Coordination of cell proliferation and differentiation during *C. elegans* development

Suzanne Aletta Ruijtenberg

ISBN: 978-90-393-6389-8

Cover: Microscopy images made during my PhD with in the background a painting made by my grandmother Letty Wijga-van der Hoeven (Oma). On the backside the *C. elegans* lineage, as described by Sulston and Horvitz, is shown.

Coordination of cell proliferation and differentiation during *C. elegans* development

Coördinatie tussen celdeling en celspecialisatie tijdens de ontwikkeling van *C. elegans*

(met een samenvatting in het Nederlands)

Proefschrift

ter verkrijging van de graad van doctor aan de Universiteit Utrecht op gezag van de rector magnificus, prof. dr. G.J. van der Zwaan, ingevolge het besluit van het college voor promoties in het openbaar te verdedigen op woensdag 16 september 2015 des middags te 2.30 uur

door

Suzanne Aletta Ruijtenberg

geboren op 19 juli 1985 te Seria, Brunei

Promotor: Prof. dr. S.J.L. van den Heuvel

Content

General introduction

Coordination of cell proliferation and differentiation

Suzan Ruijtenberg & Sander van den Heuvel

Manuscript in preparation for publication in *Cell Cycle*

Developmental Biology, Faculty of Sciences, Department of Biology, Utrecht University,
Padualaan 8, 3584 CH Utrecht, The Netherlands.

1

Introduction

The formation of a complex multi-cellular organism from a single fertilized egg is an intriguing yet highly complex process. It requires the generation of large numbers of cells, which at the appropriate times need to obtain specialized functions and morphologies, while assembling into well-defined structures, tissues, and organs. Most cells follow a gradual process of specialization with a final step, terminal differentiation, characterized by acquisition of a fully differentiated post-mitotic state. Examples include neurons, muscles and bone cells formed from proliferating precursor cells that shut down the cell cycle machinery while activating cell-type specific transcriptional programs. The temporal coupling between cell cycle withdrawal and differentiation is crucial for normal growth and development, and continues to be critical for tissue homeostasis and cell replacement throughout life. In contrast, a failure to arrest proliferation and loss of differentiation can lead to a variety of diseases and are hallmarks of cancer cells. Deregulation of proliferation control genes has been long known to contribute to carcinogenesis. Interestingly, recent insights in the frequency of genetic alterations in human cancer also highlight a widespread disruption of differentiation-related chromatin regulators and cell-type specific transcription factors in human cancer. The tight coupling between proliferation and differentiation makes it difficult to determine whether the disturbance of both cell cycle regulation and cell differentiation underlies tumor formation, or whether one follows from the other. Here, we examine the molecular mechanisms that connect cell cycle exit to cell differentiation, and consider the potential implications for cancer and regenerative medicine.

Cell cycle regulation

Cyclin Dependent Kinases (CDKs) are the master regulators of the cell division cycle. Dependent on the activity of CDK-cyclin complexes in the G1-phase, cells either arrest cell division or commit to go through another cell cycle (Figure 1). This decision depends on extracellular signals, and cell-intrinsic information such as CDK levels at the end of the previous cell cycle (Spencer *et al.*, 2013). Stimulation of quiescent cells with mitogens and growth factors induces expression of D-type cyclins (D1, D2, D3 in mammals) and activation of CDK4/6-cyclin D kinases (Choi and Anders, 2014) (Figure 2). CDK4/6-cyclin D is responsible for the initial phosphorylation of the retinoblastoma tumor suppressor (Rb) protein. This phosphorylation is thought to weaken the interaction between pRb and the heterodimeric transcription factor E2F/DP (together referred to as E2F). As a consequence, some activating E2Fs are released, which triggers the transcription of E2F-dependent genes. These pRb/E2F regulated target genes include cyclin E and many other cell cycle genes. Activation of CDK2-cyclin E leads to further phosphorylation and inactivation of pRb, release of E2F, and full commitment to S-phase entry (Figure 2) (van den Heuvel and Dyson, 2008).

In addition to pRb-mediated transcriptional repression, several other levels of control counteract progression from G1 into S-phase. This includes ubiquitin-dependent degradation of positive regulatory proteins, and blocking of CDK activation by CDK

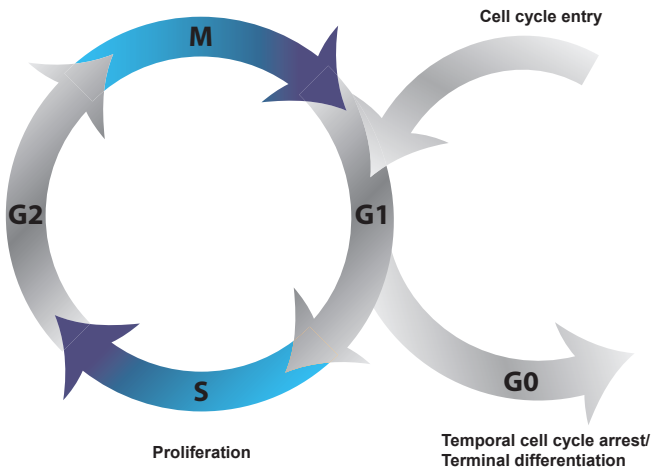

Figure 1. Cell cycle entry and exit. In order to create two new daughter cells from a single mother cell, cells go through a series of events that form part of a larger control network, together called the cell cycle. The sequential events of the cell cycle are duplication of the genetic information through DNA replication during S-phase, equal segregation of this DNA into two daughter nuclei during mitosis, and finally, creation of two new cells during the process of cytokinesis. In most cell cycles, the S- and M-phases are separated by two Gap-phases, called G1 and G2. During development, cells can decide to continue cell division or to exit from the cell division cycle and enter a state referred to as G0. Exit from the cell cycle can either be temporal during quiescence or permanent during the process of terminal differentiation.

inhibitory proteins (CKIs). Ubiquitin-dependent degradation of cell cycle proteins is primarily regulated at the level of substrate recognition by E3 ubiquitin ligases. E3 ligases with important functions in G1/S inhibition are the Anaphase Promoting Complex/Cyclosome (APC/C) in association with the FZR1/Cdh1 coactivator, and Skp1, Cullin, F-box factor (SCF) complexes (Bassermann *et al.*, 2014). Likewise, CKIs from two distinct families contribute to G1/S control in mammals (Figure 2) (Sherr and Roberts, 1999). CKIs of the INK4 protein family, such as $p16^{INK4A}$, bind to CDK4/6 kinases and prevent their interaction with D-type cyclin subunits. In contrast, CKIs of the CIP/KIP family block the activity of CDK-cyclin complexes through their association. The CIP/KIP family consists of $p21^{Cip1}$, $p27^{Kip1}$ and $p57^{Kip2}$ and is particularly important for inhibiting CDK2-cyclin E. Members of both CKI families contribute to cell cycle exit and their increased expression has been observed in differentiating cells. The importance of these CKIs is further underscored by the fact that loss of CKIs can lead to unperturbed proliferation, and by the functional inactivation of $p16^{INK4A}$ in a wide variety of human cancers (Sherr and Roberts, 1999).

Coordinating G1 length with differentiation

The decision to continue to divide or to exit from the cell cycle is made in response to a variety of signals during the G1-phase of the cell cycle. A long standing question has been

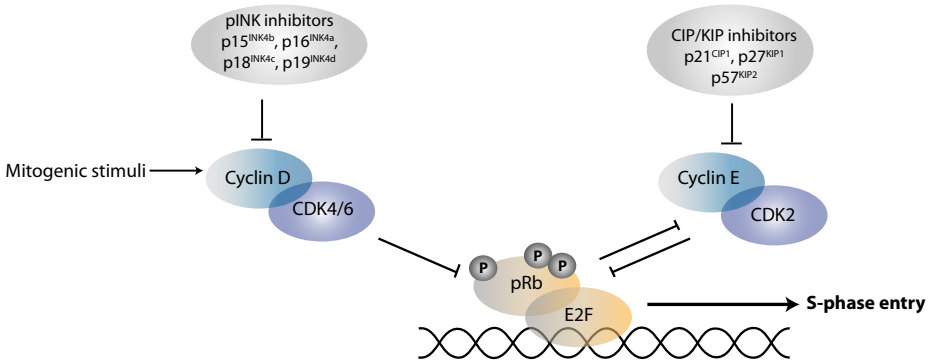

Figure 2. Regulation of the G1/S transition. The main CDK-cyclin complexes that promote progression through G1 are CDK4/6 in association with D-type cyclins and CDK2 together with cyclin E. These kinases counteract association of the retinoblastoma tumor suppressor (Rb) family with E2F transcription factors, thereby allowing transcriptional activation of S-phase genes. E2F refers to heterodimeric transcription factors that contain an E2F and DP family protein. Some E2F subunits are primarily transcriptional activators (E2F1, E2F2, E2F3), and are blocked by pRb binding. Other E2Fs are transcriptional repressors (E2F4, E2F5) and act in conjunction with the pRb family. E2F6, E2F7, and E2F8 are repressors of transcription that do not bind pRb family proteins. The pRb protein family consists of pRb, p107, and p130.

whether cells need to be in G1-phase to respond to differentiation-inducing signals, and if the length of the G1-phase is a regulating factor in the process. Indeed, early studies with embryonal carcinoma cells indicated that differentiation can be rapidly induced in G1, but not in S-phase (Mummery *et al.*, 1987). Moreover, the G1-phase appears to lengthen coincident with increased differentiation response during the progression from pluripotent stem cells to lineage-restricted progenitors and final divisions that precede cell cycle withdrawal. In fact, undifferentiated cells in the early embryo of many animal systems, including flies (*Drosophila melanogaster*), frogs (*Xenopus laevis*), and zebrafish (*Danio rerio*), undergo very rapid cell divisions that entirely lack G1- and G2-phases. This may be relevant for maintenance of the undifferentiated state, or simply reflect that syncytial divisions (*Dm*) and cell cleavages (*Xl, Dr*) do not include cell growth, and therefore may not need Gap phases. Very short cell division cycles have also been observed during mammalian embryogenesis, but only after preimplantation embryos reach the blastocyst stage. Subsequent cell cycles vary in length, with the shortest cell cycles (± 3 hr) reported after implantation, for cells that move through the primitive streak during gastrulation (Mac Auley *et al.*, 1993; Ciemerych and Sicinski, 2005). Similarly, embryonic stem cells established from the inner cell mass of preimplantation embryos have unusual cell cycles with a short G1-phase of approximately 2 hours.

All these short embryonic cycles are characterized by the absence of active CDK inhibitors and constitutively high levels of CDKs and Cyclins, especially CDK2-cyclin E (Stead *et al.*, 2002; White and Dalton, 2005; Filipczyk *et al.*, 2007; Lange and Calegari, 2010; Singh

et al., 2013). Interestingly, these cell cycle profiles start to change upon induced differentiation, or during specific development transitions such as the specification of the three germlayers in mice. The activity of CDKs drops during these processes and becomes more cell cycle-dependent. This coincides with establishment of a functional CDK4/6-cyclin D–pRb pathway and increased expression of cell cycle inhibitors. As a consequence, cell cycles become longer and include an extensive G1-phase.

The importance of this G1 lengthening during lineage commitment was demonstrated in mouse and human embryonic stem cells. Increasing the levels of CDK2-cyclin E activity, the main driver of the cell cycle in these cells, reduced the cell cycle length and obstructed differentiation. Decreasing CDK2-cyclin E levels had the opposite effect (Richard-Parpaillon *et al.*, 2004; Filipczyk *et al.*, 2007; Kim *et al.*, 2009). Thus, low G1 CDK-cyclin activity and a short G1-phase may be causally related to the maintenance of the undifferentiated state of embryonic stem cells. As a possible explanation, cells appear most sensitive to differentiation factors during the G1-phase. Keeping G1 very short or absent might prevent the induction of differentiation during early development. Conversely, introducing an extended G1-phase during later stages of development allows more time to respond to external signals and accumulate differentiation-inducing transcription factors (Mummery *et al.*, 1987; Sela *et al.*, 2012; Barta *et al.*, 2013; Calder *et al.*, 2013; Coronado *et al.*, 2013; Dalton, 2013).

Remarkably, recent studies demonstrated that signals received in early versus late G1 can have different outcomes (Dalton, 2013; Pauklin and Vallier, 2013). In response to TGFβ-related signaling, pluripotent human embryonic stem cells in early G1 formed endoderm, while late G1 cells showed neurectodermal specification. The difference was traced to activation of CDK4/6-cyclin D, which phosphorylated and blocked nuclear import of Smad2/3, thereby preventing endoderm and allowing neurectodermal differentiation. These data emphasize the intimate connection between G1 length, G1 CDK-cyclin activation and the response to developmental and differentiation-inducing signals.

In addition to extension of the G1-phase upon lineage commitment of stem cells, lengthening of the G1-phase also occurs when progenitor cells start to give rise to daughter cells that initiate terminal differentiation. The contribution of G1 lengthening in progenitor cells has been well investigated in the developing mouse brain. The neural progenitors go through a well-organized pattern of division to first form intermediate progenitors and finally terminally differentiated neurons. Interestingly, as progenitors switch from proliferative divisions to neurogenic divisions, the time in G1-phase has been observed to increase from approximately 3 to 12 hours (Calegari *et al.*, 2005; Salomoni and Calegari, 2010). Similar to embryonic stem cells, experimental manipulation of the G1-phase of neuronal progenitors influenced their differentiation. Inhibition of cyclin E levels caused lengthening of G1 in the progenitors, coincident with a premature switch from proliferative to neurogenic divisions. Interfering with the levels of CDK4-cyclin D activity had a comparable effect. Moreover, knockout of cyclin D1 increased neurogenesis at the expense of progenitor expansion in the retina, whereas overexpression of cyclin D1 and CDK4 led to shortening of G1-phase and a delay in neurogenesis (Calegari and Huttner, 2003; Lange *et al.*, 2009).

The examples above indicate that cell cycle lengthening is not simply a consequence of differentiation. Cell cycle progression and differentiation are tightly linked, and shorting or lengthening of G1 correlates with a decrease or increase in differentiation potential, respectively. Therefore, G1 lengthening might be an important aspect of lineage commitment and terminal differentiation (O'Farrell *et al.*, 2004; White *et al.*, 2005; Singh and Dalton, 2009; Li *et al.*, 2012; Singh *et al.*, 2013)

Temporal versus permanent cell cycle exit

In contrast to permanent cell cycle exit upon differentiation, cells can also temporarily exit the cell cycle. This reversible non-dividing state, known as quiescence, is common during development, and during maintenance of adult stem cells as well as progenitors such as resting lymphocytes. Quiescence is usually studied in tissue culture cells exposed to stimuli such as serum starvation, contact inhibition or loss of adhesion (Blomen and Boonstra, 2007). The mechanisms that induce quiescence *in vivo* are more complex and less well characterized (Blomen and Boonstra, 2007; Buttitta and Edgar, 2007; O'Farrell, 2011). Expression of CDK inhibitors of the CIP/KIP family, which predominantly inhibit CDK2-cyclin E, are particularly associated with the quiescent state both *in vivo* and in tissue culture. Interfering with these inhibitors disrupts cell cycle exit and quiescence and can therefore lead to, for example, depletion of the hematopoietic stem cell pool *in vivo* (Cheng *et al.*, 2000; Matsumoto *et al.*, 2011).

Both temporal and permanent cell cycle exit involve induction of negative cell cycle regulators and inhibition of positive regulators. What then determines the difference between temporal and permanent cell cycle exit, and why do some cells only temporarily exit the cell cycle while permanent differentiation programs are initiated in others? The finding that quiescence does not simply result from arrested cell division may provide an important cue (Coller *et al.*, 2006). Human fibroblasts can be arrested by $p21^{Cip1}$ expression, but this does not induce a gene expression profile that characterizes the quiescent state. Moreover, introduction of MyoD in proliferating or $p21^{Cip1}$-arrested fibroblasts induces muscle differentiation, while quiescent fibroblasts resist differentiation. Thus, the quiescent state may actively prevent differentiation in order to retain the ability to resume proliferation. Expression of the transcriptional repressor Hairy and Enhancer of Split1 (HES1) has been proposed as a possible mechanism for preventing terminal differentiation of quiescent cells (Coller *et al.*, 2006; Sang *et al.*, 2008).

The main difference between temporal and permanent cell cycle exit, however, probably depends on the activation of differentiation-inducing transcription factors and the concomitant changes in gene expression during differentiation. This altered transcriptional program also depends on chromatin regulators and needs to be coordinated with the cell cycle machinery in order to induce the functional and morphological changes and the transition from proliferating precursor cells to differentiated post mitotic cells. Below we will discuss how the combinatorial activity of transcription factors, chromatin regulators and the cell cycle machinery coordinates cell cycle exit with differentiation.

Model systems to study the coordination between proliferation and differentiation

The temporal coupling between cell cycle exit and differentiation has been observed and studied in a wide diversity of cell types and model organisms. In particular, the formation of muscle fibers and differentiated neurons provide relatively well-defined programs of proliferative stem cell divisions that transition through committed progenitors to terminally differentiated cells (Figure 3). In fact, myogenesis has long served as a model for the antagonism between proliferation and differentiation. Early studies identified the key myogenic transcription factor MyoD, and found that it induced muscle specific gene expression as well as expression of the $p21^{Cip1}$ cell cycle inhibitor (Tapscott *et al.*, 1988; Halevy *et al.*, 1995).

Studies of skeletal muscle differentiation have made extensive use of the C2C12 mouse myoblast cell line, as well as primary myoblasts in culture, and differentiation of progenitors such as satellite cells in model organisms. Differentiation involves an initial determination step of proliferative myoblasts formation, which is followed by exit from the cell cycle

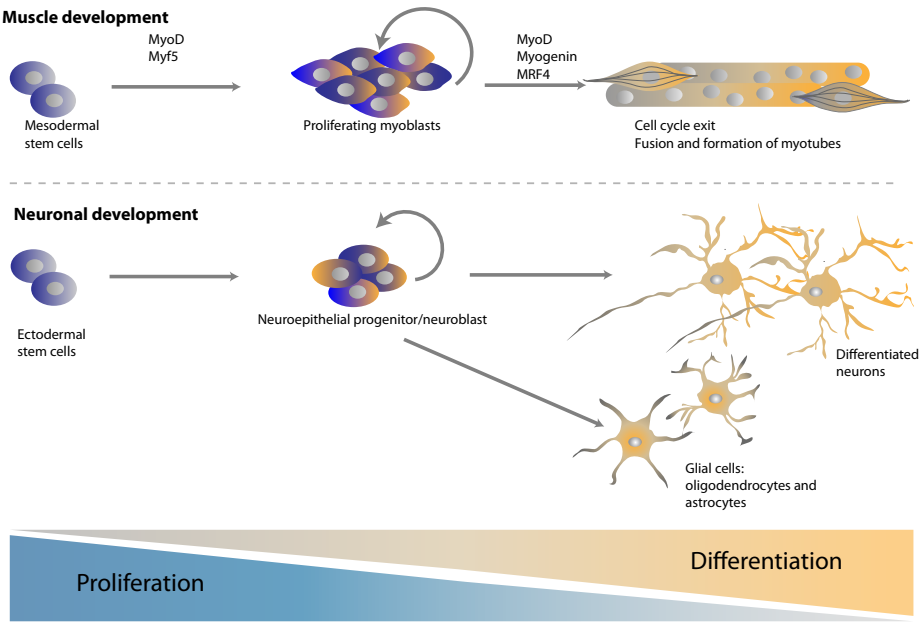

Figure 3. Model systems to study the coordination of cell cycle exit and differentiation. To study the temporal coupling between cell cycle exit and differentiation both muscle and neuronal development have served as powerful model systems. Differentiated muscle cells and neurons are formed from precursor cells that first become lineage restricted, then committed precursors that continue proliferative divisions, and finally terminally differentiate into post-mitotic cells. This requires the activation of myogenic and pro-neuronal transcription factors and is often accompanied by the upregulation of negative cell cycle regulators.

and fusion to form multi-nucleated myotubes (Figure 3). A network of helix-loop-helix (bHLH) myogenic regulatory factors (MRFs) controls the determination and differentiation steps. In addition to the myoblast determination protein (MyoD), the MRFs include myogenic factor 5 (Myf5), Mrf4 (also known as Myf6) and Myogenin. MyoD and Myf5 serve as the main myogenic determination factors, while Myogenin as well as MyoD and Mrf4 act later during the terminal differentiation of myoblasts into muscle fibers (Figure 3). In addition to the important fundamental insights in how transcription factors control cell differentiation, recent studies of muscle development emphasize the contribution of miRNAs and chromatin regulators in this process (Braun and Gautel, 2011; Puri and Mercola, 2012; Buckingham and Rigby, 2014)

Also, several neurogenesis models have been used to study the reciprocal relationship between proliferation and differentiation. Insight has come from induced neuronal differentiation of embryonic carcinoma or neuroblastoma cell lines in tissue culture. Moreover, highly sophisticated developmental studies have been performed in *Drosophila*, *Xenopus* and mice. Recently, human pluripotent stem cells have been successfully induced to acquire specific neuronal fates, and even to form multi-layered cerebral organoid structures (mini-brains) in 3D culture (Lancaster and Knoblich, 2014). Although the exact mechanisms of neuronal development varies between systems, neuronal development starts in general from a neuroepithelial progenitor, which can give rise to neuronal-restricted and glia-restricted progenitors (Figure 3). Glia-restricted precursors can generate oligodendrocytes and astrocytes, while neuronal progenitors contribute to formation of all the different neurons of the central and peripheral nervous system (Holland, 2001; Dehay and Kennedy, 2007; Paridaen and Huttner, 2014). This neuronal differentiation process depends on the expression of the right combination of transcription factors, and is often accompanied by upregulation of negative cell cycle regulators. The pro-neuronal bHLH transcription factors of the Neurogenin (Neurog), NeuroD, and Achaete scute-like 1 (Ascl1) families are critical for neurogenesis. Interfering with these transcription factors or with the cell cycle machinery influences the coordination between proliferation and differentiation and thereby the final number of differentiated neurons in the brain (Wilkinson *et al.*, 2013; Paridaen and Huttner, 2014). A major question is how the differentiation-inducing transcription factors and cell cycle regulators interact to initiate and maintain the non-proliferative differentiated state of neurons.

Are cell proliferation and differentiation mutually exclusive or co-regulated?

The co-occurrence of cell cycle exit and terminal differentiation as observed in neurons, muscles, blood, bone, and other cell types could theoretically result from one of two different underlying principles. First, the processes of cell division and cell differentiation could be mutually exclusive. This would be the case if differentiation can only occur when cells have exited the cell cycle, or when cell division depends on the cells being in an undifferentiated state. Alternatively, cell cycle exit and differentiation could be jointly regulated

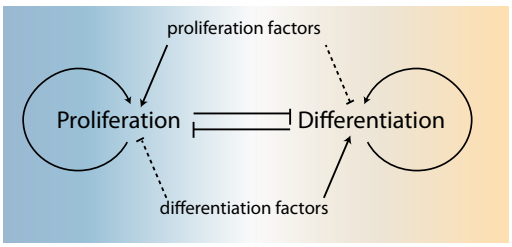

Figure 4. Coordination of proliferation and differentiation. Tight coordination between cell cycle exit and differentiation has been observed in many systems. This results most likely from both negative and positive feedback mechanisms. As a consequence, proliferation is promoted and differentiation inhibited in dividing cells, while the opposite occurs in differentiated cells.

in time and coupled by feedback mechanisms (Figure 4). In case of a dependent relation, proliferation and differentiation could never coincide. If the processes are co-regulated, however, they may be uncoupled through specific deregulations.

Some specific examples have been reported of coincident occurrence of cell division and a highly differentiated state *in vivo*. For instance, loss of Rb allows proliferation of post-mitotic hair cells in the mouse inner ear, and in part, these cells remain functional (Sage *et al.*, 2005). Similarly, conditional inactivation of multiple Rb-family members in the mouse eye causes terminally differentiated neurons to resume proliferation while maintaining a differentiated status (Ajioka *et al.*, 2007). In *Drosophila*, simultaneous activation of E2F and G1 CDK-cyclins causes overproliferation of terminally differentiated cells in the eyes and wings (Buttitta *et al.*, 2007, 2010). While cardiac muscle cells are notoriously post-mitotic, mouse HL-1 cells derived from cardiac muscle combine proliferation with maintenance of a differentiated phenotype (White *et al.*, 2004). Remarkably, even normal cardiomyocytes can proliferate to promote regeneration of the neonatal mouse heart, a capacity that is lost soon after birth (Porrello *et al.*, 2011; Mahmoud *et al.*, 2013). These observations all indicate that proliferation and differentiation are not necessarily incompatible, and thus that cell cycle exit and differentiation are likely jointly regulated rather than co-dependent.

The low frequency of coincident proliferation/terminal differentiation phenotypes indicates that the coordinated regulation is very tight. This stringency likely comes from two different origins. First, there is a substantial degree of redundancy in the regulatory network, in particular in the control of proliferation. Hence, in most tissues, loss of a single regulator has a limited effect, and two or more redundantly acting controls will rarely be altered by chance. Moreover, the presence of positive and negative feedback mechanisms are likely to enforce all-or-none decisions. Consequently, cells either exist in a stable proliferative state or in a differentiated post-mitotic state. A regulatory network with a high degree of redundancy and feedback control can create robust control and effectively accomplish mutually exclusive states (Figure 4) (Gérard *et al.*, 2012).

Inhibition of differentiation by positive cell cycle regulators

A possible mechanism to coordinate proliferation and differentiation is to control the function of cell-type specific transcription factors in a cell cycle-dependent manner. Indeed, crosstalk between cell cycle genes and differentiation-inducing transcription factors has

been reported, again with studies of MyoD leading the way. While MyoD is present in proliferating myoblasts and associated with regulatory regions of many genes, induction of differentiation and muscle specific gene expression is delayed until cell proliferation seizes. This regulation has long been known to relate to CDK-cyclin activity. Overexpression of the cell cycle regulator Cyclin D1 was found to inhibit MyoD induced myogenesis and more specifically MyoD transcriptional activity (Rao *et al.*, 1994; Skapek *et al.*, 1995; Guo and Walsh, 1997). This effect appeared CDK4-cyclin D kinase-activity-dependent and partly Rb independent. As an attractive hypothesis, MyoD could be phosphorylated and inhibited by CDK4-cyclin D, but evidence for such phosphorylation has not been found (Skapek *et al.*, 1996; Lazaro *et al.*, 2002). Instead, CDK4-MyoD mutual inhibition through complex formation has been described (Zhang *et al.*, 1999a), but it remains unclear if this interaction is physiologically significant (Kitzmann and Fernandez, 2001).

Several groups, however, reported direct phosphorylation of MyoD by CDK2-cyclin E. MyoD is phosphorylated at multiple residues *in vivo*. One of these residues, Ser200, was found to be specifically phosphorylated by CDK2-cyclin E *in vitro* (Kitzmann *et al.*, 1999; Reynaud *et al.*, 1999; Tintignac *et al.*, 2000). Providing support for *in vivo* significance, roscovitin, a chemical CDK2 and CDK1 inhibitor, and overexpression of $p57^{Kip2}$ each prevented MyoD-Ser200 phosphorylation (Reynaud *et al.*, 1999; Tintignac *et al.*, 2000). MyoD-Ser200 phosphorylation corresponds to increased turnover of MyoD at the end of G1 (Song *et al.*, 1998; Kitzmann *et al.*, 1999; Tintignac *et al.*, 2000). By preventing MyoD accumulation and concomitant induction of muscle differentiation, this mechanism may contribute to continued myoblast proliferation.

Phosphorylation of MyoD by CDK2-cyclin E likely follows from CDK4-cyclin D induced Rb-inhibition. Thus, this does not explain the observed Rb-independent obstruction of myogenesis by CDK4-cyclin D. However, direct phosphorylation by CDK4-cyclin D was found to control transcriptional activation by MEF2, which acts together with MyoD in muscle differentiation (Lazaro *et al.*, 2002). Together with phosphorylation of additional factors associated with MyoD and MEF2 by other kinases, this likely controls the switch from transcriptional repression to activation of muscle specific genes (Singh *et al.*, 2015).

Phosphorylation by CDK-cyclin complexes has also been suggested to regulate the function of neurogenesis-inducing transcription factors. Examination of the proneuronal differentiation factor *neurogenin 2* (Ngn2) from *Xenopus* and mouse cells revealed extensive phosphorylation *in vivo*. Both mouse and *Xenopus* Ngn2 contain 9 potential CDK-phosphorylated Ser residues (each followed by Pro), and cyclin A and cyclin B kinases efficiently phosphorylated Ngn2 *in vitro*. Mutating these residues to non-phosphorylatable Ala residues increased the activity of Ngn2 as an inducer of neurogenesis. Moreover, progressive phosphorylation in mitotic extracts appeared to correlate with reduced DNA binding in mobility shift assays (Ali *et al.*, 2011; Hindley *et al.*, 2012). Similar result were obtained for the bHLH neurogenic transcription factor Achaete-Scute Homologue 1 (Ascl1, Mash1) (Ali *et al.*, 2011). As an interesting hypothesis, progressive multi-site phosphorylation could affect the affinity of these transcription factors in a cell cycle-dependent fashion, changing them from binding only to promoters accessible in proliferating precursor cells to the more

closed regulatory regions of differentiation promoting genes when CDK levels drop (Byun *et al.*, 2005; Hardwick and Philpott, 2014).

Antagonistic regulation of differentiation-inducing factors by CDK2-cyclin E complexes may be used broadly, as indicated by examples in highly diverse systems. One of these systems is the *Drosophila* neuroblast (Berger *et al.*, 2005; Jeong *et al.*, 2011). *Drosophila* neuroblasts typically divide asymmetrically, combining self-renewal with the generation of a ganglion mother cell. This ganglion mother cell divides once again to give rise to two differentiated neurons. The transcription factor Prospero is deposited exclusively to the ganglion mother cell during the asymmetric neuroblast division. Prospero enters the nucleus of this cell and induces a transcriptional program required for neuronal differentiation. Its asymmetric distribution depends on cortical localization in the neuroblast, while localization to the nucleus is required for differentiation. In the absence of Cyclin E, nuclear localization of Prospero is observed in both neuroblast daughter cells, leading to premature neuronal differentiation (Berger *et al.*, 2005, 2010). In contrast, ectopic cyclin E expression induces asymmetric prospero distribution in a normally symmetrically dividing neuroblast. Thus, Cyclin E controls prospero localization and function directly or indirectly.

CDK2-cyclin E has also been implicated in antagonizing cell differentiation in *C. elegans* (Fujita *et al.*, 2007; Jeong *et al.*, 2011). One example is reminiscent of *Drosophila* Prospero and involves an asymmetric cell division in the somatic gonad (Fujita *et al.*, 2007). Upon loss of cyclin E, some of these divisions become symmetric, with the daughter cell that normally remains temporally quiescent also becoming a Distal Tip Cell, a fate normally acquired only by its sister cell. A quite different example of CDK2-cyclin E regulated control of a differentiation-inducing factor is seen during the transition of germ line stem cells into differentiated gametes (Jeong *et al.*, 2011). This decision involves a switch from mitotic cell division to entry into meiotic prophase. Meiotic entry and/or arrest of cell division is promoted by the GLD-1 (defective in Germ Line Development) protein, which associates with mRNA targets and inhibits their translation. Several lines of evidence indicate that GLD-1 is a direct substrate of CDK2-cyclin E *in vivo* and *in vitro.* As a consequence of CDK2-cylin E-dependent GLD-1 phosphorylation, GLD-1 levels remain low in the stem cells of the germ line, and premature cell cycle exit and meiotic entry are prevented (Jeong *et al.*, 2011). Interestingly, GLD-1 also represses cyclin E mRNA translation, allowing a double negative feedback loop and abrupt transition from mitosis to meiosis (Biedermann *et al.*, 2009; Fox *et al.*, 2011; Jeong *et al.*, 2011).

The examples described above illustrate how CDK-cyclin phosphorylation may directly counter the activity of differentiation-inducing factors. This provides a potential mechanism for how the onset of differentiation may depend on an extended G1-phase with low CDK-cyclin activity.

Negative cell cycle regulators promote differentiation

While positive cell cycle regulators prevent differentiation, negative cell cycle regulators promote differentiation. In particular, members of the CIP/KIP family of CDK inhibi-

tors are important to connect cell cycle exit and differentiation. Obviously, these cell cycle inhibitors interfere with the activity of CDKs and thereby overcome negative regulation of differentiation-inducing factors. In addition, in some cases CKIs may contribute functions independent from cell cycle exit. For example, direct binding of $p57^{Kip2}$ to MyoD has been reported to stabilize MyoD, thereby promoting differentiation (Reynaud *et al.*, 1999, 2000). In addition, $p27^{Kip1}$ is sufficient for cell cycle arrest of mouse oligodendrocyte precursors, yet $p21^{Cip1}$ is also needed to promote full differentiation (Zezula *et al.*, 2001). The N-terminal part of *Xenopus,* p27 (Xic1) also appeared to contribute a cell cycle independent function in the differentiation of multiple cell types (Hardwick and Philpott, 2014). While these functions of CIP family members are not well understood, they have been implicated in stabilization of differentiation-inducing transcription factors.

In cooperation with CIP family members, transcriptional co-repressors of the Rb family promote cell differentiation. This role relates at least in part to the inhibition of cell cycle progression by complexes of pRb and E2F family proteins (van den Heuvel and Dyson, 2008). In addition, pRb has been reported to associate with cell-type specific transcription factors, including MyoD, Myogenin, C/EBP, PU.1, NF-IL6, Pax-3 and AP-2 (Lipinski and Jacks, 1999; Müller and Helin, 2000; Morris and Dyson, 2001; Korenjak and Brehm, 2005). Such interactions may help prevent transcriptional activation of differentiation specific genes in proliferating precursor cells, as has also been reported for Rb-E2F-related complexes (Dimova *et al.*, 2003). It is thought that pRb fulfills these transcriptional repressor functions in differentiation in part via the recruitment of various chromatin regulators, as will be discussed below. In some cases, however, pRb complexes can promote transcription of cell-type specific genes (Korenjak and Brehm, 2005). The best-described example is the differentiation of liver macrophages, which is critical for completion of erythropoiesis (Iavarone *et al.*, 2004). In this process, pRb can bind the ETS-domain transcription factor PU.1 as well as the antagonistically acting Id2 bHLH domain transcriptional repressor. PU.1 is needed for myeloid gene expression, which is repressed by pRb association. Surprisingly, $Rb^{-/-}$ knockout cells showed reduced expression of genes specific for the macrophage and dendritic branch of the myeloid lineage. This indicated a positive role for pRb in transcription, due to sequestering the PU.1 antagonist Id2, thereby allowing PU.1-activated transcription (Iavarone *et al.*, 2004). What determines whether pRb associates with PU.1 or Id2 is currently not understood.

As a third level of regulation, targeted protein degradation plays an important role in cell cycle progression and differentiation. One of the E3 ligases involved in ubiquitin-dependent destruction of cell cycle proteins is the Anaphase Promoting Complex/Cyclosome (APC/C). Association of the APC/C with either the Cdc20 or FZR1/Cdh1 co-activator determines substrate recognition. During muscle differentiation of C2C12 cells, APC/C^{Cdh1} targets both the cell cycle regulator Skp2 and the early myogenic differentiation factor Myf5 for degradation (Li *et al.*, 2007). The degradation of Skp2 results in elevated levels of the CIP/KIP inhibitors p21 and p27. By contrast, degradation of the early myogenic factor Myf5 is required for myogenic fusion. Thus, by promoting cell cycle arrest and ensuring the

presence of the correct combination of transcription factors, the APC/C^{Cdh1} functions as a dual function regulator that links cell cycle exit to differentiation (Li *et al.*, 2007).

The CIP/KIP inhibitors, pRb and APC/C^{Cdh1} are all well established inhibitors of G1 progression, which will likely promote differentiation through their effects on G1 CDK-cyclins and lengthening of G1. The examples above illustrate how G1 inhibitors may also directly regulate differentiation-related transcription factors. Thus, negative and positive regulators of the cell cycle each appear to be involved in the regulation of cell differentiation, directly as well as indirectly. As a consequence, cell cycle exit becomes coordinated with terminal differentiation.

The role of differentiation-inducing transcription factors in cell cycle progression

During terminal differentiation, cell type specific transcription factors induce extensive changes in gene expression, thereby executing one specific specialization program out of a wide variety of possibilities. To coordinate differentiation with cell cycle exit, the induction of cell-type specific genes needs to go along with altered expression of cell cycle regulators. Interestingly, several transcription factors that promote differentiation of muscle cells, neurons, or blood cells also control expression of cell cycle genes. This dual function in transcriptional regulation of cell-type specific genes and cell cycle genes was first observed for MyoD, which triggers expression of the cell cycle inhibitors $p21^{CIP1}$ and $p57^{KIP2}$ (Guo *et al.*, 1995; Halevy *et al.*, 1995; Parker *et al.*, 1995; Figliola and Maione, 2004; Vaccarello *et al.*, 2006; Busanello *et al.*, 2012). MyoD can directly bind $p21^{CIP1}$ and $p57^{KIP2}$ promoter sequences in committed precursors, but their transcriptional activation is delayed until the initiation of differentiation (Cao *et al.*, 2010; Zalc *et al.*, 2014). Most importantly, knockout of $p21^{CIP1}$ and $p57^{KIP2}$ impairs skeletal muscle development *in vivo*, with defective muscle fibres that resemble those of myogenin knockout mice (Zhang *et al.*, 1999b). These data point to an essential role for these CIP/KIP inhibitors in cell cycle arrest during muscle formation. These mechanisms appear widely used. For instance, two key transcription factors required for erythrocyte development and maturation, EKLF and GATA-1, directly control the expression levels of $p21^{CIP1}$ (Papetti *et al.*, 2010; Siatecka *et al.*, 2010).

Neurogenin is required for neural commitment and also appears to act as a dual function regulator of differentiation and cell cycle arrest. Studies in chicken spinal cords addressed whether Neurogenin 2 (Ngn2) directly regulates cell cycle genes (Lacomme *et al.*, 2012). The authors examined which genes showed altered expression directly after ectopic Ngn2 expression in early embryos, at the time of neuronal commitment but before full differentiation. This revealed inhibition of patterning genes, induction of differentiation-related genes, and simultaneously reduced expression of positive cell cycle regulators. In particular D-, E- and A-type cyclins showed reduced expression at this early stage (Lacomme *et al.*, 2012). With the possible exception of Cyclin E2, the transcriptional repression however, did not appear to be directly mediated by Ngn2 (Lacomme *et al.*, 2012).

The *Drosophila* neurogenic factor Prospero, described above, also provides an example of a transcription factor which promotes upregulation of neuron specific genes together with inactivation of positive cell cycle genes. Examination of Prospero mutant embryos showed continued proliferation despite the initiation of early steps of neuronal differentiation. Loss of Prospero coincided with severe upregulation of cyclin E, cyclin A and String/Cdc25, while ectopic Prospero expression reduced their expression (Li and Vaessin, 2000). Thus, neuronal differentiation factors promote cell cycle exit, although direct regulation of cell cycle genes by neurogenic transcription factors is not well documented.

In the previous section we discussed how cell cycle genes control differentiation. Here, we showed examples of differentiation factors directly controlling cell cycle progression. By making the activity of differentiation genes dependent on cell cycle genes and the activity of cell cycle regulators on differentiation factors, tight coordination between cell cycle exit and differentiation can be established.

The role of chromatin regulators in coordinating cell cycle exit with differentiation

In the previous paragraphs we focused on how cell cycle regulators and cell type specific factors act together to ensure temporal coupling between cell cycle arrest and differentiation. The transcriptional changes involved in differentiation are not achieved by transcription factors alone, but rather in coordination with a large variety of chromatin remodeling factors. Gene transcription requires binding of transcription factors to regulatory DNA sequences in promoter and enhancer elements. Whether these transcription factors can bind and become activated depends on the chromatin state. Open chromatin, called euchromatin, allows transcription factor and polymerase access and is permissible for gene expression. In contrast, more densely packed closed chromatin, called heterochromatin, contributes to gene silencing. The chromatin composition and packaging of DNA is regulated by multiple mechanisms including DNA methylation, histone modification (including phosphorylation, methylation, acetylation and ubiquitylation), incorporation of histone variants and ATP-dependent chromatin remodeling (Chen and Dent, 2014). Multi-subunit chromatin modification complexes covalently attach methyl groups and other modifications to DNA or histones, or remove such modifications. This either directly affects chromatin compaction or contributes to the binding of effector molecules. ATP-dependent chromatin remodelers, on the other hand, use the energy of ATP hydrolysis to exchange, move or eject histones. Together, these regulators determine the accessibility of the DNA to transcription factors, co-regulators and RNA polymerase complexes. Below, we will discuss chromatin regulators that are particularly important in regulating cell cycle control, lineage commitment, and terminal differentiation. This includes pRb-containing modification complexes, transcriptional repressors of the Polycomb Group, and the activating Trithorax Group members. The SWI/SNF ATPase-dependent chromatin remodeling complexes will receive special attention because of their central role in cell division and differentiation decisions.

pRb-dependent chromatin remodeling

Proteins of the pRb family repress transcription by binding the transactivation domain of E2F transcription factors. In addition, pRb family proteins contribute to active gene silencing through the recruitment of chromatin regulatory proteins (for reviews see: van den Heuvel and Dyson, 2008; Gordon and Du, 2011; Talluri and Dick, 2012; Sadasivam and DeCaprio, 2013). Co-repressors reported to associate with pRb include histone deacetylases (HDACs), ATPases of the SWI/SNF chromatin remodeling complex, histone methyltransferases (HMTs), the DNA methyltransferase DNMT1, and histone binding proteins such as HP1. Whether these interactions, often detected by co-immunoprecipitation, reflect functional cooperation *in vivo* is difficult to proof. Nevertheless, it is quite well documented that HDAC activity corresponds to pRb/E2F localization and contributes to transcriptional repression of cyclin E, cyclin A and other E2F targets during cell cycle exit (Gordon and Du, 2011; Talluri and Dick, 2012). Recruitment of an HDAC co-repressor complex to pRb/E2F-regulated promoters has been reported to depend on SWI/SNF function (Gunawardena *et al*., 2007). The direct physical interaction between pRb and the SWI/SNF-Brg1/Brm subunits remains debated (Talluri and Dick, 2012). In support of a functional interaction, however, Rb, E2F and SWI/SNF mutations show genetic interaction in model organisms (Staehling-Hampton *et al*., 1999; Cui *et al*., 2004, Chapter 6). In *C. elegans*, SWI/SNF loss of function and Rb family null mutations show strong genetic enhancement (Cui *et al*., 2004). This supports concerted functions that, at least in part, do not depend on direct physical interaction between the proteins.

The methyltransferases (HMTs) found associated with pRb contribute to the formation of general gene silencing marks. This includes the HMT Suv39h1, which is responsible for trimethylation of lysine 9 of histone H3 (H3K9me3), a repressive histone methylation mark associated with heterochromatin. H3K9 trimethylation allows binding of the heterochromatin binding protein HP1, which is an important step in transcriptional repression. Notably, deacetylation, trimethylation and HP1 binding of H3K9 are three sequential steps in gene silencing, carried out by three different chromatin regulators found in association with pRb. The HMTs Suv4–20 h1 and h2 also associate with pRb and are responsible for bi- and tri-methylation of H4K20. These methylations create a binding site for the lethal malignant brain tumor protein L(3)MBT (Trojer *et al*., 2007). L(3)MBT has also been reported to form part of a silencing complex that contains pRb as well as a HP1 family member. Thus, through enzymatic activities and protein association, the chromatin regulators associated with pRb have the potential to induce chromatin compaction and repression of gene transcription. These combined activities likely contribute to the stable silencing of cell cycle genes during cell cycle exit.

Genetic studies in *C. elegans* and biochemical experiments in *Drosophila* resulted in the identification of a large Rb-related protein complex that possibly lacked chromatin-regulatory enzymes. Genes encoding components of this complex are needed for stable repression of *lin-3* EGF in the *C. elegans* epidermis. De-repression of *lin-3* EGF by two simultaneous mutations induces extra precursor cells to form vulval tissue, and thus gives rise to a synthetic Mulva (synMuv) phenotype. *C. elegans* Rb-related (LIN-35), E2F-like (EFL-1),

DP-like (DPL-1) and several other conserved proteins all belong to the same synMuv B class, indicating that these proteins function within a genetic pathway or in association. Purification of RB/E2F complexes from *Drosophila* embryos revealed a repressor complex containing fly RB (RBF), E2F2, MYB and in addition four conserved synMuv B proteins (Korenjak *et al*., 2004). This DREAM (*Drosophila* RBF, E2F, and Myb) complex is not only similar to the *C. elegans* synMuv B complex, but also closely related to a mammalian complex that contains repressive E2F4 and E2F5 and the pRb-related protein p130 (Sadasivam and DeCaprio, 2013). Importantly, the components of these complexes remained associated through multiple biochemical steps, and were genetically identified because of their overlapping functions in *C. elegans*. Therefore, DREAM and synMuvB probably are *in vivo* relevant RB/E2F-related protein complexes.

Surprisingly, the *Drosophila* and human DREAM complex did not appear to contain obvious enzymatic activities. This could question whether chromatin regulators are truly required for the Rb-related repressor functions *in vivo*. An independently purified Myb-MuvB complex that largely corresponds to DREAM was found to contain associated Rpd3 HDAC and L(3)MBT proteins (Lewis *et al*., 2004). These proteins were not detected in *Drosophila* DREAM, human p130-E2F4/5, or *C. elegans* synMuv B complexes (Harrison *et al*., 2006, 2007). However, *C. elegans hda-1* HDAC1, *hpl-1* HP1, and *lin-61* L(3)MBT all show substantial phenotypic overlap with synMuv B genes. Moreover, *Drosophila* DREAM binds specifically to deacetylated histone H4 tails (Korenjak *et al*., 2004), and L(3)MBT requires Myb-MuvB/DREAM for its chromosomal recruitment (Blanchard *et al*., 2014). These data are consistent with functional and (weak) physical interactions between DREAM/MuvB and chromatin modifying complexes, leading to gene silencing.

Only a subset of the *C. elegans* synMuv B genes contributes to cell cycle arrest (Boxem and van den Heuvel, 2002). In contrast, all synMuv B genes prevent inappropriate *lin-3* EGF expression and several are needed for the silencing of germline specific genes in somatic cells (van den Heuvel and Dyson, 2008; Petrella *et al*., 2011; Xiao *et al.,* 2011). Derepression of germline genes in synMuv B mutants is most obvious in the intestine and skin, two tissues with continued S-phases throughout larval development. Similarly, *Drosophila* DREAM subunits are required for the permanent repression of sex and differentiation specific genes in proliferating S2 cells and embryos. Importantly, these fly dE2F2/RBF complexes remain present despite high CDK activity (Dimova *et al*., 2003; Dimova and Dyson, 2005). Thus, while some Rb/E2F complexes repress cycle genes during cell cycle exit, other E2F/Rb-related complexes repress cell-type specific gene expression in cycling cells. The mammalian p130-E2F4/5 DREAM complex deviates from this paradigm and mediates gene silencing specifically in quiescent or G0 arrested cells (Litovchick *et al*., 2007).

Polycomb and Trithorax Group genes and developmental control of differentiation

Chromatin regulators of the Polycomb Group (PcG) and the antagonistically acting Trithorax Group (TrxG) have emerged as key players of developmental gene regulation. PcG

and TrxG proteins contribute to the epigenetic regulation of many processes, including cell cycle control, stem cell maintenance, cell fate determination, and terminal differentiation (Schuettengruber *et al.*, 2007, 2011; Laugesen and Helin, 2014). PcG and TrxG genes were originally identified in *Drosophila*, through their roles in the maintenance of the proper pattern of Hox gene expression. Since, homologues of *Drosophila* PcG and TrxG genes have been found to be conserved in a wide variety of multi-cellular organisms and are now known to repress or activate, respectively, transcription of many genes.

PcG proteins form multi-subunit protein complexes, of which Polycomb Repressor Complex 1 and 2 are the most important. Both of these complexes contain a subunit with catalytic activity. The Ring protein of PRC1 catalyzes ubiquitylation of H2A at lysine residue K119. EZH (Enhancer of Zeste), one of the core subunits of the PRC2 complex, is an HMT responsible for the methylation of lysine 27 of histone H3 (Müller *et al.*, 2002). Other PRC2 subunits are needed for this HMT activity, and one of the PRC1 subunits recognizes H3K27me3. Thus, PRC1 recruitment is likely coupled to PRC2 function. While binding of ubiquitylated H2AK119 by PRC1 probably contributes to chromatin compaction, plants and worms appear to lack a PRC1-related complex. These and other data indicate that PRC2 activities also contribute directly to transcriptional repression, although the mechanism is currently not understood.

Trithorax Group proteins oppose PcG protein-mediated transcriptional repression and contribute to maintenance of an activate chromatin state. TrxG proteins form a highly diverse class and include proteins with histone modifying activities, components of chromatin remodeling complexes and DNA binding proteins (Schuettengruber *et al.*, 2011). The best-known TrxG representative is the histone methyltransferase MLL1. MLL1 catalyzes histone H3 K4 trimethylation (H3K4me3), which is associated with active transcription. Several MLL complexes also contain histone acetlyltransferase (HAT) activity, while other TrxG proteins form part of a variety of ATP-dependent chromatin remodeling complexes, including SWI/SNF (see below).

In light of proliferation versus differentiation control, PcG and TrxG genes are of particular interest because of their important contribution to lineage commitment. As embryonic stem cells become committed progenitors, remarkable changes in their chromatin structure occur that even can be observed by light and electron microscopy (Efroni *et al.*, 2008). The chromatin of embryonic stem cells is open in general, while the chromatin of lineage-committed cells becomes more compact and less accessible to transcriptional activators. Even though the chromatin structure of embryonic stem cells promotes transcriptional activation, maintenance of the pluripotent state requires that developmental genes remain silenced. This dual goal may be achieved by marking differentiation-related genes with bivalent domains, regulatory regions containing both the activating H3K4me3 and inactivating H3K27me3 histone modifications (Bernstein *et al.*, 2006). While bivalent domains prevent gene transcription, they also maintain the potential for later activation. During differentiation, most of the bivalent domains lose one of the two modifications and become monovalent, leaving either activating or inactivating marks (Bernstein *et al.*, 2006; Voigt *et al.*, 2013) .

In addition to their role in lineage commitment, PcG and TrxG proteins are important during terminal differentiation. Genome wide analysis of human embryonic fibroblasts showed PcG protein binding and H3K27me3 modification of many genes involved in neuronal, bone, muscle, hematopoietic and epithelial differentiation (Bracken *et al.*, 2006). During retinoic acid-induced neuronal differentiation, PcG binding and H3K27me3 marks decreased progressively from neuron specific genes (Bracken *et al.*, 2006; Mikkelsen *et al.*, 2007). These and other results support that PcG-mediated gene silencing prevents premature expression of cell-type specific genes.

Conditional knockout of the *Ring1* PRC1 and *EZH2* PRC2 genes revealed a direct role in the timing of gene repression in neural progenitors. In these studies, PcG inactivation interfered with downregulation of *neurogenin1* and delayed the switch from divisions that produce neurons to those producing astrocytes (Hirabayashi *et al.*, 2009). Thus PcG-mediated gene repression is an important mechanism in the timing of developmental decisions. In contrast to PcG, the TrxG gene *Mll1* was found to be required for neurogenesis in the mouse post-natal brain (Lim *et al.*, 2009). Conditional knockout of *Mll1* in subventricular zone neural stem cells prevented their neuronal differentiation. The transcription factor *Dlx2* was identified as the critical target of MLL1 in this process. *Dlx2* contains a bivalently marked promoter, which depends on MLL1 binding for activation (Lim *et al.*, 2009). This example illustrates how the combined activity of PcG and TrxG proteins determines the expression of genes that control important developmental transitions, including neuronal differentiation.

As shown for neurons, muscle differentiation also involves PcG protein-mediated chromatin remodeling. In proliferating mouse C2C12 myoblasts, H3K27me3 marks muscle specific genes, while this silencing mark is absent from the promoters of cell cycle genes at this stage. This is in contrast to later stages of muscle differentiation, when differentiation genes become expressed, and cell cycle genes are marked by the H3K27me3 repressive mark (Caretti *et al.*, 2004; Blais *et al.*, 2007). Curiously, pRb inactivation caused loss of H3K27 trimethylation, re-expression of cell cycle genes, and cell cycle re-entry of terminally differentiated muscle cells (Blais *et al.*, 2007). Further examination supports that silencing of cell cycle genes coincides with trimethylation of H3K27 and not H3K9 in this system (Blais and Dynlacht, 2007; Asp *et al.*, 2011).

PcG proteins may be recruited to MyoD bound promoters in proliferating myoblasts to prevent that the presence of MyoD automatically leads to differentiation. In agreement with this idea, overexpression of the PcG protein EZH inhibits muscle differentiation (Caretti *et al.*, 2004). However, PcG proteins have much broader functions, as indicated by the results of ChIP-seq analysis of differentiating C2C12 cells (Cao *et al.*, 2010). This study revealed MyoD binding at the promoters of thousands of genes, of which only a subset showed modified expression during muscle differentiation. These and other findings indicate that PcG proteins act broadly as global transcriptional repressors in the maintenance of cellular homeostasis.

Despite a global role, PcG proteins are crucial for suppressing cell-type specific gene expression, antagonizing cell cycle arrest and maintaining the undifferentiated state. As an

interesting example, ectopic expression of MyoD induces muscle differentiation of *C. elegans* precursor germ cells, but only when combined with knockdown of PcG gene function (Patel *et al.*, 2012). The best example of a PcG-controlled cell cycle regulator is the *ink4A* tumor suppressor locus. As first described for the *bmi1* PRC1 component, PcG protein overexpression results in repression of this locus, while PcG gene knockout in mice leads to increased expression of $p16^{INKA}$ and $p19^{ARF}$, and interferes with cell proliferation (Popov and Gil, 2010; Jacobs *et al.*, 1999; Voncken *et al.*, 2003; Dietrich *et al.*, 2007; Martinez and Cavalli, 2014). TrxG proteins counteract PcG repression of this locus, which probably provides the best-characterized example of PcG-TrxG antagonism in gene regulation.

SWI/SNF-dependent chromatin remodeling in differentiation and cell cycle regulation

The switching/sucrose non fermenting (SWI/SNF) subclass of TrxG proteins currently receives much scientific attention (de la Serna *et al.*, 2006; Wilson and Roberts, 2011). This was triggered by the recent discovery of an unexpectedly high frequency of mutations in SWI/SNF subunit genes in human cancer (Kadoch *et al.*, 2013; Kandoth *et al.*, 2013; Wang *et al.*, 2014). Moreover, it is becoming increasingly clear that the SWI/SNF complex plays a critical role in lineage commitment and terminal differentiation in a wide variety of tissues and cell types (Armstrong *et al.*, 1998; Kowenz-Leutz and Leutz, 1999; de la Serna *et al.*, 2001, 2006; Lessard *et al.*, 2007; Juliandi *et al.*, 2010; Wilson and Roberts, 2011). SWI/SNF-mediated chromatin remodeling predominantly contributes to transcriptional activation, and is needed for proper expression of approximately 6 % of all genes in yeast (Holstege *et al.*, 1998).

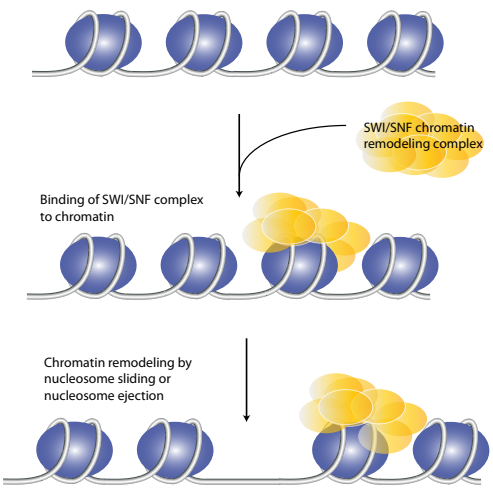

Figure 5. Chromatin remodeling by the SWI/SNF complex. The SWI/SNF complex is a conserved chromatin-remodeling complex that uses ATP hydrolysis to alter the chromatin state and DNA accessibility. Binding of the SWI/SNF complex to chromatin reduces the interaction between DNA and histones, allowing either sliding or ejection of histones. This creates a more open and accessible chromatin structure, or possibly the reverse. Histones are shown in blue, the multi-subunit SWI/SNF complex in yellow.

SWI/SNF complexes are highly conserved chromatin remodelers, which use the energy of ATP hydrolysis to mobilize nucleosomes, thereby altering DNA accessibility and regulating transcription (Figure 5). The complex consists of several core subunits, including the ATPase subunit Brahma (BRM) in *Drosophila,* and either BRM or BRM-related Gene 1 (BRG1) in mammals (Figure 6). The other core components are the BRG1-associated factors BAF155, BAF170 and SNF5 (BAF47, INI1). These subunits are present in all SWI/SNF complexes, and when combined as purified proteins they reconstitute remodeling activity to the same level as the entire SWI/SNF complex (Phelan *et al.*, 1999). In addition to this catalytically active core, SWI/SNF complexes contain a large number of associated subunits. Based on the associated subunits, two subclasses of SWI/SNF complexes are distinguished, BAF and PBAF, which contain the BAF250/ARID1/Osa and BAF180/PBRM signature subunits, respectively (Figure 6).

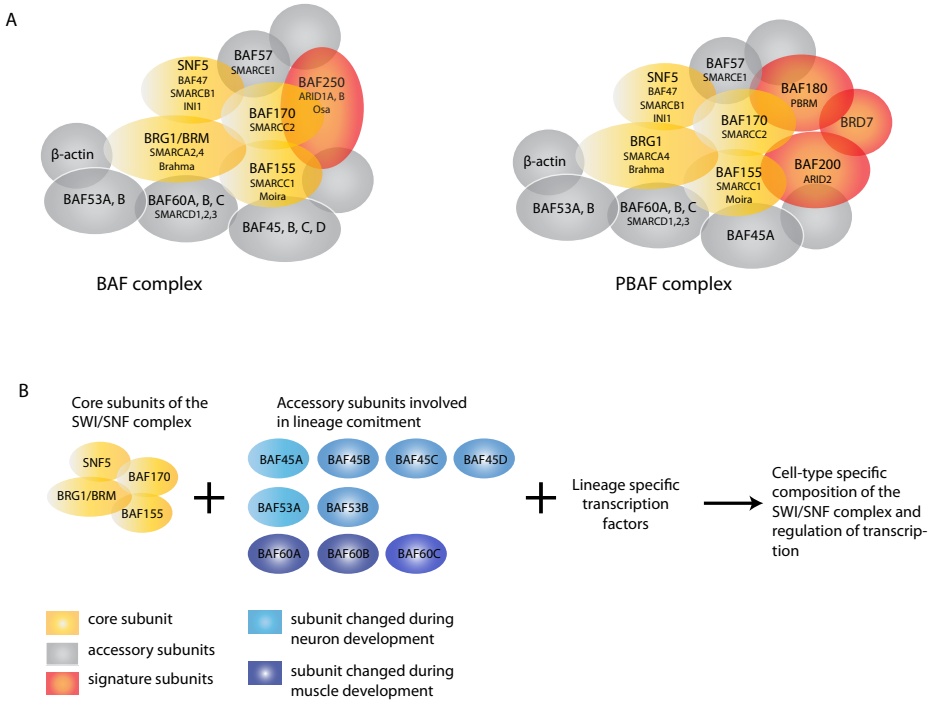

Figure 6. Subunit composition of the SWI/SNF complex. (A) The SWI/SNF complex consist of several core subunits (yellow) in association with additional accessory subunits (grey) and signature subunits (red) which are mutually exclusive for either the BAF complex (BAF250/ARID1) or the PBAF complex (BAF180/PBRM, BRD7 and BAF200/ARID2). All subunits have multiple names dependent on the nomenclature used. While not used in the text, the systematic SMARC (SWI/SNF-related, Matrix-associated, Actin-dependent Regulator of Chromatin) nomenclature is included in (A). For simplicity in figure B only the BAF names are used. (B) The core subunits (yellow) of the SWI/SNF complex assemble together with accessory subunits to ultimately form a functional complex. Dependent on the incorporated associated subunits, the complex may interact with specific transcription factors and exert cell type or differentiation-specific functions. Here, some of the variants described to be specifically incorporated during neuronal or muscle differentiation are shown in blue.

Importantly, several of the associated SWI/SNF subunits are encoded by multiple genes (Figure 6). At least some of these variants show lineage specific and differentiation-stage specific expression and complex association. For example, BAF45a and BAF53a need to be associated with the SWI/SNF complex in proliferating neuronal progenitors, but are exchanged for BAF45b/c and BAF53b when these cells exit the cell cycle and differentiate (Lessard *et al.*, 2007). Moreover, three different genes encode BAF60 variants (Figure 6), but BAF60c is the only subunit expressed in mesodermal precursors of cardiomyocytes and myoblasts (Puri and Mercola, 2012). BAF60c interacts with the GATA4 cardiac transcription factor and with MyoD, and is required for the formation of differentiated heart and skeletal muscle. As such, BAF60c is currently the best-described example of a variant subunit that bridges the SWI/SNF complex to differentiation-inducing transcription factors.

The SWI/SNF complex could fulfill its role in differentiation by increasing DNA accessibility for transcription factor binding, or by binding transcription factors in order to locally change the chromatin to provide access for additional factors, co-activators and the RNA polymerase complex. Both mechanisms have been proposed for muscle differentiation. On the one hand, association of the SWI/SNF BRG1 subunit with the myogenin promoter was found to precede association of MyoD (de la Serna *et al.*, 2005). In contrast, as described above, the muscle specific BAF60c subunit interacts with MyoD before binding to DNA (Puri and Mercola, 2012). Dependent on the specific gene and cell type, recruitment of SWI/SNF components may precede, coincide with or follow promoter binding of cell-type specific transcription factors.

The examples above describe critical contributions of the SWI/SNF complex in cell differentiation. Does this mean that SWI/SNF-mediated chromatin remodeling is required for coordinating cell cycle arrest with cell type specific gene expression? Several reports have linked the SWI/SNF complex to the regulation of cell cycle genes, including the INK4A-ARF locus, $p21^{Cip1}$, cMyc, cyclin D, and cyclin E. While such connections may be indirect and follow from differentiation, at least some of these genes appear directly regulated by the SWI/SNF complex. Addressing this topic, several studies made use of malignant rhabdoid tumors that contain inactivating mutations in the human SNF5/BAF47 gene. Reintroduction of SNF5 into these tumor cells resulted in upregulation of $p16^{INK4a}$ and $p15^{INK4b}$ expression and arrest of cell division (Kia *et al.*, 2008; Wilson *et al.*, 2010). Coincidently, SNF5 expression induced extensive chromatin remodeling and removal of PRC1 and PRC2 PcG complexes from the INK4a-INK4b locus. As described above, PcG complexes silence the INK4A-ARF locus, hence PcG gene knockout and SNF5 activation both lead to increased expression of $p16^{INK4A}$. These observations fit with the identification of SWI/SNF genes as members of the Trithorax group of genes, which antagonize PcG-mediated transcriptional repression (Wilson *et al.*, 2010). Mechanistically, activation of the SWI/SNF complex replaces PcG proteins at the promoters of their joint target genes. In agreement with these functions, loss of SWI/SNF activity has been shown to result in PcG-mediated silencing of the INK4A locus, leading to continued proliferation and a stem cell-like signature (Popov and Gil, 2010; Kia *et al.*, 2008; Wilson *et al.*, 2010).

Similar to the $p16^{INK4}$ CDK4/6 inhibitor, expression of $p21^{CIP1}$ is also directly controlled by the SWI/SNF complex. Downregulation of several SWI/SNF components leads to $p21^{CIP1}$ loss, while re-expression of SNF5 in malignant rhabdoid tumor cells induces $p21^{CIP1}$ expression, independently of p53 (Kuwahara *et al.*, 2010, 2013). ChIP experiments showed strong $p21^{CIP1}$ promoter association of SNF5, in the proximity of the transcription start site and together with RNA Polymerase II association. The BAF specific subunit BAF250b expressed in HeLa cells also directly controls $p21^{Cip1}$ expression and induces cell cycle arrest (Inoue *et al.*, 2011). These data support direct transcriptional activation of $p21^{CIP1}$ by the SWI/SNF BAF complex, and indicate that $p21^{CIP1}$ is an important mediator of SWI/SNF-dependent cell cycle arrest (Hendricks *et al.*, 2004; Kang *et al.*, 2004; Chai *et al.*, 2005; Kuwahara *et al.*, 2010, 2013; Inoue *et al.*, 2011).

While SWI/SNF is considered predominantly a transcriptional activator, SWI/SNF-dependent repression of positive cell cycle regulators, including cyclins D and cyclin E, has also been reported (Brumby *et al.*, 2002; Zhang *et al.*, 2002; Alarcon-Vargas *et al.*, 2006; Baig *et al.*, 2010, Chapter 6 of this thesis). Loss of the SNF5 core subunit of SWI/SNF results in upregulation of cyclin D1 expression. Pharmacological inhibition, or genetic ablation of cyclin D1 in rhabdoid tumor cells inhibited tumor growth, indicating that the elevated levels of cyclin D in these tumors contribute to their uncontrolled proliferation (Zhang *et al.*, 2002; Tsikitis *et al.*, 2005; Alarcon-Vargas *et al.*, 2006; Lünenbürger *et al.*, 2010; Smith *et al.*, 2011). A mechanism proposed for the SWI/SNF-dependent repression of cyclin D and cyclin E involves recruitment of HDAC1 and concomitant inhibition of transcription through histone deacetylation (Zhang *et al.*, 2000, 2002). HDAC recruitment to SWI/SNF bound promoters may be used more broadly for SWI/SNF-mediated gene repression (Nagl *et al.*, 2007; Flowers *et al.*, 2009).

During the past decades, chromatin remodeling and the composition of the epigenetic landscape have emerged as key mechanisms underlying a wide variety of processes, including the balance between proliferation and differentiation. Several lines of evidence have shown direct interactions between chromatin-remodeling complexes, in particular those described here, with cell cycle regulators and genes required for differentiation. By regulating both the expression of differentiation factors and cell cycle regulators, chromatin-remodeling complexes fulfill a highly important role in cell cycle exit specifically employed during differentiation.

Creating all-or-nothing transitions from proliferating precursors to differentiated cells.

As concluded above, robust control over the proliferation versus differentiation decision likely results from redundant regulators and feedback control mechanism (Figure 7). For example, three Rb-related transcriptional repressors and three CIP/KIP family CDK inhibitors contribute to cell cycle exit in mammals. Redundancies are observed between the two families, and between members of each individual family of G1/S inhibitors. Notably, Rb family or CIP/KIP family triple knockout mice are viable until approximately day 10

or day 13 of gestation, respectively (e.g. Wirt *et al.*, 2010; Tateishi *et al.*, 2012). This indicates that cell cycle exit and differentiation can occur in the absence of an entire class of cell cycle inhibitors. Our studies in *C. elegans* emphasize this conclusion and show that at least five different levels of regulation promote cell cycle arrest during differentiation (Chapter 6 and Figure 7). These regulators display a high degree of redundancy, are individually not sufficient for reliable control, yet in combination create highly robust "all-or-nothing" decisions in cell cycle exit.

An important double negative feedback appears to operate in the proliferation-differentiation decision: G1 CDK-cyclins antagonize differentiation-inducing transcription factors, while these transcription factors in turn antagonize CDK-cyclin activation. The mutual antagonism between PcG and TrxG genes, in particular the TrxG-SWI/SNF class, is an integral part of this network. Several other levels of control likely help reinforce the two mutually exclusive states, such as regulation of protein degradation by E3 ubiquitin ligases, and regulation of mRNA stability by miRNAs. The mutual antagonism is expected to create bistability: cells could either be in a state of proliferation without differentiation, or shut down the cell cycle and acquire a differentiated status. However, if this is true, then how can cells make the transition from proliferating precursor cells to post-mitotic differentiated cells?

Undergoing such a switch requires a substantial disruption of the initial equilibrium. This can be accomplished by overexpression of a single critical regulator, for instance as discussed for the ectopic expression of MyoD or cell cycle inhibitors. *In vivo*, most developmental transitions are likely accomplished through alteration of multiple players at the same time. The trigger for these alterations will come from external signals, cell intrinsic information, or a combination of both. Many external factors can induce transitions, including cytokines, mitogens, growth factors, Notch, Wnt/Wgl, Hedgehog, and TGFβ-BMP

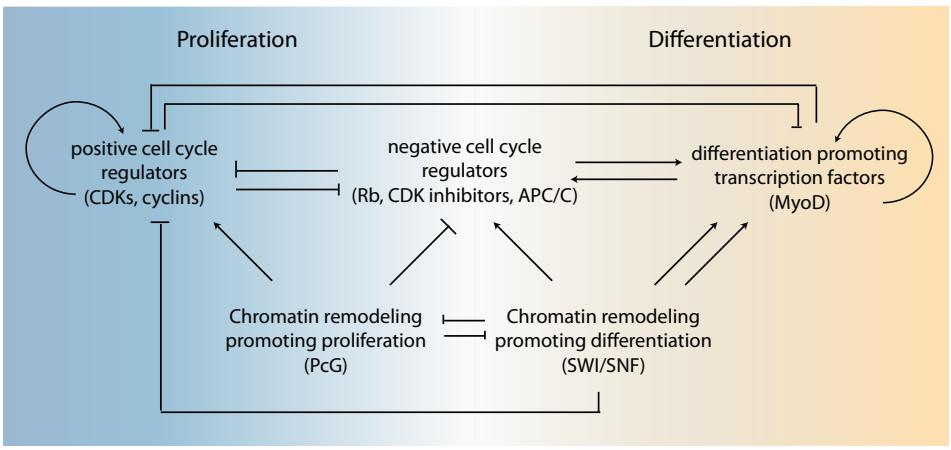

Figure 7. Robust control over the proliferation versus differentiation decision. A regulatory network of cell cycle regulators, transcription factors, lineage-specific SWI/SNF complexes, and chromatin modification complexes induce the all-or-nothing transition from proliferating precursors to differentiated post-mitotic cells.

ligands. Examples of cell intrinsic information are transcription regulators that become unequally distributed during asymmetric cell division. External or internal factors that disrupt an initially stable situation can trigger differentiation-inducing transcription factors to become active, displacement of PcG proteins by SWI/SNF complexes, induction of CDK inhibitors, repression of G1 cyclin transcription, and activation of cell-type specific gene expression. While these mechanisms likely apply to differentiation in general, much of the regulation is cell-type specific, which greatly adds to the complexity of the proliferation-differentiation decision.

Probably the best-understood example of differentiation is the formation of muscle fibers from proliferating myoblasts. While myogenic regulatory factors are known to act in a switch-like circuitry, the presence of external proliferation and differentiation-inducing factors determines which MRFs are expressed and functional. Growth factors and mitogenic signals prevent MyoD induced activation of muscle specific genes. As discussed above, this involves phosphorylation of MyoD by CDK2-cyclin E, as well as phosphorylation of the collaborating MEF2 transcription factor by CDK4/6-cyclin D (Lazaro *et al.*, 2002). Reduction of growth factors leads to downregulation of this inhibitory phosphorylation and allows differentiation.

Illustrating the simultaneous alteration of multiple controls, differentiation signals induce p38 MAPK activation with critical regulatory functions in muscle formation. Before differentiation of C2C12 mouse myoblasts, the SWI/SNF BAF60c subunit associates with MyoD and localizes to promoters (Puri and Mercola, 2012). Activated p38 MAPK phosphorylates BAF60c, which triggers the assembly of a functional SWI/SNF complex onto the preassembled MyoD/BAF60c pioneer complex (Forcales *et al.*, 2012). In addition, p38 MAPK phosphorylates MEK2, which induces recruitment of an MLL2-menin TrxG activation complex (Rampalli *et al.*, 2007). An additional p38 MAPK pathway leads to release of co-repressors and recruitment of co-activators to the MyoD and MEF2 transcription factors at target gene promoters (Singh *et al.*, 2015). Thus, growth-factor reduction and differentiation-inducing signals can both induce differentiation by activating transcription from MyoD-MEF2 occupied promoters.

In conclusion, a regulatory network of cell cycle regulators, transcription factors, lineage specific SWI/SNF complexes, and chromatin modification complexes (Figure 7) induce the all-or-nothing transition from proliferating precursors to differentiated post-mitotic cells. While complex, a deeper understanding of these regulatory networks and their cell-type specific variations has the potential to lead to improved possibilities for regenerative medicine and cancer treatment.

Disturbing the balance between proliferation and differentiation: Cancer development

The same mechanisms required to link cell cycle arrest to differentiation are often compromised in cancer cells, leading to unperturbed proliferation and a failure to differentiate (Hanahan and Weinberg, 2011). Indeed, loss of the control mechanisms discussed

above, including cell cycle regulation, differentiation, and chromatin remodeling, all have been shown to contribute to tumor development. Although disturbed in cancer cells, the link between proliferation and differentiation still seems to exist, at least in some cases. Overexpression of cell cycle inhibitors can be sufficient for differentiation induction. For instance, overexpression of the CDK inhibitors $p21^{Cip1}$, $p27^{Kip1}$, $p19^{ARF}$, and $p16^{INK4A}$ inhibit proliferation and also induce differentiation in a variety of tumor cells (Kranenburg et al., 1995; Liu et al., 1996; Adachi et al., 1997; Matushansky et al., 2000). Similarly, overexpression of differentiation-inducing transcription factors promotes both differentiation and cell cycle arrest. The role of differentiation-inducing transcription factors in tumorigenesis has been best-characterized for the transcription factors PU.1 and GATA-1 in Acute leukemia (AML) and mouse erythroleukemia (MEL) cell lines. During development, PU.1 is required for the generation of myeloid precursor cells as well as common lymphoid precursors (Tenen, 2003; Rosenbauer and Tenen, 2007). Early loss of PU.1 can prevent myeloid differentiation, allowing continuous proliferation of precursor cells without differentiation and contributing to cancer development. However, PU.1 has an opposite role during erythroid differentiation, where it blocks differentiation into mature erythrocytes by inhibiting the transcription factor GATA-1. In agreement with this role, loss of PU.1 in MEL cell lines stimulated these cells to re-enter a differentiation program as well as terminal growth arrest (Tenen, 2003; Papetti and Skoultchi, 2007; Choe *et al.*, 2010). These examples demonstrate that the tight link between proliferation and differentiation can still exist in malignancies, and that inhibition of the cell cycle machinery in cancer cells can promote differentiation, while stimulating differentiation can result in cell cycle arrest.

For many years, cancer has been considered a genetic disease, driven by the acquisition of sequential mutations in tumor suppressors and proto-oncogenes. More recently, it has become evident that cancer development also involves epigenetic changes and chromatin remodeling. Mutation of one of the core subunits of the SWI/SNF complex, SNF5/SMARCB1, was discovered to be the causative event for the onset of malignant rhabdoid tumors as early as 1998 (Versteege *et al.*, 1998). This provided the first link between ATPase-dependent chromatin remodeling and tumor suppression. Loss of function of a variety of SWI/SNF subunits has since been identified in a broad range of cancers. Strikingly, SWI/SNF subunit genes were found to be collectively mutated in approximately 20% of all tumors, placing them amongst the most frequently mutated genes in human cancer (Kadoch *et al.*, 2013; Kandoth *et al.*, 2013; Kim and Roberts, 2014; Wang *et al.*, 2014)

The fact that SWI/SNF-dependent chromatin remodeling influences both proliferation and differentiation may explain their frequent mutation in cancer. Work focusing on malignant rhabdoid tumors indicated that loss of SWI/SNF activity leads to the deregulation of multiple pathways, which might explain why the inactivation of a single factor is sufficient to cause tumor formation (Kim and Roberts, 2014; Wang *et al.*, 2014). In addition to the SWI/SNF complex, mutations in other chromatin regulators, including the PcG proteins discussed above, are also associated with tumor development. In agreement with a role for PcG proteins in stem cell maintenance and inhibition of differentiation, PcG proteins can function as proto-oncogenes and are found upregulated in a variety of tumors types (Spar-

mann and van Lohuizen, 2006). These findings all highlight that the intimate connection between proliferation and differentiation, and the important roles of chromatin regulators in coordinating these processes, are of great fundamental and clinical importance.

The nematode *C. elegans* as a model organism to study cell cycle exit during differentiation

Here we use the nematode *Caenorhabditis elegans* (*C. elegans*) to study the mechanisms underlying cell cycle exit and the link between cell cycle arrest and differentiation in the context of a developing animal. This small round worm of approximately 1 mm in length was originally introduced as a model system by Sydney Brenner in the early 60ths (Brenner, 1974; Sulston and Brenner, 1974). Since then, it has become a leading model organism for studies of a wide variety of processes, including cell fate and cell division control (Ankeny, 2001; Jorgensen and Mango, 2002). Among the reasons for the success of *C. elegans* in these studies are the relatively short generation time, its highly invariant cell linage and its reproducible pattern of cell division. This combined with the transparency of the animal allows life imaging of all cells and cell divisions (Sulston, 1977; Sulston and Schierenberg, 1983). Equally important are the availability of strong and efficient forward and reverse genetic approaches and high quality genomic DNA sequence and annotation information. Particularly appealing for cell cycle studies is the fact that it is exactly known when each cell divides and which cells will be formed. Since cell division patterns are almost invariant in wild-type animals, disruption of division control can be easily recognized and quantitatively characterized. Defects in cell division can be precisely described by determining the number of cells in a specific lineage, while temporal changes in cell cycle progression can be quantified by following cell divisions over time.

As an additional advantage, many cell cycle regulators that exist as gene families in higher eukaryotes are represented by single genes in *C. elegans*. Examples include the various subtypes of CDKs and earlier mentioned G1 regulators. This relatively simple cell cycle machinery has helped to identify cell cycle proteins and contributed to our understanding of the factors that control progression through the cell cycle. Cell cycle progression in the context of a developing animal may use mechanisms that are not important for single cell eukaryotes and cells in tissue culture. For example, in early embryonic cycles of *C. elegans*, S and M phases rapidly follow each other, and Gap phases are kept very short. The regulation of these cell divisions must differ from normal somatic cell cycle control. Another example is the endoreplication cycle, during which rounds of DNA replication continue in the absence of M phases as is observed in the intestine and epidermis of *C. elegans* (Kipreos, 2005a). Indeed, several conserved, general cell cycle regulators have displayed lineage specific contributions and requirements. For instance, inactivation of the sole *C. elegans* Rb family member *lin-35* causes overproliferation in the intestine, while other cell types are not affected, indicating cell-type specific requirements. The combined features of *C. elegans* make this animal ideally suited for the genetic identification of developmental cell division control mechanisms.

Below we will describe the factors that control progression through the cell cycle during postembryonic development of *C. elegans*, with a particular focus on G1 regulators.

G1 control in *C. elegans*

Several genetic screens have identified mutations that alter normal cell lineage (*lin* mutants) (Sulston, 1977; Horvitz and Sulston, 1980; Sulston and Horvitz, 1981). Some of the genes defined by these mutations turned out to code for classical regulators of cell cycle progression. Cell division fails in some *lin* mutants, while other mutants display an overproliferation phenotype. For example, extra cell divisions were observed in *cul-1* (formerly *lin-19*), *lin-23* (βTrCP), and *lin-35* (Rb) mutants. However, mutants with truly uncontrolled overproliferation have never been found, indicating that cell cycle exit and differentiation are tightly controlled in *C. elegans*.

Progression through G1 in metazoans involves the activity of CDK4-cyclin D and CDK2-cyclin E. In *C. elegans,* single genes encode a D-type cyclin (*cyd-1*), CDK4/6 homologue (*cdk-4*), E-type cyclin (*cye-1*), and a CDK2 homologue (*cdk-2*) (Park and Krause, 1999; Fay and Han, 2000; Boxem and van den Heuvel, 2001; Brodigan *et al*., 2003). While candidate null *cyd-1* or *cdk-4* mutants complete embryogenesis except for a few final divisions, CYD-1 is, in contrast to its role in *Drosophila* and mice, essential for all post embryonic divisions in *C. elegans* (Meyer *et al*., 2002; Emmerich *et al*., 2004; Kozar *et al*., 2004). During L1 development of *cyd-1* mutants, cells migrate to the proper position but fail to initiate cell division or initiation of DNA replication as wild-type animals do (Boxem and van den Heuvel, 2001). *C. elegans cye-1* is essential for cell cycle progression at an earlier developmental stage. While most embryonic divisions are unaffected in *cyd-1* mutants, RNAi against *cye-1* results in an embryonic arrest at approximately the 100-cell stage (Fay and Han, 2000). A critical function of CDK4-cyclin D in mammalian cells is phosphorylation and inactivation of the Rb protein. In *C. elegans*, the Rb family is represented by the single gene *lin-35*. Indeed, LIN-35 also appears to be a downstream target of CDK-4/CYD-1 in *C. elegans*. First, inactivation of *lin-35* can partially rescue the lack of cell division and DNA replication in *cyd-1* and *cdk-4* mutants (Boxem and van den Heuvel, 2001). In addition, LIN-35 is efficiently phosphorylated by CDK-4/CYD-1 *in vitro* (The *et al*., 2015, Chapter 3). Inactivation of *lin-35* causes extra division of intestinal nuclei and combined inactivation of *lin-35* and other negative G1 regulators further enhances this phenotype, classifying *lin-35* as a negative regulator of cell cycle exit (Boxem and van den Heuvel, 2001; The *et al*., 2015). While CDK inhibitors of the pINK family have not been identified in *C. elegans*, two CIP/KIP inhibitory genes, *cki-1* and *cki-2,* have been identified as negative cell cycle regulators. The CKI-1 and CKI-2 proteins are predicted to be equally similar to the mammalian CDK inhibitors $p21^{CIP}$ and $p27^{KIP}$. However, only *cki-1* has been identified as a strong inhibitor of cell cycle progression whereas the effect of *cki-2* is limited. Loss of *cki-1* causes extra divisions in a number of different cell types and results in embryonic lethality (Hong *et al*., 1998; Feng *et al*., 1999; Boxem and van den Heuvel, 2001; Clayton *et al*., 2008). In addition to Rb- and CKI-dependent cell cycle inhibition, progression through G1 is also counteracted by targeted protein degradation. This involves the Skp1, Cullin, F-box factor (SCF) complex and the Anaphase Promoting Complex/Cyclosome (APC/C) E3 ubiquitin ligases (Kipreos, 2005b; Polley *et al*., 2014). The first mutants described to have an overproliferation phenotype in multiple postembryonic lineages defined the *cul-1* and *lin-23*

(βTrCP) genes, which encode $SCF^{\beta TrCP}$ components (Horvitz and Sulston, 1980; Sulston and Horvitz, 1981; Kipreos *et al*., 1996, 2000). While it has been suggested that SCF mainly controls the levels of CYE-1 to inhibit G1 progression, it is not unlikely that CYD-1 is a SCF target as well (Fay and Han, 2000). Moreover, *lin-23* (βTrCP) has been implicated in the degradation of the CDK activating phosphatase *cdc25.1* (Hebeisen and Roy, 2008). Gain of function mutations that likely remove the βTrCP phosphodegron of CDC-25.1 cause extra divisions of intestinal nuclei (Clucas *et al*., 2002; Kostić and Roy, 2002). This is most likely the consequence of increased CDC-25.1 levels, leading to premature and enhanced activation of G1 CDK-cyclin complexes. Substrate specificity of the APC/C initially depends on interaction with its co-activator CDC20 during early mitosis and subsequntely on FZR1 during late mitosis and G1-phase. Loss of the FZR-1 function in *C. elegans* causes a synthetic phenotype together with *lin-35* loss of function (Fay *et al*., 2002), and combined loss of *lin-35* and *fzr-1* completely bypass the requirement for CDK-4/CYD-1 (The *et al*., 2015). These observations indicate that LIN-35 mediated transcriptional repression and APC/C^{FZR-1}-mediated protein degradation act in parallel to prevent S-phase entry. Based on data in other systems, phosphorylation of LIN-35 by CDK-4/CYD-1 is assumed to release activating E2Fs and leads to expression of E2F target genes, including *cye-1*. Three different E2F like transcription factors have been identified in *C. elegans: efl-1, efl-2,* and *efl-3*. The function in cell cycle control is best described for *efl-1*. Inactivation of *efl-1* leads to a similar phenotype as inactivation of *lin-35,* indicating that *efl-1* is a negative regulator of G1 and most likely acts as a transcriptional repressor, rather than activator. Indeed, EFL-1 has similarity to the human repressive E2Fs E2F4 and E2F5 (Ceol and Horvitz, 2001; Boxem and van den Heuvel, 2002). While EFL-1 may repress rather than promote transcription during vulva development, EFL-1 seems to function as an activating transcription factor in germ cells (Chi and Reinke, 2006). In the germ line, EFL-1 and EFL-2 likely function as a heterodimers with DPL-1, the *C. elegans* DP homologue, since loss of E2Fs and DPL-1 affects the expression of a similar set of target genes. Because the recently identified EFL-3 protein most likely represents a homologue of the mammalian repressive E2F7 and E2F8, no activating E2F has been identified in *C. elegans* thus far (Winn *et al*., 2011). An activating E2F would be expected however, based on the observation that *dpl-1* DP contributes both to transcriptional activator and repressor functions (Ceol and Horvitz, 2001; Boxem and van den Heuvel, 2002; Korzelius *et al*., 2011). Moreover, many S-phase promoting genes including *cye-1* and genes encoding MCM subunits of the DNA helicase complex have multiple canonical E2F binding sites in their promoter regions, suggesting the E2F-dependent expression of these S-phase promoting genes (Brodigan *et al*., 2003; Korzelius *et al*., 2011).

In summary, progression through G1 is controlled by both positive and negative regulators. While CDK-4/CYD-1 and CDK-2/CYE-1 act as positive regulators of the G1 to S-phase transition, their activity is counteracted by the combined activity of several negative regulators. LIN-35-mediated transcriptional repression, inactivation of CDK activity by CKIs, and targeted protein degradation by the SCF and the APC/C^{FZR-1} are conserved and parallel mechanisms, used to prevent uncontrolled S-phase entry and overproliferation in *C. elegans*.

Cell-type specific cell cycle regulation during development

C. elegans L1 larvae hatch with approximately 550 cells. During the subsequent larval stages, specific precursor cells go through several rounds of division to contribute to the formation of the intestine, muscles, neurons, hypodermis, and vulva (Sulston, 1977). Quantification of cell numbers and real time imaging of postembryonic divisions have provided powerful strategies for cell cycle studies. In this thesis we focus on the examination of the number of several different cell types, most importantly precursor cells of the intestine, cells in the ventral nerve cord, and mesoblast lineage (Figure 8). The intestinal cells are formed and become specialized during embryonic development. The majority of these cells undergoes one round of nuclear division at the end of the first larval stage and all intestinal nuclei complete a full cycle of endoreduplcation during each larval stage. Possibly as a consequence of the continued activity of the cell cycle machinery and DNA replication, intestinal nuclei have previously been shown to be sensitive to disruption of normal cell cycle control. The importance of proper G1 control in these cells is demonstrated by their dependence on all known G1 regulators: CDK-4 and CYD-1 are required for nuclear division in the intestine, while *lin-35*, *cki-1*, *fzr-1,* and *cdc25.1* all contribute to temporal arrest (Boxem and van den Heuvel, 2001; Clucas *et al*., 2002; Fay *et al*., 2002; Kostić and Roy, 2002). The ventral nerve cord is formed by 15 juvenal motor neurons and neuronal P-daughter cells that arise during postembryonic development from the ventral cord precursor cells "P". P cells are a set of precursor cells which migrate from the ventral lateral side to the ventral side of the animal and give rise to neurons, nuclei of the hypodermis, and the vulval precursor cells (VPCs). These VPCs are formed during the first larval stage, after which they temporarily exit the cell cycle and only start to divide again in mid-L3 to form the vulva. This temporal G1 arrest was found to be dependent on *cki-1* activity, as loss of *cki-1* leads to reversal of this G1 arrest and overproliferation in the VPCs (Hong *et al*., 1998). Subsequent screens identified the *cdc-14* phosphatase as well as *lin-1* and *lin-31* transcription factors as upstream regulators of *cki-1* in this lineage (Saito *et al*., 2004; Clayton *et al*., 2008). Thus both division of nuclei in the intestine and proliferation of ventral cord precursors have been highly informative in identifying the mechanisms that control cell cycle progression and cell cycle exit in the context of a multi-cellular organism.

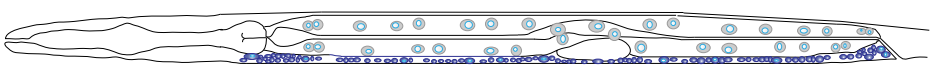

Figure 8. Graphical impression of *C. elegans* at the L2 stage, highlighting the cells in the ventral nerve cord (dark blue) and intestine (grey). Anterior (head region) is to the left and dorsal side up.

In addition to the intestine and the ventral cord precursor cells, the mesoblast lineage has particularly attractive characteristics to study the link between cell cycle exit and differentiation. The mesoblast goes through several rounds of division, generating daughter cell that enter multiple periods of temporal arrest and terminal differentiation. The mesoblast (M) precursor cell of postembryonic mesoderm is formed during early embryogenesis

and remains quiescent until halfway the first larval stage. During subsequent divisions, 16 daughter cells are generated, that undergo terminal differentiation, while two additional cells, known as sex myoblasts (SMs) migrate anteriorly to align with the gonad during L2 development. During late L3, the SMs re-enter the cell cycle and start to give rise to in total 16 cells, which will form the sex muscles required for egg laying (Krause and Liu; Sulston, 1977; Sulston and Schierenberg, 1983). Using the mesoblast lineage as a model system allowed us to address the factors that are required for cell cycle exit during differentiation, how these factors act together and how cell cycle exit is coordinated with terminal differentiation. Better understanding of these regulators and mechanisms in a developing animal will not only increase our fundamental knowledge about cell cycle regulation but may also provide important insights in regeneration of damaged tissues and inappropriate proliferation of cancer cells.

Scope and outline of this thesis

Spatio-temporal control of development and tissue homeostasis require a perfect balance between cell proliferation and differentiation. On the one hand, proliferation is needed to form cells in sufficient numbers and replace those that are lost. On the other hand, cells need to exit the cell cycle and acquire specialized functions at the appropriate time during development. Deregulation of the mechanisms underlying this balance can lead to unperturbed proliferation and a failure to differentiate, a hallmark of cancer cells. While obviously of great importance, it remains only partially understood how proliferation and differentiation are coordinated during development. In order to better understand these mechanisms, we use the small nematode *Caenorhabditis elegans* (*C. elegans*). *C. elegans* provides a very attractive model system for cell cycle studies because of its highly invariant pattern of cell division, the possibility of efficient genetics and its transparency allowing life imaging of all cells and cell divisions. Moreover, studying cell cycle regulation in a developmental context may allow the identification of mechanisms that are not required for single cell eukaryotes and cells in tissue culture.

The proteins and protein complexes that initiate and control DNA replication in *C. elegans* are reviewed in **Chapter 2**, with a particular focus on developmental-stage and tissue-specific regulation. **Chapter 3 to 7** contain experimental work regarding the mechanisms required for cell cycle exit during development. Progression through the cell cycle, as reviewed in Chapter 1, is dependent on the activity of CDK-cyclin complexes. In **Chapter 3** we describe the critical functions of the G1 CDK-cyclin complex CDK4-cyclin D. To regulate the G1-S transition, CDK4-cyclin D phosphorylates and inhibits the function of the negative cell cycle regulators Rb and FZR1 in *C. elegans* as well as human breast cancer cells.

In **Chapter 4 and 5** we examine the irreversibility of the post-mitotic state of terminally differentiated muscle cells and neurons in *C. elegans*. By overexpression of the G1 CDK-cyclins and inactivation of negative regulators of cell division we were able to induce partial cell cycle re-entry in both muscle cells and neurons. Moreover, micro-array analysis of these muscle cells provided insights in the transcriptional program activated upon cell cycle re-entry in terminally differentiated cells. Experiments in rat-hippocampal neurons suggested that mechanisms involved in maintenance of a non proliferative state in terminally differentiated neurons may be conserved between *C. elegans* and a mammalian system.

As cells progress from proliferating precursor cells to terminally differentiated cells, they exit the cell cycle and initiate cell-type-specific differentiation programs. To study the mechanisms required for cell cycle exit during differentiation we developed a CRE-loxP-based conditional knockout and lineage tracing system for *C. elegans*. In **Chapter 6** we describe the development and use of this system to unravel the mechanisms underlying cell cycle exit during differentiation. By combing cell-type specific knockouts with genetic screening, we found that previously identified G1 regulators, members of the SWI/SNF chromatin remodeling complex, and lineage specific transcription factors act together to ensure cell cycle exit during muscle differentiation in *C. elegans*. Combined inactivation of these regulators caused a failure in cell cycle exit and tumorous like proliferation. In **Chap-**

ter 7 we further describe and explore the possibilities of the CRE-loxP-based recombination system in *C. elegans*, including the generation of cell-type specific inducible expression and the development of a split-CRE system.

A summarizing discussion is provided in **Chapter 8**.

Chapter 2

Regulation of DNA synthesis and replication checkpoint activation during *C. elegans* development

Suzan Ruijtenberg, Sander van den Heuvel & Inge The

An adapted version is published as a book chapter in the book "DNA Replication and Related Cellular Processes", edited by dr. Jelena Kusic-Tisma. ISBN: 978-953-307-775-8, InTech

Developmental Biology, Faculty of Sciences, Department of Biology, Utrecht University, Padualaan 8, 3584 CH Utrecht, The Netherlands.

Introduction

Replication of the DNA during the synthesis (S) phase of the cell cycle is one of the most critical aspects of cell division. DNA replication must be highly accurate and tightly controlled to maintain genomic integrity over many rounds of cell division. This is particularly important during animal development, since genetic instability can lead to cell death, birth defects, developmental abnormalities and diseases such as cancer. The developmental context also adds specific constraints to S-phase regulation. For instance, variations in DNA replication control are needed to accommodate the rapid embryonic divisions in early embryos, the production of haploid germ cells, and the generation of polyploid tissues. A comprehensive understanding of DNA replication requires insight in these developmental aspects of S-phase control. Here, we review the initiation of DNA replication in the genetic animal model *Caenorhabditis elegans* (*C. elegans*), with a focus on developmental-stage and tissue-specific regulation.

Caenorhabditis elegans

Caenorhabditis elegans (*C. elegans*) was introduced as a model organism in the 1960s by Sydney Brenner and became, in a relative short time, one of the leading model organisms in biological research (Ankeny, 2001). One of the appealing aspects of this nematode is its rapid and reproducible development from the one-cell embryo to the adult stage (Sulston and Horvitz, 1977). The invariance, combined with the fact that the animals are transparent and contain a relatively low number of cells (adult hermaphrodites contain only 959 somatic cell nuclei), has made it possible to record the entire somatic cell lineage of *C. elegans* (Sulston and Horvitz, 1977, 1981; Horvitz and Sulston, 1980). Knowing when each cell normally divides is a major benefit for studies of the cell cycle. Efficient genetics has allowed identification of mutations that alter the normal cell lineage (*lin* mutants), some of which affect DNA replication or DNA content (Horvitz and Sulston, 1980; Sulston and Horvitz, 1981). As an additional advantage, many cell cycle regulators that exist in gene families in higher eukaryotes are represented by single genes in *C. elegans*, which helps identification of gene function and determination of the hierarchy of gene functions in regulatory pathways.

While these aspects make *C. elegans* suitable for cell cycle studies, there are additional reasons for adding this animal to the repertoire of cell cycle models. Studies of DNA replication in the context of a developing organism may identify regulatory mechanisms that are not important for single cell eukaryotes and cells in tissue culture. The developmental context adds an extra layer of S-phase regulation. For instance, in meiosis, two rounds of chromosome segregation follow each other without intervening S-phase, while in endoreplication cycles, rounds of DNA replication continue in the absence of M-phases. In addition, a broad range of models also increases the potential for uncovering important aspects of DNA replication control. For example, studies in *C. elegans* identified a CUL-4/DDB-1 E3 ubiquitin ligase complex as an important inhibitor of DNA re-replication, which is functionally conserved in mammals (Zhong *et al.*, 2003; Arias and Walter, 2007; Kim and Kipreos, 2007a). In addition, defects in DNA synthesis were found to cause lineage-specific

delays in cell division in *C. elegans*, through a checkpoint mechanism that also contributes to the difference in timing of founder cell division in the early embryo (Encalada *et al.*, 2000; Brauchle *et al.*, 2003). Furthermore, our recent results support tissue-specific contributions of a conserved general regulator of DNA replication, MCM-4 (Korzelius *et al.,* 2011). Below, we describe the currently known factors that control DNA replication in *C. elegans*, as well as their functions in particular stages of development and specific cell types. Several techniques used for analysis of DNA replication in *C. elegans* are summarized in BOX 1.

The factors that regulate DNA replication

The regulation of DNA replication in eukaryotes involves two discrete steps. First, pre-replication complexes assemble at sites of replication initiation ("origin licensing"), and subsequently, the actual initiation of DNA synthesis can be triggered ("origin firing"). Comprehensive studies aimed at identifying all components involved in DNA replication have not been reported for *C. elegans*. However, functional annotations by the *C. elegans* genome sequence consortium have revealed orthologs of many DNA replication components (www.wormbase.org). In addition, some DNA replication genes have been identified through mutations, and genome-wide RNA interference (RNAi) has confirmed that most putative replication components exert critical functions (Encalada *et al.,* 2000; Korzelius *et al.,* 2011; Sonnichsen *et al.,* 2005). Despite their clear conservation, certain well-known replication genes currently appear to lack *C. elegans* counterparts (see Table 1). For instance, in eukaryotes ranging from yeast to human, the origin recognition complex (ORC) has been found to consist of 6 subunits, ORC1 to ORC6. At present, ORC-2 is the only ORC protein identified in *C. elegans*, and its function has not been characterized in detail.

Recruitment of the ORC is normally the first step in pre-replication complex assembly, which is followed by association of the CDC6 and CDT1 proteins. *C. elegans* does contain legitimate CDC-6 and CDT-1 orthologs, which are essential for DNA replication and required for embryonic as well as larval viability (Kim and Kipreos, 2008, 2007a, 2007b; Kim *et al.,* 2007). Simultaneous overactivation of CDC-6 and CDT-1 leads to extensive re-replication, which underscores the role of CDC-6 and CDT-1 as critical regulators of origin licensing.

Studies in other systems have shown that CDC6 and CDT1 are needed to load the minichromosome maintenance (MCM) protein complex onto the replication origins. The MCM complex consists of 6 proteins, MCM2 to MCM7, which is thought to act as the helicase that unwinds the DNA at the replication origins. *C. elegans* contains orthologs of all six MCM genes, which are known as *mcm-2* to *mcm-7* and cause similar embryonic lethal phenotypes when inactivated by RNAi (Sonnichsen *et al.*, 2005). MCM-4 was initially identified through a mutation in the *lin-6* gene, and is the only *C. elegans* MCM protein studied in detail (Korzelius *et al.,* 2011). MCM-4 is expressed in all dividing cells during embryonic and postembryonic development. It is strongly induced just prior to the G1/S transition in somatic cells and disappears when cells exit the cell cycle. MCM-4 localizes to the cell nucleus in interphase, while in mitosis MCM-4 localization becomes diffuse

BOX1: *C. elegans* DNA replication analysis. One of the advantages of the use of *C. elegans* as a model system is that the animal is fully transparent, which allows the use of Differential Interference Contrast (DIC, also known as Nomarski) microscopy for live observations of cell division. Moreover, expression and localization of the green fluorescent protein (GFP) and other fluorophores can be followed by time-lapse microscopy. Introduction of transgenes with tissue or cell type-specific promoters that drive expression of GFP or GFP-tagged fusion proteins is a routine procedure in *C. elegans* (Mello and Fire, 1995). However, transgenes are usually silenced in the germline and in early embryos, which can be avoided by integrating a single copy transgene through DNA particle bombardment or the MosSCI technique (Praitis *et al.*, 2001; Frokjaer-Jensen *et al.*, 2008). We have recently applied the MosSCI strategy for integration of a single copy transgene expressing an MCM-4::mCherry protein fusion, which rescues *mcm-4* null mutants and shows a similar expression pattern and subcellular localizations as the endogenous MCM-4 protein (Korzelius *et al.*, 2011 and our unpublished results).

In addition to gene expression studies, DNA replication itself can be visualized in multiple different ways. The most quantitative method makes use of determination of the DNA content. The DNA content of a cell correlates with the cell cycle phase: cells in G1 have a ploidy of 2n; S-phase cells between 2n and 4n; and cells in the G2 and M-phases 4n. To measure the DNA content, animals are fixed and stained with a dye that fluoresces when bound to DNA, such as propidium iodide, Hoechst 33258, or DAPI (4'6'- diamidino-2-phenylindole dihydrochloride). The most accurate method, but also the most time consuming, for in situ quantification is analysis of the fluorescence signal in confocal serial sections of propidium iodidestained nuclei (Boxem *et al.,* 1999; Feng *et al.*, 1999; Zhong *et al.*, 2003). The accuracy of this method makes it ideal for experiments in which small differences in DNA content must be distinguished, e.g. when comparing cells in G1 vs S-phase.

In order to investigate if cells go through the process of DNA replication, or whether DNA replication takes place at specific times of development, incorporation of the thymidine analogues 5-bromo-2'-deoxyuridine (BrdU) or 5-ethynyl-2'-deoxyuridine (EdU) can be used. BrdU incorporation can be detected by immunostaining with specific anti-BrdU antibodies. EdU detection is based on a copper (Cu^{1+}) catalyzed covalent "click" reaction between an azide attached to a fluorescent dye and the alkyne group of EdU (Salic and Mitchison, 2008). While BrdU detection in *C. elegans* has been possible for some time (Boxem *et al.,* 1999), the EdU method is new and has been applied only in a few recent studies (Figure 1) (Cinquin *et al.*, 2010; Korzelius *et al.,* 2011). The EdU method has a major advantage over BrdU staining: while BrdU detection requires DNA denaturation, this step is not needed in the EdU procedure. As a result, EdU incorporation can be combined with immunostaining with antibodies, which can be a great help in visualizing cells of interest.

Flow cytometry is commonly used for DNA quantification in other systems. Although this technique is not widespread, flow cytometry has been used to produce accurate measurements of DNA content for freshly dissociated *C. elegans* cells (Bennett *et al.*, 2003). The dissociated *C. elegans* cells represented multiple cell types, which reduces the utility of the DNA distribution information. This limitation can be avoided by using strains in which cells of interest are marked with transgenes that express GFP (or other fluorescent tags). GFP expression can be used to gate cells of interest in the flow cytometry analysis so that the DNA distribution of only the GFP expressing cells is analyzed. In future studies, this coupling of selective GFP expression with propidium iodide staining will probably be applied more broadly in the analysis of the DNA distribution of specific tissues and cells of interest.

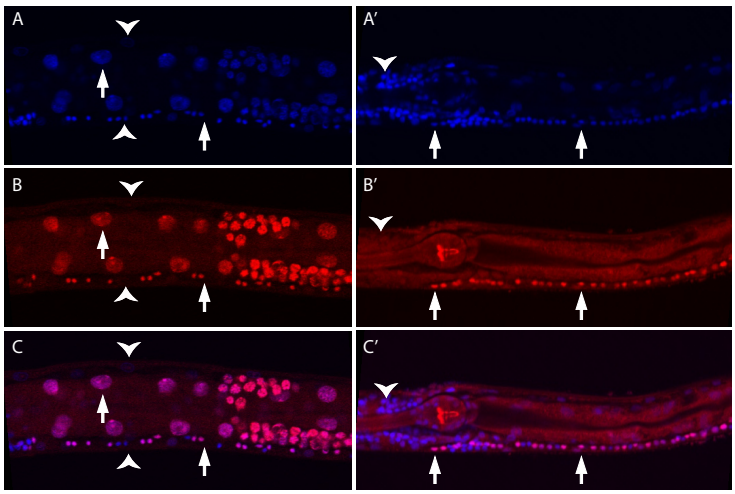

Figure 1. EdU incorporation and staining visualizes DNA replication in *C. elegans* larvae. EdU incorporation in cells of the ventral nerve cord in a first stage larva (A, B, and C) and nuclei in the intestine of an early L4 larva (A', B', and C') are indicated by arrows. Panels show DNA staining by DAPI (A and A'), EdU staining (B and B') and merged images (C and C'). Note that cells that completed S-phase prior to EdU addition stain with DAPI but do not incorporate EdU, such as the neurons indicated by arrowheads. One arm of the developing gonad is visible at the right (A', B', C').

throughout the cell upon nuclear envelope breakdown. In late anaphase, MCM-4 starts to colocalize with the DNA, presumably licensing the DNA for the next round of S-phase (Figure 2). The absence of DNA replication, as observed in *mcm-4* mutants, might be expected to trigger a checkpoint that delays mitotic entry. However, *mcm-4* mutants enter mitosis in the absence of DNA replication and, initially, with normal timing, suggesting that is not only required for DNA replication but also activates a checkpoint that monitors completion of DNA replication (Korzelius *et al.,* 2011). This second function corresponds to the results obtained in studies with other organisms, which clarified the requirement of the MCM complex in activation of the DNA damage and replication checkpoints (Labib *et al*., 2001; Zou and Elledge, 2003). In addition to these well conserved functions, *mcm-4* also displays a tissue-specific requirement in *C. elegans*, which will be discussed below (Korzelius *et al.,* 2011).

Activation of the MCM2-7 complex is needed for opening the DNA helix and allowing the DNA polymerases to start DNA replication. This activation marks the end of origin licensing and the start of origin firing (Labib and Diffley, 2001). Studies in several organisms have shown that the onset of S-phase requires CDK (Cyclin Dependent Kinase) and DDK (Dbf4-dependent Cdc7 kinase) activity to promote activation of the MCM2-7 helicase, while at the same time the recruitment of pre-replication complexes is inhibited (Bousset and Diffley, 1998; Nguyen *et al*., 2001; Remus *et al*., 2005). CDKs and DDK4 are not only required for the activation of the MCM complex, they also trigger the assembly of

Table 1. Homologues of DNA replication components. * Based on homology searches only

Protein Name	*S. cerevisiae*	*S. pombe*	*D. melanogaster*	Mammals	*C. elegans*
Prereplication complex					
Orc1-6	Orc1-6	Orc1-6	Orc1-6	Orc1-6	ORC-2
Cdc6	Cdc6	Cdc18	Cdc6	Cdc6	CDC-6
Cdt1	Cdt1/Tah11/ Sid2	Cdt1	DUP	Cdt1	CDT-1
Mcm2	Mcm2	Mcm2/ Cdc19/Nda1	Mcm2	Mcm2	MCM-2
Mcm3	Mcm3	Mcm3	Mcm3	Mcm3	MCM-3
Mcm4	Cdc54/mcm4	Cdc21	DPA	Mcm4	MCM-4
Mcm5	Cdc46/Mcm5	Mcm5/Nda4	Mcm5	Mcm5	MCM-5
Mcm6	Mcm6	Mcm6/Mis5	Mcm6	Mcm6	MCM-6
Mcm7	Cdc47/Mcm7	Mcm7	Mcm7	Mcm7	MCM-7
Preinitiation complex					
Mcm10	Mcm10/Dna43	Cdc23	Mcm10	Mcm10	Y47D3a.28
Cdc45	Cdc45/Sld4	Sna41/Cdc45	Cdc45	Cdc45	F34D10.2
Sld3	Sld3	Sld3	-	-	-
Dbp11	Dbp11	Cut5/Rad4	Mus101	TopBP1	MUS-101
Sld2	Sld2/Drc1	Drc1	-	-	-
Sld5	Sld5	Sld5	Sld5	Sld5	Y113G7B.24
Psf1	Psf1	Psf1	Psf1	Psf1	R53.6*
Psf2	Psf2	Psf2	Psf2	Psf2	F31C3.5*
Psf3	Psf3	Psf3	Psf3	Psf3	-
Kinases					
Cdc7	Cdc7	Hsk1	Cdc7	Cdc7	C34G6.5
Dbf4	Dbf4	Dfp1	Chiffon	Dbf4/Ask/ Drf1	-

additional factors. This results in the formation of a "pre-initiation complex" that contains a large and still growing group of proteins, such as Cdc45, Mcm10, RPA, and the DNA polymerases α and ε (McGarry and Kirschner, 1998; Bell and Dutta, 2002; van Leuken *et al.*, 2008; Méchali, 2010). Most of these factors have not been identified or investigated in *C. elegans*, and the formation and function of the pre-initiation complex in *C. elegans* therefore remains elusive (Table 1). In animal systems, Geminin acts as an inhibitor of CDT-1, which is degraded in mitosis in an APC/C-dependent fashion (McGarry and Kirschner, 1998; van Leuken *et al.*, 2008). *C. elegans* Geminin GMN-1 also associates with CDT-1 and inhibits origin licensing when added to frog egg extracts (Yanagi *et al.*, 2005). GMN-1 inhibition results in germline defects and intestinal abnormalities with chromatin bridges. Thus, Geminin may be an example of a metazoan-specific regulator of DNA replication initiation.

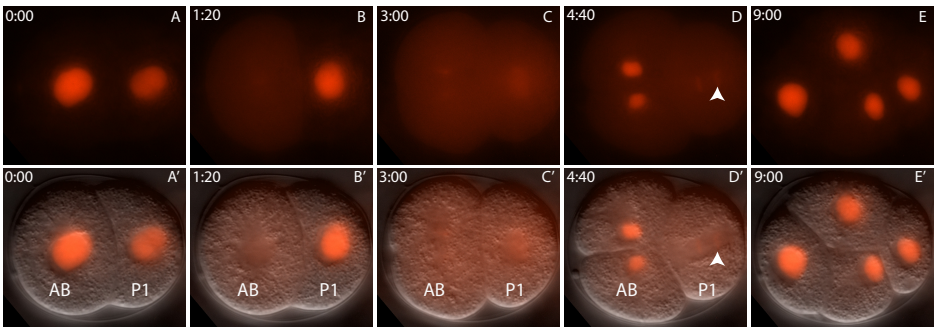

Figure 2. Time-lapse fluorescence microscopy shows expression and localization of MCM-4 in an early embryo. MCM-4 is fused to mCherry and expressed from the mcm-4 promoter (A-E). Merged images of the DIC and fluorescence channels are shown in the bottom panels (A'-E'). The red MCM-4::mCherry fluorescence is visible in the anterior AB and posterior P1 cell in the two stage embryo (A and A'). Note that the AB cell enters mitosis before the P1 cell (B and B'). MCM-4 can be detected on the chromosomes in late anaphase (arrowhead in P1 cell, D and D')

Preventing re-replication

When DNA replication is initiated, origin licensing should be prevented, as re-firing of only a single origin may lead to gene amplification and could have dramatic consequences. Hence, all eukaryotes use multiple levels of control to prevent more than one round of DNA synthesis within a single S-phase, although the exact players and mechanisms differ somewhat between species. In general, there are two mechanisms used to prevent re-replication: firstly, formation of the pre-replication complex (prior to S-phase) and the activation of the origins (during S-phase) are temporally separated, and secondly, proteins required for the formation of the pre-replication complex are inactivated as soon as DNA replication starts (Blow and Dutta, 2005; Machida *et al.*, 2005; Arias and Walter, 2007). Surprisingly, despite the importance of a single round of DNA replication and the redundant levels of control, certain single gene mutations cause substantial re-replication. As an important example, *C. elegans cul-4* displays such a re-replication phenotype (Zhong *et al.*, 2003).

cul-4 encodes the core subunit of a cullin-based E3 ubiquitin ligase that targets substrate proteins for ubiquitylation and degradation. Kipreos and coworkers studied the effects of *cul-4* inhibition by RNAi in the epithelial stem-cell like "seam" cells in the *C. elegans* skin. Interestingly, they observed that *cul-4* RNAi resulted in seam cells with up to a 100n DNA content and showed that this results from extensive re-replication rather than failed mitosis (Zhong *et al.*, 2003). As mentioned above, a key mechanism of preventing re-replication is inactivation of the components that form the pre-replication complex. Indeed, it was shown that *cul-4* is required for the degradation of one of these components. When *cul-4* is inhibited, CDT-1 levels do not drop at the end of G1 but remain constant throughout S-phase, indicating that CUL-4 is required for S-phase degradation of CDT-1. Subsequent studies in *C. elegans* and other systems demonstrated that CUL-4 in association with the DNA damage binding protein 1 (DDB-1) recognizes CDT-1 as a substrate (Blow and Dutta, 2005; Arias and Walter, 2007; Kim and Kipreos, 2007a, 2007b). However, degradation

of CDT-1 by CUL-4 is not the whole story, since expression of stable CDT-1 alone does not cause noticeable re-replication. CUL-4 was also found to be responsible for the localization of CDC-6, another member of the pre-replication complex. CDC-6 normally accumulates in the nucleus during G1 phase, and is exported from the nucleus to the cytoplasm during S-phase. The activity of CUL-4 turned out to be needed for nuclear export of CDC-6. Thus, CUL-4 inactivation deregulates two essential factors of the pre-replication complex. High nuclear levels of both CDT-1 and CDC-6 in S-phase allow continued origin licensing and promote re-replication (Kim and Kipreos, 2007a; Kim *et al.*, 2007).

Although intriguing, the mechanism by which CUL-4 regulates nuclear export of CDC-6 in S-phase was not immediately apparent. However, two clues were available: CDC6 nuclear export is regulated by Cyclin-CDKs in other systems, and, similar to the human homolog, the amino terminus of *C. elegans* CDC-6 contains multiple nuclear localization signals flanked by potential CDK phosphorylation sites (Kim and Kipreos, 2007b;

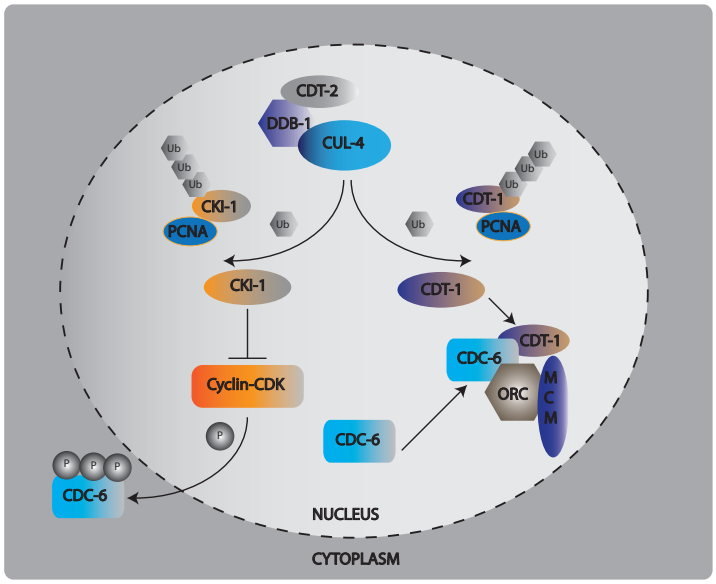

Figure 3. Preventing re-replication. Inactivation of CDT-1 and CDC-6 in S-phase provides a key mechanism for preventing re-replication. The cullin RING ubiquitin E3 ligase (CRL) complex CRL-4^{Cdt2} is critical in the inactivation of CDT-1 as well as CDC-6. $CRL4^{Cdt2}$ contains the cullin protein CUL-4, adaptor DDB-1 and substrate recognition unit CDT-2. This complex recognizes its substrates in association with PCNA. CDT-1 and a CDK inhibitor of the Cip/Kip family, CKI-1, contain a PCNA interacting protein (PIP) motif in the N-terminus and are degraded by $CRL4^{Cdt2}$. As PCNA is an auxiliary factor of DNA polymerases, the degradation of CDT-1 and CKI-1 can be coupled to DNA replication. Inactivation of CKI-1 allows activation of S-phase CDK/Cyclin kinases. CDK phosphorylation of the CDC-6 N-terminus promotes nuclear export of CDC-6. Because of its control of two critical pre-replication complex components, CUL-4 inactivation leads to extensive re-replication in *C. elegans* (see text for further details).

Kim *et al.*, 2007, 2008). Phosphorylation at these sites coincides with nuclear export, as demonstrated by phosphospecificantibody staining, and mutation of all six CDK sites prevented nuclear export. Thus, CUL-4 could promote nuclear export by stimulating CDK phosphorylation of the CDC-6 N-terminus. This is likely accomplished by degradation of a CDK inhibitor of the Cip/Kip family, known as CKI-1 in worms, Dacapo in flies and $p21^{Cip1}$ in vertebrates (Figure 3) (Bondar *et al.,* 2006; Higa *et al.,* 2006; Kim and Kipreos, 2007a, 2007b; Kim *et al.,* 2008; Korzelius *et al.,* 2011).

In each of these models, a cullin RING ubiquitin E3 ligase (CRL) has been identified that contains CUL-4, DDB-1, and a substrate recognition unit CDT-2. This $CRL4^{Cdt2}$ complex recognizes its substrates in an unusual manner. CKI-1, $p21^{Cip1}$ and CDT-1 all contain a PCNA interacting protein (PIP) motif in the N-terminus (Havens and Walter, 2009). PCNA is an auxiliary factor of DNA polymerases, which forms a ring around the DNA and acts as a sliding clamp. Because interaction with PCNA is a prerequisite for $CRL4^{Cdt2}$ substrate ubiquitylation, degradation of the CKI and CDT-1 substrates is coupled to DNA replication. In summary, upon association with PCNA, the CDK-inhibitor CKI-1 is recognized by $CRL4^{Cdt2}$ and targeted for degradation. This allows S-phase Cyclin-CDKs to phosphorylate CDC-6, which triggers CDC-6 export from the nucleus. In addition to CKI-1, $CRL4^{Cdt2}$ also targets PCNA-bound CDT-1 for ubiquitin-dependent proteolysis. In *C. elegans*, CDC-6 nuclear export and CDT-1 degradation are two redundant mechanisms that prevent rereplication (Figure 3) (Kim and Kipreos, 2007b; Korzelius and van den Heuvel, 2007). Because *C. elegans* does not show redundancy for the $CRL4^{Cdt2}$ E3 ligase in CDT-1 degradation, the function of this complex has been more obvious in *C. elegans*.

Activation of the DNA replication checkpoint in early embryos

Incomplete DNA replication activates an S-phase checkpoint, which delays progression through the cell cycle to create time for repair (Branzei and Foiani, 2010). Central in this checkpoint is the ATR-Chk1 protein kinase pathway, which is activated by lesions created by stalled replication forks. Active Chk1 phosphorylates downstream cell cycle regulators such as the CDC25 phosphatase that controls the activity of CDK1. This S-phase checkpoint is generally not functional in early embryos. For example, inhibition of DNA replication with a low concentration of hydroxyurea (HU) does not affect cell cycle progression in embryos of *Drosophila*, *Xenopus,* or zebrafish (Hartwell and Weinert, 1989). However, the situation is quite different in early *C. elegans* embryos, which not only contain an active S-phase checkpoint, but also activate the ATR-1/Chk-1 pathway as part of normal development (Encalada *et al.*, 2000; Brauchle *et al.*, 2003).

The first division of the *C. elegans* zygote is unequal and generates a larger anterior blastomere, AB, and smaller posterior blastomere, P1. These cells give rise to different daughter cell lineages. For instance, P1 continues an additional three asymmetric divisions to produce the germline precursor P4 (Sulston and Schierenberg, 1983). In addition to the different fates, cell division in the AB and P1 lineages also occurs with a different timing, with the AB cell dividing approximately 2 minutes earlier than the P1 cell (visible in Figure 2).

Interestingly, *atl-1* ATR and *chk-1* function contributes to this asynchrony of cell division in normal embryos (Brauchle *et al.*, 2003). Double inactivation of *atl-1* and *chk-1* reduced the time between mitotic entry (nuclear envelope breakdown) of AB and P1 from 125 sec in the wild-type to 75 sec after *atl-1*/*chk-1* RNAi. Thus, somehow the P1 blastomere might preferentially and highly reproducibly activate the S-phase checkpoint. Asymmetric division of the zygote is needed for this distinction between AB and P1 (Brauchle, et al. 2003).

Preferred checkpoint activation in P1 is also visible in mutants with defects in DNA replication, or embryos treated with HU, which inhibits ribonucleotide reductase (Brauchle *et al.,* 2003; Encalada *et al.,* 2000, 2005; Korzelius *et al.,* 2011). Both the zygote (P0) and P1 daughter are able to delay mitosis by about 12 minutes when replication is compromised, while the AB daughter halts for only a few minutes. Inactivation of *atl-1* and/or *chk-1* prevents these delays, indicating that this is a legitimate, though limited, phase checkpoint response. The different response of the P1 versus AB lineage has been interpreted as protection of the germline against replication errors. Surprisingly, however, the checkpoint response to DNA damage (rather than replication arrest) appears actively repressed in the P1 lineage (Holway *et al.*, 2006). Bypassing the checkpoint could serve to maintain the relative timing of blastomere divisions, which is an essential part of development.

The MCM helicase is needed for activation of the replication checkpoint

Defects in some replication components trigger a checkpoint arrest, while others do not. For instance, partial loss of function of *div-1*, which encodes a DNA polymerase α-subunit, gives rise to substantial cell cycle delays (Encalada *et al.*, 2000). The same is true for inhibition of ribonucleotide reductase by HU treatment or *rnr-1* RNAi (Brauchle *et al.*, 2003). However, *mcm-4* inactivation interferes with DNA synthesis without the induction of a checkpoint response (Korzelius *et al.*, 2011). Cells in *mcm-4*(RNAi) embryos and *mcm-4* mutant larvae enter mitosis at the appropriate time and continue chromosome segregation as well as cell division. Moreover, RNAi of *mcm-4* suppressed the checkpoint delay induced by *rnr-1* inhibition. These data indicate that MCM-4 is not only required for DNA replication but also for activation of the S-phase checkpoint. Genome fragmentation has also been reported for *cdt-1*(RNAi) and *cdc-6*(RNAi) embryos. Thus, the assembly of a pre-replication complex appears to be needed to trigger the S-phase checkpoint.

Studies in other organisms support these observations and have demonstrated that activation of the DNA damage and replication checkpoints requires MCM helicase activity. Recruitment of Replication Protein A (RPA) to single-stranded DNA is probably the actual checkpoint trigger (Zou and Elledge, 2003). The helicase activity of MCM proteins generates ssDNA, through unwinding the DNA at the replication fork. Stalling of replication forks, e.g. after HU treatment, causes uncoupling of the MCM helicase from DNA polymerase activity (Byun *et al.*, 2005). Consequently, fork stalling leads to an accumulation of ssDNA, which recruits additional RPA and causes activation of the checkpoint kinases ATR and Chk1. The formation of replication forks and the generation of ssDNA both

require MCM function. This explains why *C. elegans mcm-4* loss of function prevents DNA synthesis without activation of the replication checkpoint.

Endoreplication: polyploidy required for growth

Endoreplication cycles bypass mitosis while DNA replication continues, which results in a doubling of the ploidy during each endocycle. Endoreplication commonly occurs in specific cell types during metazoan development. In *C. elegans*, only two tissues become polyploidy as a result of endoreplication: the intestine and the epidermis (formally known as hypodermis). Intestinal cells endoreplicate during each larval stage, increasing the ploidy to 4n at the transition from first to second larval stage and leading to intestinal nuclei with 32n DNA in adult animals (Hedgecock and White, 1985).

The situation in the epidermis is more complex. Epidermal nuclei reside in syncytia, sharing a common cytoplasm without separating membranes. The largest epidermal syncytium is hyp7, which covers most of the body except for regions of the head and tail (Hedgecock and White, 1985). In each larval stage, stem-cell like precursors in the epidermis, known as "seam cells", divide to create novel seam cells and daughter cells that fuse with the hyp7 syncytium (Sulston and Horvitz, 1977). Ultimately, this creates a syncytium with 133 nuclei. The newly created epidermal cells duplicate their genomic DNA prior to fusion, so that they enter the syncytium as 4n nuclei (Hedgecock and White, 1985). Endoreplication has been reported to occur in adult stage hyp7 nuclei, although the level varies between nuclei, with an average ploidy of 10n to 12n in older adults (Figure 4) (Flemming *et al.*, 2000; Morita *et al.*, 2002; Nystrom *et al.*, 2002). Why these two cell types, the skin and intestine, undergo endoreplication is not fully understood. It has been speculated that endoreplication is used to maintain the integrity of these tissues, while allowing increased genome ploidy to support increases in cell volume and metabolic activity (Kipreos, 2005). In many organisms however, endoreplication has been correlated with growth. Indeed, the *C. elegans* epidermis and intestine grow extensively during larval development, and endoreplication in the epidermis has been correlated with the size of the entire animal.

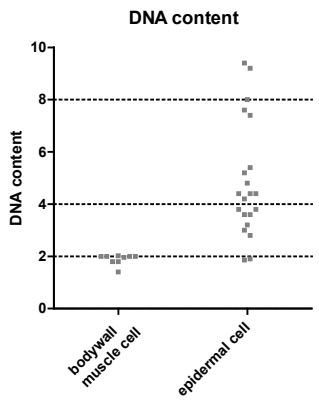

Figure 4. DNA endoreplication in the epidermis. Quantification of DNA content based on propidium iodide staining. Nuclei of the body wall muscles are used as a reference for 2n DNA content. The epidermal nuclei show increased ploidy with up to 8n DNA content. The DNA content of epidermal nuclei further increases in concert with growth of late stage adults. Each dot represents a single nucleus.

Several observations support this conclusion. Hydroxyurea (HU) treatment of adult animals, in which somatic cell proliferation has been completed, prevents endoreplication in the epidermis as well as growth of the animals. (Lozano *et al.*, 2006). In contrast, tetraploid animals are 40% larger in volume than wild type worms, which closely corresponds to the increase in epidermal polyploidy (from average 11.2n to 16.7n, in adults at 148 hrs.). Furthermore, the first generation homozygous *cye-1* cyclin E mutants survive till adulthood because of maternal CYE-1 supplies and these animals show reduced endoreplication in the epidermis and a corresponding reduction in body size (Lozano *et al.*, 2006). Finally, *mcm-4* mutants fail DNA replication and are severely growth retarded and larval lethal. Specific expression of MCM-4 in the epidermis of such mutants is sufficient to rescue larval growth and lethality (Korzelius *et al.,* 2011). Thus, the polyploidy of the epidermis contributes to the body size of the adult animal.

Tissue specific regulation of DNA replication

Interestingly, endoreplication in the epidermis is regulated by a TGF-β signal transduction pathway. *C. elegans* uses several different TGF-β pathways to control a variety of developmental processes, including growth. Mutations in components of this pathway lead to smaller and thinner adult animals (small phenotype: Sma). The ligand for the growth pathway is DBL-1, which is homologous to DPP/BMP-4 (Suzuki *et al.*, 1999; Morita *et al.*, 2002). DBL-1 signals through the Type I and II TGF-βserine/threonine kinase receptors SMA-6 and DAF-4, respectively, to the downstream SMAD transcriptional regulators SMA-2, SMA-3 and SMA-4 (Savage-Dunn, 2005). Notably, *daf-4* and *sma-2* mutants are not only small and thin, but also show reduced ploidy of epidermal nuclei (Flemming *et al.*, 2000; Nystrom *et al.*, 2002).

A critical downstream target of the DBL-1 pathway has also been identified: *lon-1* (Maduzia *et al.*, 2002; Morita *et al.*, 2002). Homozygous *lon-1* mutant animals are longer than normal (Lon phenotype), while overexpression of *lon-1* leads to a small phenotype. Several observations indicate that *lon-1* acts downstream of the SMA-6 TGF-β type I receptor: double *sma-6; lon-1* mutants are still somewhat long, and *lon-1* mRNA levels are increased in *sma-6* mutants. Surprisingly, *lon-1* encodes a putative transmembrane protein, related to the plant pathogenesis-related protein 1 (PR-1) and human glioma-pathogenesis related protein (GliPR-1). This LON-1 protein is expressed and required in the epidermis, and anti-LON-1 antibodies showed localization to apical junctions (Morita *et al.*, 2002). LON-1 is claimed to repress endoreplication, based on the increased epidermal ploidy in *lon-1*(e185) and *lon-1*(RNAi) adults. However, two other *lon-1* mutations show somewhat reduced ploidy compared to wild-type (Morita *et al.*, 2002). Thus, although further research is needed, there is strong evidence that the DBL-1 ligand, produced in a set of neurons, activates a TGF-β/SMA pathway, which inhibits *lon-1* expression in the epidermis, and thereby allows endoreplication and growth of the adults.

The TGF-β/SMA/LON-1 pathway should somehow connect to the cell cycle in order to regulate endoreplication. Based on the Sma phenotype of *cye-1* mutants, it has been pro-

posed that Cyclin E is the key regulator (Lozano *et al.*, 2006). Cyclin E mutant mice also show defects in trophoblast endoreplication (Parisi *et al.*, 2003), and the fluctuating activity of Cyclin E with its kinase partner CDK-2 drives endoreplication in *Drosophila* (Claycomb and Orr-Weaver, 2005; Lilly and Duronio, 2005). However, TGF-β/SMA/LON-1 signaling could also act more upstream of *cye-1*, e.g., in the regulation of *cyd-1* Cyclin D. *cyd-1* mutants are also small, and *C. elegans* Cyclin D is needed for endoreplication, at least in the intestine (Boxem and van den Heuvel, 2001). At least in *C. elegans*, Cyclin D is essential for G1/S progression and induction of S-phase genes such as MCM proteins (Boxem and van den Heuvel, 2001, 2002; Korzelius *et al.,* 2011).

The *cyd-1* and *mcm-4* mutants show an interesting phenotypic difference. Homozygous mutants of either *cyd-1* or *mcm-4* complete embryogenesis, because of maternal supplies, fail DNA replication from the first larval stage onward, and show severe growth retardation. However, only *mcm-4* mutants show larval lethality, which is fully suppressed by expression of *mcm-4* from an epidermis-specific promoter (Korzelius *et al.,* 2011). The ability to arrest the cell cycle probably underlies the difference between *cyd-1* and *mcm-4* mutants: post-embryonic blast cells in *cyd-1* mutants arrest prior to S-phase entry, while they continue abnormal mitosis in *mcm-4* mutants. As a result, the structural integrity of the epidermis is lost only in *mcm-4* mutants, which often causes larval death. Thus, not absence of DNA replication but lack of an S-phase checkpoint response may lead to death of the animal.

In conclusion

Studies of DNA replication in *C. elegans* have thus far been limited. Given the variation of well-established models for replication studies, which include budding and fission yeast, *Xenopus* egg extracts, cells in culture, *in vitro* systems and even flies, one could question the need for studying S-phase in the worm. However, several important mechanistic insights have been obtained from observations of DNA replication-defective phenotypes in the worm. Moreover, such analyses have emphasized the variation in regulatory mechanisms between different developmental stages and in different cell types, underscoring the need for studies of replication control in a developmental context. The combination of its large embryonic cells, strong cell biology, genetic tractability and highly reproducible lineage now allows for a detailed analysis of the assembly of prereplication and replication initiation complexes in real time in *C. elegans*. High-throughput studies have already defined RNAi phenotypes for many known DNA replication components, and have identified currently uncharacterized genes with similar phenotypes. Thus, *C. elegans* increasingly adds an attractive developmental animal system for gene discovery, functional characterizations *in vivo*, and live imaging of replication component localizations.

Chapter 3

Rb and FZR1/Cdh1 determine CDK4/6-cyclin D requirement in *C. elegans* and human cancer cells

Inge The[1,*], **Suzan Ruijtenberg**[1,*], Benjamin P. Bouchet[2], Alba Cristobal[3], Martine B.W. Prinsen[1], Tim van Mourik[1], John Koreth[4], Huihong Xu[5,] Albert J.R. Heck[3], Anna Akhmanova[2], Edwin Cuppen[6], Mike Boxem1,Javier Muñoz[3,†], & Sander van den Heuvel[1]

*** these authors contributed equally to the work**

An adapted version of this manuscript has been published in *Nature Communications*, 2015

1. Developmental Biology, Faculty of Sciences, Department of Biology, Utrecht University, Padualaan 8, 3584 CH Utrecht, The Netherlands. **2.** Cell Biology,Faculty of Sciences, Department of Biology, Utrecht University, Padualaan 8, 3584 CH, Utrecht, The Netherlands. **3.** Biomolecular Mass Spectrometry and Proteomics Group, Bijvoet Center for Biomolecular Research and Utrecht Institute for Pharmaceutical Sciences, Utrecht University, Padualaan 8, 3584 CH Utrecht, The Netherlands. **4**. Hematologic Oncology, Dana-Farber Cancer Institute, 450 Brookline Avenue, Boston, Massachusetts 02215, USA. **5**. Department of Pathology and Laboratory Medicine, Boston University School of Medicine and Boston Medical Center, 670 Albany Street, Boston, MA, USA. 6. Hubrecht Institute, Uppsalalaan 8, 3584 CT Utrecht, The Netherlands. † Present address: Spanish National Cancer Research Centre (CNIO), Proteo-Red-ISCIII, Melchor Férnandez Almagro, 3, 28029 Madrid, Spain.

Abstract

Cyclin Dependent Kinases 4 and 6 (CDK4/6) in complex with D-type cyclins promote cell cycle entry. Most human cancers contain overactive CDK4/6-cyclin D, and CDK4/6-specific inhibitors are promising anti-cancer therapeutics. Here, we investigate the critical functions of CDK4/6-cyclin D kinases, starting from an unbiased screen in the nematode *Caenorhabditis elegans*. We found that simultaneous mutation of *lin-35*, a retinoblastoma (Rb)-related gene, and *fzr-1*, an orthologue to the APC/C co-activator Cdh1, completely eliminates the essential requirement of CDK4/6-cyclin D (CDK-4/CYD-1) in *C. elegans*. CDK-4/CYD-1 phosphorylates specific residues in the LIN-35 Rb spacer domain and FZR-1 amino terminus, resembling inactivating phosphorylations of the human proteins. In human breast cancer cells, simultaneous knockdown of Rb and FZR1 synergistically bypasses cell division arrest induced by the CDK4/6-specific inhibitor PD-0332991. Our data identify FZR1 as a candidate CDK4/6-cyclin D substrate and point to an APC/C^{FZR1} activity as an important determinant in response to CDK4/6-inhibitors.

Introduction

Cyclin Dependent Kinases (CDKs) in association with cyclin subunits are the key regulators of cell division in eukaryotes (Malumbres and Barbacid, 2009). Active CDK-cyclin complexes promote progression through the cell division cycle by phosphorylating critical substrates. The decision to initiate cell division occurs in the G1-phase and involves expression of D-type cyclins in response to mitogenic signaling (Choi and Anders, 2014). These cyclins assemble with CDK4 or CDK6 (CDK4/6), to form kinase complexes that are best known for their phosphorylation of the retinoblastoma (Rb) tumour suppressor protein. Rb family proteins associate with E2F transcription factors and act as transcriptional repressors of cyclin E and other S-phase genes. The initial phosphorylation of Rb by CDK4/6-cyclin D is thought to weaken its repressor function, while subsequent phosphorylation by CDK2-cyclin E completely inactivates Rb function and allows full commitment to S-phase entry.

Strong support for the *in vivo* importance of this cell cycle control pathway has come from human cancer studies. Overexpression of CDK4/6 or D-type cyclins and inactivation of the CDK4/6 antagonist p16INK4A/CDKN2A or Rb tumour suppressor are common in human cancer (Kandoth *et al.*, 2013). These events are largely mutually exclusive, in support of p16INK4A, CDK4/6, D-type cyclins and Rb acting in a single regulatory pathway. At the same time, various studies have indicated that phosphorylation of Rb is not the only catalytic activity of CDK4/6-cyclin D kinases (Anders *et al.*, 2011; Lee *et al.*, 2014). Additional substrates of cyclin D kinases have been described, the best characterized of which are the Rb-related proteins p107 and p130, and transcription factors SMAD3 and FOXM1 (Matsuura *et al.*, 2004; Anders *et al.*, 2011; Choi and Anders, 2014). To what extent phosphorylation of these targets contributes to carcinogenesis is currently unknown.

Results from studies in mice have caused doubt on whether the functions of CDK4/6-cyclin D kinases are essential for proliferation. Knockout of a single D-type cyclin gene causes limited defects and mice that lack all three D-type cyclins still develop until mid-to-late gestation (Kozar *et al.*, 2004). Similarly, CDK4/CDK6 double knockout mice complete organogenesis and extensive cell proliferation, with death due to anaemia occurring only in the late stages of embryogenesis (Malumbres *et al.*, 2004). In contrast to normal development, cancer formation in various mouse models depends strongly on CDK4/6-cyclin D kinase activity (Yu *et al.*, 2001; Puyol *et al.*, 2010; Choi *et al.*, 2012; Sawai *et al.*, 2012). This difference in requirement appears to provide a window of opportunity for therapeutics that block cancer growth, while sparing normal cells. Small molecule inhibitors with high specificity for CDK4/6 have been identified, with PD-0332991 as the leading example (Fry *et al.*, 2004; Toogood *et al.*, 2005). PD-0332991 induces proliferation arrest in a substantial subset of human cancer cell lines and inhibits cancer formation in mouse models (Fry *et al.*, 2004; Finn *et al.*, 2009; Puyol *et al.*, 2010; Choi *et al.*, 2012). Based on these results and recent Phase II and Phase III clinical trials, CDK4/6 inhibitors currently receive much attention as promising anti-cancer therapeutics (Guha, 2012, 2013; Brower, 2014). Although there are substantially increased progression-free survival rates of cancer patient populations in

several studies, biomarkers that predict a positive response to CDK4/6 inhibitor treatment are currently not known. It will be of great clinical importance to reveal which cancer genotypes correspond to cell cycle arrest, or even senescence and apoptosis, in response to inhibitor treatment, and which bypass routes may be used by cancer cells to acquire resistance to CDK4/6-specific inhibitors.

In this study, we examine the critical functions of the CDK4/6 cyclin D kinase, making use of the evolutionary conserved regulation of cell cycle entry in metazoans. Our observations in the nematode *C. elegans* support that Rb-mediated transcriptional repression and APC/C^{FZR1}-mediated protein degradation act in parallel to inhibit G1/S progression, and that phosphorylation by the CDK-4/CYD-1 cyclin D kinase counteracts these inhibitory functions. Importantly, we also observed synergy between Rb and FZR1 knockdown in bypassing the proliferation arrest induced by treatment of human breast cancer cells with the CDK4/6 inhibitor PD-0332991. Our results indicate that the level of APC/C^{FZR1} activity is an important contributing factor in response of cancer cells to CDK4/6 inhibitor treatment.

Results

C. elegans CDK-4/CYD-1 has multiple critical substrates. We followed a genetic approach to reveal critical functions of CDK4/6 kinases. Cell cycle entry in *C. elegans* involves a CDK4/6-Rb pathway with limited redundancies (Figure 1A)(van den Heuvel and Dyson, 2008). Single genes encode for a *C. elegans* CDK4/6 kinase CDK-4, a D-type cyclin CYD-1, and a member of the Rb protein family, LIN-35. Candidate null mutations in *cyd-1* or *cdk-4* result in a general arrest of cell division in the G1-phase during larval development, slow growth and complete sterility (Figure 1B)(Boxem and van den Heuvel, 2001). Inactivation of *lin-35* Rb by RNA interference (RNAi) or putative null mutation (*n745* and *n2239* alleles) suppresses the *cdk-4* CDK4/6 and *cyd-1* cyclin D mutant phenotype in part. Although *lin-35* Rb loss allows post-embryonic cell division in *cyd-1* and *cdk-4* mutants, double mutant animals that lack *lin-35* and *cyd-1*, or *lin-35* and *cdk-4*, remain small and sterile (Figure 1B) (Boxem and van den Heuvel, 2001). In addition, quantification of cell numbers in the intestine and ventral nerve cord showed that the division of post-embryonic precursor cells remains limited in such double mutants (Figure 1C,D) (Boxem and van den Heuvel, 2001, 2002). These data indicate that the CDK-4/CYD-1 kinase promotes cell cycle entry not only by inhibiting LIN-35 Rb but also through additional critical activities.

Additional functions could involve phosphorylation of other substrates or, as has been suggested for mammalian CDK4/6-cyclin D complexes (Choi and Anders, 2014), sequestration of CDK-inhibitory proteins (CKIs; Figure 1A). To examine whether the additional function of CDK-4/CYD-1 requires kinase activity, we expressed a FLAG-tagged kinase-dead (KD) form of CDK-4 in *lin-35*, *cdk-4* double-null mutants. As a control, we expressed wild-type (WT) *cdk-4::flag* introduced as a single-copy integrated transgene. Transgene-expressed WT *cdk-4::flag* completely rescued the *cdk-4(gv3)*-null mutant phenotype (Supple-

mentary Figure 1). Expression of KD CDK-4D128E::FLAG, however, neither alleviated the *cdk-4-null* phenotype nor improved rescue when combined with *lin-35* Rb inactivation (Supplementary Figure 1). These data demonstrate that CDK-4/CYD-1 has one or more critical phosphorylation targets in addition to LIN-35 Rb.

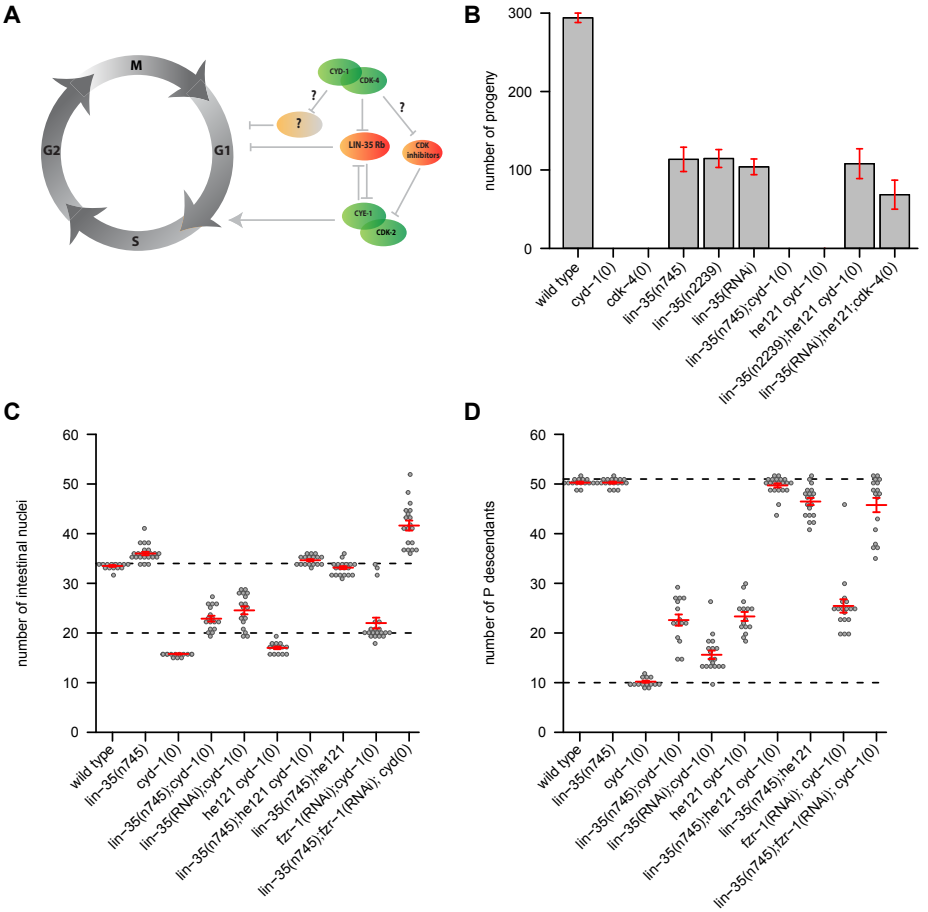

Figure 1. Simultaneous *lin-35* Rb and *fzr-1* loss of function eliminates *cyd-1* and *cdk-4* requirement. (A) Model for cell cycle entry in *C. elegans* illustrating more than one critical function of CYD-1/CDK-4. (B) Quantification of total progeny numbers (bars) for animals of the indicated genotypes. (C) Quantification of the number of intestinal nuclei for the indicated genotypes. (D) Quantification of the number of descendants of the P2–P10 ventral cord precursor cells for the indicated genotypes. The candidate-null alleles used are *cyd-1(he112)*, *cdk-4(gv3)* and the *lin-35* alleles *n745* and *n2239*. Total broods were counted of at least two animals of each genotype and total cell numbers in the indicated tissues of at least ten animals of each genotype. Graphs show mean ± s.e.m., each dot (C,D) represents a single animal.

LIN-35 Rb and FZR-1 loss eliminates CDK-4/CYD-1 requirement

To identify critical substrates, we performed a genetic screen for mutations that suppress the cell division arrest and sterility of *lin-35*, *cyd-1* double mutant animals. In a large-size screen (410,000 haploid genomes), we identified only a single mutant with complete rescue of the *lin-35(n745);cyd-1(he112)* phenotype. The mutant animals with this *he121* suppressor mutation appeared normal and produced progeny numbers similar to *lin-35* single mutants (Figure 1B). Quantification of cell numbers further supported that postembryonic cell divisions in *cyd-1(he112)* mutants were fully restored by simultaneous *lin-35* inactivation and *he121* mutation (Figure 1C,D). In fact, the triple mutant larvae showed slightly higher than normal numbers of intestinal nuclei, again resembling the *lin-35* single-mutant phenotype (Figure 1C, note: the normal intestine never has more than 34 nuclei). Combining *lin-35* RNAi with the *he121* mutation also restored cell division and fertility in *cdk-4(gv3)*-null mutants (Figure 1B). Thus, rescue of the cell cycle arrest phenotype does not result from allele-specific suppression of *cyd-1(he112)*. Instead, the combined *lin-35* and *he121* mutations appear to abolish *cdk-4*/*cyd-1* requirement. Interestingly, the homozygous *he121* mutation also caused some suppression of the cell division arrest of *cyd-1* mutants with normal *lin-35* Rb function (Figure 1C,D; note: *cyd-1(he112)* larvae always have 16 intestinal nuclei). These data indicate that the *he121* mutation disrupts a negative regulator of cell cycle entry, which acts in parallel to *lin-35* Rb.

We mapped the *he121* mutation to chromosome 2, to the right of *dpy-10* and close to map position 1. Whole-genome sequencing of the *lin-35(n745);he121 cyd-1(he112)* strain revealed a nonsense mutation in the fourth codon of the *fzr-1* FZR1 predicted open reading frame (CAT to TAG; Glu to Stop). *C. elegans fzr-1* encodes a co-activator and substrate specificity factor of the anaphase-promoting complex (APC/C) that is closely related to human FZR1 (also known as Cdh1), *Drosophila fizzy related (fzr)* and budding yeast Cdh1/Hct1 (Sigrist and Lehner, 1997; Visintin *et al.*, 1997; Fay *et al.*, 2002). The APC/C^{FZR1} E3 ubiquitin ligase targets specific proteins for degradation in late mitosis and early G1. APC/C^{FZR1} is known to inhibit G1/S progression, which appears to agree with *he121* being an *fzr-1* allele. Additional observations support this conclusion: fosmid and plasmid clones carrying genomic *fzr-1* sequences complemented the *he121* phenotype when introduced as transgenes (Supplementary Table 1). Further, RNAi of *fzr-1*, obtained by soaking first stage (L1) larvae, rescued the cell cycle defects in *lin-35*, *cyd-1* double mutants and allowed production of viable offspring (Supplementary Table 2). However, *fzr-1* RNAi and the *fzr-1(ku298)* strong loss-of-function mutation predominantly induced lethality and sterility when combined with *lin-35* loss of function, as previously reported (Fay *et al.*, 2002). In combination with *cyd-1* loss, or double *lin-35*, *cyd-1* mutations, strong *fzr-1* RNAi also resulted in a higher number of nuclear divisions in the intestine, compared with the *fzr-1(he121)* mutation (Figure 1C, note: the P-derived neuroblasts examined in Figure 1D are somewhat RNAi insensitive). This combination of results indicates that *he121* is a partial loss-of-function allele of *fzr-1*. The effect of the *he121* early termination codon may be weakened by ribosomal readthrough, translation initiation at a downstream ATG, or alternative usage of promoter sequences and splice sites. The requirement for an *fzr-1* allele to simultaneously suppress *cyd-1*

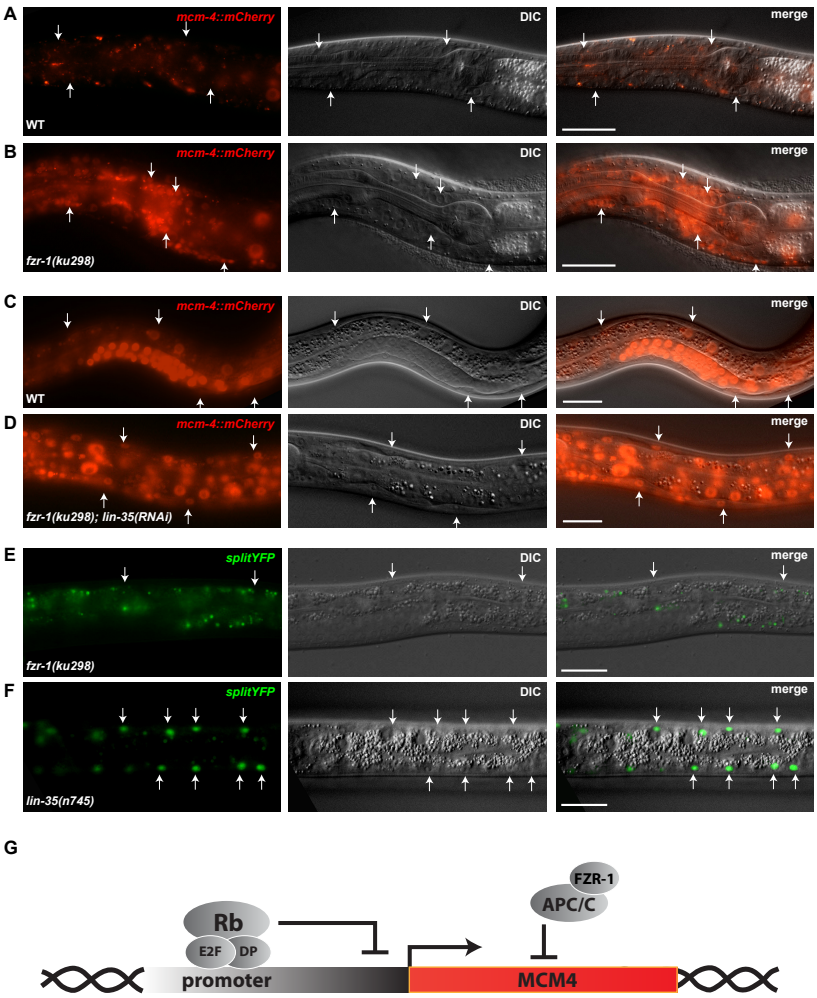

Figure 2. Differentiated cells in *lin-35; fzr-1* double mutants express S-phase reporters. (A–D) Animals containing a translational S-phase reporter of genomic *mcm-4* sequences, encoding an MCM-4 DNA replication helicase subunit fused to mCherry. (A) WT animal, head region. (B) *fzr-1(ku298)* mutant, head region. Note MCM-4::mCherry protein expression in many neurons of the nerve ring around the pharynx. (C) WT animal and (D) *fzr-1(ku298);lin-35(RNAi)* mutant. Note MCM-4::mCherry protein expression in body wall muscle cells (bwm), exclusively in the double mutant. (E,F) Animals containing a 'split YFP' transcriptional S-phase reporter, with the N-terminal half of YFP expressed under control of the mcm-4 G1/S-induced promoter, and C-terminal YFP expressed from the musclespecific *myo-3* promoter. (E) *fzr-1(ku298)* and (F) *lin-35(n745)* mutant. Note YFP expression in post-mitotic muscle cells, only in *lin-35(n745)* mutants. (G) Model illustrating parallel functions in cell cycle arrest through transcriptional repression by LIN-35 Rb and protein degradation by APC/C^{FZR-1}. Arrows indicate individual cells that either do not express (A,C,E) or express (B,D,F) the reporter. Experiments were repeated four (D) or more times with many animals. Scale bars, 20 μm.

loss and avoid synthetic lethality with *lin-35* may explain the identification of a rare partial loss-of function *fzr-1* mutation in a large-size screen.

Table 1. S-phase marker expression in muscle cells				
Body wall muscle	**WT**	***fzr-1***	***lin-35***	***lin-35; fzr-1***
MCM-4::mCherry protein expression	- (many)	- (1/96)	- (1/82)	+ (152/186)
mcm-4 promoter activity	- (many)	- (many)	+ (288/300)	+ (ND)

Quantification of the number of animals expressing the *mcm-4* translational or transcriptional S phase reporter in differentiated body wall muscle cells of wild type animals (WT), *fzr-1(ku298)* mutants, *lin-35(n745)* mutants or double mutants. -/+ indicates expression, between brackets: number of animals with reporter expression versus total number examined.

Arrest of cell cycle entry by FZR-1 and LIN-35 Rb

To examine cooperation between *fzr-1* and *lin-35* in cell cycle arrest, we tested how inactivation of these genes affects expression of *mcm-4* S-phase reporter constructs. MCM-4 is a subunit of the replicative helicase complex, which we previously observed to accumulate in G1/S, and to be induced by cyclin D and cyclin E CDK activity (Korzelius *et al.*, 2011a, 2011b). We used a *Pmcm-4::MCM-4::mCherry* reporter to detect *mcm-4* transcription and protein expression. Remarkably, loss of *fzr-1* function by RNAi or use of the *ku298* allele resulted in MCM-4::mCherry protein expression in post-mitotic neuronal cells (Figure 2A,B). This indicates that the strict G0/G1-phase arrest of differentiated neurons involves *fzr-1* function (Figure 2B). Neurons did not initiate DNA synthesis in *fzr-1* mutants, based on the absence of EdU (5-ethynyl-20-deoxyuridine) incorporation, and MCM-4::mCherry was not detected in other differentiated cells, such as muscle cells (Supplementary Figure 2). *lin-35* Rb mutants did not display deregulated expression of MCM-4::mCherry in any cell-type (Table 1). To specifically examine loss of transcription regulation, we designed a split yellow fluorescent protein (YFP) reporter combination for detection of S-phase gene activation in differentiated muscle cells. We combined expression of an N-terminal YFP fragment (*Pmcm-4::nzYFP*) under the control of a cell cycle promoter, with expression of a carboxy-terminal YFP fragment from a muscle specific promoter (*Pmyo-3::czYFP*). In contrast to WT or *fzr-1* mutant animals (Figure 2E), muscle-specific YFP fluorescence was observed in *lin-35* mutants, indicating that the *mcm-4* promoter is activated or de-repressed in the mutant muscle cells (Figure 2F). Combining *lin-35* Rb and *fzr-1* mutations in *Pmcm-4::MCM-4::mCherry* transgenic animals caused broad expression of the MCM-4::mCherry fusion protein, including body wall muscle expression (MCM-4::mCherry expression in bwm of 152/186 animals; Figure 2D and Table 1). Thus, LIN-35 Rb-mediated transcriptional repression and APC/C^{FZR1}-mediated protein degradation act in parallel to prevent S-phase gene expression, not only in cells that are temporarily quiescent but also in differentiated postmitotic cells (Figure 2G).

Posttranslational regulation of FZR-1 and LIN-35 function

We wondered whether the FZR-1 protein levels or localization are cell cycle-regulated and reflect cell cycle stage-specific functions. We created transgenic animals that express FZR-1 with an N-terminal green fluorescent protein (GFP) tag, to be able to follow the FZR-1 protein throughout development in living animals. The GFP::FZR-1 fusion protein is functional, as it rescues the lethal phenotype of *lin-35(n745);fzr-1(ku298)* double mutants. Transgenic animals showed expression of GFP::FZR-1 in many somatic cells during larval development, at levels that varied in a cell-type- and developmental stage-dependent manner (Figure 3, left panels). In developmentally arrested L1 larvae, GFP::FZR-1 expression was detectable in the cytoplasm and nucleus of postembryonic precursor cells, with the highest levels in nuclei of the syncytial epidermis (hyp7) and intestine, and lowest levels in epidermal seam cells (Figure 3A and Supplementary Figure 3). Initiation of cell cycle entry during larval development coincided with a substantial increase in nuclear GFP::FZR-1 (observed in ventral cord precursor (P) cells, vulval precursor cells, intestinal cells and seam cells; Figure 3A–C). Subsequent phases of temporal or permanent cell cycle arrest corresponded

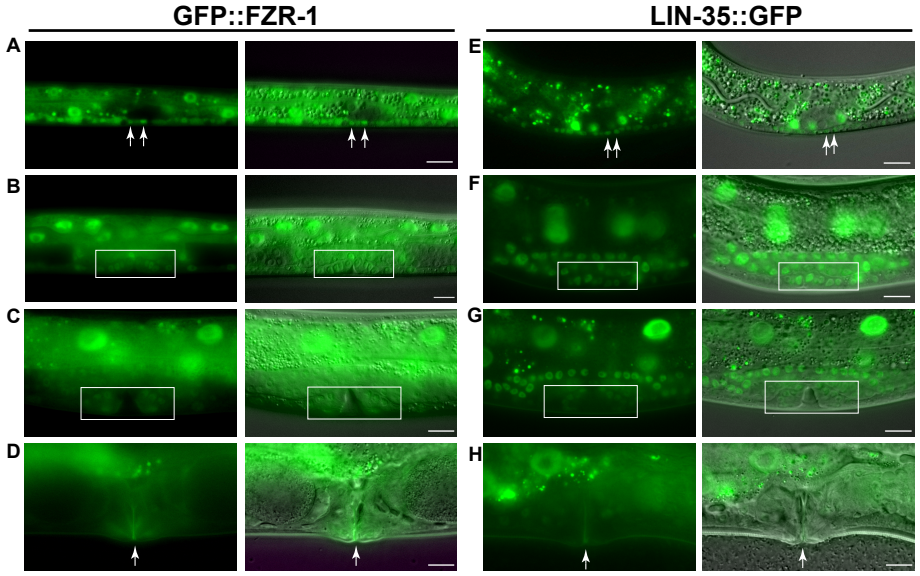

Figure 3. Expression of GFP-tagged FZR-1 and LIN-35 Rb correlates with cell cycle progression. (A–H) Fluorescence microscopy images of GFP expression and corresponding overlays of fluorescence and DIC images. (A,E) First-stage (L1) larvae showing GFP::FZR-1 (A) and LIN-35::GFP (E) expression. Arrows indicate dividing P cells with high expression levels. Dark spots in the ventral nerve cord are post-mitotic juvenile neurons. (B–D and F–H) Vulval development during the L3 stage. The vulval precursor cells (VPCs) close to the gonad migrate and divide to form the vulva (white boxes). The dividing VPCs express GFP::FZR-1 (box in B,C) and LIN-35::GFP (box in F,G). On completion of vulva formation, expression of FZR-1::GFP and LIN-35::GFP disappears from vulval cells (arrows in D and H). Images illustrate observations of many animals on multiple days. Scale bars, 10 μm.

to a gradually declining GFP::FZR-1 signal (Figure 3D, vulval precursor cells). Similarly, cells in *cyd-1* mutants that fail to enter S-phase showed reduced GFP::FZR-1 expression (Supplementary Figure 3). Hence, GFP::FZR-1 levels are high in actively cycling cells and decrease in cells arrested in G0/G1. It is surprising that GFP::FZR-1 levels are relatively low in G0/G1, when APC/C^{FZR-1} is active. This could possibly result from FZR-1 acting as an activator as well as a substrate of the APC/C E3 ubiquitin ligase. Alternatively or in addition, FZR-1 and other negative cell cycle regulators may be transcriptionally induced during cell division, to allow immediate arrest when needed. Notably, expression of LIN-35::GFP also correlated with cell division and decreased after cell cycle exit (Figure 3, right panels). The abundance of LIN-35 and FZR-1 in dividing cells indicates that the activity of these negative regulators of cell cycle progression is predominantly controlled at levels other than protein expression.

LIN-35 Rb and FZR-1 are CDK-4/CYD-1 kinase substrates

Our genetic observations demonstrate that the CDK-4/CYD-1 kinase is required for cell cycle entry, unless *lin-35* Rb and *fzr-1* are simultaneously inhibited. The simplest explanation for these findings is that LIN-35 and FZR-1 are the main targets of CDK-4/CYD-1, and that phosphorylation inhibits LIN-35 and FZR-1 function. Similar to Rb, FZR1 (Cdh1) activity is known to be temporally regulated by CDK activity (Zachariae *et al.*, 1998; Jaspersen *et al.*, 1999; Pesin and Orr-Weaver, 2008). Activation of APC/C^{FZR1} follows mitotic cyclin destruction and CDK1 inactivation in anaphase. In the next cell cycle, phosphorylation of FZR1 at the G1/S transition and association with the Emi1 pseudo-substrate inhibitor are thought to switch off APC/C^{FZR1} activity (Reimann *et al.*, 2001; Pesin and Orr-Weaver, 2008). Although in particular CDK2-cyclin A has been implicated in this phosphorylation (Lukas *et al.*, 1999), it appears likely to be that CDK4/6-cyclin D contributes to overcoming APC/C^{FZR1}-mediated G1 inhibition when cell cycle entry depends on this kinase. To test this possibility, we performed kinase assays *in vitro*, thereby avoiding indirect phosphorylation events by other CDKs and making use of the well-established substrate specificity of CDK4/6-cyclin D kinases *in vitro*. In these assays, we used *C. elegans* CDK-4/CYD-1 expressed and immunopurified from HEK 293T cells in combination with the bacterially expressed substrates GST-LIN-35 and GST-FZR-1. Autoradiography and mass spectrometric analysis revealed efficient and specific phosphorylation of both substrates (Figure 4A). LIN-35 Rb was phosphorylated by CDK-4/CYD-1 at Ser714 and Thr719, located between the pocket A and B regions (Figure 4C). These phosphorylations resemble Ser608 and Ser612 phosphorylation of human Rb, which reduce the affinity for E2F by promoting self-association between the Rb pocket loop and E2F-binding site of Rb (Dick and Rubin, 2013). Although human CDK4/6-cyclin D can phosphorylate Ser608 and Ser612, the specificity of this phosphorylation remains disputed (Narasimha *et al.*, 2014).

Mass spectrometric analysis of *in vitro* phosphorylated FZR-1 revealed eight CDK-4/CYD-1-phosphorylated residues in the N-terminal half of FZR-1 (Figure 4D). Phosphopeptides containing these residues were abundant in the WT CDK-4 kinase reactions and

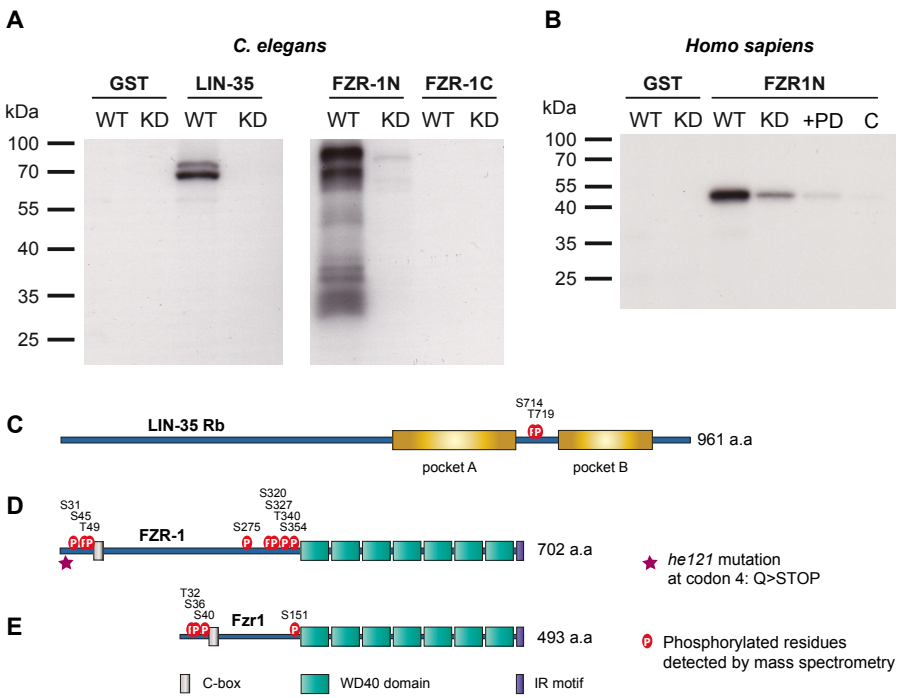

Figure 4. Phosphorylation of FZR1 by the CDK4-cyclin D kinase. (A) Autoradiogram following SDS–PAGE of in vitro kinase assays. FLAG-tagged C. elegans CDK-4 (WT) or KD CDK-4 (KD) were immunopurified and incubated with ^{32}P-γ-ATP, and the purified GST protein alone, or GST-fused to either the LIN-35 pocket region, FZR-1 N-terminus or FZR-1 C-terminus. (B) Same as in A, but kinase assays were performed with FLAG-tagged human CDK4 (WT) or KD CDK4 (KD), in the presence of GST alone or GST-fused to the human FZR1 N-terminus. The KD control showed some kinase signal in multiple experiments, probably through contaminating kinases. In the +PD lane, 0.9 μM of the CDK4/6 inhibitor PD-0332991 was added to the reaction with CDK4 (WT). Last lane (C) shows a negative control kinase assay, using anti-FLAG IP from cells transfected with empty vector. Illustration of the C. elegans LIN-35 protein showing the location of the two CDK-4 phosphorylated residues (P) in the spacer region between the pocket A and B domains. (D) Illustration of the *C. elegans* FZR-1 protein, indicating the positions of CDK-4 phosphorylated residues (P) and protein domains. The asterisk marks the *he121* mutation. The C-box is located at a.a. 59–65, the 7 WD40 domains start at a.a. 388, the final two a.a. form the IR motif. (E) Illustration of the H. sapiens FZR1 protein, the positions of the CDK-4 phosphorylated residues (P) and protein domains are indicated. C- box: a.a. 43–55, the 7 WD40 domains start at a.a. 182, the final two a.a. form the IR motif. All kinase assays and mass spectrometric analysis of the *C. elegans* proteins were performed twice, mass spectrometry of human FZR1 once.

were either not detectable or present at very low levels in the kinase dead CDK-4 control (Supplementary Table 3). All eight phosphorylated residues are followed by a proline residue and four are part of a T/SPxR/K consensus CDK phosphorylation site. For compari-

son, we also expressed human CDK4-cyclin D2 and found efficient phosphorylation of a human FZR1 N-terminal fragment (Figure 4B). Mass spectrometric analysis identified four residues that were differentially phosphorylated by CDK4-cyclin D2 compared with the KD CDK4 control (Figure 4E). These four phosphorylated residues of human FZR1 are also part of prolinecontaining sites. Moreover, their location in the FZR1 N-terminal domain is similar to the location of the CDK-4/CYD-1-phosphorylated residues of *C. elegans* FZR-1 and at least two of the phosphosites are evolutionarily conserved (*C.e.* Ser45, Thr49 versus *H.s.* Ser36, Ser40). A previous study showed that mutation to alanine of four conserved CDK consensus sites prevented inactivation of human FZR1 (Cdh1) (Lukas *et al.*, 1999). Two of these sites, Ser40 and Ser151, were phosphorylated by CDK4 in our *in vitro* kinase assays. Moreover, previous quantitative phosphorylation analysis showed cell cycle-dependent *in vivo* phosphorylation of FZR1 at five N-terminal serine residues, including Ser32, 36 and 151 (Dephoure *et al.*, 2008). Together, our data indicate evolutionarily conserved inhibitory phosphorylation of Rb and FZR1 proteins, and are consistent with LIN-35 and FZR-1 inactivation in G1 through phosphorylation by CDK-4/CYD-1.

LIN-35 Rb and FZR-1 probably are CDK-4/CYD-1 targets *in vivo*

We considered alternative or complementary mechanisms for the elimination of CDK-4/CYD-1 requirement following Rb and FZR-1 reduction. Based on results in other systems, loss of FZR-1 might allow persistence of mitotic cyclins into the next G1-phase, or lead to premature CDK-2/CYE-1 cyclin E activation. The inappropriate activity of cyclin B or cyclin E kinases could bypass the CDK-4/CYD-1 kinase requirement. Immunohistochemical staining of *fzr-1(he121)* and *fzr-1(ku298)* mutants indicated normal degradation of CYB-1 cyclin B1 and CYB-3 cyclin B3 in mitosis (Supplementary Figure 4A–C). This is in agreement with mitotic cyclin degradation by APC/C in association with the Cdc20/Fizzy substrate specificity factor. Immunohistochemical staining of CYE-1 cyclin E also did not reveal apparent abnormalities, as CYE-1 expression was only detected in cells expected to be in S-phase. Western blotting experiments were not conclusive but at most indicated slightly increased CYE-1 levels in *fzr-1(ku298)* and *lin-35(n745)*; *fzr-1(he121)* larvae (Supplementary Figure 4). Human APC/CFZR1 regulates SCF^{Skp2} and thereby $p21^{Cip1}$ and $p27^{Kip1}$ degradation (Bashir *et al.*, 2004; Wei *et al.*, 2004). In analogy, activation of CDK-2/CYE-1 could also indirectly result from CKI-1 CIP/KIP depletion following *fzr-1* loss. However, CKI-1::GFP levels were increased, rather than decreased, following RNAi of *fzr-1*, indicating that this control is not conserved in *C. elegans* (Supplementary Figure 5). Thus, although CDK-2/cyclin E may replace CDK-4/CYD-1 function, our data favour a model in which CDK-4/CYD-1 kinase activity is required to counter LIN-35 Rb- and APC/C^{FZR1}-mediated G1 inhibition.

CDK4/6 inhibitor-induced arrest of human cancer cells

Given our results in *C. elegans*, we wondered whether human tumour cells require CDK4/6-cyclin D activity to counteract APC/C^{FZR1}. To test this possibility, we combined

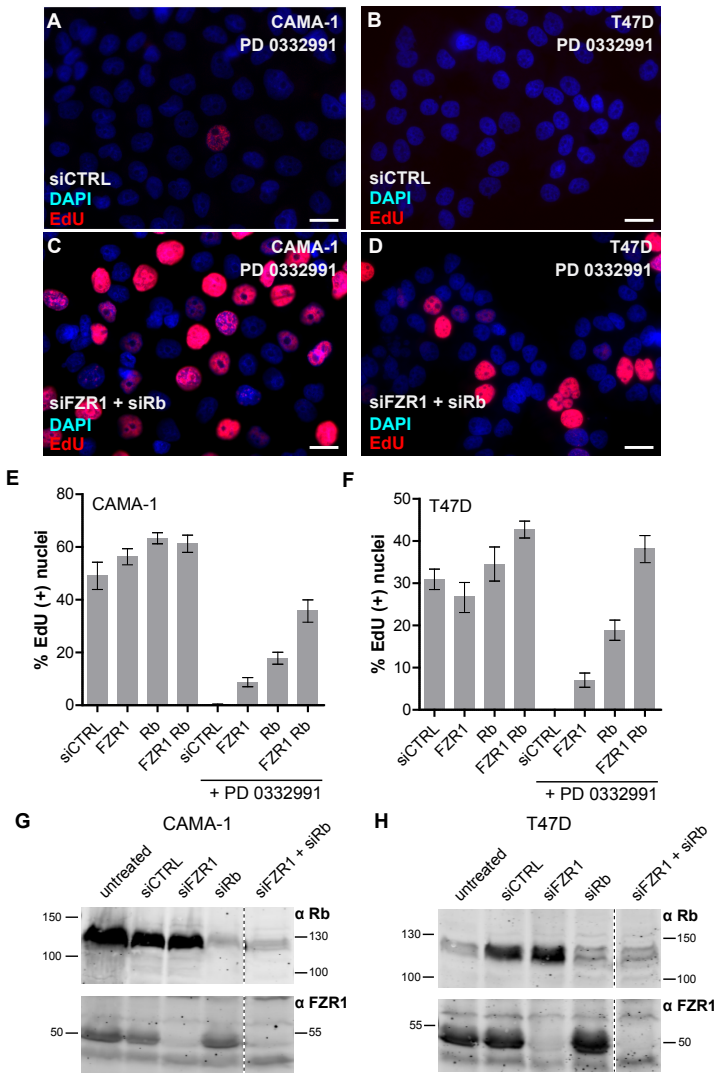

Figure 5. Knockdown of Rb and FZR1 overcomes cell cycle arrest induced by CDK4/6-inhibitor treatment of human breast cancer cell lines. (A–D) Representative immunofluorescence images of a field of CAMA-1 (A,B) and T47D (C,D) cells, following visualization of DNA replication by EdU incorporation and staining, and nuclei with DAPI staining. Cells were first transfected with nonspecific control siRNAs (siCTRL) (A,C), or combined FZR1- and Rb-specific siRNAs (B,D), treated with the CDK4/6 inhibitor PD-0332991 (500 nM) and subsequently incubated with EdU. Scale bar, 10 μm. (E,F) The percentage of EdU-positive nuclei counted for CAMA-1 (E) or T47D (F) cells treated with siRNA pools as indicated, in the absence or presence of PD-0332991 (500 nM). (G–H) Western blottings of CAMA-1 (G) or T47D (h) total cell lysates, following transfection with the indicated siRNA pools. Blots were probed with either anti-Rb or anti-FZR1 antibodies. All aspects of the experiments were performed twice, with similar results.

treatment of human breast cancer cells with the CDK4/6-specific inhibitor PD-0332991 with knockdown of Rb and FZR1. As expected, treatment with 500nM PD-0332991 induced cell division arrest in CAMA-1 luminal type breast cancer cells and T47D ductal mammary carcinoma cells. We examined incorporation of the thymidine analog EdU, which confirmed that the arrested cells lack DNA synthesis, and thus S-phase (Figure 5A,B). Transfection of CAMA-1 and T47D cells with pools of small interfering RNAs (siRNAs) targeting Rb or FZR1 messenger RNA caused substantial downregulation of the corresponding proteins (Figure 5G,H). FZR1 knockdown resulted in limited rescue of the cell cycle arrest induced by PD-0332991 in CAMA-1 and T47D cells (Figure 5E,F). The effect of Rb knockdown was somewhat stronger, but still limited. In contrast, double inhibition of FZR1 and Rb strongly rescued the cell cycle arrest induced by PD-0332991 in both cell-types (Figure 5C–F). These synergistic interactions between Rb and FZR1 closely resemble the observed interactions between cdk-4 CDK4/6, *cyd-1* cyclin D, *lin-35* Rb and *fzr-1* FZR1 in *C. elegans* (Figure 1C,D). Together, our data indicate that not only the mutant or WT status of Rb but also the expression levels of FZR1 and functional activity of the APC/C^{FZR1} E3 ligase will determine how cancer cells respond to CDK4/6 inhibitor treatment.

Discussion

We found that combined inhibition of the Rb transcriptional repressor and the FZR1 APC/C co-activator eliminates the normal requirement for CDK4/6-cyclin D kinase activity in *C. elegans* and human breast cancer cells. In addition, we showed that CDK4-cyclin D phosphorylates FZR1 and Rb at multiple target sites *in vitro*. These phosphorylated residues are present at very similar locations in the *C. elegans* and human Rb and FZR1 proteins. Previous studies have shown that phosphorylation at these sites corresponds to inhibition of human Rb or FZR1 (Lukas *et al.*, 1999; Dick and Rubin, 2013). As CDK4/6-cyclin D kinases are notoriously selective even *in vitro*, these combined observations make FZR1 a candidate novel target for regulation by cyclin D kinase phosphorylation.

FZR1 is a well-known CDK substrate, but previous studies have largely focused on inactivating phosphorylations that occur following the G1/S transition, in particular phosphorylation by CDK2-cyclin A and mitotic CDK1 (Zachariae *et al.*, 1998; Jaspersen *et al.*, 1999; Lukas *et al.*, 1999; Pesin and Orr-Weaver, 2008). Our findings imply that regulation of APC/C^{FZR1} by CDK4/6-cyclin D forms part of the molecular network controlling passage through the G1 restriction point. At least one study in yeast implicated G1-CDKs in the inactivation of APC/C^{Cdh1} (Amon *et al.*, 1994). However, other experiments showed that degradation of at least some of the substrates of APC^{Cdh1} continues into S-phase, and that S-phase cyclins are required for full APC/C^{Cdh1} inactivation (Huang *et al.*, 2001). Based on these data and our own results, we hypothesize that the inactivating phosphorylation of FZR1 may follow a pattern similar to Rb phosphorylation. As such, initial cyclin D kinase phosphorylation might weaken the G1 inhibitory function of APC/C^{FZR1}. Combined with

a simultaneous reduction in Rb-mediated transcriptional repression by CDK4/6-cyclin D phosphorylation, this may allow some induction of CDK2-cyclin E activity. Phosphorylation by CDK2-cyclin E fully inactivates Rb and possibly APC/C^{FZR1}, triggering a positive feedback loop and commitment to S-phase entry. Further experimentation will be needed to test this model, and to explain how association with pseudo-substrate inhibitors, which provide an alternative mechanism for APC/C^{FZR1} inactivation, contributes to this switch.

The observed contribution of FZR1 loss in eliminating CDK4/6-cyclin D requirement could involve a more indirect mechanism. Mutation of Cdh1/Hct1 in yeast or fzr in *Drosophila* allows persistence of mitotic cyclins beyond M phase (Schwab *et al*., 1997; Sigrist and Lehner, 1997). This ectopic cyclin expression triggered S-phase in pheromone-exposed yeast cells and *Drosophila* cells that undergo a final mitosis (Irniger and Nasmyth, 1997; Sigrist and Lehner, 1997). Our EdU incorporation experiments in *C. elegans* did not reveal ectopic S-phases, even when *fzr-1* was strongly inactivated. Moreover, *lin-35(0); fzr-1(he121)* double mutants and *fzr-1* strong loss of function mutants showed normal cyclin B1 (CYB-1) and cyclin B3 (CYB-3) degradation in mitosis. Therefore, we do not expect that persistence of mitotic cyclins is responsible for the *fzr-1* phenotype. The APC/C in association with its other co-activator, FZY-1 (Cdc20), probably retains prolonged activity in the absence of FZR-1 and suffices for mitotic cyclin degradation, as has been observed in human cells (Skaar and Pagano, 2008; Clijsters *et al*., 2013).

As an alternative possibility, premature activation of cyclin E kinase activity could bypass cyclin D-kinase requirement in *lin-35* Rb, *fzr-1* double mutants. Although loss of Rb is likely to lead to de-repression of *cye-1* cyclin E transcription, reduced APC/C^{FZR-1} activity has been reported to alleviate CDK2-cyclin E kinase inhibition in human cells (Bashir *et al*., 2004; Wei *et al*., 2004). The latter effect involves the F-box factor SKP2, which acts as the substrate specificity factor of the E3 ubiquitin ligase SCF. SKP2 is one of the best-characterized targets for APC/C^{FZR1} in human cells. Hence, downregulation of APC/C^{FZR1} activity leads to increased SCF^{SKP2} function, and thereby to degradation of its substrates, the $p21^{Cip1}$ and $p27^{Kip1}$ CDK inhibitors (Bashir *et al*., 2004; Wei *et al*., 2004). The protein expression level of CKI-1, the *C. elegans* homologue of Cip1/Kip1, was increased in *fzr-1* mutants, rather than reduced, compared to WT. This indicates that the link between APC/C^{FZR1} and Cip1/Kip1 regulation is probably not conserved in *C. elegans*. Therefore, we favour the model that LIN-35 Rb and FZR-1 are the two critical targets for inhibitory phosphorylation by the CDK-4/CYD-1 kinase, which when removed allow cyclin D-kinase-independent cell cycle entry.

We cannot exclude that the above-mentioned indirect mechanisms for elimination of CDK4/6-cyclin D requirement contribute to the escape from PD-0332991-induced arrest of human cancer cells following Rb and FZR1 knockdown. Independent of the mechanism, however, it is important to realize that reduced FZR1 levels correspond to reduced sensitivity for CDK4/6-specific inhibitors. At least three different CDK4/6-specific inhibitors are in variouS-phases of clinical trials with human cancer patients (Guha, 2012, 2013; Brower, 2014). Given the promise of these inhibitors in cancer treatment, it will be important to identify which genetic makeup corresponds with sensitivity to, or allows escape from, drug

treatment. Although mutations in FZR1 are not common, the level of FZR1 protein expression and functional activity can be compromised in human cancer (Skaar and Pagano, 2008). Probably reflecting this reduced activity, overexpression of the APC/C^{FZR1} substrate SKP2 has been observed in a subset of human cancers with poor prognosis (Signoretti *et al.*, 2002; Frescas and Pagano, 2008). Future studies should determine whether expression levels of FZR1 or its proteolytic targets such as SKP2 provide prognostic markers for the response of cancer cells to CDK4/6 inhibitor treatment.

Materials and Methods

C. elegans culture

Strains used are described in the Supplementary Table 4. Strains were cultured on Nematode Growth Medium (NGM) plates seeded with *Escherichia coli* OP50 according to standard protocol. All experiments were conducted at 20°C, unless indicated otherwise. Feeding RNAi was performed on NGM plates supplied with 50 mg/ml Ampicillin and 2mM IPTG. Soaking RNAi was performed as previously described (van der Voet *et al.*, 2009), using synchronized L1 larvae obtained by hypochlorite treatment and hatching of eggs in M9 medium with 0.05% Tween-20. L1 larvae were soaked in 10 ml dsRNA solution for 23 h at 20°C, transferred to NGM plates with OP50 and allowed to develop for the appropriate amount of time.

Genetics and whole-genome sequencing

For mutagenesis, L4 animals of strain SV357, *lin-35(n745)/dpy-5(e61) unc-29(e91)* I; *rol-1(e91) cyd-1(he112)/mnC1[dpy-10(e128) unc-52(e444)]* II, were collected in 1ml M9 medium with 0.05% Tween-20, followed by addition of 20 ml of ethyl methane sulfonate and incubation for 6 h at room temperature. The F2 progeny was examined for fertile Rol animals. For genetic mapping of *he121*, we used mutations with visible phenotypes and single-nucleotide polymorphisms in Hawaiian strain CB4856. These experiments placed *he121* to the right of *dpy-10(e128)* and left of *rol-1(e91)*, probably close to position 1 cM on chromosome II. We performed highthroughput next-generation sequencing (SOLid) of three different strains. One was the backcrossed *he121* mutation strain isolated in the screen (SV383), one strain contains the *he121* mutation and homozygous *cdk-4(gv3)*, but no longer carries *cyd-1(he112)* (SV789), and one strain (SV331) was a precursor of the strain used in the mutagenesis. Whole-genome sequencing revealed three missense or nonsense mutations associated with *he121*: mutations in *cdc-14* (II, 1.07 cM), *sra-3* (II, 1.53 cM) and *fzr-1* (II, 1.62 cM). In contrast to *fzr-1*, soaking with dsRNA of *cdc-14*, *sra-3* or the combination did not suppress the *cyd-1(he112)* phenotype. Moreover, through recombination with a *dpy-10(e128) unc-4(e120)* chromosome, we were able to remove the *cdc-14* and *sra-3* mutations but not the *fzr-1* muta-

tion. The resulting *dpy-10(e128) fzr-1(he121) rol-1(e91) cyd-1(he112)* animals (strains SV1303 and SV1304) remained fertile on *lin-35* RNAi plates.

DNA plasmid construction and transgenics

To create the *cdk-4wt::flag* and *cdk-4kd::flag* microparticle bombardment constructs, we cloned a genomic EcoRV fragment containing the entire *cdk-4a* coding region as well as 3,466 bp of upstream and 770 bp of downstream sequences into vector pBluescript SK(+). To add a flag tag, site-directed mutagenesis was used to create an MfeI site at the stop codon (changing CAAGTGA to CAATTGA). A linker containing the flag tag, created by annealing oligonucleotides FLAG tag linker F and FLAG tag linker R was inserted into this MfeI site. For the KD construct, QuickChange site-directed mutagenesis was used to create an Asp/Asn substitution at aminoacid position 187 using primers Asp187Asn F and Asp187Asn R. To generate the final microparticle bombardment constructs, both the WT and KD *cdk-4* constructs were cloned into the *unc-119(wt)* vector pDP#MM016b (Maduro and Pilgrim, 1995). These constructs were subsequently transformed into *unc-119(ed3)* worms by microparticle bombardment (Praitis *et al.*, 2001).

Pmcm-4::mcm-4::mCherry::mcm-4UTR was generated by cloning the *mcm-4::mCherry* insert into the MosScI vector pCFJ178—Ti10882 (IV), followed by single-copy integration into the genome.

To create splitYFP reporters, we generated *myo-3::NLSegl-13::nzYFP* and *myo-3::NLSegl-13::czYFP* constructs. The myo-3 promoter was isolated from pPD93.97 (A. Fire) and cloned into the pCGS1 vector. The nzYFP and czYFP-coding sequences were isolated from T4#712 and T4#713, respectively, and cloned into the pCGS1-*Pmyo-3* vector. A *C. elegans egl-13* nuclear localization signal was placed in frame between promotor and splitYFP DNA sequences. The *myo-3* promoter of *myo-3::NLSegl-13::nzYFP* and *myo-3::NLSegl-13::czYFP* constructs were replaced by the *mcm-4* promoter, which was PCR amplified with primers mcm-4prom F and mcm-4prom R. Upstream ATGs and part of the 50-untranslated region (UTR) were removed from *mcm-4::NLSegl-13::nzYFP* and *mcm-4::NLSegl-13::czYFP*, to obtain higher transgene expression. To construct MosSCI vectors, the *myo-3::nzYFP* and *myo-3::czYFP* were cloned in the vectors pCFJ151-p5605 (II) and pCFJ178—Ti10882 (IV), respectively. *mcm-4::NLSegl-13::czYFPnATG* was cloned in the pCFJ178—Ti10882 (IV) backbone. Integrated transgenic lines were generated as described (Frokjaer-Jensen *et al.*, 2008).

To create *GFP::fzr-1* fosmid WRM0635dH03 (Sourse BioScience) was used as a PCR template for *fzr-1* genomic sequences. PCR fragments of 2.2 kb *fzr-1* promoter sequences, codon-optimized GFP (Redemann *et al.*, 2011) (0.87 kb, a kind gift of the Hyman lab), *fzr-1*-coding genomic sequences (3.4 kb) and *fzr-1* 30-UTR (0.95 kb) were ligated together and cloned into pBluescript. Transgenic lines were generated by microinjection with *myo-2::tdTomato* as a co-injection marker, and strains with a high percentage of transmission as detected by expression of *myo-2::TdTomato* were used for FZR-1 protein expression and localization studies. In *fzr-1* rescue experiments, fosmid WRM0635dH03 was injected, to-

gether with *myo-2::GFP* in strain SV439. Two transgenic lines transmitting the extrachromosomal array were further examined: SV1258 (Line 1) and SV1259 (Line 2).

To create *lin-35::GFP* fosmid WRM063cF08 (Source Bioscience) containing 20 kb upstream and 9.5 kb downstream sequences surrounding *lin-35* was used to generate *lin-35::GFP* with a recombination-based approach described previously (Tursun *et al.*, 2009) . This homologous genetic engineering technique in bacteria allowed us to integrate the GFP tag into a large genomic region of almost 40 kb, probably containing all the native regulatory sequences required for proper *lin-35* expression. To generate *cki-1::gfp*, the GFP tag was integrated into fosmid WRM0611ch10 (Source Bioscience) by using the same recombination technique described above.

To express *C. elegans cdk-4::3xFLAG* and cdk-4KDD187N::3xFLAG in human cells, *cdk-4* was PCR amplified with primers: cdk-4 XhoI_50 F and cdk-4 _1026_HdIII R, and cloned into XhoI and HindIII sites of pBluescript. *The cdk-4_KDD187N* mutation was generated by site-directed mutagenesis with cdk-4KD primer. The 3xFLAG fragment was PCR amplified from the p3xFLAG-myc-CMV-24 expression vector (Sigma) with the primers 3xFLAG_HdIII F and 3xFLAG_PstI R, and cloned behind *cdk-4* and *cdk-4KD* in pBluescript. Both *cdk-4* and *cdk-4KD* were cloned behind the cytomegalovirus (CMV) promoter of pEGFP-N1 (BD Biosciences, GenBank accession code U55762). To express human CDK-4::3xFLAG and CDK-4KDD158N::3xFLAG, plasmids pCMV-Cdk-4-HA and pCMV-Cdk4NFG-HA (Addgene, van den Heuvel (van den Heuvel and Harlow, 1993)) were digested with XhoI and BstXI. A double-stranded G-block oligonucleotide *H.s._cdk-4_FLAG* was ligated into the XhoI/BstXI site, resulting in an in-frame 3xFLAG-tagged construct.

To express *C. elegans* CYD-1 cyclin D in human cells, *cyd-1* complementary DNA was PCR amplified from *pCGSmyo-3::cyd-1* with the following primers: *cyd-1*_1 EcoRI_F and *cyd-1*_1218 SalI_R. The resulting PCR fragment was cloned behind the pCMV promoter of pEGFP N1. Fragments encoding the N or C terminus of *C. elegans* FZR-1 were PCR amplified from a *C. elegans* cDNA library with *fzr-1*_1 SalI-F and *fzr-1*_1197 Not1-R for the N terminus and for the C terminus, *fzr-1*_988 EcoRI-F and *fzr-1*_2107 NotI-R. Subsequently, the PCR fragments were cloned into pGEX 4T-3. For GST-LIN-35, a *lin-35* fragment encoding the extended C-terminal region with the A and B pocket domains was amplified by PCR from a cDNA library with *lin-35*_1486 SmaI-F and *lin-35*_2883_NotIR, and cloned into pGEX 4T-2.

To generate human GST-FZR1 proteins, fzr1 cDNA was PCR amplified from a Homo sapiens cDNA library with fzr1_Hs_EcoRI_1 F and fzr1_Hs_NotI_598 R, and cloned into the EcoRI/NotI sites of pGEX4T-3, resulting in an in-frame GST fusion protein. The constructs were introduced into *E. coli* BL21 and expression was induced with 2mM IPTG for 3 h. The GST fusion proteins were purified by binding to Glutathione Sepharose beads (GE Healthcare).

Immunostaining and antibodies

Immunohistochemical analyzes and staining of DNA with propidium iodide or 40,6-diamidino-2-phenylindole (DAPI) were performed as previously described (van den Heuvel and Kipreos, 2012). EdU labelling and staining were performed according to a protocol using the Click-IT EdU Alexa Fluor 594 kit (Life Technologies) as previously described (Korzelius *et al.*, 2011b; van den Heuvel and Kipreos, 2012). Primary antibodies used for immunofluorescent staining are as follows: mouse anti-CYE-1 (1:150, 17C8, a kind gift of E. Kipreos), mouse anti-AJM-1 (1:20, MH27, Developmental Studies Hybridoma Bank), rabbit anti-CYB-3 (1:100), mouse anti-FZR-1 (1:100, DH01, Thermo Scientific), mouse anti-Rb (1: 1,000, 4H1, Cell Signaling Technology). For anti-FLAG immunopurifications M2 anti-FLAG beads (Sigma) were used. Western blotting was performed as previously described d45, using the following antibodies: rabbit anti-FLAG (1:5,000, F7425, Sigma), rabbit anti-GFP (1:1,000, Invitrogen), mouse anti-Tubulin (1:2000, T9026, Sigma), mouse anti-CYE-1 (1:2,000, 17C8, a kind gift of E. Kipreos), rabbit anti-CYB-3 (affinity purified 1:2,000) (van der Voet *et al.*, 2009). Cell numbers were determined in synchronized animal populations, following fixation with Carnoy's solution and staining of DNA with propidium iodide (van den Heuvel and Kipreos, 2012). No statistical method was used to predetermine sample size; instead, total cell numbers were counted for the indicated tissues in at least ten animals for each genotype. Usually, all available mutant animals were quantified.

Microscopy analysis

Microscopy was performed at 20 °C. Two microscope setups were used: a wide-field immunofluorescence microscope and a spinning disc confocal microscope. The wide-field fluorescence microscope is a Zeis Axioplan2 upright microscope equipped with a HAL 100 halogen visible light source controlled by an internal shutter, an HXP 120 C metal halide fluorescence light source controlled by a Uniblitz VMM-D1 shutter, a X25/0.8 NA imm Corr objective with DIC slider, X 63 and X 100 Plan-APOCHROMAT 1.4 NA objectives with DIC sliders, a DIC polarizer and an Axiocam MRm CCD monochrome camera. The filter turret is equipped with the following Zeiss filter sets: filter set 34 for DAPI (excitation: 390/22 nm band pass, dichroic mirror: 420 nm, emission: 460/50 nm band pass), filter set 13 for GFP (excitation: 470/20 nm band pass, dichroic mirror: 495 nm, emission: 505–530 nm band pass), filter set 46 for YFP (excitation: 500/20nm band pass, dichroic mirror: 515 nm, emission: 535/30 nm band pass), filter set 31 for mCherry (excitation: 565/30 nm band pass, dichroic mirror: 585 nm, emission: 620/60 nm band pass) and a DIC analyzer cube. The microscope and camera are controlled by Zeiss Axiovision 4.x imaging software. Confocal images were obtained with a Zeiss LSM 700 confocal microscope.

Immunoprecipitation and *in vitro* kinase assays

pCMV plasmids expressing *C. elegans* CDK-4::3xFLAG or CDK-4^{KDD187N}::3xFLAG were co-transfected with a pCMV::CYD-1 expression vector in HEK 293T cells (PAA, Pasch-

ing, Austria). Cells were lyzed and immunoprecipitated in CDK-4 buffer (Matsushime *et al.*, 1994) with M2 beads (Sigma). Kinase assays were performed as described by incubation of the immunoprecipitation beads for 30 min at 25 °C, with bacterially produced GST only or GST fused to the *C. elegans* FZR-1 N-terminus (a.a. 1–406), the FZR-1 C-terminus (a.a. 330–702) or the extended pocket region of LIN-35 (a.a. 496–961). The reaction was performed in kinase buffer containing 200 mM ATP, 50mM HEPES at pH 7.5, 10mM $MgCl_2$, 1mM EGTA, 2mM dithiothreitol phosphatase inhibitors (Roche) and 20 µCi [γ-32 P]ATP for radioactive kinase assays. Reactions were terminated by the addition of SDS (4 x sample buffer) (Galli et al., 2011). A similar experiment was performed with human CDK4 and KD CDK4^{D158N}, co-transfected and expressed with cyclin D2. Kinase assays were performed with GST only or GST fused to the *H. sapiens* FZR1 Nterminus (a.a. 1–199). The CDK4/6 inhibitor PD-0332991 was added to a final concentration of 0.9 µM.

Mass spectrometry

The mass spectrometry proteomics data have been deposited to the ProteomeXchange Consortium (Vizcaíno *et al.*, 2014) via the PRIDE partner repository (see accession codes section). Gel lanes (WT and KD) were cut into different bands, which were treated with 6.5mM dithiothreitol for 1 h at 60 °C for reduction and 54 mM iodoacetamide for 30 min for alkylation. The proteins were digested overnight with trypsin at 37 °C. The resulting peptides were extracted with 10% formic acid. The samples were analyzed using a Proxeon Easy-nLC 1000 (Thermo Scientific) connected to a QExactive mass spectrometer (Thermo Scientific). The injected samples were first trapped (Dr Maisch Reprosil C18, 3 µm, 2c m, 100 µm) at a maximum pressure of 600 bar with solvent A (0.1% formic acid in water) before being separated on an analytical column (Agilent Poroshell EC-C18, 2.7 µm, 40 cm, 50 µm) at a stable temperature of 40 °C. Peptides were chromatographically separated by a 90-min gradient from 7% to 30% solvent B (0.1% formic acid in acetonitrile) at a flow rate of 100 nl/min. The column eluent was directly introduced into the electrospray source of the mass spectrometer. The electrospray voltage was set to 1.7 kV using a fused silica capillary (360 µm o.d., 20 µm i.d., 10 µm tip i.d., constructed in-house). The mass spectrometer was used in a data dependent mode, which automatically switched between MS and MS/MS using a Top10 method (higher-energy collision dissociation fragmentation). Alternatively, samples were also analyzed in an Agilent HPLC 1200 series (Agilent) connected to an LTQ Orbitrap Velos (Thermo Scientific) using a data-dependent decision tree as before (Muñoz *et al.*, 2012).

Proteome data analysis

Raw files were processed using Proteome Discoverer 1.4 (version 1.4.1.14, Thermo Scientific). Mascot (Matrix Science, version 2.4) was used as a search engine against a combined database of the human and *E. coli* proteomes in which GST-Frz1 and GST-LIN-35 sequences were added. Carbamidomethylation (C) was set as a fixed modification, and oxida-

tion (M) and phosphorylation (STY) were set as variable modifications. The PhosphoRS 3.0 node was used for the phosphosite localization. Trypsin was specified as enzyme and up to two missed cleavages were allowed. The following parameters were used: 50 p.p.m. for the precursor mass tolerance and 0.05 Da for the fragment ion tolerance (0.5 Da for iontrap data). Data filtering was performed using Percolator, resulting in 1% false discovery rate. Additional filters were applied as follows: search engine rank 1 peptides, minimum of 7 residues per peptide and Mascot ion score above 20. Extracted ion chromatograms were obtained for each phosphopeptide in both the KD and WT kinase (CDK4) experiments. The intensities of all the phosphopeptides containing the same phosphosite(s) were summed (for example, missed cleavages and methionine oxidation) to obtain a total signal in each experiment. The intensities for the different charge states of the same phosphopeptide (for example, 2+, 3+, 4+ and so on) were also summed. When multiple phosphopeptides were identified from the same chromatographic peak, only one value was used for the calculation. Normal peptides (that is, non-phosphopeptides) from FZR1 were used to normalize the data between the two samples.

Cell culture and inhibitor assays

HEK293T cells were cultured in 50% DMEM/50% F10 with L-glutamine (Lonza) supplemented with 10% FCS and antibiotics. Cell transfections were performed with 25 kD linear polyethyleninmine (Polysciences) (van der Vaart *et al.*, 2013). CAMA-1 and T47D cells were cultured in RPMI-1640 medium (Life Technololgies), supplemented with 10% FCS. Cells were seeded on coverslips and transfected for 3 days with 10nM of ON-TARGET plus SMARTpool siRNA (Thermo Scientific) targeting FZR1 and/or RB1, using HiPerFect as previously described, and compared with cells transfected with luciferase-targeting siRNA (Dambournet *et al.*, 2011). The CDK4/6 inhibitor PD 0332991 was added in a concentration of 500 nM in dimethyl sulfoxide for 24 h. The Click-iT EdU Imaging Kit (Life Technologies) assays were performed according to the manufacturer's instructions. Briefly, cells transfected for 3days with siRNA were incubated 7 h with 20mM EdU, fixed, stained using Click-iT EdU Alexa Fluor 594 Imaging Kit and counterstained with DAPI. For quantification, ten independent fields spanning duplicate experiments were imaged for Alexa Fluor 594 and DAPI fluorescence, and counted for EdU nuclear positivity relative to total number of nuclei per field.

Additional information

Accession codes: The mass spectrometry data were deposited in ProteomeXchange with the accession code PXD001501.

Acknowledgements

We thank E. Kipreos, A. Hyman, and A. Pozniakovsky for reagents; A. Thomas for critically reading the manuscript; and members of the van den Heuvel and Boxem groups for help and critical comments. Several strains were provided by the CGC, which is funded by NIH Office of Research Infrastructure Programs (P40 OD010440). This work is part of research program 819.02.016, financed by the Netherlands Organization for Scientific Research (NWO). B.P.B. was supported by a Marie Curie Intra-European Fellowships for Career Development 273872, NWO ALW provided support for TvM (CGDB graduate program grant from NWO H01.205), M.B. (Innovational Research Incentives Scheme VIDI grant 864.09.008) and A.A. (ALW VICI 865.08.002). We acknowledge the PRIDE team for proteomics data dissemination.

Author contributions

I.T. and S.R. contributed to the experimental design, performed most *C. elegans* experiments, analyzed the data, and participated in manuscript preparation. B.P.B. performed and analyzed the experiments with breast cancer cells, with help from A.A. J.M. and A.C. performed the mass spectrometry experiments and data analysis, with help from A.J.R.H. H.X. identified the *he121* allele, J.K. participated in the genetic mapping, M.B.W.P. performed phenotypic characterizations, E.C. contributed whole-genome sequencing and data analysis. T.v.M. assisted with the kinase assays. M.B. participated in the *C. elegans* experiments and provided feedback on the manuscript. S.v.d.H. designed the experiments, assisted with data analysis and prepared the manuscript.

Supporting Information

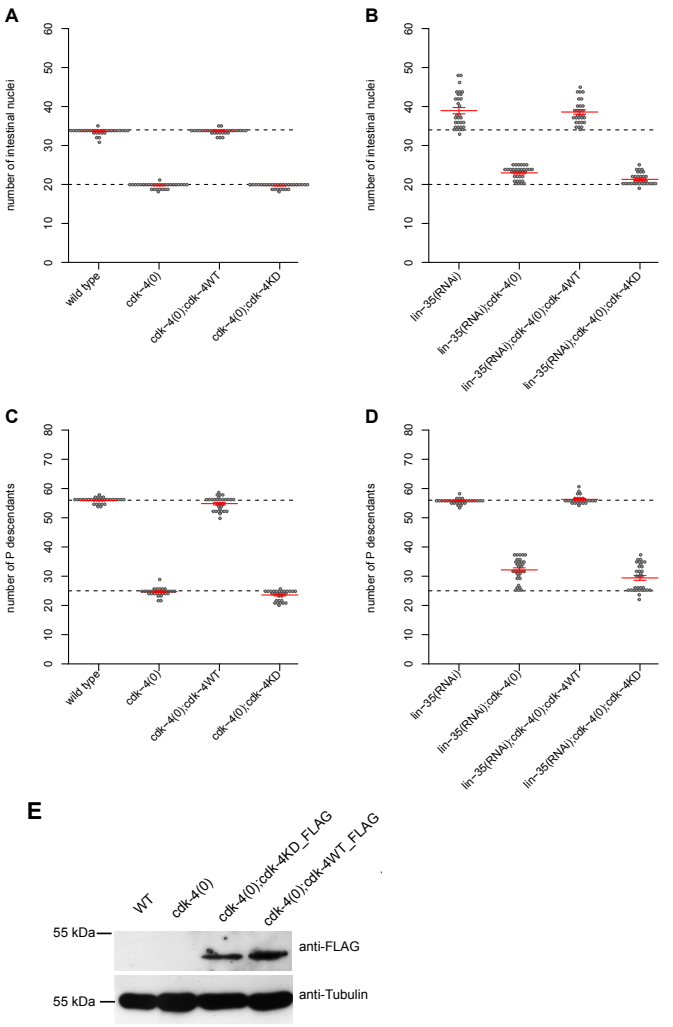

Supplementary Figure 1. Wild-type but not kinase-dead CDK-4 rescues cell division in *cdk-4* mutant animals. (A, B) Quantification of the number of intestinal nuclei for the indicated genotypes in the absence (A) or presence (B) of *lin-35* RNAi. (C, D) Quantification of the number of P cell descendants in the ventral nerve cord for the indicated genotypes, in the absence (C) or presence (D) of *lin-35* RNAi. (E) Western blot demonstrating expression of CDK-4WT-FLAG and CDK-4KD-FLAG. Equal amounts of total protein of the indicated strains were used for immunoprecipitation (IP) with anti-FLAG beads, followed by SDS-PAGE and immunobotting. Blots were probed with anti-FLAG antibodies to detect transgene expressed CDK-4. The anti-tubulin blot illustrates equal amounts of protein used in the IP reactions. The Graphs show mean ± s.e.m.; each dot represents a single animal. Total cell numbers were counted for the indicated tissues in at least 20 animals for each genotype

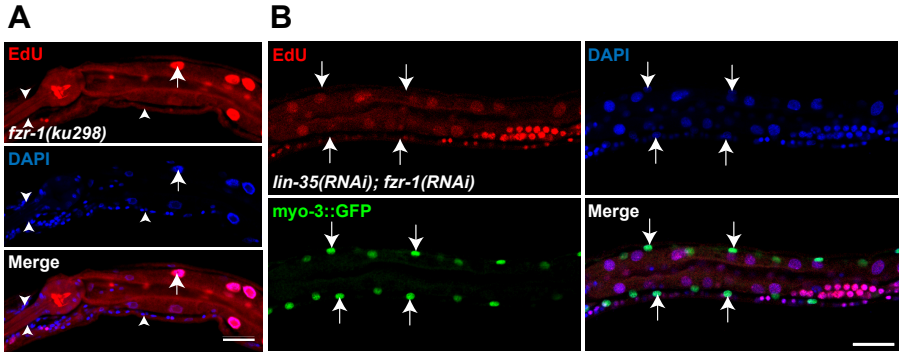

Supplementary Figure 2. Loss of *lin-35* and *fzr-1* does not lead to EdU incorporation in differentiated neurons and muscle cells. (A, B) Representative immunofluorescence images of EdU incorporation and staining experiments. (A) A *fzr-1(ku298)* mutant animal. EdU incorporation is seen in intestinal nuclei (arrow), which undergo endoreplication during larval development. Note that EdU is not incorporated in differentiated neurons in the head region and ventral nerve cord (arrowheads). (B) A *lin-35(RNAi); fzr-1(RNAi)* animal. Note that EdU incorporation is not detected in the body wall muscle cells (arrows) which are visualized by *Pmyo-3::GFP* (green). All stained *fzr-1(ku298)* animals (many) were examined in three independent EdU labeling-staining experiments, staining of *lin-35(RNAi)*; *fzr-1(RNAi)* larvae was performed once, with 28 animals analyzed. Anterior is to the left in all panels. Scale bar, 20 μm.

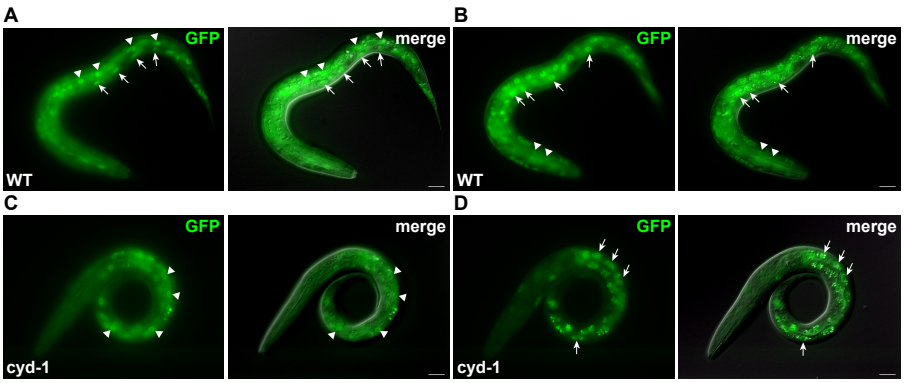

Supplementary Figure 3. GFP::FZR-1 expression in a wild type animal and *cyd-1* mutant larva. (A, B) In the starved L1 larva GFP::FZR-1 can be detected in the hypodermal nuclei (arrowheads in A), P cells (arrows in a), head neurons (arrowheads in B) and intestinal cells (arrows in B). (C, D) In cyd-1 starved L1 larva GFP-FZR-1 is seen in the hypodermal cells (arrowheads in C) and intestinal cells (arrows in D). Dorsal is up in all pictures. The images represent observations of > 20 individual animals in >4 independent experiments for each genotype. Scale bar, 10 μm.

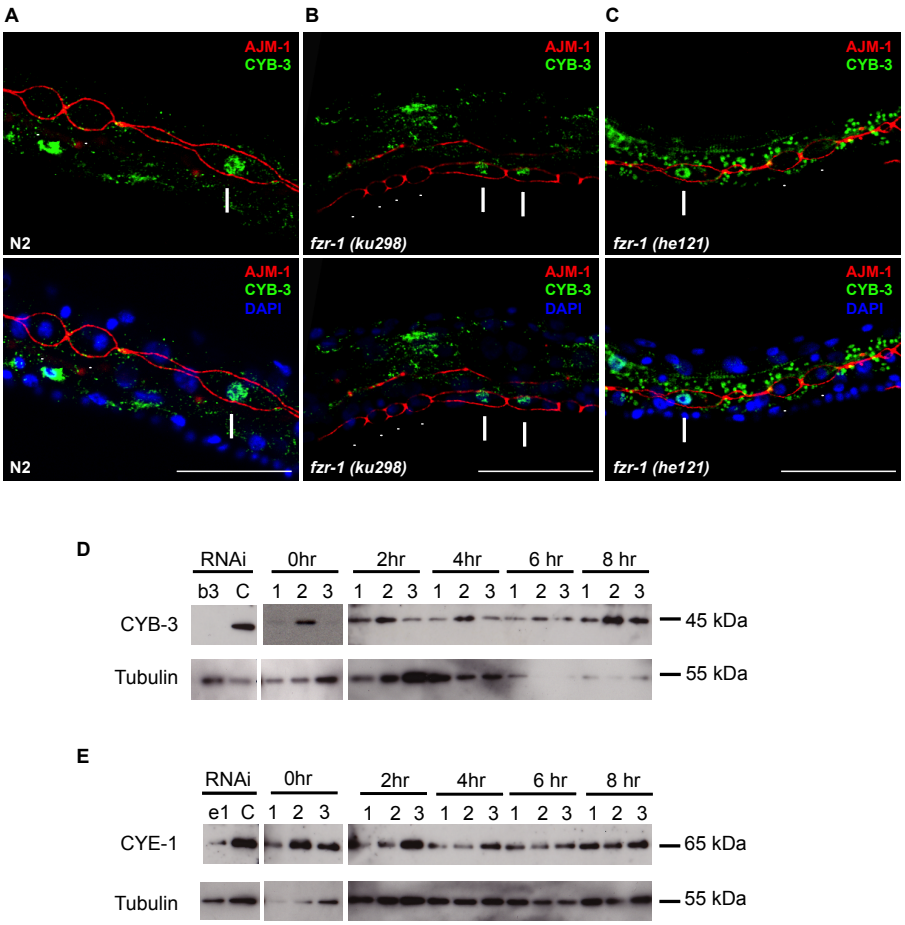

Supplementary Figure 4. Normal degradation of cyclin B3 (CYB-3) in *fzr-1* mutants. (A-C) Representative fluorescence microscopy images, following immunohistochemical analysis of CYB-3 expression in wild-type N2 (A), *fzr-1(ku298)* (B), and *fzr-1(he121)* (C) animals. Epithelial seam cell junctions are visualized with anti-AJM-1 staining, DNA with DAPI. Arrows indicates cells prior to division, in which CYB-3 levels are high. Arrowheads indicate cells that have just divided, in which expression of CYB-3 was not detected. (D, E): Western blot analysis of cyclin levels in C. elegans larvae from 0 to 8 hr of L1 development. (D) Upper panel anti-CYB-3 staining, lower panel anti-Tubulin. (E) Upper panel: anti-CYE-1, lower panel anti-Tubulin. As controls, *C. elegans* were fed with either *cyb-3* dsRNA (D: b3) or *cye-1*dsRNA (E: e1). Total embryo lysates of wild-type (N2, lanes 1), *fzr-1(ku298)* (lanes 2) or *lin-35(n745); fzr-1(he121) cyd-1(he112)* (lanes 3) mutants were immunoblotted and incubated with the indicated antibodies. Immunostaining and immuoblotting experiments were performed twice. All successfully stained animals with mitotic cells (n=5, n=8) were examined. Scale bar, 20 μm.

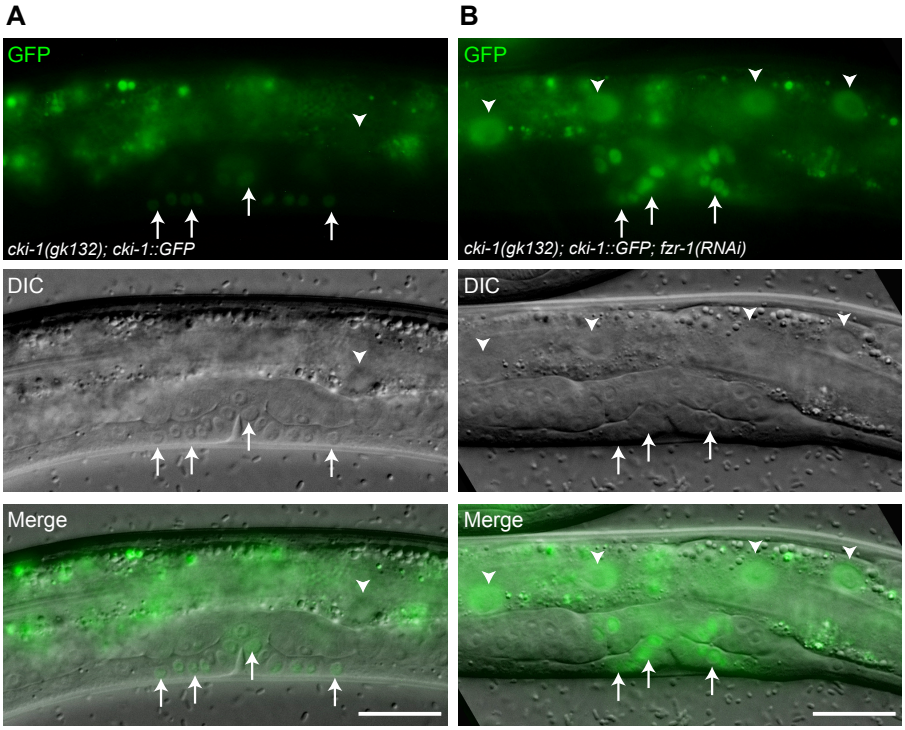

Supplementary Figure 5. CKI-1::GFP expression increases following *fzr-1* RNAi. (A,B) Representative fluorescence microscopy images of *cki-1*(0) L3 larvae expressing CKI-1::GFP from a fosmid-based transgene. The animal in (B) was treated with *fzr-1* RNAi. Note the increased CKI-1::GFP expression in the vulval cells (arrows) and intestinal nuclei (arrowheads). The experiment was repeated twice, each time > 20 animals were examined for each condition. Scale bar, 20 μm.

Supplementary Table 1. Fosmid rescue of *fzr-1(he121)* as detected by reversion of *lin-35; he121 cyd-1* fertility and normal development.

	Rol animals	% fertile	% non-fertile	% wt vulva	% no vulva	% abnormal vulva	% n.d.
Line 1 (n=110)	GFP+ (n=63)	1.6	98.4	0	70	17.4	12.7
	GFP- (n=47)	100	0	100	0	0	0
Line 2 (n=141)	GFP+ (n=60)	0	100	0	73.3	23.3	3.3
	GFP- (n=81)	96.3	3.7	60.5	0	1.2	38.3

Examination of Rol progeny from two balanced lines containing an extrachromosomal array with *myo-2::GFP* and a fosmid containing the *fzr-1* genomic region. Loss of fertility and normal development of lin-35(RNAi); rol-1 he121 cyd-1 offspring correlates strongly with the presence of the extrachromosomal array. Animals with a wild-type vulva, no vulva, or abnormal vulva (often protruding) are shown as percentages of the number of animals with or without pharyngeal GFP expression (indicating inheritance of the array). n.d.: % of animals not analyzed for the vulval phenotype.

Supplementary Table 2. Soaking RNAi of *fzr-1* rescues the fertility of *lin-35; cyd-1* animals

concentration *fzr-1(RNAi)* (ng per µl)	**# fertile F1**	**# F2 progeny**
no RNAi	0	n.a.
50	3	20
		6
		6
500	2	23
		6
1000	1	17
2000	1	24

For each concentration 6 animals were tested. The number of fertile F1 is indicated and for each fertile animal the number of viable F2 progeny.

Supplementary Table 3. Quantitative MS analysis of LIN-35, FZR-1 and FZR1 phosphorylation levels in kinase assays

***C.elegans* LIN35 SEQUENCE**	SITE	CDK-4/ CYD-1 WT	CDK-4 Kinase dead/CYD-1	Ratio CDK-4 WT/KD
LNSYSPIKFTPIK	S714	9,72 x 10^6	Not Detected	Infinite
LNSYSPIKFTPIK	T719	6,89 x 10^6	Not Detected	Infinite
LNSYSPIKFTPIK	S714, T719	1,8 x 10^6	Not Detected	Infinite
***C.elegans* FZR1 SEQUENCE**	SITE	CDK-4/ CYD-1 WT	CDK-4 Kinase dead/CYD-1	Ratio CDK-4 WT/KD
TLGPHNSPVKSMSTNSSAHTSPR	S31	9,41 x10^9	1,72 x 10^8	54,7
TLGPHNSPVKSMSTNSSAHTSPR	S31/S45	6,51 x10^7	Not Detected	Infinite
SMSTNSSAHTSPRVTPTK	T49	4,27 x10^8	6,41 x 10^6	66,5
SMSTNSSAHTSPRVTPTK	S45/T49	2,17 x10^9	9,64 x10^5	2253,5
SMSTNSSAHTSPRVTPTK	S41/S45/T49	1,17 x10^8	Not Detected	Infinite
SMSTNSSAHTSPR	S45	2,38 x10^7	5,58 x10^5	42,6
YHSINSDDDSGFK	S77	3,83 x10^5	Not Detected	Infinite
ISGAESPTMAQMMEPR	S275	2,35 x10^9	3,21 x10^6	733,8
APPPALPLSPIVQK	S320	2,67 x10^7	Not Detected	Infinite
APPPALPLSPIVQKQSPAR	S320/S327	2,16 x10^7	Not Detected	Infinite
SLFTYSAKTTPVK	S336/T340	2,25 x10^8	Not Detected	Infinite
SLFTYSAKTTPVK	T340	2,62 x10^7	Not Detected	Infinite
SLFTYSAK	Y335	3,65 x10^7	2,79 x10^6	13,1
YGGQATTTATSPFGGPFGVDSQR	S354	3,84 x10^6	Not Detected	Infinite
HUMAN FZR1 SEQUENCE	SITE	Cdk4/Cyd2 WT	Cdk4 Kinase dead/Cyd2	Ratio CDK-4 WT/KD
GSPNSMDQDYER	"-S4"	6,76 x10^5	1,46 x10^5	4,62
GSPNSMDQDYER	Y5	1,89 x10^6	3,62 x10^6	0,52
TLTPASSPVSSPSK	T32	2,35 x10^7	6,24 x10^6	3,77
TLTPASSPVSSPSK	S36	3,66 x10^7	8,00 x10^6	4,59
TLTPASSPVSSPSK	S40	1,06 x10^7	3,17 x10^6	3,35
SSPDDGNDVSPYSLSPVSNK	S149	8,61 x10^5	1,08 x10^6	0,79
SSPDDGNDVSPYSLSPVSNK	S151	4,54 x10^6	Not detected	Infinite
SSPDDGNDVSPYSLSPVSNKSQK	S157	1,59 x10^6	1,66 x10^6	0,95

Phosphopeptides from LIN-35 and FZR1 were identified by LC-MS/MS. Extracted ion chromatograms (AREAS) were obtained for each phosphopeptide in both the kinase dead and wild type (CDK4/CYD1) experiments. The intensities of all the phosphopeptides containing the same phosphosite(s) were summed to obtain a total signal in each experiment. The intensities for the different charge states of the same phosphopeptide (e.g. 2+, 3+, 4+...) were also summed.

Supplementary Table 4. Strains used in this study	
EMS mutagenesis	
SV35:	*lin-35(n745)/dpy-5(e61) unc-29(e91) I; rol-1(e91) cyd-1(he112)/mnC1[dpy-10(e128) unc-52(e444)] II*
whole genome sequencing	
SV331	*lin-35(n745) I; rol-1(e91) cyd-1(he112)/mnC1[dpy-10(e128) unc-52(e444)] II; lin-15(n767) X*
SV383	*lin-35(n745) I; rol-1(e91) he121 cyd-1(he112) II*
SV789	*he121 rol-1(e91) II; cdk-4(gv3) IV*
cdk-4 rescue experiments	
SV913	*cdk-4(gv3) X/+; he Is22 [Pcdk-4::cdk-4KD:: flag::cdk-4 3'UTR]*
SV916	*cdk-4/+ X*
SV929	*unc-119(ed3) III; cdk-4(gv-3)X; vmIs9[unc-119; Pcdk-4::cdk-4::flag::cdk-4 3'UTR]*
brood size	
SV314	*rol-1(e91) cyd-1(he112)/mnC1[dpy-10(e128) unc-52(e444)] II*
SV216	*lin-35(n745) I*
SV1444	*lin-35(n2239) I*
SV439	*fzr-1(he121) rol-1(e91) cyd-1(he112)/mnC1[dpy-10(e128) unc-52(e444)] II*
SV981	*lin-35(n2239) I; fzr-1(he121) rol-1(e91) cyd-1(he112)II*
SV1303	*dpy-10 (e128) fzr-1(he121) rol-1(e91) cyd-1(he112) II*
SV1304	*dpy-10 (e 128) fzr-1(he121) rol-1(e91) cyd-1(he112) II*
SV789	*he121 rol-1(e91) II; cdk-4(gv3) X on lin-35(RNAi)*
fzr-1(RNAi) soaking	
SV1231	*lin-35; rol-1 cyd-1/mnC1; heSi45[Pmcm-4::mcm-4::mCherry::mcm-4 3'UTR; unc-119+] IV*
fzr-1 fosmid expression	
SV1258	*fzr-1(he121) rol-1(e91) cyd-1(he112)/mnC1; heEx427[fosmid WRM0635dH03; Pmyo-2::gfp]*
SV1259	*fzr-1(he121) rol-1(e91) cyd-1(he112)/mnC1; heEx428[fosmid WRM0635dH03; Pmyo-2::gfp]*
egfp::fzr-1, lin-35::gfp and cki-1::gfp	
SV1430	*fzr-1(ku298) unc-4(e120) II; heEx505[Plin-48::TdTomato; Pfzr-1::mEGFP::fzr-1::fzr-1 3'UTR]*
SV1454	*rol-1(e91) cyd-1(he112)/mIn1; heEx505[Plin-48::TdTomato; Pfzr-1::mEGFP::fzr-1::fzr-1 3'UTR]*
SV1269	*unc-119(ed3) III; heSi45[Pmcm-4::mcm-4::mCherry] IV; heEx510[Plin-35::lin-35::GFP on fosmid wrm063cf08]*
SV1275	*cki-1(gk132); heEx512[Pcki-1::cki-1::GFP on fosmid WRM0611ch10 ; Plin-48::TdTomato]*
S-phase reporter lines	
SV1067	*unc-119(ed3) III; heSi45[Pmcm-4::mcm-4::mCherry::mcm-4 3'UTR; unc-119+] IV*
SV1263	*lin-35 (n745)/dpy-5(e61) unc-29 (e403); heSi73[Pmyo-3:: NLSegl-13::nzyfp] II; heSi74[Pmcm-4:: NLSegl-13::czyfp] IV; lin-15A(n767) X*
SV1175	*fzr-1(ku298) unc-4(e120) II; unc-119(ed3) III; heSi45[Pmcm-4::mcm-4::mCherry::mcm-4 3'UTR; unc-119+] IV*
SV859	*heIs11[myo-3::H2B::GFP]*
Cyclin antibodies staining and immunoblots	
MH1829	*fzr-1(ku298) unc-4(e120) II*
SV981	*lin-35(n2239) I; fzr-1(he121) rol-1(e91) cyd-1(he112) II*

Chapter 4

Caenorhabditis elegans Cyclin D/CDK4 and Cyclin E/CDK2 induce distinct cell cycle re-entry programs in differentiated muscle cells

Jerome Korzelius[1], Inge The[1], **Suzan Ruijtenberg**[1], Martine B. W. Prinsen[1], Vincent Portegijs[1], Teije C. Middelkoop[1], Marian J. Groot Koerkamp[2], Frank C. P. Holstege[2], Mike Boxem[1] & Sander van den Heuvel[1]

An adapted version of this manuscript has been published in *Plos Genetics*, 2011

1. Developmental Biology, Faculty of Sciences, Department of Biology, Utrecht University, Padualaan 8, 3584 CH Utrecht, The Netherlands. **2.** Molecular Cancer Research, University Medical Center Utrecht, Universiteitsweg 100, 3584 CG Utrecht, The Netherlands.

Abstract

Cell proliferation and differentiation are regulated in a highly coordinated and inverse manner during development and tissue homeostasis. Terminal differentiation usually coincides with cell cycle exit and is thought to engage stable transcriptional repression of cell cycle genes. Here, we examine the robustness of the post-mitotic state, using *Caenorhabditis elegans* muscle cells as a model. We found that expression of a G1 Cyclin and CDK initiates cell cycle re-entry in muscle cells without interfering with the differentiated state. Cyclin D/CDK4 (CYD-1/CDK-4) expression was sufficient to induce DNA synthesis in muscle cells, in contrast to Cyclin E/CDK2 (CYE-1/CDK-2), which triggered mitotic events. Tissue-specific gene-expression profiling and single molecule FISH experiments revealed that Cyclin D and E kinases activate an extensive and overlapping set of cell cycle genes in muscle, yet failed to induce some key activators of G1/S progression. Surprisingly, CYD-1/CDK-4 also induced an additional set of genes primarily associated with growth and metabolism, which were not activated by CYE-1/CDK-2. Moreover, CYD-1/CDK-4 expression also down regulated a large number of genes enriched for catabolic functions. These results highlight distinct functions for the two G1 Cyclin/CDK complexes and reveal a previously unknown activity of Cyclin D/CDK-4 in regulating metabolic gene expression. Furthermore, our data demonstrate that many cell cycle genes can still be transcriptionally induced in post-mitotic muscle cells, while maintenance of the post-mitotic state might depend on stable repression of a limited number of critical cell cycle regulators.

Introduction

During the terminal stages of differentiation, cells usually arrest proliferation and permanently exit the division cycle. Insight in how this post-mitotic state is established and maintained is of both fundamental and clinical importance. Entry into the cell cycle requires activation of Cyclin Dependent Kinases (CDKs) in the G1 phase of the cell cycle. These kinases promote expression of cell cycle genes that are controlled by E2F/DP (together named "E2F") transcription factors (for review: van den Heuvel and Dyson, 2008). CDK inhibitors (CKIs), such as $p21^{Cip1}$ and $p27^{Kip1}$, counteract cell cycle entry through association with Cyclin/CDK complexes and inhibition of their activity. In addition, members of the retinoblastoma protein (pRb) family inhibit cell cycle entry through repression of E2F-regulated cell cycle genes (Cobrinik, 2005). When activated in the G1 phase, Cyclin D/CDK4(6) and Cyclin E/CDK2 kinases phosphorylate pRb, which prevents its association with E2F and allows activating E2F transcription factors to induce S-phase gene expression. Differentiation signals are thought to induce cell cycle arrest through activation of negative regulators of G1 progression, probably in parallel with chromatin remodeling and modification complexes that induce stable repression of cell cycle genes (Jacobs *et al.*, 1999; Blais *et al.*, 2007; Buttitta and Edgar, 2007).

Only a few examples have been reported of post-mitotic cells that re-enter the cell cycle while maintaining the differentiated state. In *Drosophila*, expression of E2F together with the Cdc25c phosphatase String or Cyclin E/CDK2 induces continued division of differentiated cells during eye and wing development (Buttitta *et al.*, 2007). In mammals, loss of the pRb tumor suppressor allows proliferation of certain terminally differentiated cells, such as the post-mitotic hair cells of the mouse inner ear (Sage *et al.*, 2005). In addition, inactivation of pRb family members can result in the development of retinoblastoma or related tumors from fully differentiated neurons (Ajioka *et al.*, 2007; Xu *et al.*, 2009). Thus, at least some terminally differentiated cells that are normally arrested can be induced to initiate cell proliferation with no apparent dedifferentiation.

In this study, we use the nematode *C. elegans* to examine the cell cycle arrest associated with terminal differentiation. *C. elegans* shows a tight inverse relationship between proliferation and differentiation, and a highly reproducible pattern of terminal differentiation (Sulston and Horvitz, 1977; Sulston and Schierenberg, 1983). Except for 55 'blast' cells, all cells differentiate and become post-mitotic before embryonic development completes. The single Cyclin D (*cyd-1*) and CDK4/6 (*cdk-4*) genes are essential for G1/S progression in postembryonic development (Park and Krause, 1999; Boxem and van den Heuvel, 2001), while the single Rb-family member, *lin-35*, and the *cki-1* and *cki-2* Cip/Kip inhibitors act as negative regulators of cell cycle entry (Hong *et al.*, 1998; Lu and Horvitz, 1998; Boxem and van den Heuvel, 2001, 2002; Saito *et al.*, 2004; Buck *et al.*, 2009). Notably, *lin-35* Rb inactivation combined with *cki-1*/*cki-2* inhibition causes only limited over-proliferation in blast-cell lineages (Boxem and van den Heuvel, 2001), JK and SvdH, unpublished observations). Thus, in *C. elegans*, cell cycle exit can occur without a functional pRb family protein, as was recently also observed in mice (Wirt *et al.*, 2010).

Here, we examine to what extent terminally differentiated *C. elegans* body-wall muscle cells respond to, or resist, cell cycle inducing signals. Expression of G1 Cyclin/CDK combinations triggered expression of S-phase genes and partial cell cycle re-entry in differentiated muscle cells, while not interfering with the differentiation status. Tissue-specific transcriptional profiling and single molecule FISH experiments revealed that CYD-1/CDK-4 and CYE-1/CDK-2 induce a substantial and overlapping set of genes that are strongly associated with cell cycle functions. However, CYD-1/CDK-4 also triggered up-regulation or downregulation of large numbers of genes with metabolism-associated functions, and induced DNA replication, in contrast to CYE-1/CDK-2. Notably, several key G1/S regulators, such as *cye-1*, *cdc-25.1*, and *cdk-2*, were not induced by CYD-1/CDK-4. Thus, differentiated muscle cells remain remarkably flexible for cell cycle induction, while at the same time, robust repression of a few key regulators appears to maintain a stable post-mitotic state.

Results

G1 Cyclin/CDK induction overcomes cell cycle quiescence

We set out to examine if cell cycle entry can be induced by transcriptional induction of single G1 Cyclins (CYD-1 Cyclin D or CYE-1 Cyclin E), CDKs (CDK-4, CDK-2, or CDK-2AF, a mutated form of CDK-2 that lacks the negative Tyr14 and Thr15 phosphorylation sites), or combined expression of CYD-1/CDK-4, CYE-1/CDK-2 or CYE-1/CDK-2AF. We first examined the effects of G1 Cyclin/CDK transgene expression in cells that are temporarily arrested (quiescent) but not terminally differentiated. In wild-type larvae that hatch from the egg, precursor cells of the post-embryonic lineages remain quiescent under starvation conditions. When food is added, development resumes and postembryonic blast cells initiate proliferation (Hong *et al.*, 1998). Expression of any of the three Cyclin/CDK combinations from the intestinespecific *elt-2* promoter prevented the normal cell cycle arrest in the intestine of late embryonic and starved L1 animals (see Figure S1). Based on BrdU incorporation, DNA replication continued in starvation-arrested larvae with intestinal Cyclin/CDK expression (Figure S1D). The number of intestinal nuclei in these starved L1 animals regularly exceeded the maximal number of 34 nuclei in normal adults (Figure S1B and S1F). Expression of either CYD-1 or CYE-1 alone was sufficient to trigger nuclear division and DNA replication, whereas CDK expression alone did not induce an apparent cell cycle response (Figure S1E and S1F, and data not shown). This probably indicates that the temporally arrested cells contain residual CDK proteins, but not G1 Cyclins. We conclude that transcriptional induction of a G1 Cyclin is sufficient to prevent cell cycle quiescence of intestinal cells.

Cyclin/CDK expression in muscle leads to cell cycle re-entry during larval development

Next, we examined if G1 Cyclin/CDK expression could trigger cell cycle re-entry in terminally differentiated body-wall muscle. The *C. elegans* larva is born with 81 fully differentiated body-wall muscle cells (Sulston and Horvitz, 1977). We chose the *myo-3* promoter (*Pmyo-3*) to drive expression of Cyclins and CDKs in muscle, as the muscle myosin gene *myo-3* is turned on in post-mitotic embryonic body-wall muscle (Fire and Waterston, 1989; Fox *et al.*, 2007). When expressed from this promoter, CYE-1 and CDK-2AF showed muscle-specific expression in immunostaining, and complex formation in immunoprecipitation/western blotting experiments (Figure S2). Next, we introduced the different Cyclin/CDK combinations together with a reporter construct, *Pmyo-3::GFP::H2B*, to facilitate the detection of muscle nuclei, and generated strains with integrated arrays to avoid mosaic expression (Figure 1A).

In contrast to our findings in the intestine, animals expressing any of the three Cyclin/CDK combinations in muscle hatched with a normal complement of muscle nuclei

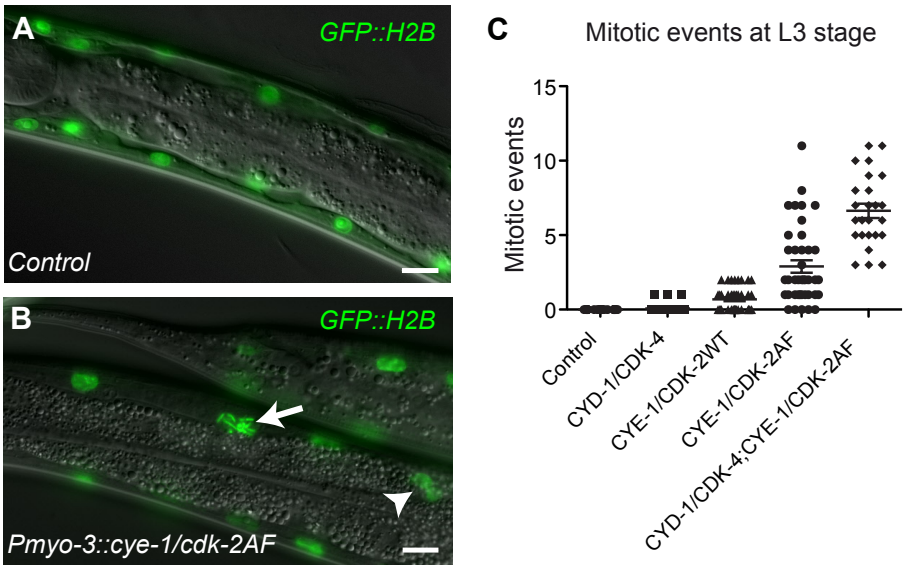

Figure 1. G1 Cyclin/CDK expression induces mitotic events in body-wall muscle cells. (A) Control animal expressing the GFP::H2B fusion protein in body-wall muscle. (B) Animals that express CYE-1, CDK-2AF and GFP::H2B together from the *myo-3* promoter show chromosome condensation (arrow) and nuclear division (arrowhead) in differentiated body-wall muscle. (C) Quantification of mitotic events for each Cyclin/CDK combination at the L3 stage. Each dot represents the number of mitotic muscle nuclei (with condensed DNA, metaphase or anaphase figures or nuclear division) in a single animal. In each animal, 58 muscle nuclei anterior of the prospective vulva were counted, to exclude muscle cells formed during post-embryonic development in the Mesoblast lineage. The highest mitotic index was 12% (7/58) in the strain with both Cyclin/CDKs. Error bars represent s.e.m.

(Figure S3A and S3B). Thus, *Pmyo-3*-driven Cyclin/CDK expression does not lead to extra muscle cell division during embryogenesis. However, from the L2 stage onwards, some body-wall muscle cells started to show signs of mitosis, including chromosome condensation, chromosome congression, anaphase and nuclear division, sometimes even resulting in clusters of small nuclei (Figure 1B; Figure S3C-S3E). In contrast to quiescent intestinal cells, expression of CYD-1 or CYE-1 alone did not induce mitotic events in differentiated muscle cells. CYE-1/CDK-2AF was much more efficient in inducing mitotic events than CYD-1/CDK-4, while CYE-1/CDK-2WT expression gave an intermediate effect (Figure 1C). Western blotting experiments indicated that the extent of mitotic induction did not correspond to the protein expression level, but rather the type of CDK (and Cyclin) expressed (Figure S4). The combination of CYD-1/CDK-4 and CYE-1/CDK-2AF caused the strongest mitotic induction (Figure 1C).

We looked for additional indications of cell cycle re-entry in body-wall muscle cells. Staining for the mitosisspecific phospho-histone H3S10 epitope readily visualized mitotic nuclei in the body-wall muscle of CYE-1/CDK-2AF animals (Figure 2A and 2B). Moreover, we observed expression of S-phase reporters in muscle cells. One of these reporters uses the *rnr-1* ribonucleotide reductase promoter to express tdTomato in frame with a destruction box-containing N-terminal CYB-1 Cyclin B fragment (Korzelius *et al.*, 2011). In addition, we used a transgenic strain with a single-copy translational fusion of *C. elegans MCM-4::mCherry* under its native promoter. Both reporters were completely silent in body-wall muscle of normal larvae. In contrast, MCM-4::mCherry was detectable as early as the L1 stage in all body-wall muscle cells of CYD-1/CDK-4 and CYE-1/CDK-2AF-expressing animals (Figure 2C and 2D, and data not shown). Expression of *rnr-1::CYB-1desBox::tdTomato* became detectable from the L2 stage onward, and even remained detectable in the muscle of adult animals.

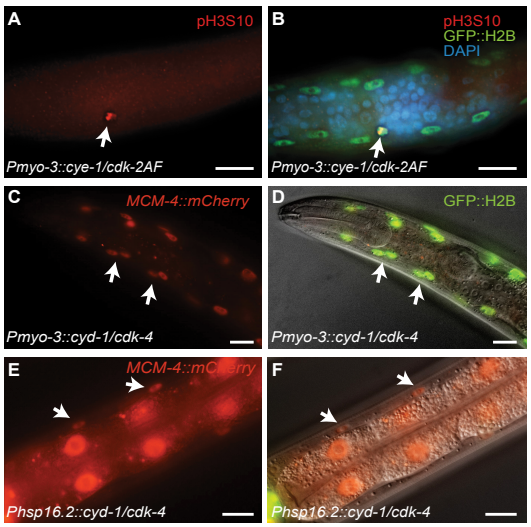

Figure 2. G1 Cyclin/CDK expression induces S and M phase markers in larval muscle. (A,B) A body-wall muscle cell expressing CYE-1/CDK-2AF stains positive for the mitosis-specific phospho-histone H3S10 epitope (arrow). (C,D) Expression of the S-phase marker *Pmcm-4::MCM-4::mCherry* (MCM4) in all body-wall muscle cells of an adult animal expressing CYD-1/CDK-4 from the *myo-3* promoter. (D) merged image of MCM-4::mCherry, GFP::H2B and DIC. (E,F) Expression of the *Pmcm-4::MCM-4::mCherry* S-phase marker in an L4 animal after heat-shockinduced expression of CYD-1/CDK-4 at the L2/L3 stage. (F) merged image of MCM-4::mCherry and DIC. Arrows point to muscle nuclei, scale bars indicate 10 µm.

Importantly, heat-shock promoter driven expression of CYD-1 and CDK-4 during larval development also induced S-phase reporter gene expression. After heat-shock, we observed MCM-4::mCherry expression in the body-wall muscle of *hsp-16.2::CYD-1/hsp-16.2::CDK-4* transgenic strains (Figure 2E and 2F; in 3 of 3 strains), but never in control heat-shock treated animals without the Cyclin/CDK transgenes (n= 50 animals examined). Even adult animals showed MCM-4 expression after heat-shock induction of CYD-1 and CDK-4, further illustrating that the S-phase reporter could be turned on after terminal differentiation. Together, these results indicate that at least some cell cycle genes are not irreversibly silenced in post-mitotic muscle cells.

C. elegans Cyclin D/CDK-4, but not Cyclin E/CDK-2, induces S-phase in muscle cells

Next, we tested if G1 Cyclin/CDK expression is sufficient for induction of DNA replication in differentiated muscle cells. We used two independent methods to detect DNA synthesis. First, we examined incorporation of EdU, a thymidine analogue that can be used to visualize DNA replication in combination with antibody staining of muscle nuclei (Salic and Mitchison, 2008; Korzelius *et al.*, 2011). We stained L4 animals for both EdU and GFP and analyzed muscle cells anterior of the vulva, to exclude muscles formed in the postembryonic Mesoblast lineage. To our surprise, only in 2 out of 35 CYE-1/CDK-2AF expressing animals EdU incorporation was detectable in a few muscle cells, while all other

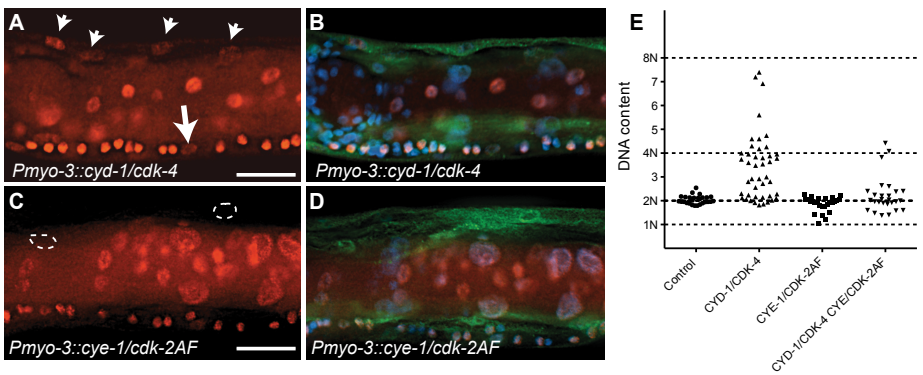

Figure 3. C. elegans Cyclin D/CDK-4 induces DNA replication in muscle. (A-D) Detection of EdU incorporation in body-wall muscle nuclei. (A,C) EdU staining, (B,D) merged image of EdU, GFP and DAPI staining. EdU-positive nuclei are readily detectable in CYD-1/CDK-4 expressing body-wall muscle (A, arrowheads), but not in CYE-1/CDK-2AF expressing body-wall muscle (C, circles). For comparison, the arrow in (A) indicates a Pn.p cell, which completed one round of DNA replication in the presence of EdU. (E) Quantitative determination of DNA content reveals DNA replication in CYD-1/CDK-4 expressing muscle cells. Each dot indicates the DNA content, based on propidium iodide staining, of a single body-wall muscle nucleus. Pn.p nuclei in the ventral cord were used as 2n controls. L3/L4 stage larvae were stained in A-D, GFP staining reveals muscle expressed GFP::H2B and CDK-2/4::Venus.

muscle nuclei were completely EdU negative (Figure 3C and 3D, circles). In contrast, the anterior of more than half (19/35) of the CYD-1/CDK-4 animals contained clearly EdU positive body-wall muscle cells (Figure 3A and 3B, arrowheads).

Quantitative determination of DNA content based on propidium iodide (PI) intercalation confirmed and expanded these results (Figure 3E). While body-wall muscle in the *Pmyo-3::H2B::GFP* control strain showed a G1 DNA content (2n), muscle cells with CYD-1/CDK-4 expression often contained a larger amount of DNA, which corresponded to a partly or completely duplicated genome (4n). CYE-1/CDK-2 expressing muscle cells did not contain more than 2n DNA, and very few muscle cells with combined expression of CYD-1/CDK-4 and CYE-1/CDK-2 contained 4n DNA (Figure 3E). Thus, CYD-1/CDK-4 promotes DNA replication, while CYE-1/CDK-2 even appears to inhibit induction of DNA synthesis by CYD-1/CDK-4. Together, CYE-1/CDK-2AF expression in differentiated muscle triggers S-phase gene expression and mitosis, but not DNA replication, while the CYD-1/CDK-4 combination induces a more normal cell cycle that includes DNA replication in S phase, but usually arrests prior to M-phase.

Activation of a cell-cycle transcriptional program without loss of muscle differentiation

Our combined data indicate that differentiated body-wall muscle cells can re-enter the cell cycle post-embryonically in response to G1 Cyclin/CDK expression. Next, we wanted to examine if the observed cell cycle re-entry coincides with loss of muscle differentiation. Animals expressing G1 Cyclin/CDK complexes in the body-wall muscle appear phenotypically normal and show apparently normal sinusoidal movement (Figure 4C). To examine muscle structure, we stained animals for UNC-15/Paramyosin, a component of thick muscle filaments in *C. elegans* (Moerman and Williams, 2006). Muscle cells in L4 and adult CYE-1/CDK-2AF animals displayed a normal pattern of thick muscle filaments, even when nuclei with clear mitotic figures were present (Figure 4A and 4B). These data support the idea that CYE-1/CDK-2AF expression does not change muscle structure and function.

To obtain a more comprehensive picture of the changes induced by CYD-1/CDK-4 and CYE-1/CDK-2AF expression, we performed tissue-specific mRNA profiling of body-wall muscles. Key to this approach is muscle-specific expression of a FLAG-tagged PAB-1 poly(A)-binding protein (Roy *et al.*, 2002). As a validation of the method, immunopurification of PAB-1-crosslinked mRNA from *Pmyo-3::FLAG::PAB-1* transgenic animals yielded mRNAs that were highly enriched for muscle-expressed genes (Table S1). We next compared the mRNA profiles of control L1 animals (carrying the *Pmyo-3::GFP::H2B* and *Pmyo-3::FLAG::PAB-1* transgenes), and L1 animals that, additionally, expressed CYE-1/CDK-2AF or CYD-1/CDK-4 in muscle cells. Most genes in CYD-1/CDK-4 or CYE-1/CDK-2AF expressing muscle cells were not significantly up- or down regulated (Figure S5A and S5B, Table S2). This includes nearly all muscle-specific genes, confirming maintenance of the muscle-specific fate (see below).

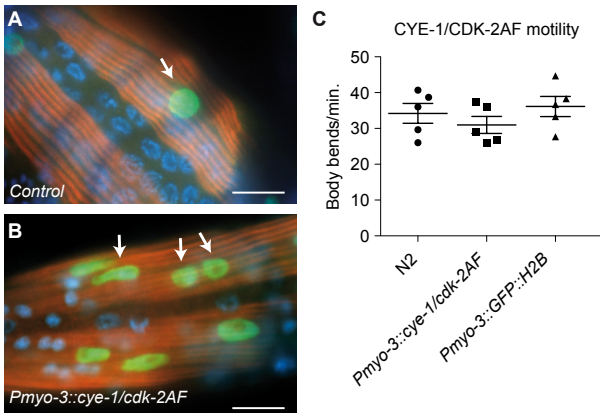

Figure 4. Animals with mitotic body-wall muscle retain normal motility and muscle structure. (A,B) UNC-15/Paramyosin staining (red) of a control (*Pmyo-3::GFP::H2B)* line and a line with muscle expression of CYE-1 and CDK-2AF. Arrows mark GFP (green) expressing nuclei of body-wall muscle cells. (B) Body-wall muscle in both animals show thick filament structures, despite the signs of mitosis (arrows). (C) Motility assay of L4 larvae: N2 wild type, SV858 (*Pmyo-3::CYE-1/CDK-2AF*), and SV859 (*Pmyo-3::GFP::H2Bcontrol*). Each dot represents a single animal. Error bars represent s.e.m., scale bars indicate 10 μm.

A set of 219 genes was significantly upregulated (fold-change ≥2, $p<0.05$) in CYE-1/CDK-2AF animals compared to the control strain. Manual annotation of these induced genes and GO-term enrichment analysis using Funcassociate (Berriz *et al.*, 2003) revealed a large overrepresentation of genes involved in various aspects of the cell cycle, including G1/S regulation, DNA replication, DNA damage response, mitosis, cytokinesis and checkpoint control (Figure 5B and 5E, Table S2). Similar to CYE-1/CDK-2AF, CYD-1/CDK-4 expression in the body-wall muscle induced a set of 395 genes with a strong cell cycle signature (Figure 5A, Table S2).

The majority of genes upregulated in CYE-1/CDK-2AF were also upregulated in CYD-1/CDK-4 muscle (Figure 5C and 5D). The overlapping gene set has a particularly strong cell cycle signature, with over 60% of the genes with functional annotations in a cell cycle category (Figure 5D and 5E). Interestingly, CYD-1/CDK-4 also induced a set of 143 genes (> 2x, $p<0.05$) that are not significantly upregulated by CYE-1/CDK-2AF expression ($p>0.05$) (Table S2, Table S3). These genes were enriched for GO terms related to biosynthesis, though at adjusted P values slightly above 0.05 (0.055 to 0.092). Manual annotation confirmed that many of these genes (45 of 87 genes with recognizable homologues) have ascribed cellular growth and metabolism functions (Figure 5A, Table S2). This suggests that CYD-1/CDK-4 does not only activate a cell-cycle transcriptional program, but also functions in G1 to stimulate cellular growth and metabolism associated gene expression.

A major function of G1/S Cyclin/CDK complexes is the activation of E2F transcription factors through inhibitory phosphorylation of pRb proteins (van den Heuvel and Dyson, 2008). We therefore analyzed the promoter sequences of genes upregulated in CYD-1/

CDK-4 or CYE-1/CDK-2AF for enrichment in consensus transcription factor binding sites (Materials and Methods), including a *C. elegans*-specific profile for the EFL-1 (E2F) transcription factor (Kirienko and Fay, 2007). We analyzed the promoter regions of 439 genes upregulated ≥ 2 fold in CYD-1/CDK-4 or CYE-1/CDK-2AF expressing muscle. In both sets of promoters the highest scoring transcription factor site motif was that of E2F1, while the *C. elegans*-specific EFL-1 site ranked fifth and third respectively (Table S4). These results are consistent with the activation of a set of E2F target genes by both CYD-1/CDK-4 and CYE-1/CDK-2. We next analyzed the 143 genes upregulated in CYD-1/CDK-4 animals but not in CYE-1/CDK-2 animals. This set of genes was hardly enriched for E2F1 and EFL-1 sites (Table S4). Together with the functional annotations, these results indicate that CYD-1/CDK-4 and CYE-1/CDK-2 induce a core set of E2F regulated cell cycle genes, while CYD-1/CDK-4 also activates a set of genes with a broader range of functions.

CYE-1/CDK-2 expression in muscle caused down-regulation of only 50 genes with no functional enrichment. In contrast, CYD-1/CDK-4 expression also resulted in down-regulation (≥ 2x, $p<0.05$) of a substantial set of 555 transcripts (Table S5). This group shows a remarkable enrichment with GO terms related to catabolic processes, including peptidase, lipase, esterase and hydrolase activities. While muscle cells remain functional and morphologically normal, 60 of the down-regulated genes are normally highly expressed in muscle (Table S4). Thus, CYD-1/CDK-4 causes upregulation of cell-cycle and biosynthesis associated genes, as well as down-regulation of genes primarily associated with biodegradation and energy production.

Key G1/S regulators are not induced by G1 Cyclin/CDK expression in muscle

Despite the robust induction of many E2F targets, some key activators of G1/S progression were not induced. For instance, in CYD-1/CDK-4 expressing muscle, the induction factor (log^2, mean of 4 experiments) was 0.11 for *cye-1* Cyclin E, 0.04 for *cdk-2*, and -1.3 for *cdc-25.1*. These genes are well-established E2F targets in mammals, *Drosophila*, and, at least *cye-1* and *cdc-25.1*, also in *C. elegans* (Duronio and O'Farrell, 1995; Kirienko and Fay, 2007). These observations suggest that in contrast to many other E2F targets, the actual regulators that promote cell cycle entry may be more tightly repressed. We used single molecule FISH analysis to verify the gene expression analysis. This method makes use of approximately 48 individually labeled short oligonucleotide probes, which together allow detection of individual mRNA molecules (Raj , 2008). As a first test, we examined *myo-3* mRNA abundance. The control strain, expressing *myo-3::H2B::GFP* in muscle, and four different strains with muscle-induced G1 Cyclin/CDK expression, all showed readily detectable fluorescent *myo-3* mRNA spots in the cytoplasm of muscle cells (Figure 6A–6C, 6G). Very similar numbers were obtained in different strains and experiments; illustrating that single molecule FISH gives reproducible results (Figure 6G, and data not shown). Next, we used this technique to examine mRNA levels of the E2F-target *mcm-6*. All muscle cells with G1 Cyclin/CDK expression showed substantial *mcm-6* mRNA induction as early as 3 hrs of postembryonic

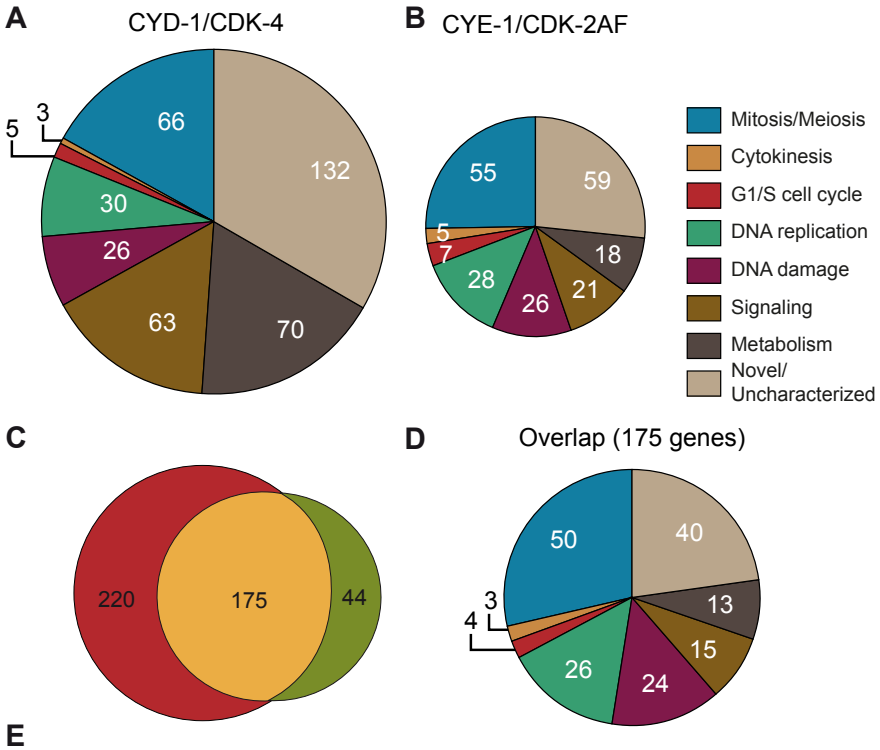

E

Mitosis/Meiosis	DNA replication	DNA damage	G1/S cell cycle
cyb-3 (Cyclin B)	*mcm-2–7* (MCM)	*chk-1* (Chk-1)	*cki-1* (p27)
air-1 (Aurora A)	*pri-1* (DNA Primase)	*scc-1* (RAD21)	*cki-2* (p27)
plk-1 (Polo Kinase)	*pri-2* (DNA Pimase)	*msh-6* (MUTS)	*dpl-1* (DP)
bub-1 (BUB1)	*rfc-3 (RFC3)*	*brd-1* (BARD1)	*skpt-1* (Skp1 related)
zen-4 (Kinesin 6)	*rfc-4 (RFC4)*	*msh-2* (MSH2)	
bmk-1 (Kinesin 5)	Y53F4B.3 (DNA Polε)	*exo-3* (APEX exonuclease)	
spdl-1 (Spindly)	*pcn-1* (PCNA)	*cku-70* (XRCC6)	

Figure 5. Microarray analysis reveals induction of cell-cycle gene transcripts in differentiated muscle cells. (A,B) Functional annotation of genes significantly increased more than 2-fold in *Pmyo-3::CYD-1/CDK-4* and *Pmyo-3::CYE-1/CDK-2AF* muscle cells. A large overrepresentation of genes involved in various stages of the cell cycle is seen in both data sets, as well as a distinct increase in the proportion of metabolism and signaling genes in CYD-1/CDK-4 animals. (C) Overlap in more than 2-fold upregulated genes between CYE-1/CDK-2AF and CYD-1/CDK-4 body-wall muscle cells. The majority of the genes induced by CYE-1/CDK-2AF are also induced in CYD-1/CDK-4, but the latter also contains a substantial number of non-cell cycle genes. (D) Functional annotation of the genes present in the overlap between CYD-1/CDK-4 and CYE-1/CDK-2AF reveals a strong (60%) representation of known cell cycle genes. (E) Table of representative cell cycle genes and their orthologs that are induced by both CYD-1/CDK-4 and CYE-1/CDK-2AF (>2-fold upregulated).

L1 development, in agreement with the microarray data (Figure 6H). Induction of *mcm-6* was observed in CYE-1/CDK-2AF and CYE-1/CDK-2 expressing strains, and in two independent CYD-1/CDK-4 strains, including one with low levels of CYD-1/CDK-4 expression in muscle (CYD-1/CDK-4 #2; Figure 6H, Figure S4).

The microarray data showed weak upregulation of the Leucyl amino-acyl tRNA synthetase gene *lrs-2* in muscle with CYD-1/CDK-4 (induction factor 1.38) but not in CYE-1/CDK-2AF expressing muscle (induction 0.04). FISH experiments showed the same trend: strain 2 with only low CYD-1/CDK-4 expression showed *lrs-2* upregulation, while even the high CYE-1/CDK-2 expressing strain did not differ from the control (Figure 6I). In contrast, *cye-1* mRNA was nearly absent in CYD-1/CDK-4 expressing muscle cells, with occasionally a single or at most two small dots in muscle cells (Figure 6E, 6J). Thus, the

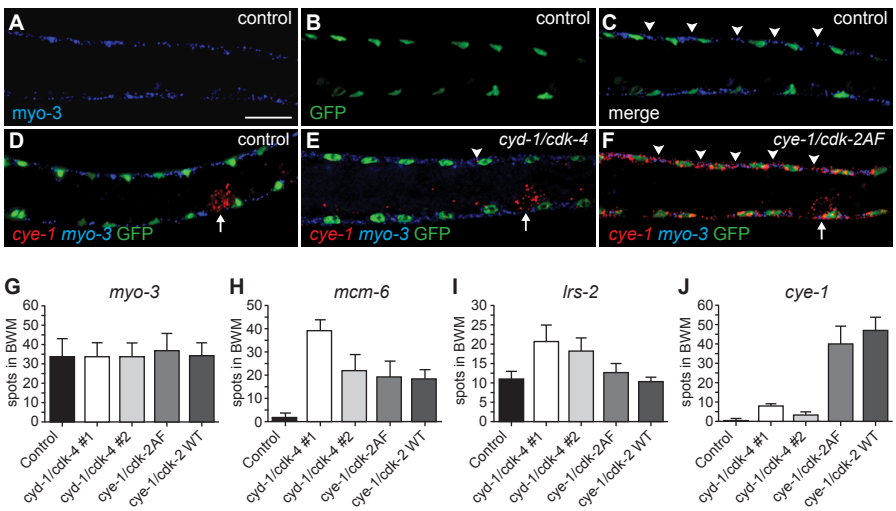

Figure 6. Single molecule FISH shows gene expression in individual muscle cells and limited *cye-1* induction by CYD-1/CDK-4. (A-F) Single mRNA molecules labeled with probes against myo-3 (blue) or cye-1 (red) mRNA. Muscle nuclei are marked in green by *Pmyo-3::H2B::GFP*. Analyzed are strains expressing only *Pmyo-3::H2B::GFP* (control, SV859: A-D), and *Pmyo-3::H2B::GFP* together with *Pmyo-3::CYD-1/CDK-4* (SV857: E) or *Pmyo-3::CYE-1/CDK-2AF* (SV858: F). Arrowheads indicate areas of *myo-3* mRNA (C) or *cye-1* mRNA (E, F) expression in dorsal body-wall muscle cells. Arrows in (D-F) indicate cye-1 expression in the gonad. Scale bar indicates 10 µm, all panels show the same magnification. (G-J) Quantification of the number of fluorescent spots in seven body-wall muscle cells located anterior of the gonad on the dorsal side of animals. All animals were hybridized with *myo-3* probes to identify body-wall muscle cells. Signal corresponding to mRNA molecules of *myo-3*(G), *mcm-6* (H), *lrs-2* (I), or *cye-1* (J) were counted. The strains analyzed are SV859 (control), SV857 (*cyd-1/cdk*-4 #1), SV860 (*cyd-1/cdk-4* #2), SV858 (*cye-1/cdk-2AF*) and SV861 (*cye-1/cdk-2WT*). Note that overlap between spots greatly reduced the counted number of *myo-3* and *mcm-6* mRNAs. In contrast, the few and small *cye-1* labeled spots are likely all single mRNA molecules.

single molecule FISH experiments support our conclusions from the microarray data, and show with single cell resolution that *cye-1* mRNA expression is not even induced in a subset of muscle cells.

Discussion

In this study, we demonstrate that post-mitotic *C. elegans* muscle cells remain remarkably competent to express cell cycle genes, and that cell cycle re-entry can occur coincident with the differentiated state. In addition, we demonstrate differential activity of CYD-1/CDK-4 versus CYE-1/CDK-2 in the regulation of gene expression. These results challenge prevailing views on the irreversible commitment to cell cycle exit upon terminal differentiation and the linear pathway of CDK activities.

To our knowledge, our data show for the first time that the CYD-1/CDK-4 complex controls expression of metabolic genes, in addition to cell cycle genes. These transcriptome data fit well with observations that Cyclin D is directly controlled by mitogenic signals as the most upstream regulator in cell cycle entry (reviewed in Sherr, 2004), and that *Drosophila* Cyclin D and Cdk4 predominantly act to promote growth rather than cell cycle progression (Datar *et al.*, 2000; Meyer *et al.*, 2000). While many studies implicate Cyclin D and Cyclin E CDKs as regulators of the Rb/E2F module, our data provide strong support for CYD-1/CDK-4 control of additional transcription factors. Interestingly, Cyclin D has been observed to interact with several transcriptional regulators, to localize to promoters, and to affect transcription independently of CDK4/6 (e.g., Bienvenu *et al.*, 2010). It will be of great interest to find if these results relate to our observations, and what molecular mechanisms underlie the regulation of metabolic genes by Cyclin D/CDK4. As a potential substrate, several metabolic genes that are specifically up-regulated (e.g. *acs-2*) or down-regulated (e.g. *ech-9*/F01G10.3) by CYD-1/CDK-4 are transcriptional targets of NHR-49, a member of the Hepatocyte Nuclear Factor 4 (HNF4) family of nuclear hormone receptors (Van Gilst *et al.*, 2005).

CYD-1/CDK-4 also induced DNA replication in muscle, while CYE-1/CDK-2, in contrast, appeared to antagonize DNA synthesis. As a possible explanation, DNA synthesis might depend on a growth-related signal that is uniquely induced by CYD-1/CDK-4. Alternatively, or in addition, the different effects of the two Cyclin/CDK combinations may result from different roles in DNA replication origin licensing. CYE-1/CDK-2 antagonizes the formation of DNA pre-replication complexes (pre-RCs), at least in some cell types (Mailand and Diffley, 2005; Kim *et al.*, 2007; Korzelius and van den Heuvel, 2007). This activity helps to restrict DNA replication to only once per cell cycle. The observed induction of DNA replication in muscle cells indicates that CYD-1/CDK-4 does not share this CYE-1/CDK-2 function, but allows the formation and function of pre-RCs. In arrested intestinal cells, CYE-1 Cyclin E was sufficient to induce DNA replication, which points to an important difference in the arrested state of quiescent versus post-mitotic cells.

Progression from temporary arrest to irreversible cell cycle exit is thought to depend on epigenetic silencing of cell cycle promoters (e.g., (Jacobs *et al.*, 1999)). Our transcriptional profiling indicates that such a repressive chromatin state can be reversed at many cell cycle promoters. As Cyclin/CDK expression does not appear to induce full cell division of body-wall muscle, additional safeguards probably inhibit proliferation. Our expression studies indicate that these safeguards focus on a limited number of critical regulators. Interestingly, expression of E2F in differentiating *Drosophila* eye and wing cells, and differentiation of mouse Rb family triple knockout cells have also revealed additional levels of control that impinge on Cyclin E during terminal differentiation (Buttitta *et al.*, 2010; Wirt *et al.*, 2010).

Coincident differentiation and proliferation has been observed in some situations, such as proliferating horizontal interneurons in mouse retinoblastoma, proliferating $pRb^{(-/-)}$ hair cells of the mouse inner ear, and *Drosophila* wing hairs and eye cells expressing E2F and Cyclin E (Sage *et al.*, 2005; Ajioka *et al.*, 2007; Buttitta *et al.*, 2007). Our preliminary results indicate that CYD-1/CDK-4 expression also triggers S-phase gene expression in differentiated *C. elegans* neurons (data not shown). Together, the different examples indicate potential for finding a common set of gene alterations that can induce cell proliferation in terminally differentiated cells. Despite the success of induced pluripotent stem cells, this could ultimately provide an attractive regeneration strategy, in particular if limited proliferation could be achieved without genome-wide remodeling of the chromatin and loss of the differentiated state.

Materials and Methods

Strains, molecular cloning, and transgenes

All strains and culture conditions are listed in Text S1. Expression constructs for *cye-1*, *cyd-1*, *cdk-4*, *cdk-2*, *cdk-2AF*, and GFP::H2B were created using a 2.4 Kb *myo-3* promoter (PCGS1 (*Pmyo-3*), body-wall muscle expression) or a 5 kb *elt-2* promoter (intestinal expression (Fukushige *et al.*, 1998)). Coding sequences of Venus YFP with *C. elegans*-optimized codons (a kind gift of Yuichi Iino) were inserted before the translational stop in all CDK constructs. The CDK-2AF mutant was created by mutating two conserved Wee1 phosphorylation sites (Thr25-to-Ala and Tyr26-to-Phe) by sitedirected mutagenesis. *Pmcm-4::MCM-4::mCherry::mcm-4 3'UTR* was recently described (Korzelius *et al.*, 2011) and integrated as a single copy using the MosSCI technique (Frokjaer-Jensen *et al.*, 2008). The *Prnr::CYB-1DesBox::TdTomato* marker expresses an N-terminal 100 amino acid part of *C. elegans* CYB-1 (N-CYB-1), which harbors a KEN destruction box sequence for recognition by the APC/C coupled to the TdTomato fluorophore (Korzelius *et al.*, 2011). Multiple transgenic lines were analyzed for each Cyclin/CDK combination. Representative lines with 40-70% F2 transmission were selected for gamma irradiation. Integrated lines were backcrossed with N2 a minimum of 4 times before analysis.

Immunostaining and detection of DNA replication

For immunostaining of larval stages, animals were fixed in methanol (5 minutes at -20 °C) and acetone (20 minutes at -20 °C) according to (Korzelius *et al.*, 2011). BrdU and EdU staining were performed as described (Boxem *et al.*, 1999; Korzelius *et al.*, 2011). Primary antibodies used: rabbit anti-phospho-H3S10 (1:200, Abcam), mouse anti-GFP (1:100, Sigma), mouse anti-CYE-1 (E. Kipreos, 1:200), rabbit anti-GFP (1:100, Molecular Probes), mouse monoclonal antibody 5-23 to UNC-15 (1:3, tissue supernatant, Developmental Studies Hybridoma Bank). Secondary antibodies used: Donkey anti-mouse FITC or TexasRed and Donkey anti-rabbit FITC or TexasRed (1:200, Jackson Immunolaboratories). Quantitative DNA measurements were performed as previously described (Boxem *et al.*, 1999a). In short, series of Z-sections were taken of propidium iodide-stained animals with a confocal scanning laser microscope, and pixel intensities of all sections were added and recalculated to DNA content, using Pn.p ventral cord precursor nuclei as a 2n DNA standard.

Tissue-specific microarray analysis

Tissue-specific mRNA was isolated from synchronized L1 larvae fed for 3 hours by purification of the poly-A binding protein FLAG::PAB-1 specifically expressed in body-wall muscle cells of L1 larvae (Roy *et al.*, 2002). Poly(A) RNA was isolated essentially as described (Roy *et al.*, 2002). Four independently grown biological samples were used for each different line: SV912 (control), SV911 (CYE-1/CDK-2AF), and SV985 (CYD-1/CDK-4). Array data is submitted to Array Express accession no.: E-TABM-886. Procedures used in the hybridizations, data analysis and transcription factor analysis are detailed in Text S1.

Functional analysis

Manual annotation of genes upregulated ≥2-fold was done using WormBase (release WS207). GO-term enrichment was determined using Funcassociate (Berriz *et al.*, 2003).

Single-molecule Fluorescence In Situ Hybridization

Single molecule Fluorescence In Situ Hybridization was performed as described by (Raj *et al.*, 2008). Starved L1 animals were fed for three hours on OP50, followed by fixation in 4% formaldehyde and hybridization with sets of the 48 labeled oligonucleotide probes. Images were taken with a DeltaVision Core wide-field microscope, quantification of the number of mRNAs was performed using the 3D imaging software Volocity version 5 (Perkin Elmer). For quantification, a region of interest was drawn around seven body-wall muscle nuclei, located anteriorly from the gonad on the dorsal side of the animal, to exclude cells in the ventral nerve cord and mesoblast lineage. Further details on the procedure, microscopy and data analysis are provided in Text S1.

Acknowledgements

We thank Harmjan Vos for help with dye-labeling and purification of oligonucleotides, Judith Kimble and Sarah Crittenden for the EdU labeling protocol, Edward Kipreos for reagents, David Fay and Natalia Kirienko for unpublished data, Michael Krause for comments on the manuscript, and Christian Berends for help with the French pressure cell. Several nematode strains used in this work were provided by the *Caenorhabditis* Genetics Center.

Author Contributions

Conceived and designed the experiments: JK IT SvdH. Performed the experiments: JK IT SR MBWP VP TCM MJGK. Analyzed the data: JK IT SR MJGK MB SvdH. Contributed reagents/materials/analysis tools: MJGK FCPH. Wrote the paper: JK MB SvdH.

Supporting Information

C. elegans strains and culturing

C. elegans strains were cultured on NGM plates seeded with E. coli strain OP50 as described (Stiernagle, 2006) at 20 °C unless indicated otherwise. For synchronization, animals were treated with hypochlorite solution, followed by hatching of the eggs in M9 medium with 0.05% Tween-20. Larvae were then allowed to develop for the appropriate amount of time.

The following strains were used in this study: N2 Bristol wild-type, SV822 *heEx288[Pelt-2::CYE-1; Pelt-2::CDK-2AF::Venus;Pmyo-2::GFP]*. SV326 *rtIs14[elt-2::GFP; osm-10::HT150Q]*. SV1030 *rtIs14; heEx345[Pelt-2::CDK-4::Venus; Pmyo-2::TdTomato]*. SV1031 *rtIs14; heEx346[Pelt-2::CYD-1; Pelt-2::CDK-4::Venus; Pmyo-2::TdTomato]*. SV857 *heIs9[Pmyo-3::GFP::H2B; Pmyo-3::CYD-1; Pmyo-3::CDK-4::Venus]*. SV858 *heIs10[Pmyo-3::GFP::H2B; Pmyo-3::CYE-1; Pmyo-3::CDK-2AF::Venus]*. SV859 *heIs11[Pmyo-3::GFP::H2B]*. SV860 *heIs12[Pmyo-3::GFP::H2B; Pmyo-3::CYD-1; Pmyo-3::CDK-4::Venus]*. SV861 *heIs44[Pmyo-3::GFP::H2B; Pmyo-3::CYE-1; Pmyo-3::CDK-2::Venus]*. SV1076 *unc-119(ed3); heIs47[Pmcm-4::MCM-4::mCherry]; heIs9*. SV1077 *unc-119(ed3); heIs47; heIs10*. SV852 *heIs10; heIs10[Prnr-1::CYB-1DesBox::TdTomato; p*RF4 *rol-6(+)]. SV1118 unc119(ed3); heIs47; heEx388[Phsp16.2::CYD-1;Phsp-16.2::CDK-4;Pmyo-2::GFP]*. SD1075 *gaIs146[Pmyo-3::FLAG::PAB-1; Psur-5::GFP]*. SV911 *heIs10; gaIs146*. SV912 *heIs11; gaIs146*. SV985 *gaIs146; heIs9*. SV1195 *heIs9; heIs10*.

For heat-shock induced expression: synchronized L2/L3 stage SV1118 animals expressing CYD-1/CDK-4 from the *hsp-16.2* heat-shock promoter were placed for 40 min. at 33 °C in a water bath and a second heat shock was given 15 hours later. Animals were examined for expression of the S-phase marker *Pmcm-4::MCM-4::mCherry* 8 hours after the second heat shock.

Microarray Hybridizations and Data Analysis

Microarrays were *C. elegans* Gene Expression Microarrays V1 (Agilent Technologies), with 2x 21000 60-mer probes in a 4x44K layout. RNA amplification, labeling, and hybridizations were performed as described (van de Peppel *et al.,* 2003; Roepman *et al.,* 2005) with a minimum of 50 ng immunoprecipitated RNA from each sample. After automated data extraction using Imagene 8.0 (BioDiscovery), print-tip loess normalization was performed on mean spot-intensities (Yang *et al.,* 2002). Dye bias was corrected with a within-set estimate according to (Margaritis *et al.,* 2009). Statistical analysis was through MAANOVA (Wu *et al.,* 2003). In a fixed effect analysis, sample, array, and dye effects were modeled. P-values were determined by a permutation F2-test, in which residuals were shuffled 5000 times globally. Probes with $p<0.05$ after family-wise error correction were considered significantly changed. Agilent probe names were matched to gene names from Wormbase release WS200.

Transcription factor site analysis

To identify transcription factor binding sites enriched in different gene sets we used the Clover program (Frith *et al.,* 2004) together with the Jaspar CORE set of non-redundant transcription factor binding site profiles (modification date 10-12-2009) (Portales-Casamar *et al.,* 2010). In addition, we added a *C. elegans* specific E2F profile (Kirienko and Fay, 2007). For each gene we defined the promoter as the sequence from 1000 bp upstream of the first splice variant to the -1 position of the most downstream splice variant. For genes in operons, the promoter sequence of the first gene in the operon was analyzed. To identify absolute E2F transcription site numbers (table S4), we used the TFBS perl module (Lenhard and Wasserman, 2002). Sequence logos were drawn using Weblogo (Crooks *et al.,* 2004).

Motility assays, microscopy and quantification

Motility assays were performed by determining the average number of body bends per minute in a three-minute interval for each animal as described (Robatzek and Thomas, 2000). For UNC-15 Paramyosin staining of L4/adult worms, we used a modified version of the Finney-Ruvkun whole-mount staining protocol (Bettinger *et al.,* 1996). For observation of H2B::GFP localization in live animals, synchronized larvae were anaesthetized with 10 mM Sodium Azide. Extra division events were quantified at L3 and L4 stages by counting the number of cells that had mitotic phenotypes (including cells with extra nuclei, nuclei with condensed DNA, and nuclei in the various stages of mitosis) anterior of the prospective vulva. Photographs were taken with an Axioplan 2 microscope mounted with an Axiocam mRM camera (Zeiss Microscopy). Scalebars are 10 μm. Quantitive data and graphs were produced using GraphPad Prism Version 5 for Mac (GraphPad Software) and Excel 2008 for Mac (Microsoft).

Co-immunoprecipitation of CYE-1/CDK-2AF::VENUS complex

For co-immunoprecipitation of the CYE-1/CDK-2AF::Venus complex, N2 and SV837 (see *C. elegans* strains and culturing) animals were homogenized by grinding in liquid nitrogen and transferring the worm debris into 4 ml chilled lysis buffer (20 mM Tris-HCl (pH 8.3), 137 mM NaCl, 1% Nonidet P-40, 2 mM EDTA, protease inhibitor cocktail (Roche Diagnostics), 0.14% β-mercapto-ethanol), followed by treatment of the lysate in a French pressure cell. 1 mg of protein was used for the IP experiments and 50 μg was used for direct lysate samples. Immunoprecipitation was performed by incubating 500 μl lysate with either anti-CYE-1 (a kind gift of Michael Krause) or anti-GFP (Molecular Probes) covalently coupled to ProtG and ProtA beads respectively. Negative control immunoprecipitations were performed with mouse anti-SD15 (a kind gift of Nick Dyson), 5 μl of ascitus coupled to protG beads, and rabbit anti-eIF-4E (a kind gift of Adri Thomas) coupled to protA beads. Following immunoprecipitation, 20 μl of each sample was loaded on an 8% polyacrylamide gel. Proteins were blotted on PVDF membrane (Amersham Bioscience). Blots were incubated with mouse anti-CYE-1 (M.Krause, 1:750), rabbit anti-GFP (Invitro-

gen,1:500) or monoclonal mouse anti-actin (MP Bio Medicals, 1:1000). Goat anti-mouse-peroxidase and goat anti-rabbit peroxidase (Jackson Immunolaboratories) were used as secondary antibodies. The chemiluminescent detection reaction was performed using a Biorad ECL kit (Biorad) and the blot was subsequently exposed to hypersensitive film (Amersham Hyperfilm, GE healthcare).

Single molecule Fluorescence In Situ Hybridization

Single molecule Fluorescence In Situ Hybridization was performed as described in (Raj *et al.,* 2008). In brief, 48 oligonucleotides probes directed against the coding sequence of *myo-3*, *mcm-6*, *lrs-2,* and *cye-1* were designed on the single molecule FISH website (www.singlemoleculefish.com) and ordered with 3'-modifications from BioSearch Technologies. All 48 oligonucleotides were pooled and labeled with succinimidyl esters of either Tetramethylrhodamine (TMR) (Invitrogen) or Cy5 (GE Healthcare) and purified by reverse phase liquid chromatography using a C18 polymeric reversed phase column (VYDAC 218TP™ Series). Starved L1 animals were fed for three hours on OP50, followed by fixation in 4% formaldehyde and hybridized with the lableled 48 nucleotides probes. Hybridization of these animals was performed in 100 µl hybridization solution to which 9.3 ng of the myo-3 probes coupled to TMR was added, and 3.7 ng of *mcm-6*, 18.4 ng of *lrs-2,* or 8.6 ng of *cye-1* probes coupled to Cy5. Following overnight incubation at 32 ºC, samples were washed 4x 1 hour with wash buffer at 32 ºC. Shortly before imaging, samples were mounted in anti-bleach buffer.

Western blot analysis

Western blotting experiments were performed as previously described (Boxem *et al.,* 1999). In short: animals from various strains were grown and equal numbers of L4 animals (80) were harvested. 2x Laemmli sample buffer was added to the worm pellet, samples were boiled for 10 minutes, divided in two and separated on a 12% SDS-PAGE gels. Blots were probed with rabbit anti-GFP (Abcam, 1:1000 dilution), and mouse anti-tubulin (Sigma, 1:1000 dilution).

Imaging and quantification

Images were taken with a DeltaVision Core wide-field microscope, equipped with a 100x oil-immersion objective (Applied Precision) and a Cascade 2 EMCCD® 1K camera (Photometrics) using SoftWorx acquisition software version 4 (Applied Precision). Exposure times used for both TMR and Cy5 were 2 seconds. Stacks were acquired automatically with 0.20 microns between the Z-slices.

Quantification of the number of mRNAs was performed using the 3D imaging software Volocity version 5 (Perkin Elmer). A region of interest was drawn around seven body wall muscle nuclei, located anteriorly from the gonad on the dorsal side of the animal,

to exclude cells in the ventral nerve cord and mesoblast lineage. Expression of myo-3 mRNA in the cytoplasm was used to localize the body wall muscle cells. The results were statistically analyzed with GraphPad Prism version 5 (GraphPad Software Inc), using an unpaired t-test.

Supporting Figures

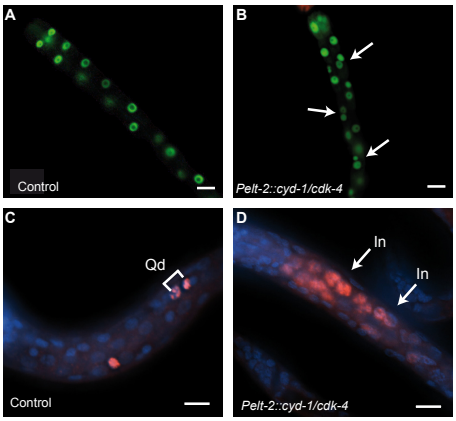

E

Strain	n	% BrdU-positive
N2	many	0
Pelt-2::cdk-4::Venus	50	0
Pelt-2::cyd-1	43	12
Pelt-2::cyd-1/cdk-4::Venus	51	51
Pelt-2::cye-1/cdk-2AF::Venus	37	46

F

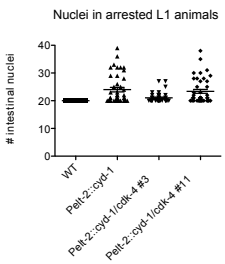

Supplementary Figure 1. Expression of G1 Cyclin/CDK combinations in the intestine of arrested L1 larvae leads to extra nuclear divisions and DNA synthesis. (A-B) L1 animals carrying an integrated *Pelt-2::GFP* marker alone (A) or in combination with CYD-1/CDK-4 expressed from the intestinal *elt-2* promoter (B). Arrows indicate clusters of extra nuclei. (C-D) BrdU incorporation in the intestine of wild-type starved L1 control animals (C) or animals expressing CYD-1/CDK-4 in the intestine (D). Control L1 arrested animals have no BrdU positive intestinal cells, only the Q neuroblast daughters (C, brackets) and some epidermal V-cells occasionally escape arrest. The intestine of the *Pelt-2::CYD-1/CDK-4* animal shows an extensive amount of intestinal cells that have undergone DNA replication during starvation-induced quiescence (D, arrows). (E) Quantification of the percentage of animals staining positive for BrdU in the gut in representative lines of each Cyclin/CDK combination. (F) Quantification of the number of intestinal nuclei in arrested L1 animals. Note that expression of CYD-1 alone is sufficient to trigger cell cycle progression in the gut. Each dot represents a single animal. Error bars represent s.e.m.

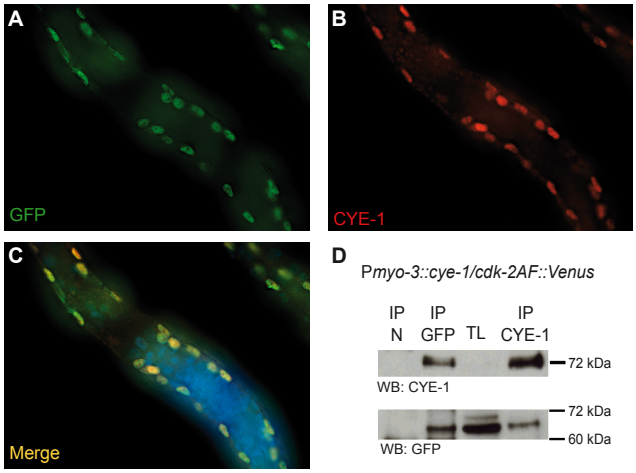

Supplementary Figure 2. Expression of CYE-1 and CDK-2AF::Venus in the body wall muscle. (A-C) Immunostaining of CYE-1 and GFP in SV858 (*Pmyo-3::GFP::H2B; Pmyo-3::CYE-1/CDK-2AF::Venus*) L1 larva. GFP antibody staining visualizes the body wall muscle nuclei (A), the CYE-1 staining shows nuclear localization of CYE-1 protein in the body wall muscle (B). (C) Merge of A and B. (D) Immunoprecipitation of the CYE-1/CDK-2AF::Venus complex. CYE-1 migrates with an apparent molecular weight of, 72 kDa. The CDK-2AF::Venus fusion protein is detected at 66 kDa with anti-GFP antibodies. The CYE-1/CDK-2AF::Venus interaction was detected in both the CYE-1 and GFP immunoprecipitations.

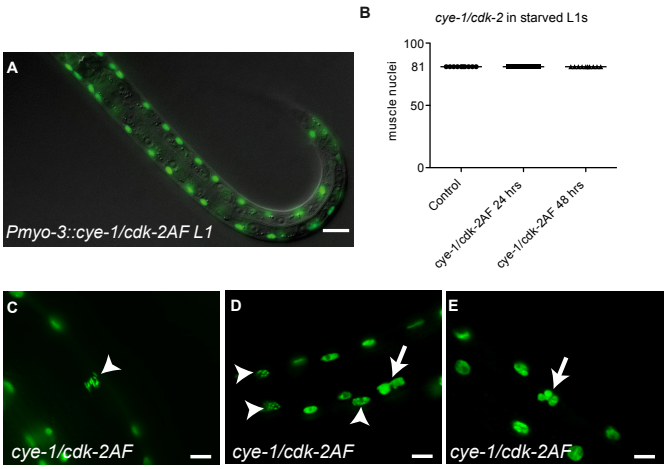

Supplementary Figure 3. Body wall muscle expressing CYE-1/CDK-2AF show mitotic events during larval development. (A) GFP-DIC picture of a starvation-arrested L1 animal expressing CYE-1/CDK-2AF from the *myo-3* promoter. No extra nuclei or mitotic nuclei are observed at this stage. (B) Quantification of muscle nuclei in control animals (expressing only *Pmyo-3:GFP::H2B* in their muscle) and CYE-1/CDK-2AF L1 animals after 24 or 48 hours of L1 arrest. N=15 animals for each condition. Each dot represents a single animal. Error bars represent s.e.m. (C,D,E) During larval development, mitotic body wall muscle nuclei become apparent. L3 stage animals that express *Pmyo-3::CYE-1*, *Pmyo-3::CDK-2AF* and *Pmyo-3::GFP::H2B* show DNA condensation (C,D, arrowheads) and abnormal nuclear divisions (D,E, arrows) in differentiated body wall muscle.

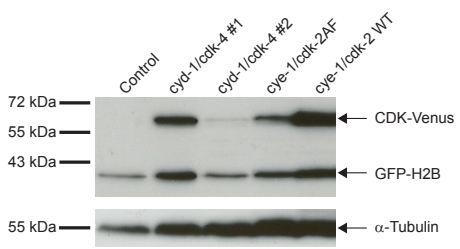

Supplementary Figure 4. Western blot analysis of CDK and H2B expression levels in transgenic strains. Total protein lysates of transgenic animals with muscle expression of GFP::H2B alone (control, SV859), or together with Cyclin D/CDK-4::Venus (SV857: *cyd-1/cdk-4* #1, SV860: *cyd-1/cdk-4* #2) or Cyclin E/CDK-2::Venus (SV858: *cye-1/cdk-2AF,* SV861: *cye-1/cdk-2WT*) were separated by SDS PAGE electrophoresis and blotted. The upper panel was probed with an anti-GFP antibody and shows CDK-2/4::Venus (70 and 66 kDa resp., upper arrow) and GFP::H2B (41.5 kDa, lower arrow) protein bands. The lower panel contains the same samples, probed with anti-a-Tubulin (55 kDa) as a loading control (arrow points to a-Tubulin). Note that the *cyd-1/cdk-4* #1 strain shows higher levels of transgene expression than the *cye-1/cdk-2AF* strain. These strains were used in all subsequent experiments, except for *cyd-1/cdk-4* #2, which was only used in the experiments shown in Figure 6.

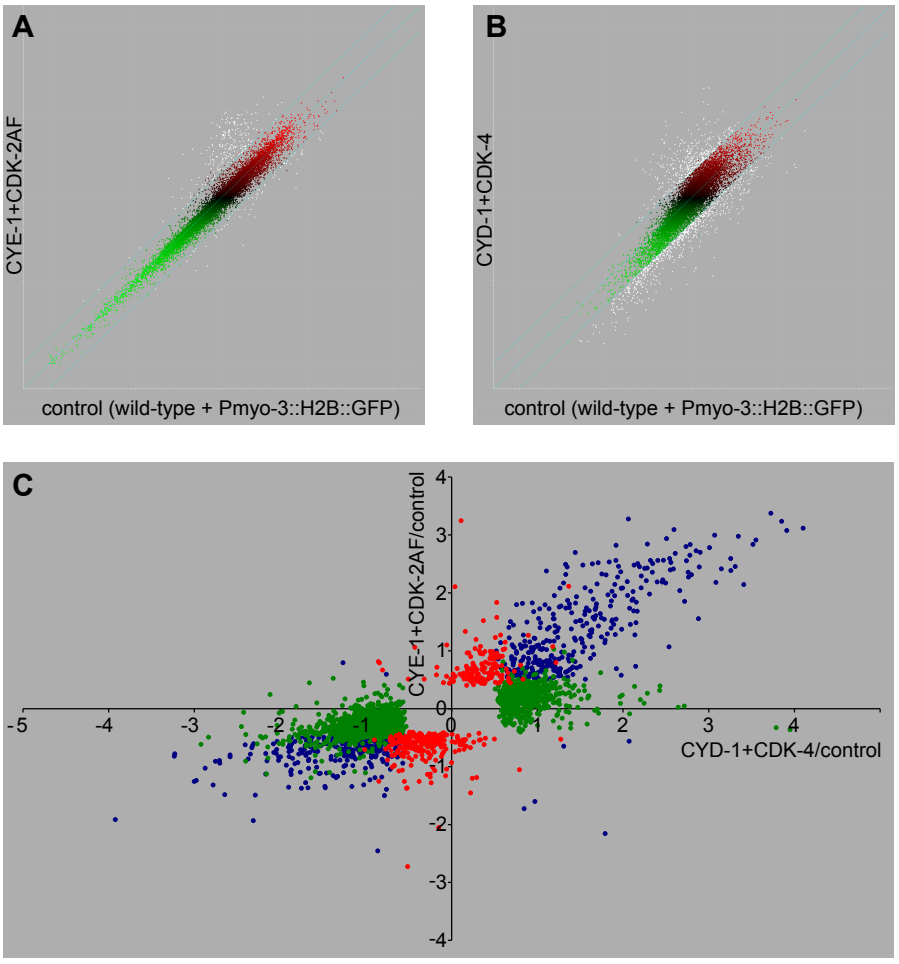

Supplementary Figure 5. Scatterplot representation of expressed genes. (A,B) Microarray signal intensities for CYE-1/CDK-2AF (A) and CYD- 1/CDK-4 (B) expressing muscle compared to control muscle IP (SV912). The experiment was repeated four times for each line. The intensities of all genes are shown after background subtraction, normalization, and merging of replicate culture dye swap hybridizations. MAANOVA statistical analysis was performed to determine genes with significantly different mRNA expression. White data points mark genes that are significantly changed ($p < 0.05$) and have a ≥2-fold change. Values are plotted on a $\log^{10}$ scale. Y-axis: CYD-1/CDK-4 (SV985) or CYE-1/CDK-2AF (SV911) PAB-1 IP RNA versus total RNA, X-axis: Control (SV912) PAB-1 IP RNA versus total RNA. (C) Plot of significantly changed genes ($p < 0.05$) in CYE-1/CDK-2AF (Yaxis) and CYD-1/CDK-4 (X-axis). Colors for each data point indicate in which set(s) the gene is significantly changed (green: CYD-1/CDK-4, red: CYE-1/CDK-2AF). Values are plotted on a $\log^2$ scale.

Supporting Tables

Of each table, the first 8 rows are shown to indicate the type of available data and analysis. Full tables are available at *http://journals.plos.org/plosgenetics/article?id=10.1371/journal.pgen.1002362*

Supplementary Table 1. List of genes enriched ≥2-fold in muscle (PAB-1 IP versus total RNA) and GO-term analysis of these genes. The experiment was repeated four times for each line. The intensities of all genes are shown after background subtraction, normalization, and merging of replicate culture dye swap hybridizations. MAANOVA statistical analysis was performed to determine genes with significantly different mRNA expression. * Fold change of PAB-1 IP vs total RNA from SV912 (control). ** p-values of 0 and 1 indicate actual values of < 0, 0002 and > 0,9998 respectively.

Probe details of genes enriched in muscle

Probe_ID	WB_ID	Gene	Public name	$\log^2$(PAB-1 IP/ total RNA)*	p-val**
A_12_P102918	WBGene00003369	C36E6.3	*mlc-1*	5,2706523	0
A_12_P119811	WBGene00000653	M195.1	*col-77*	3,8247577	0
A_12_P119150	WBGene00006789	F11C3.3	*unc-54*	3,4472089	0
A_12_P119150	WBGene00000088	F32A7.6	*aex-5*	3,4472089	0
A_12_P103356	WBGene00018519	F46H5.3	*F46H5.3*	3,3433083	0
A_12_P103253	WBGene00004429	Y48G8AL.8	*rpl-17*	3,3098965	0
A_12_P108149	WBGene00006764	ZK721.2	*unc-27*	3,2570846	0
A_12_P116585	WBGene00003769	B0213.6	*nlp-31*	3,2542357	0

GO term analysis of genes enriched in muscle

Overrepresented attributes

N	X	LOD	P	P_adj	attrib ID	attrib name
3	3	2,26	0,00005	0,0330	GO:0005865	striated muscle thin filament
6	13	1,35	0,00000	0,0010	GO:0006099	tricarboxylic acid cycle
6	13	1,35	0,00000	0,0010	GO:0046356	acetyl-CoA catabolic process
6	15	1,25	0,00001	0,0040	GO:0009109	coenzyme catabolic process
6	15	1,25	0,00001	0,0040	GO:0051187	cofactor catabolic process
7	15	1,36	0,00000	0,0010	GO:0006084	acetyl-CoA metabolic process
8	16	1,42	0,00000	<0,001	GO:0006096	glycolysis
7	21	1,13	0,00001	0,0010	GO:0007517	muscle organ development

Supplementary Table 2. Lists of genes enriched ≥2-fold in CYD-1/CDK-4, CYE-1/CDK-2AF, both, or exclusively in one of the strains.

Genes enriched by CYD-1/CDK-4 expression

WB_ID	Gene	Public	Functional category	log^2 fold change
WBGene00006795	Y50E8A.4	*unc-61*	cytokinesis	1,84
WBGene00000064	T04C12.5	*act-2*	cytokinesis	1,51
WBGene00006793	W09C5.2	*unc-59*	cytokinesis	1,23
WBGene00003422	Y47G6A.11	*msh-6*	DNA damage	3,07
WBGene00008641	F10B5.5	*pch-2*	DNA damage	2,73
WBGene00000498	Y39H10A.7	*chk-1*	DNA damage	2,40
WBGene00004737	F10G7.4	*scc-1*	DNA damage	2,21
WBGene00004721	ZC328.4	*san-1*	DNA damage	2,19

Genes enriched by CYD-1/CDK-4 expression, but not enriched by CYE-1/CDK-2AF expression

WB_ID	Gene	Public	Functional category	log^2 fold change
WBGene00004391	T23G5.1	*rnr-1*	DNA repl.	1,32
WBGene00018909	F56A3.2	*F56A3.2*	DNA repl.	1,15
WBGene00004808	F46A9.4	*skr-2*	G1/S	1,08
WBGene00009221	F28F8.2	*acs-2*	metabolism	3,79
WBGene00007203	B0564.3	*B0564.3*	metabolism	2,64
WBGene00009512	F37H8.3	*F37H8.3*	metabolism	1,72
WBGene00017797	F25G6.2	*F25G6.2*	metabolism	1,59
WBGene00019730	M02D8.4	*M02D8.4*	metabolism	1,58

Genes enriched by CYE-1/CDK-2AF expression

WB_ID	Gene	Public name	Functional category	log^2 fold change
WBGene00006795	Y50E8A.4	*unc-61*	cytokinesis	2,53
WBGene00006793	W09C5.2	*unc-59*	cytokinesis	1,34
WBGene00013038	Y49E10.19	*ani-1*	cytokinesis	1,23
WBGene00020527	T15B7.15	*T15B7.15*	cytokinesis	1,22
WBGene00000064	T04C12.5	*act-2*	cytokinesis	1,21
WBGene00003422	Y47G6A.11	*msh-6*	DNA damage	3,00
WBGene00008641	F10B5.5	*pch-2*	DNA damage	2,80
WBGene00004721	ZC328.4	*san-1*	DNA damage	2,45

Supplementary Table 2 continued

Genes enriched by CYE-1/CDK-2AF expression, but not enriched by CYD-1/CDK-4 expression

WB_ID	Gene	Public	Functional category	log^2 fold change
WBGene00013038	Y49E10.19	*ani-1*	cytokinesis	1,23
WBGene00000871	C37A2.4	*cye-1*	G1/S	3,25
WBGene00002068	C27A2.3	*ify-1*	G1/S	2,11
WBGene00019362	K03E5.3	*cdk-2*	G1/S	2,10
WBGene00000776	T03E6.7	*cpl-1*	metabolism	1,08
WBGene00008803	F14E5.5	*lips-10*	metabolism	1,07
WBGene00019899	R05G6.5	*R05G6.5*	metabolism	1,03
WBGene00015975	C18E3.6	*cas-2*	metabolism	1,02

Genes enriched both by CYD-1/CDK-4 expression and CYE-1/CDK-2AF expression

WB_ID	Gene	Public	Functional category	log^2 (CYD-1/CDK-4 fold change)	log^2 (CYE-1/CDK2AF fold change
WBGene00006795	Y50E8A.4	*unc-61*	cytokinesis	1,84	2,53
WBGene00000064	T04C12.5	*act-2*	cytokinesis	1,51	1,21
WBGene00006793	W09C5.2	*unc-59*	cytokinesis	1,23	1,34
WBGene00003422	Y47G6A.11	*msh-6*	DNA damage	3,07	3,00
WBGene00008641	F10B5.5	*pch-2*	DNA damage	2,73	2,80
WBGene00000498	Y39H10A.7	*chk-1*	DNA damage	2,40	2,19
WBGene00004737	F10G7.4	*scc-1*	DNA damage	2,21	2,29
WBGene00004721	ZC328.4	*san-1*	DNA damage	2,19	2,45

Supplementary Table 3. Fold change of all probes enriched in CYD-1/CDK-4 or CYE-1/CDK-2AF lines (p-value < 0.05)

Levels of probes enriched in CYD-1/CDK-4 or CYE-1/CDK-2AF lines

Probe_ID	Gene	Public name	log^2(CYD-1/CDK-4 fold change)	log^2(CYE-1/CDK2AF fold change)
A_12_P108907	B0207.4	*air-2*	4,1011122	3,1183761
A_12_P107620	C23G10.11	*C23G10.11*	3,9486008	-0,36256527
A_12_P114433	T06E6.2	*cyb-3*	3,9092931	3,0764081
A_12_P119342	ZC404.8	*spn-4*	3,8509294	3,2363131
A_12_P111695	F28F8.2	*acs-2*	3,7857912	-0,32729646
A_12_P103129	T05G5.3	*cdk-1*	3,7253049	3,3765616
A_12_P112247	R06F6.1	*cdl-1*	3,5497431	2,9127816
A_12_P102536	T09B4.5	*T09B4.5*	3,5152961	2,8372847

Supplementary Table 4. Transcription factor binding sites enriched in the promoters of Cyclin/CDK-induced genes. Includes sequence logos for the recognition sites of the transcription factors identified in the promoter analysis. The Clover raw score indicates how frequently a motif is present. For E2F sites, this score is 44 for the set of 143 genes upregulated in CYD-1/CDK-4 animals but not in CYE-1/CDK-2 animals, as compared to 167 ± 7 on average for a random selection of 143 genes induced by CYD-1/CDK-4 as well as CYE-2/CDK-2AF.

Enriched ≥ 2-fold in CYD-1/CDK-4			
Rank	TF	Raw-score	p-value
1	E2F1	306	<0.001
2	SPT23	279	<0.001
3	RSC3	259	<0.001
4	SUM1	234	0.033
5	EFL-1	222	<0.001
Enriched ≥ 2-fold in CYE-1/CDK-2AF			
Rank	TF	Raw-score	p-value
1	E2F1	231	<0.001
2	RSC3	207	<0.001
3	EFL-1	185	<0.001
4	SPT23	157	<0.001
5	SUM1	149	<0.001
Enriched only in CYD-1/CDK-4, not in CYE-1/CDK-2AF			
Rank	TF	Raw-score	p-value
1	CHA4	53	<0.001
2	SUT1	47	<0.001
3	E2F1	44	0.012
4	RSC3	41	<0.001
5	btd	38	0.003
12	EFL-1	24	<0.001

Subset of 143 genes from both enriched >2-fold, 100 randomizations		
TF	Average Raw-score	Average p-value
E2F1	167.32 ± 7.25	<0.001
EFL-1	136.46 ± 10.78	<0.001

Absolute TF site numbers					
Dataset	Promoters analyzed	E2F1 sites	E2F1 sites/ promoter	EFL-1 sites	EFL-1 sites/ promoter
Enriched in CYD-1/CDK-4	378	1276	3,38	614	1,62
Enriched in CYE-1/CDK-2AF	211	781	3,70	375	1,78
Enriched only in CYD-1/CDK-4	139	386	2,78	200	1,44
Whole genome	18362	49126	2,68	18941	1,03

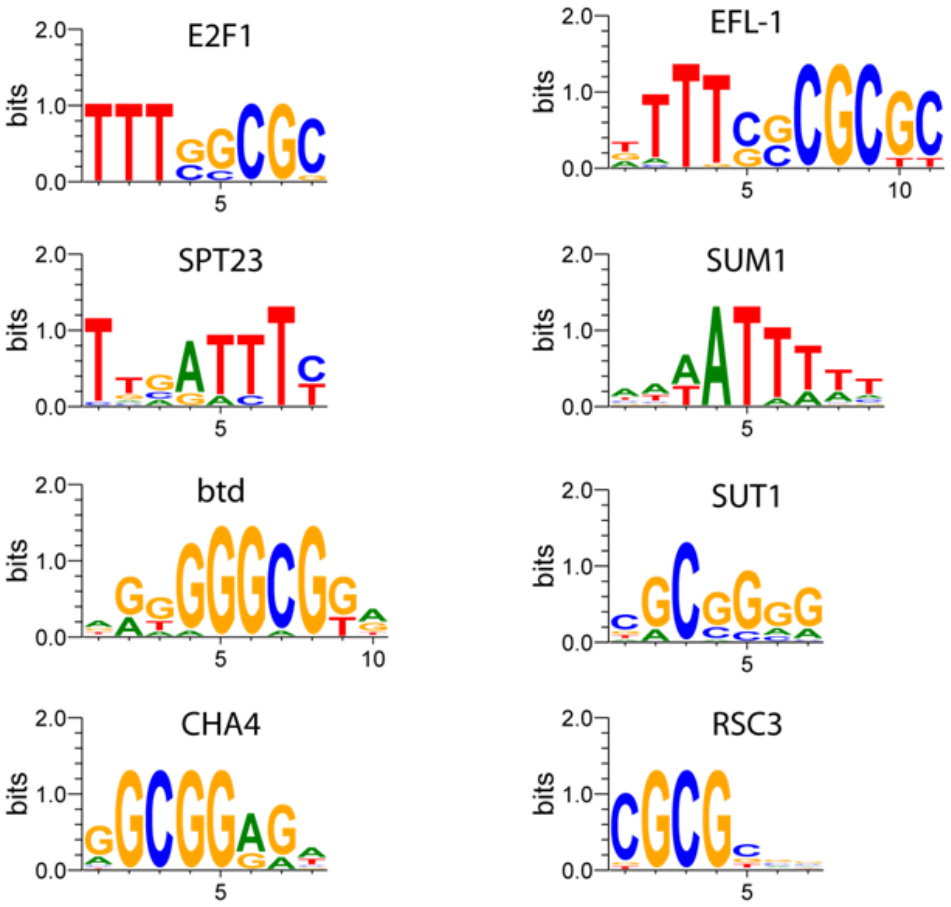

Supplementary Table 5. Lists of genes downregulated ≥2-fold in CYD-1/ CDK-4, and genes upregulated ≥2-fold in control muscle cells that are downregulated ≥2-fold in CYD-1/CDK-4. Includes GO-term analysis of these genes.

Genes downregulated by CYD-1/CDK-4 expression			
WB_ID	Gene	Public	log^2 fold decrease
WBGene00006439	T27E9.1	*ant-1.1*	-3,92
WBGene00022292	Y75D11A.3	*Y75D11A.3*	-3,23
WBGene00021050	W05H9.3	*W05H9.3*	-3,23
WBGene00010485	K01H12.2	*ant-1.3*	-3,00
WBGene00020140	T01B11.4	*ant-1.44*	-2,98
WBGene00022291	Y75D11A.2	*Y75D11A.2*	-2,92
WBGene00003474	T08G5.10	*mtl-2*	-2,87
WBGene00020380	T09B4.6	*T09B4.6*	-2,84

Chapter 5

Examining cell cycle arrest of terminally differentiated neurons in *C. elegans* and rat hippocampal cultures

Suzan Ruijtenberg[1], Inge The[1], Stephan Kersten[1], Tim van Mourik[1], Henri Weigand[1], Marijn Kuijpers[2], Casper C. Hoogenraad[2] & Sander van den Heuvel[1]

1. Developmental Biology, Faculty of Sciences, Department of Biology, Utrecht University, Padualaan 8, 3584 CH Utrecht, The Netherlands. **2.** Cell Biology, Faculty of Sciences, Department of Biology, Utrecht University, Padualaan 8, 3584 CH Utrecht, The Netherlands.

Abstract

During development, tight coordination between cell division and cell differentiation is needed to form cells in the right numbers and with the correct specialized functions. Proliferating precursor cells that undergo terminal differentiation permanently lose the capacity to divide. Here we examine the post-mitotic state of terminally differentiated neurons using *C. elegans* and primary mammalian neuronal cultures as model systems. This dual approach enabled us to combine the power of *C. elegans* genetics with functional validation in a mammalian system. We found that forced expression of CDK4-cyclin D was sufficient to induce partial cell cycle re-entry in both *C. elegans* osmo-sensory neurons and primary mammalian neuronal cultures. In addition, our preliminary studies indicate that the pRb tumor suppressor and FZR1 co-activator of the Anaphase Promoting Complex/Cyclosome (APC/C) act in parallel to promote cell cycle arrest of differentiated mammalian hippocampal neurons. These results agree with observations in *C. elegans* and indicate that the mechanisms that maintain the post-mitotic state are evolutionarily conserved. In order to identify novel critical regulators required for maintenance of a post-mitotic state in terminally differentiated neurons, we performed a candidate-based RNAi screen as well as a forward genetic screen in *C. elegans*. The forward genetic screen identified candidate mutants in which the induction or maintenance of cell cycle withdrawal may be disturbed during neuronal differentiation. While further analysis will be required to understand the phenotypes of these mutants, our work identified functionally conserved mechanisms that contribute to cell cycle arrest in coordination with neuronal differentiation.

Introduction

Proper development requires tight coordination between cell proliferation and differentiation. During embryogenesis, extensive proliferation expands the number of cells, while adult organisms consist largely of post-mitotic functionally specialized cell types. Proliferation and differentiation show a remarkable inverse relationship, with terminally differentiating cells losing the capacity to divide (Myster and Duronio, 2000; Zhu and Skoultchi, 2001; Buttitta and Edgar, 2007). The decision whether to continue cell division or to exit from the cell cycle depends on the activity of Cyclin Dependent Kinases (CDKs). When activated, CDK4/6-cyclin D and CDK2-cyclin E promote progression from G1 into S-phase. One of the key functions of these G1 CDK-cyclin complexes is phosphorylation of the Rb tumor suppressor protein. Phosphorylation of pRb allows its release from E2F transcription factors and subsequent E2F-dependent activation of S-phase genes (van den Heuvel and Dyson, 2008).

The activity of G1 CDK-cyclin complexes is inhibited by their binding to CDK inhibitory proteins (CKIs) such as p16 INK4A, $p21^{Cip1}$ and $p27^{Kip1}$. In addition to inhibition by pRb and CKI, progression through G1 can also be inhibited by ubiquitin-mediated protein degradation of cell cycle regulators. Cell cycle mediated protein degradation involves the Skp1, Cullin, F-box factor (SCF) complex and the Anaphase Promoting Complex/Cyclosome (APC/C) E3 ubiquitin ligases (Cardozo and Pagano, 2004; Skaar and Pagano, 2008, 2009; Wäsch *et al.*, 2010). The substrate specificity of the APC/C depends on interaction with its co-activators CDC20 and FZR1 (Cdh1). FZR1 binds to and activates the APC/C during late mitosis and G1 and plays an important role in cell cycle regulation.

Exit from the cell division cycle can either be temporal, during quiescence, or permanent, during terminal differentiation. The main difference between temporal and permanent cell cycle exit most likely depends on activation of differentiation-inducing transcription factors (TFs) and the concomitant changes in gene expression. Activation of these TFs, together with chromatin regulators and the inhibition of the cell cycle machinery induces functional and morphological changes, leading to a permanent switch from proliferating precursor cells to differentiated post mitotic cells (Buttitta and Edgar, 2007).

Cell cycle exit during differentiation is a tightly regulated process. Nevertheless, some terminally differentiated cells have been observed to re-enter the cell cycle. For instance, combined loss of function of Rb and p19 ARF in mice proved sufficient for cell cycle re-entry of post-mitotic muscle cells (Pajcini *et al.*, 2010). Similarly, loss of Rb-induced proliferation of post-mitotic differentiated hair cells in the mouse inner ear (Sage *et al.*, 2005), while conditional Rb family knockout mice developed retinal eye tumors from terminally differentiated neurons (Ajioka *et al.*, 2007). This indicates that, at least in some specific terminally differentiated cell types, proliferation can coincide with terminal differentiation *in vivo*. However, such events are very rare, probably indicating that multiple levels of control normally antagonize cell cycle re-entry of terminally differentiated cells. Improved insights in the full network of regulators that restrict proliferation of terminally differenti-

ated cells will contribute to our understanding of normal development, cancer formation and regeneration.

In this study, we investigated the arrested state of terminally differentiated neurons. We examined both osmo-sensory and dopaminergic neurons in *C. elegans* as well as primary rat hippocampal neurons in culture. This dual approach allowed us to combine the power of efficient genetics in *C. elegans* with functional validation in a mammalian system. Forced expression of CDK-4/CYD-1 in *C. elegans* neurons induced partial cell cycle re-entry, marked by expression of the S-phase marker MCM-4::mCherry and DNA synthesis as detected by EdU incorporation. Similarly, loss of *fzr-1*, a co-activator of the APC/C, resulted in expression of the S-phase marker MCM-4::mCherry in differentiated neurons in *C. elegans* (The *et al.*, 2015). Interestingly, the function of CDK-4/CYD-1 and FZR-1 seems to be conserved, as similar results were obtained in rat hippocampal neurons. Moreover, loss of *fzr-1* increased the percentage of EdU positive hippocampal neurons observed upon inactivation of Rb and p53. This indicates that Rb and FZR1 act in a parallel fashion to maintain cell cycle arrest in terminally differentiated rat hippocampal neurons, which is in agreement with our previous work in *C. elegans* (The *et al.*, 2015). In order to identify novel critical regulators required for cell cycle arrest in terminally differentiated neurons, we performed a candidate-based RNAi screen as well as an unbiased forward genetic screen, in which we identified three interesting mutants. Further analysis is required to invest whether these mutants show true proliferation of terminally differentiated neurons. In summary, our work identified functionally conserved mechanisms required to maintain cell cycle arrest in terminally differentiated neurons, and we show that genetic screening has the potential to reveal additional levels of control.

Results and Discussion

S-phase re-entry in terminally differentiated neurons upon overexpression of CDK-4/CYD-1

We have previously shown that expression of CDK-4/CYD-1 and CDK-2/CYE-1 in terminally differentiated *C. elegans* body wall muscles induced partial cell cycle re-entry (Korzelius *et al.*, 2011a). Here, we investigate whether these G1 CDK-cyclin complexes execute similar effects in terminally differentiated neurons. *C. elegans* contains eight osmo-sensory neurons. Four of these are located in the head (ASH and ASI left and right) and four are located in the tail (PHA and PHB, left and right). These osmo-sensory neurons can be visualized by expression of fluorescent reporters from the *osm-10* promoter. GFP expression is first observed at the end of embryogenesis, when all osmo-sensory neurons have become fully differentiated, and continues through the larval and adult stages (Faber *et al.*, 1999; Hart *et al.*, 1999).

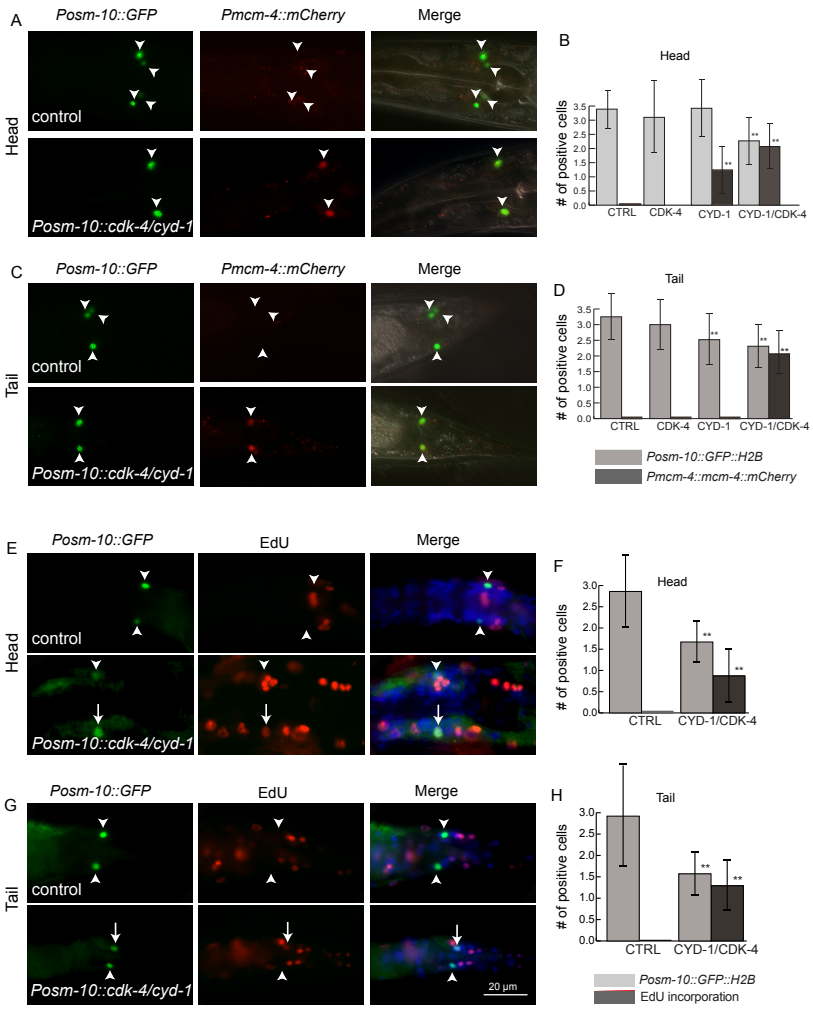

Figure 1. S-phase re-entry in terminally differentiated osmo-sensory neurons in *C. elegans*. (A-D) Analysis of *Pmcm-4::mCherry* expression in osmo-sensory neurons. (A, C) Nuclei of osmo-sensory neurons are marked by *Posm-10::GFP::H2B* (green, arrowheads). *Pmcm-4::mCherry* expression is shown in red. Note: *Pmcm-4::mCherry* (red) expression is only detected in neurons of *Posm-10::cyd-1/cdk-4* expressing animals (lower panel in A and C). (B, D) Quantification of the number of MCM-4::mCherry positive osmo-sensory neurons in the head (B) and tail (D) region upon overexpression of CDK-4, CYD-1 or CYD-1 and CDK-4. (E-H) Analysis of EdU incorporation in osmo-sensory neurons. (E, G) Fluorescence microscopy images of EdU (red) incorporation in osmo-sensory neurons (green) in control (upper panel) and *Posm-10::cyd-1/cdk-4* overexpressing animals (lower panel). Nuclei are marked with DAPI (blue). Arrowheads indicate osmo-sensory neurons negative for EdU, arrows indicate osmo-sensory neurons positive for EdU. (F, H) Quantification of the number of EdU positive osmo-sensory neurons in control and *Posm-10::cyd-1/cdk-4* overexpressing animals in the head (F) and tail (H) region. Graphs show mean ± s.e.m, ** indicates a significant difference (P <0,01) to the control group, scale bar represents 20 µm.

We expressed CDK-4/CYD-1 under the control of the *osm-10* promoter and investigated whether the GFP positive osmo-sensory neurons showed signs of cell cycle re-entry, as visualized by induction of the S-phase marker MCM-4::mCherry or EdU incorporation (Korzelius *et al.*, 2011a, 2011b). In control animals, MCM-4::mCherry expression was undetectable in GFP expressing osmo-sensory neurons (Figure 1A, upper panel). In contrast, mCherry expression was clearly observed in osmo-sensory neurons of CDK-4/CYD-1 overexpressing animals (Figure 1A-D), indicating that overexpression of CDK-4/CYD-1 can induce S-phase re-entry in terminally differentiated neurons. Next, we addressed whether overexpression of either CYD-1 or CDK-4 alone is sufficient to induce MCM-4 expression. While MCM-4::mCherry was not detectable in CDK-4 expressing neurons, overexpression of CYD-1 alone resulted in MCM-4::mCherry expression specifically in the ASI neuron (Figure 1B, D). This indicates that ectopic CYD-1 expression may be sufficient to induce E2F-dependent gene expression and partial cell cycle re-entry in a differentiated neuron.

To visualize whether CDK-4/CYD-1 is sufficient to induce DNA replication as well, we used EdU incorporation and labeling in combination with antibody staining (Salic and Mitchison, 2008; Korzelius *et al.*, 2011a). Synchronized L1 animals were put on EdU-containing plates and fixed and stained for both EdU and GFP as L4 animals. Although weak, EdU incorporation was detectable in approximately half of the GFP positive neurons in the head and most of the neurons in the tail region of animals overexpressing CDK-4/CYD-1. In contrast, EdU incorporation was never observed in osmo-sensory neurons of control animals (Figure 1E-H). These data reveal that overexpression of CDK-4/CYD-1 is sufficient to induce cell cycle re-entry, including DNA replication in S-phase. Extra neuronal nuclei or cells were, however, not observed, indicating that although these cells enter S-phase, they most likely arrest prior to mitosis. Moreover, in some of the CDK-4/CYD-1 overexpressing animals we observed a surprising decrease in the number of GFP positive neurons (Figure 1B and D). This observation suggests a loss of differentiation and associated *Posm-10::GFP* expression or, alternatively, the induction of apoptosis of osmo-sensory neurons upon overexpression of CDK-4/CYD-1. As yet, we have not performed experiments to discriminate between these possibilities.

In body wall muscle cells, overexpression of CDK-2AF, a constitutively active variant of CDK-2, together with CYE-1 did not induce EdU incorporation, but resulted in quite efficient induction of mitosis (Korzelius *et al.*, 2011a). To investigate the effect of CDK-2AF/CYE-1 expression in neurons, we introduced CDK-2AF/CYE-1 under the control of the *osm-10* promoter. In contrast to the results obtained in body wall muscle cells, no mitotic events or extra nuclei could be observed. However, the morphology of the neuronal nuclei became highly abnormal, suggesting that the overexpression of this specific combination was toxic to the cells. Therefore the effect of CDK-2AF/CYE-1 overexpression in neurons was not examined any further. Taken together, we conclude that, CDK-4/CYD-1 functions as a general, potent inducer of cell cycle re-entry in at least two different cell types in *C. elegans*.

Cell cycle re-entry in differentiated rat hippocampal neurons

Ultimately, our studies in *C. elegans* aim to reveal evolutionarily conserved mechanisms for cell cycle arrest. Hence, we set out to examine whether the observed CDK4/6-cyclin D dependency observed above applies to mammalian neurons as well. As a model system, we used primary rat hippocampal neuron cultures. These primary neurons are isolated from embryonic day 18 (E18) rat brains and cultured together with glia cells (Kaech and Banker, 2006; Kapitein *et al.*, 2010). At E18, hippocampal neurons are committed to the neuronal lineage, although functional neurites still need to develop (Dotti *et al.*, 1988). Formation of neurites starts already after a few hours in culture, when neurons form a number of immature neurites that undergo random growth and retraction. After approximately one day *in vitro* (DIV1), one of these neurites starts to extend more rapidly and becomes much longer than the others. During the next days (DIV 2-4) this extended neurite becomes a specialized axon. During the following days, the remaining neurites elongate and acquire the characteristics of dendrites, which can form synaptic contacts that enable the transmission of electrical activity (Barnes and Polleux, 2009).

In order to analyze cell cycle progression and cell cycle re-entry in rat hippocampal neuron cultures, we combined EdU incorporation with antibody staining against neuron- or glia-specific targets. To visualize differentiated neurons, we stained for the specific markers Tuj1 or β3-tubulin, while the supporting glia cells were visualized based on specific reactivity with antibodies recognizing the Glial Fibrillary Acidic Protein (GFAP) (Figure 2A, C). When EdU was provided to control cultures at DIV1, occasionally EdU incorporation could be observed in Tuj1 positive neurons. In contrast, when neurons received EdU at DIV4 or later, no EdU incorporation was observed (Figure 2A-B). The glia cells on the other hand, continued to proliferate as DNA synthesis, visualized by EdU incorporation could be detected in these cells even after four or seven days *in vitro* (Figure 2C). These data indicate that while neurons are committed to the neuronal lineage at E18, not all cells in culture have exited the cell cycle at DIV1. After the first day *in vitro* however, neurons indeed permanently exit the cell cycle and become post-mitotic.

We reasoned that starting the experiments after neurons have permanently exited the cell cycle would allow us to investigate the mechanisms that prevent cell cycle re-entry in rat hippocampal neurons. We therefore developed an experimental set-up which included transfection and addition of EdU at DIV4, followed by fixation of the cells at DIV7 to DIV10. A blue fluorescent protein (BFP) expressing plasmid was co-transfected to allow discrimination between transfected and non-transfected neurons. Forced cell cycle re-entry in neurons has previously been shown to induce apoptosis (Sumrejkanchanakij *et al.*, 2003; Herrup and Yang, 2007; Yang and Herrup, 2007). To prevent cell death, we added a plasmid encoding the anti-apoptotic protein Bcl2 to our transfection mixes.

To mimic the CDK-4/CYD-1 expression experiments in *C. elegans*, neurons were transfected with CDK4-cyclin D2 and incubated with EdU at DIV4, followed by examination of EdU incorporation at DIV7. Overexpression of CDK4-cyclin D2 induced partial cell cycle re-entry as measured by EdU incorporation, which was never observed in neurons transfected with only BFP and Bcl2 expressing plasmids (Figure 2D, F). Although only a

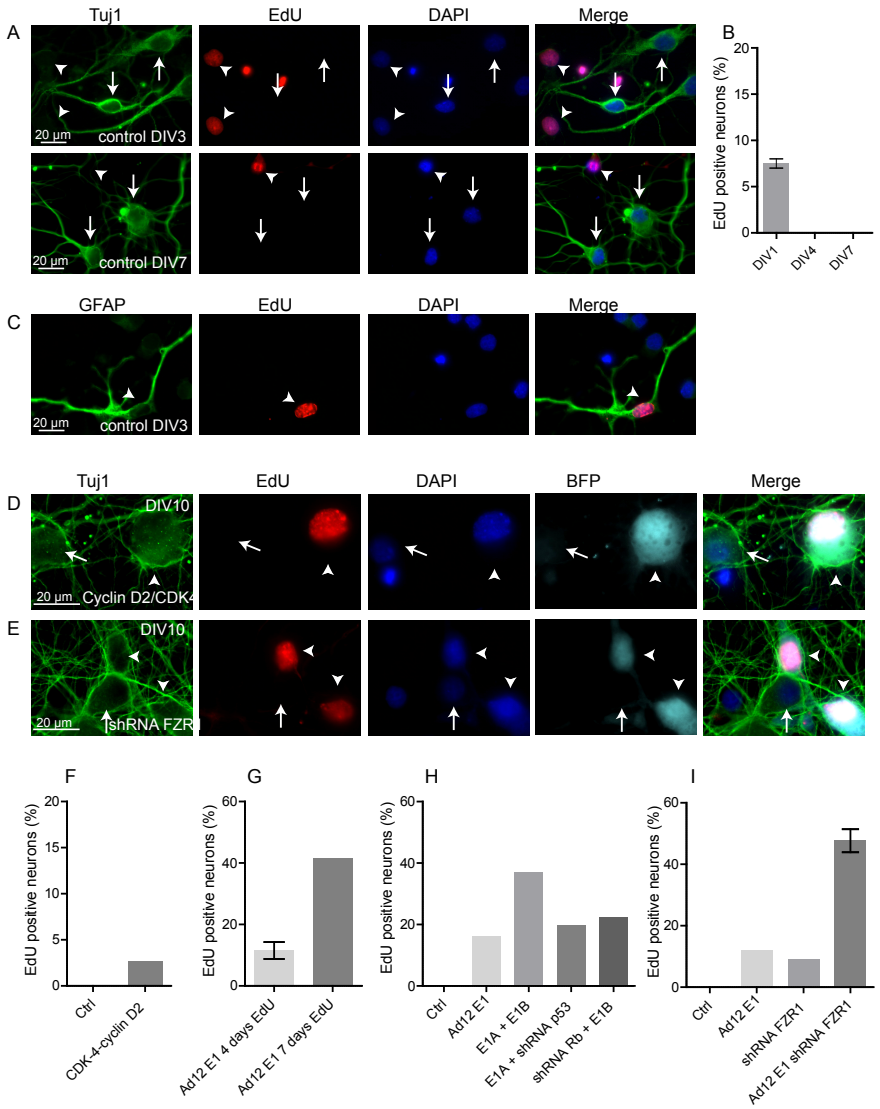

Figure 2. Partial cell cycle re-entry in terminally differentiated rat hippocampal neurons. (A, C, D, E) Fluorescence microscopy images of rat hippocampal neuron cultures transfected with the indicated constructs and stained at the indicated time points. Neurons are stained with Tuj1, marking the neuron-specific β3-tubulin isotope (green)(A, D, E), while glia cells express GFAP (C). DNA replication is visualized by EdU incorporation (red) and nuclei are marked by DAPI (blue). Transfected cells are visualized by BFP (light blue). Arrows indicate EdU negative cells, arrowheads indicate EdU positive cells. (B) Quantification of the percentage of EdU positive neurons in control cultures, to which EdU was added at DIV1, DIV4 or DIV7. (F-I) Quantification of the percentage of EdU positive neurons under the indicated conditions. Control neurons were transfected with BFP and Bcl2. Scale bar represents 20 µm. Error bars represent ± s.e.m.

low percentage of the transfected cells was positive for EdU and more extensive analysis is needed, this result indicates that CDK4-cyclin D2 is able to induce S-phase entry in rat hippocampal neurons. The low percentage of EdU positive cells may indicate that CDK4-cyclin D2 in rat hippocampal neurons is not as important for proliferation as it is in *C. elegans*, or that additional mechanisms are still able to inhibit proliferation of these cells. In addition, it is possible that CDK4 in complex with other D-type cyclins (D1 or D3) or a D-type Cyclin with CDK6, would be more potent than CDK4-cyclin D2 in inducing S phase entry in rat hippocampal neurons.

Loss of *fzr-1* induced the expression of the S-phase marker MCM-4 in a variety of different post-mitotic neurons in *C. elegans*, indicating that *fzr-1* is important in preventing cell cycle re-entry (Chapter 3, The et al., 2015). In order to investigate the role of FZR1 in rat hippocampal neurons we inhibited FZR1 expression via RNA interference. Neurons were transfected at DIV4 with shRNAs targeting FZR1, EdU was added to the cultures at DIV7 and neurons were fixed at DIV10. Inhibition of FZR1 in rat hippocampal neuron cultures resulted in EdU incorporation in approximately 10% of the neurons (Figure 2E, I). This indicates that, in agreement with the role of *fzr-1* in the maintenance of a non proliferative state in *C. elegans*, FZR1 contributes to the cell cycle arrest of mammalian neurons.

Thus, the mechanisms that maintain cell cycle arrest of terminally differentiated neurons may be conserved between *C. elegans* and mammals.

Rb family members and p53 are involved in the maintenance of a non-proliferative state in many systems and are therefore likely to fulfill a role in cell cycle exit of hippocampal neurons (Stiewe, 2007; van den Heuvel and Dyson, 2008; Polager and Ginsberg, 2009). In order to investigate the role of Rb and p53, we used two alternative strategies: expression of DNA tumor virus derived oncoproteins and shRNAs. Human adenoviruses (Ad) encode two early expressed proteins that interfere with the function of pRb and p53. Ad5 and Ad12 E1A proteins bind the pRb pocket domain and thereby compete with E2F for Rb association (Whyte *et al.*, 1988; Bandara and La Thangue, 1991; Chellappan *et al.*, 1991). The large E1B proteins interfere with the function of cellular p53, dependent on the Ad serotype either by direct sequestration or through alternative mechanisms (Sarnow *et al.*, 1982; Zantema *et al.*, 1985; van den Heuvel *et al.*, 1993). Similarly, the E6 and E7 proteins of oncogenic human papilloma viruses (HPV) interfere with the function of cellular p53 and pRb, respectively (Dyson *et al.*, 1989; Münger *et al.*, 1989; Scheffner *et al.*, 1990; Werness *et al.*, 1990). In order to inhibit Rb and p53, we transfected neurons with Ad12 E1 at DIV4, and fixed the cells three or four days later. This resulted in EdU incorporation and S-phase re-entry in approximately 10% of the transfected neurons (Figure 2G). When neurons were transfected with Ad12 E1 and grown for seven days in the presence of EdU (transfection and addition of EdU at DIV7, fixation at DIV14), more than 40% of the transfected cells was positive for EdU (Figure 2G). The high percentage in the latter suggested that DNA replication continued over time. A time-dependent increase of S-phase re-entry was also observed in similar experiments where we transfected neurons with Ad12 E1-containing transfection mixes and directly compared the percentage of EdU positive neurons after three and seven days of EdU incubation (Figure S1). Importantly, these data demonstrate

that overexpression of Ad12 E1 can force cell cycle re-entry, indicating that pRb, p53 and possibly additional cellular proteins promote maintenance of the arrested state.

To examine whether the observed effects resulted from pRb and p53 inhitibion, we used additional Rb and p53 targeting constructs. Instead of the entire Ad12 E1 region, we used Ad5 or Ad12 E1A to inactivate pRB, and only large E1B coding sequences to inhibit p53. In addition, we used and shRNAs targeting Rb and p53. Indeed, transfection of neurons with a combination of E1A from either Ad12 or Ad5 with the expression of E1B from either Ad12 or Ad5 also resulted in EdU incorporation (Figure 2H, Table S1). Combining expression of E1A with the use of shRNAs targeting p53, or combining the expression of E1B with shRNAs directed against Rb also resulted in similar amounts of EdU incorporation (Figure 2H). Additional combinations were tested and a complete overview of performed experiments is provided in Table S1. Although some of the combinations of virus constructs and shRNAs were tested only once, these experiments underscore that inactivation of Rb and to a lesser extent p53 can lead to cell cycle re-entry in post-mitotic rat hippocampal neurons.

Two parallel acting mechanisms inhibiting cell cycle progression and preventing cell cycle re-entry in terminally differentiated cells were observed in *C. elegans*: pRb family-dependent transcriptional repression and FZR1-dependent protein degradation (The *et al.*, 2015). To test whether both factors are also important for rat hippocampal neurons, we combined expression of shRNAs against FZR1 with Ad12 E1 transfection (Figure 2I). Indeed, FZR inhibition combined with Ad12 E1 introduction increased the percentage of EdU positive rat-hippocampal neurons compared to neurons transfected with Ad12 E1 or FZR1 shRNAs alone (Figure 2I). Similar results were obtained upon inactivation of APC2, one of the main subunits of the APC/C that is required for FZR1 binding (Figure S1). This demonstrates that redundant mechanisms prevent cell cycle re-entry in terminally differentiated neurons and that these mechanisms are likely to be functionally conserved between *C. elegans* and mammals.

Genetic identification of genes that contribute to the non-proliferative state of *C. elegans* neurons

In the experiments described above, overexpression of CDK-4/CYD-1 and loss of *fzr-1* induced partial cell cycle re-entry in *C. elegans* osmo-sensory neurons and rat hippocampal neurons. However, cell division and formation of new daughter cells were not observed. While this indicates the presence of additional safeguards that inhibit proliferation, it is as yet unclear which mechanisms prevent continued proliferation of terminally differentiated neurons. To be able to identify critical regulators, we performed two unbiased forward genetic screens as well as a candidate-based RNAi screen for *C. elegans* larvae with extra differentiated neurons. As in the previous experiments, we used the *Posm-10::GFP::H2B* reporter to visualize osmo-sensory neurons and screened for animals with more than the normal eight *Posm-10::GFP::H2B* positive cells present in wild-type animals. Because loss of

fzr-1 leads to partial cell cycle re-entry but not full mitosis, we used the *fzr-1(ku298)* mutation as an attractive sensitized background in these screens.

Progression from proliferative precursors to permanently arrested and fully differentiated cells is thought to depend on the combined activity of cell cycle regulators, differentiation promoting transcription factors and chromatin regulators. To investigate the role of transcription and chromatin regulators in preventing cell cycle re-entry in neurons, we performed a candidate-based RNAi screen that included 263 transcription and chromatin-related genes (Table S2 for all tested genes). *C. elegans* neurons are normally insensitive to RNAi treatment. To enable RNA interference, we introduced *nre-1(hd20)* and *lin-15B(hd126)* mutations into our *Posm-10::GFP; fzr-1(k298)* strain (Schmitz *et al.*, 2007). Indeed, RNAi against GFP was more effective in this strain compared to the non-sensitized strains (Figure S2). In spite of this sensitized protocol we did not identify any gene that upon downregulation increased the number of osmo-sensory neurons. Although negative RNAi results are little informative, these data could indicate that loss of a single transcription factor or chromatin regulator in combination with loss of the cell cycle regulator *fzr-1* is not sufficient to prevent cell cycle exit or induce cell cycle re-entry in these neurons.

In an EMS mutagenesis-based forward genetic screen, the *fzr-1(ku298)* mutant strain was again used as a sensitized background in combination with the *Posm-10::GFP::H2B* marker. We looked for mutants with more than eight GFP expressing cells. In a small-scale screen (approximately 700 haploid genomes), we identified seven mutants with additional *Posm-10::GFP::H2B* expressing cells in the head region. Two of these mutants, *he234* and *he235,* could be recovered and maintained as homozygous strains (Figure 3). Quantifications indicated near doubling of the number of GFP positive cells in the head region of *he234* and *he235* mutants (4.0 GFP positive cells in the control strain, 7.3 and 8.0 in *he234* and *he235* mutants, respectively) (Figure 3A-D). While these numbers could indicate the formation of additional osmo-sensory neurons, alternative explanations are possible. For instance, the sister cells of the ASI neurons could have failed to undergo apoptosis, and the *Posm-10* driven GFP reporter construct could be expressed aberrantly.

In order to investigate whether the identified mutations defined genes with a role in cell cycle regulation, we performed further characterizations of these two mutants. If these extra cells indeed result from continued proliferation, an increase in the number of *Posm-10* driven GFP positive cells may be expected over time. Indeed, when comparing the number of GFP positive cells in L1 animals to L3/L4 animals the number of GFP positive cells increased (Figure 3D). Likewise, dependency on *fzr-1* could indicate a cell cycle-related phenotype. To address this question we crossed out the *fzr-1(ku298)* mutation and again scored the number of *Posm-10::GFP::H2B* positive cells. In the absence of the *fzr-1(ku298)* mutation, both the *he234* and *he235* mutant strains showed fewer GFP positive cells compared to the original identified mutants (Figure 3D). This suggested that the phenotype was indeed depended on the inactivation of *fzr-1*. This dependency was further underscored by the observation that the overproliferation phenotype could be restored when *he234* and *he235* mutants with wild-type *fzr-1*, were exposed to *fzr-1* feeding RNAi (Figure 3D). While the number of animals with overproliferation was relatively low in these experi-

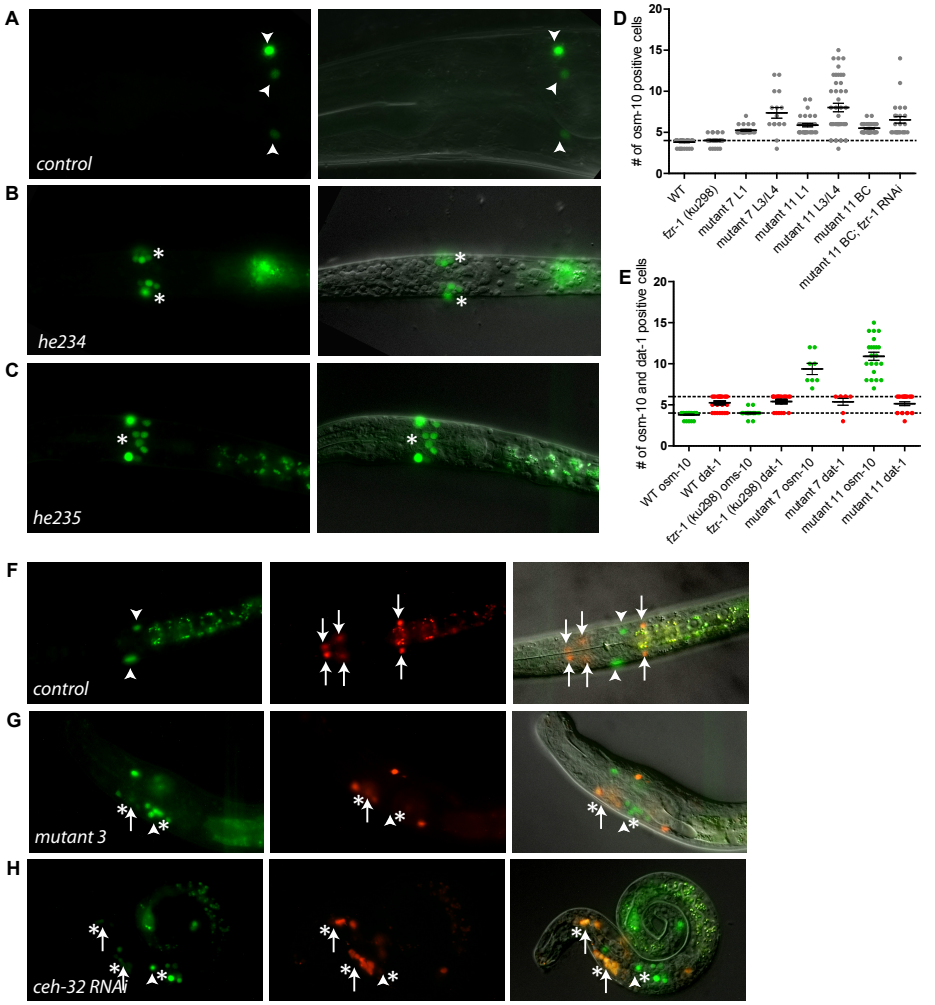

Figure 3. Identification of *C. elegans* mutants with additional osmo-sensory and dopaminergic neurons. Representative fluorescence microscopy images of (A) a control animal carrying the *Posm-10::GFP::H2B* maker (green, arrowheads), or (B-C) mutants *he234* and *he235*. * indicates the region with extra GFP positive cells. (D) Quantification of the number of *Posm-10::GFP::H2B* expressing cells in the head region in control and mutant animals. The number of cells is quantified in the L1 and L3/L4 stages and in the presence or absence of fzr-1 inactivation. (E) Quantification of the number of *Posm-10::GFP::H2B* and *Pdat-1::tdTomato* cells in control and mutant animals. Note that the number of *Pdat-1::tdTomato* expressing cells does not change in these mutants. (F) Fluorescence microscopy image of a control animal expressing both *Posm-10::GFP::H2B* (green, arrowhead) and *Pdat-1::tdTomato* (red, arrow). (G) Representative image of mutant 3 with additional *Posm-10::GFP::H2B* (green, arrowheads and *) and *Pdat-1::tdTomato* (red, arrows and *) expressing cells in the head region. (H) Representative image of a *ceh-32* (RNAi) animal with an increased number of additional *Posm-10::GFP::H2B* (green, arrowhead and *) and *Pdat-1::tdTomato* (red, arrows and *) expressing cells in the head region. Scale bar represents 20 μm. Graphs show mean ± s.e.m. and each dot represents a single animal.

ments, the number of *Posm-10::GFP::H2B* positive cells was significantly different from the observed phenotype of *he234* and *he235* mutants with wild-type *fzr-1*, not exposed to *fzr-1* RNAi, and more comparable to what we observed in the original mutant. This underscores the contribution of *fzr-1* inactivation to the phenotype.

We reasoned that, if the identified mutations define general cell cycle regulators, it is likely that more than one type of neuron is affected by these mutations. To examine the effect of the *he234 and he235* mutations in other neurons, we injected a marker for dopaminenergic neurons into the mutant strains (Figure 3E). This marker, *Pdat-1::tdTomato,* exclusively labels eight dopaminergic neurons in *C. elegans*. Six of these neurons are located in the head region (CEPD left and right, CEPV left and right, ADE left and right) and two are located in the tail region (PDE left and right) (Nass *et al*., 2002; Flames and Hobert, 2009). We quantified the number of *Pdat-1::tdTomato* expressing cells in control and *he234* and *he235* mutant animals. The number of *Pdat-1::tdTomato* expressing cells did not change in the *he234* and *he235* mutants, indicating that the observed phenotype was specific for osmo-sensory neurons (Figure 3E). This suggests that the identified mutations most likely do not define a general cell cycle regulator. Moreover, DNA replication by EdU incorporation or signs of mitosis were not observed in the osmo-sensory neuronal lineage. Together, these data indicate that the observed extra GFP positive cells do not results from proliferation of osmo-sensory neurons, but may rather reflect incorrect expression of the *Posm-10::GFP::H2B* reporter. A possible explanation for the increase in *Posm-10::GFP::H2B* expressing cells during larval development would be the accumulation of *Posm-10* driven GFP in neurons other than osmo-sensory neurons. Likewise, the dependency of the phenotype on the inactivation of *fzr-1* might be explained by the previously suggested role of *fzr-1* in neuronal differentiation (Teng and Tang, 2005; Eguren *et al*., 2011; Pick *et al*., 2013). Since clear cell cycle re-entry and neuronal proliferation was never observed in *he234* and *he235* mutants, further analysis of these mutants was halted.

We adjusted the screen with the goal of increasing the chances of identifying general regulators of cell cycle exit in neurons. Hereto, we mutagenized animals that contained a *Posm-10* driven GFP marker as well as a *Pdat-1* driven tdTomato marker in the *fzr-1(ku298)* background (Figure 3F). This genetic background allowed detection of mutants with both extra osmo-sensory neurons marked by GFP and extra dopaminergic neurons marked by tdTomato. Screening this reporter strain, we identified several mutants with additional *Poms-10::GFP::H2B* positive cells, one mutant with an increase in the number of *Pdat-1::tdTomato* labeled cells and one mutant (mutant number 3) with both extra osmo-sensory as well as dopaminergic neurons (Figure 3G). Since only mutant 3 showed the phenotype of interest, we further focused our analysis on this mutant. One of the characteristics of this mutant was a "variable abnormal" (Vab) phenotype. A Vab phenotype can be caused by altered expression of a variety of different genes that predominantly encode transcription factors and cell-junction associated proteins. Mutation of the *vab-3* gene was previously shown to increase the number of *Pdat-1* labeled cells (Doitsidou *et al*., 2008); personal communication with O. Hobert). *vab-3* encodes the *C. elegans* homologue of the Pax6/Eyeless gene and acts as an upstream regulator of *ceh-32*. *ceh-32* encodes a homeo-domain transcription factor

of the Six3/6 subfamily and was, like *vab-3*, found to be required for head morphogenesis (Dozier *et al.*, 2001). To investigate whether inactivation of these two transcription factors could mimic the phenotype of the mutants identified in our screen, we performed RNAi of *vab-3* and *ceh-32* and analyzed the number of GFP and tdTomato positive cells. *vab-3* inactivation resulted in a Vab phenotype without apparent increase in the number of osmo-sensory or dopaminergic neurons. Thus, loss of *vab-3* function is unlikely to cause the extra *Posm-10::GFP::H2B* and *Pdat1::tdTomato* positive neurons in the identified mutant. Inhibition of *ceh-32*, however, induced extra *Posm-10::GFP::H2B* and *Pdat-1::tdTomato* expressing neurons (Fig 3F,H). Since *ceh-32* encodes a homeotic transcription factor, the most likely explanation for this observed phenotype is altered cell identity and aberrant expression of the GFP and tdTomato markers, rather than an overproliferation phenotype. Further analysis will be required to discriminate between these possibilities. So far, we have no clear indications that mutant 3 shows proliferation of differentiated neurons. Continued proliferation may in fact change the differentiation status and thereby the expression of the marker used to label the neurons. The fact that we did not identify a mutant with unquestionable continuous neuronal proliferation may indicate that we have screened too few genomes or the desired phenotype may be lethal, rare or unachievable.

In conclusion, we have found that overexpression of G1 CDK-cyclin complexes or loss of *fzr-1* can lead to cell cycle re-entry in *C. elegans* neurons based on the expression of the S-phase marker *mcm-4::mCherry* and incorporation of EdU. Using rat hippocampal neuron cultures we have functionally validated these results in a mammalian system. In addition, we found that transfection of neurons with Adenovirus constructs targeting Rb and p53 resulted in cell cycle re-entry. The percentage of EdU positive neurons increased when transfection of Ad12 E1 constructs was combined with inactivating FZR1, in agreement with observations in *C. elegans* that indicated parallel functions for Rb and *fzr-1* in cell cycle arrest. Mutagenesis-based screens in *C. elegans* identified mutants with more than the wild-type number of cells expressing reporters of osmo-sensory and/or dopaminergic neurons. Further analysis and screening will be required to identify genes that control the induction and maintenance of the non-proliferative state of neurons. Approaches based on lineage-specific gene inactivation may be required to achieve this goal.

Materials and Methods

C. elegans strains and culturing

C. elegans strains were cultured on NGM plates seeded with *E. coli* OP50 according to standard protocols. Strains were maintained at 20 °C, unless otherwise indicated. RNAi clones were selected from the Ahringer and Vidal libraries (Kamath *et al.*, 2003; Rual *et al.*, 2004). For the RNAi screen, a selection of RNAi clones targeting chromatin regulators and transcription factors from the Ahringer library was used. Bacterial cultures of *E. coli*

HT115 containing L4440 empty vector, L4440 targeting GFP, or vector with genomic or ORF gene inserts were grown o/n, three times concentrated and seeded onto NGM plates containing 12.5 µg/ml Tetracycline, 100 µg/ml Ampicillin and 2 mM IPTG. Animals were synchronized by hypochlorite treatment, followed by hatching in M9 buffer. Animals were then allowed to develop for the appropriate amount of time. The following strains were used in this study:

N2 (wild type), **SV1067** *heIs45[Pmcm-4::mcm-4::mcm-4^{shortUTR}::mCherry] MosIV,* **SV1166** *heIs45[Pmcm-4::mcm-4::mcm-4^{shortUTR}::mCherry] MosIV; heEx403[osm-10::GFP::H2B; rol-6],* **SV1167** *heIs45[Pmcm-4::mcm-4::mcm-4^{shortUTR}::mCherry] MosIV; heEx404[osm-10::GFP::H2B; osm-10::CDK4flag; rol-*6], **SV1168** *heIs45[Pmcm-4::mcm-4::mcm-4^{shortUTR}::mCherry] MosIV; heEx405[osm-10::GFP::H2B; osm-10::cyd-1; rol-6],* **SV1170** *heIs45[Pmcm-4::mcm-4::mcm-4^{shortUTR}::mCherry] MosIV; heEx407[osm-10::GFP::H2B; osm-10::CDK4flag; osm-10::cyd-1; rol-6],* **SV1171** *heEx403[osm-10::GFP::H2B; rol-6],* **SV1172** *heEx407[osm-10::GFP::H2B; osm-10::CDK4flag; osm-10::cyd-1; rol-6],* **SV1194** *heIS75[osm-10::GFP::H2B],* **SV1204** *fzr-1(ku298); unc-4(e120) II; heIs75[osm-10::GFP::H2B] MosIV,* **SV1252** *fzr-1(ku298); unc-4(e120) II; heIs75[osm-10::GFP::H2B] MosIV; nre-1(hd20) lin-15B(hd126) X,* **SV1316** *heIs100[dat-1::tdTomato] MosI; fzr-1(ku298); unc-4(e120) II; heIs75[osm-10::GFP::H2B] MosIV;.* **SV1250** *he234 (mutant 7),* **SV1251** *he235 (mutant 11)*

EMS mutagenesis

For mutagenesis, L4 animals of strain SV1204 *fzr-1(ku298); unc-4(e120) II; heIs75[osm-10::GFP::H2B] MosIV* or SV1316 *heIs100[dat-1::tdTomato] MosI; fzr-1(ku298); unc-4(e120) II; heIs75[osm-10::GFP::H2B] MosIV* were collected in 4 ml M9 with 0.05% Tween-20 to which 20 µl ethyl methane sulfonate (EMS) was added. Animals were incubated in EMS solution for 6 hours at room temperature. Two to four F1 animals were put on plates and the F2 progeny was analyzed with a high power microscope (Zeiss Axioplan 2 microscope mounted with an Axiocam mRM camera) for the presence of additional *Posm-10::GFP* and/or *Pdat-1::tdTomato* expressing cells.

Plasmids and Molecular cloning

The following constructs have previously been described: Ad12, Ad5, Ad12 E1A, Ad12E1B, Ad5 E1A and Ad5 E1B, HPV E6 and HPV E7 (Jochemsen *et al.*, EMBO J 1987; Münger *et al.*, 1989; and references herein). The Adenovirus constructs were a kind gift from A.G. Jochemsen, the HPV constructs were a kind gift from K. Münger.

Previously reported expression constructs for cyclin or CDK expression under control of the *myo-3* and *elt-2* promoters (Korzelius *et al.*, 2011a) were used to re-clone the constructs for expression from the *osm-10* promoter. The *osm-10* promoter was obtained by a PCR reaction of the *Posm-10::osm-10exon1* construct in pPD49.26 (a gift of Anne Hart) using primers M13 R (CAGGAAACAGCTATGACCATG) and osm-10-BamHI (CGGGATCCCTTGCAAGATGAAATTTCCA). For creating *Posm-10::cye-1*, *cdk-4, cdk-2*

and *cdk-2AF* constructs, the *Posm-10* PCR product was digested with HindIII and BamH1 and ligated into the HindIII and BamH1 digested vectors *Pmyo-3::cye*; *Pmyo-3::cdk-4::flag*; *Pmyo-3::cdk-4::venus*; *Pmyo-3::cdk-2wt* and *Pmyo-3::cdk-2AF::venus* which resulted in removal of the *myo-3* promoter. *Posm-10::cyd-1* was created by ligation of *Posm-10* PCR product digested with PstI into the *Pelt-2::cyd-1* vector digested with SmaI and PstI, resulting in removal of the *elt-2* promoter. For the generation of *Posm-10::H2B::GFP*, *Pmyo-3::GFP::H2B* was digested with PstI, thereby removing the *myo-3* promoter and subsequently blunted by T4 polymerase (Fermentas) after which undigested *Posm-10* PCR product was ligated into the vector. To create the MosSCI *Posm-10::GFP::H2B* construct, the above *Posm-10::GFP::H2B* was cloned into the multiple cloning site of the PCFJ178 IV vector. To create the *dat-1::tdTomato* construct we replaced GFP with tdTomato in the previously published *dat-1::GFP* construct (a kind gift from R. Korswagen (Nass *et al.*, 2002). The complete sequence of *Pdat-1::tdTomato::unc-54UTR,* containing the *dat-1* promoter consisting of 716 bp immediately upstream of the initiating codon ATG was PCR amplified with the primer dat-1tdTomato Mos F ttactagtCCATGAAATGGAACTTGAATCCAG and dat-1TdTomato MOS R aactcgagaaacagttatgtttggtatattggg and cloned into PCFJ352 I Mos vector using SpeI and XhoI.

shRNA constructs

The following shRNA constructs were used in this study to inactivate FZR1, Rb, p107, p130 and APC2 in neurons: FZR1 shRNA #1 (gctactcacagaaccagat) FZR1 shRNA #2 (gctctacaaaggaatccgt), FZR1 shRNA #3 (gcgtaaacttccataggat), Rb shRNA #1 (cgctacgaagaagtttatc), Rb shRNA #2 (actcctaaatgacaacatc), Rb shRNA #3 (tacctcacattcctcgaag), p107 shRNA #1 (agctaagttaagcttaat), p107 shRNA #2 (ggaccatataatggatgct), p107shRNA #3 (gacttgttaaatccatcat), p130 shRNA #1 (agaacttgtgaaccctaat), p130 shRNA #2 (caaggtattgccaacgaaa), p130 shRNA #3 (aggagagactccaactaa), APC2 shRNA #1 (gaaggtccgagaccagcag), APC2 shRNA #2 (ctaggacattccaggaga) APC2 shRNA #3 (ccgaatgtttgtaatgact)

Cell cultures and transfections

Primary hippocampal cultures were prepared from embryonic day 18 (E18) rat brains (Jaworski *et al.*, 2009; Kapitein *et al.*, 2010). Cells were plated on coverslips coated with poly-L-lysine (30 µg/ml) and laminin (2 µg/ml) at a density of approximately 75,000/well. Hippocampal cultures were grown in Neurobasal medium (NB) supplemented with vitamine B27, 0.5 mM glutamine, 12.5 µM glutamate and penicillin/streptomycin. Hippocampal neurons were transfected after 1 day *in vitro* (DIV1) or 4 days *in vitro* (DIV4), unless otherwise indicated using Lipofectamine 2000 (L2K, Invitrogen). 1.8 µg DNA per well was mixed with 3.3 µl Lipofectamine 2000 in 100 µl NB, incubated for 30 minutes at RT, added to the neurons and incubated for 45 min at 37 °C. Next, neurons were washed with NB and transferred to the original medium. Transfection was followed by the addition of EdU

to a final concentration of 10 μM. Neurons were kept at 37 °C in 5% CO2 for 3-7 days as indicated in the text.

Immunohistochemical staining and detection of DNA replication

For EdU detection and staining of GFP positive osmo-sensory neurons in larvae, animals were synchronized by hypochlorite treatment and exposed to EdU starting from L1. L4 animals were permeabilized by freeze cracking and fixed for 5 min in ice cold methanol and 20 min ice cold acetone treatment as described previously (Salic and Mitchison, 2008; Korzelius *et al.*, 2011a, 2011b). To visualize incorporated EdU, a Click-IT reaction was performed, using the ClickIT EdU Alexa Fluor 594 kit (Invitrogen) according to the manufacturer's instructions and based on the protocol developed by S. Crittenden and J. Kimble (Salic and Mitchison, 2008). Primary mouse anti-GFP (1:100, Sigma) and secondary goat anti-mouse Alexa488 (1:200, Invitrogen) were used to stain H2B::GFP. Finally, worms were mounted in Prolong Anti-Fade Gold (Invitrogen) with 1:1000 DAPI (Sigma).

Rat hippocampal neurons were fixed in 4% paraformaldehyde with 4% sucrose in PBS, washed three times and incubated with 0.5% Triton X-100 in PBS for 20 min. The permeabilization buffer was removed and neurons were incubated with 0.5 ml of Click-it EdU reaction cocktail for 30 min, according to the manufacturer's instructions. After 30 min, the Click-it EdU reaction cocktail was removed and neurons were incubated with the indicated primary antibodies in GDB buffer (0.2% BSA, 0.8 M NaCl, 0,5% Triton X-100, 30 mM phosphate buffer pH 7.4) overnight at 4 °C. Neurons were then washed three times in PBS for 30 min, incubated with secondary antibodies in GDB for 1 hour at room temperature and washed three times in PBS for 30 min. Slides were mounted using Vectoshield mounting medium and analyzed using a Zeiss Axioplan 2 microscope mounted with an Axiocam mRM camera.

Primary antibodies used in this study include: mouse anti-GFP (1:100, Sigma), rabbit anti-β3-tubulin (1:1000, Covance), rabbit anti-phospho-H3S10 (1:200, Abcam), mouse anti-GFAP (1:20000, Sigma), mouse anti-Tuj1 (1:1000). Secondary antibodies include: goat anti-mouse Alexa488 (1:500, Invitrogen), goat anti-rabbit Alexa488 (1:500 Invitrogen), goat anti-mouse Alexa568 (1:500, Invitrogen), goat anti-rabbit Alexa568 (1:500, Invitrogen).

Supporting Information

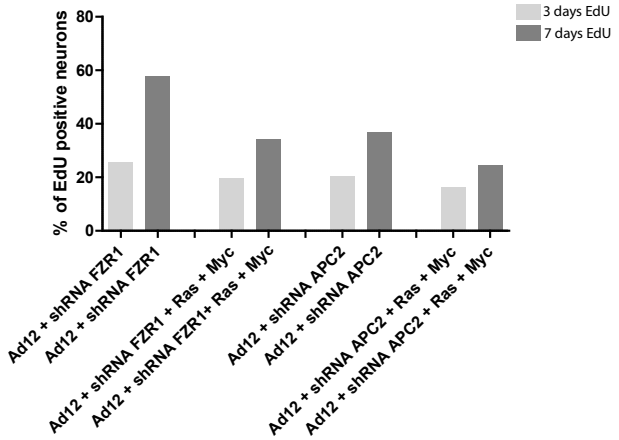

Supplementary Figure 1. Increase of the percentage of EdU positive neurons over time. Quantification of the number of EdU positive neurons after three or seven days of EdU treatment under the indicated conditions. Note that the percentage of EdU positive cells increased when cells are exposed for EdU for seven instead of three days, indicating that DNA replication continues over time. Graph shows mean ± s.e.m.

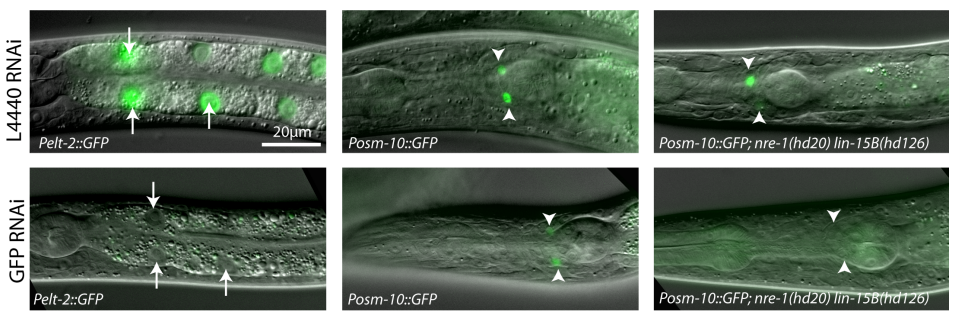

Supplementary Figure 2. Efficient GFP knockdown via RNAi in neurons of *nre-1(hd20) lin-15(hd126)* animals. (A-C) Fluorescent and DIC images of animals treated with control RNAi or RNAi against GFP (A) GFP expression in intestinal nuclei. Arrows indicate efficient GFP knockdown in intestinal nuclei (arrows). (B). GFP expression in osmo-sensory neurons. Arrowheads indicate osmo-sensory neurons which only shown partial knockdown of GFP. (C) GFP expression in osmo-sensory neurons in the *nre-1(hd20) lin-15(hd126)* containing strain. Arrowheads indicate osmo-sensory neurons and efficient GFP knockdown via RNAi. Scale bar represents 20 µm.

Supplementary Table 1. Overview of percentage of EdU positive neurons upon transfection with the indicated constructs.

condition	BFP (+)	BFP (+) EdU (+)	% of EdU (+) neurons
Experiment 8, transfection Day 4, EdU Day 4, Fixation Day 7 and 11			
ctrl	135	0	0
shRNA APC2 3 days EdU	36	0	0
shRNA APC2 7 days EdU	38	0	0
Ad12 + shRNA APC2 3 days EdU	136	35	26
Ad12 + shRNA APC2 3 days EdU	38	22	58
Experiment 13, transfection Day 4, EdU Day 4, fixation Day 8			
ctrl	100	0	0
Ad12	100	16	16
Ad12 + shRNA FZR1	100	62	62
pAd5 E1A + pAd12 E1B 54K	81	30	37
PAd5 E1A + PAd12 E1B 54K + shRNA FZR1	100	58	58
PAd5 E1A + shRNA p53	76	15	20
pAd5 E1A + shRNA p53 + shRNA FZR1	100	54	54
pAd12 E1B 54K + shRNA Rb	72	16	22
pAd12 E1B 54K + shRNA Rb + shRNA FZR1	100	26	26
shRNA p53 + shRNA Rb	100	0	0
shRNA p53 + shRNA Rb + shRNA FZR1	100	0	0
shRNA Rb + shRNA FZR1	100	5	5
HPV 16 E7 + HPV 16 E6	40	0	0
HPF 16 E7 + HPV 16 E6 shRNA FZR1	40	0	0
HPV 16 E7 + shRNA p53	40	0	0
HPV 16 E7 + shRNA p53 + shRNA FZR1	100	7	7
HPV 16 E6 + shRNA Rb	100	18	18
HPV 16 E6 + shRNA Rb + shRNA FZR1	100	25	25

BFP (+) indicates the number of transfected cells. BFP (+) and EdU (+) indicates the number of EdU positive transfected neurons

Supplementary Table 1 continued

Experiment 14,
transfection Day 4, Edu Day 7, Fixation Day 10

condition	BFP (+)	EdU (+)	% of EdU (+) neurons
ctrl	100	0	0
pAd12 E1	50	6	12
pAd12 E1A	86	34	40
3x shRb	90	45	50
3x shp107, 2x sh p130	100	0	0
pAd12 E1B 54K	100	0	0
pSuper shp53	100	0	0
3x shfzr-1	70	6	9
pAd12 E1, 3x shfzr-1	92	56	61
pAd12 E1, shfzr-1 #1	56	32	57
pAd12 E1, shfzr-1 #2	128	72	56
pAd12 E1, shfzr-1 #3	132	80	61
pAd12 E1, 3x shfzr-1	32	17	53
pAd12 E1B 54k, shRb #1	90	48	53
pAd12 E1B 54k, shRb #2	65	42	65
pAd12 E1B 54k, shRb #3	73	24	33

BFP (+) indicates the number of transfected cells. BFP (+) and EdU (+) indicates the number of EdU positive transfected neurons

Supplementary Table 2. Overview of the genes present in the RNAi screen

Gene	Gene name	Phenotype	Gene	Gene name	Phenotype
R119.6	*taf-4*	L	C29H12.5	*cec-9*	
W03D8.4		L	C32D5.5	*set-4*	
T12F5.4	*lin-59*		C04A2.2		L
C43E11.10	*cdc-6*		F10E7.11		
B0261.1		E	T07F8.4		N
T05E8.2	*hil-8*		F32A5.1	*ada-2*	
B0414.3	*hil-5*		T09A5.8	*cec-3*	
C32F10.5	*hmg-3*		C08B11.2	*hda-2*	
C32F10.2	*lin-35*		C08B11.3	*swsn-7*	L
C06A5.3			K08F8.6	*let-19*	
T23H2.3			T01B7.5		
H06O01.2	*chd-1*		T21B10.5	*set-17*	
K10D3.3	*taf-11.2*		ZK945.5		
C01H6.7	*swsn-9*		F33H1.4		
R06C7.7	*lin-61*		R166.1	*mab-10*	
C26C6.1	*pbrm-1*		R06F6.4	*set-14*	
T23G11.2	*gna-2*	E	F07A11.4		
C34B7.1			F43G6.4		
F02E9.4	*sin-3*		F43G6.6	*jmjd-1.1*	
D1081.8		L	K12D12.1	*top-2*	L
F43G9.12		L	Y17G7A.1	*hmg-12*	
F36A2.10			W09H1.2	*his-73*	L
F32H2.1		L	F15D4.1	*btf-1*	
W06D4.6	*rad-54*		ZK131.10	*his-16*	L
C12C8.3	*lin-41*	D	F08G2.2	*his-43*	L
T23D8.6	*his-68*	L	F08G2.3	*his-42*	L
T23D8.8	*cfi-1*		Y51H1A.5	*hda-10*	
T22A3.4	*set-18*		Y48B6A.14	*hmg-1.1*	
R06C1.1	*hda-3*		F26H11.3		
W02D9.3	*hmg-20*		Y53F4B.d		
B0019.1	*amx-2*		F54C4.2	*spt-4*	
B0019.2			F54C4.3	*attf-3*	L
Y18D10A.1	*attf-6*	L	C29F9.5		
M01E5.6	*sepa-1*		F23H11.1	*bra-2*	
Y40B1B.6	*spr-5*		C44F1.2	*gmeb-3*	
W04A8.7	*taf-1*	L	R13G10.2	*amx-1*	
F47G4.6	*hmg-6*		E03A3.3	*his-69*	E
K03D10.3	*mys-2*		E03A3.4	*his-70*	

Supplementary Table 2 continued					
Gene	**Gene name**	**Phentoype**	**Gene**	**Gene name**	**Phenotype**
Y105E8C.d		L	C16C10.4		
F33H2.7	*set-10*		R07E5.3	*snfc-5*	L
Y48G1A_53.a			R07E5.10	*pdcd-2*	E
Y48G8A_3051.d			C38D4.3	*mel-28*	E
F23F1.1	*nfyc-1*		C26E6.3	*ntl-9*	N
C01B12.2	*gmeb-1*		F26F4.7	*nhl-2*	
C01B12.8			C26E6.9	*set-2*	
W04H10.3	*nhl-1*		K10D2.1		
B0281.3			ZC155.2		
ZK1240.1			T24G10.2		
ZK1240.2			C05D2.5	*gak-1*	
ZK1240.3			B0336.7		
F34D6.4	*set-11*		C28H8.9	*dpff-1*	
T10D4.6			F47D12.4	*hmg1.2*	L*
H20J04.f			C56G2.15		
T05A7.4	*hmg-11*		C16A3.1		
C17G10.4	*cdc-14*	N	T26A5.7	*set-1*	L*
F59E12.1			T26A5.8		
F37A4.8	*isw-1*		F54E12.2		
T20B12.8	*hmg-4*	E	F54E12.5	*his-57*	L
ZK783.4	*flt-1*		H02I12.7	*his-65*	L
ZK112.2	*ncl-1*		F22B3.1	*his-64*	L
C14B9.6	*gei-8*		M04B2.3	*gfl-1*	
R05D3.11	*met-2*		K08E4.1	*spt-5*	L
ZK1236.2	*cec-1*		F11A10.1	*lex-1*	
F54F2.2	*zfp-1*		C25G4.4	*spe-44*	
F54F2.9			Y62E10A.e		
T23G5.6	*saeg-2*		Y57G11C.19		
F54C8.2	*cpar-1*	L	Y105C5A.a		
F58A4.3	*hcp-3*	L	Y105C5A.r		
R10E11.1	*cbp-1*	L*	Y51H4A.l		N
ZK1128.5	*swsn-2.1*		Y116A8C.22	*athp-3*	
M03C11.8			Y116A8C.13		
K01G5.2	*hpl-2*		Y41D4A_2615.a		
C44B9.4	*athp-1*		C39F7.2	*madd-2*	
Y47D3B.9	*bed-2*		T10B5.4		
Y56A3A.4	*taf-12*	E	F59A7.8		

Supplementary Table 2 continued

Gene	Gene name	Phenotype	Gene	Gene name	Phenotype
Y75B8A.6			T27C4.4	*lin-40*	N
Y49E10.6	*his-72*	L	C18G1.5	*hil-4*	
Y37D8A.9	*mrg-1*		B0238.10		
Y43F4B.1			C24G6.6	*hpo-15*	
F53A2.5	*dro-1*		VC5.4	*mys-1*	L*
T12D8.7	*taf-9*	L	F09G2.9	*attf-2*	
T12D8.1	*set-16*	L	D1014.9		
Y53G8A_6046.a			F20D6.9		N
Y55B1B_119.b			T23B12.1	*phf-30*	
Y71H2_375.b		L	F45F2.3	*his-5*	L
F15E6.1	*set-9*		F45F2.4	*his-7*	L
R08C7.3	*htz-1*		F07C3.4	*glo-4*	
R08C7.10	*wapl-1*	E	C50F4.13	*his-35*	N
F29B9.2	*jmjd-1.2*		F40F9.7	*drap-1*	N
F29B9.4	*psr-1*		T11A5.1		
R11E3.4	*set-15*		B0024.12	*gna-1*	
F41H10.6	*hda-6*		F22E12.4	*egl-9*	N
T12E12.2	*cec-6*		Y32F6A.1	*set-22*	
F38A5.13	*dnj-11*		C35A5.9	*hda-11*	
Y73B6A.f			C06H2.3	*jmjd-5*	
C17H12.13	*anat-1*		F47G9.4		
T05A12.4			T27F2.1	*skp-1*	L
F55G1.10	*his-61*	N	F55C5.6		
F55G1.2	*his-59*	E	W05B10.1	*his-74*	
F55G1.3	*his-62*	L	Y2H9A.1	*mes-4*	
F32E10.6	*cec-5*		C53A5.3	*hda-1*	L
F45E4.9	*hmg-5*		C47E8.8	*set-5*	
F17E9.13	*his-33*	L	C30G7.1	*hil-1*	
F17E9.9	*his-34*	L	F28F8.7		
F42A9.2	*lin-49*		T10C6.12	*his-3*	E
C27B7.4	*rad-26*		Y39B6B.u		L
ZK1251.1	*btas-1*		C25F9.5		
T13F2.2			Y113G7B.14		
R11A8.4	*sir-2.1*		F25C8.2	*amx-3*	
ZK593.4	*rbr-2*		F13C5.2		
F01G4.1	*swsn-4*		T04G9.1	*attf-5*	
B0035.7	*his-47*	L	C12D12.5	*sox-4*	N
T08D10.2	*lsd-1*		C10E2.3	*hda-4*	

Supplementary Table 2 continued					
Gene	**Gene name**	**Phenotype**	**Gene**	**Gene name**	**Phenotytpe**
F48D6.1	*taf-11.1*		C49F5.5		
C52B9.8			F17A2.3	*phf-32*	
ZC8.3	*set-30*		C52G5.1		
W01C8.2			T14G8.1	*chd-3*	
W01C8.3	*set-19*		K08H2.6	*hpl-1*	
W01C8.4	*set-20*		K09A11.1		
F49E10.5	*ctbp-1*		K09A11.5	*phf-33*	
K08A8.2	*sox-2*		F46G10.3	*sir-2.3*	
K09F5.5	*set-12*		F46G10.7	*sir-2.2*	
F45E1.6	*his-71*	L	C29F7.6	*jmjd-3.3*	
F22F1.1	*hil-3*		F02D10.7	*set-8*	
F22F1.3			F54B11.6	*bra-1*	
D2021.1	*utx-1*		F23D12.5	*jmjd-3.2*	
F18E9.5	*jmjd-3.1*		M163.3	*his-24*	
F36G3.2			F40E10.2	*sox-3*	
F21G4.4	*phf-34*		F53H4.1	*csb-1*	
T01C1.3			F53H4.5	*gmeb-2*	
C49F5.2	*set-6*		C11G6.1	*taf-3*	

L = lethal as expected, L* = Lethal not expected, E = expected to be lethal but not expected, N = not tested because bacteria did not grow, D = dumpy

Chapter 6

G1/S inhibitors and the SWI/SNF complex control cell-cycle exit during muscle differentiation

Suzan Ruijtenberg & Sander van den Heuvel

An adapted version of this manuscript has been published in *Cell,* 2015

Developmental Biology, Faculty of Sciences, Department of Biology, Utrecht University, Padualaan 8, 3584 CH Utrecht, The Netherlands.

Abstract

The transition from proliferating precursor cells to post-mitotic differentiated cells is crucial for development, tissue homeostasis, and tumor suppression. To study cell cycle exit during differentiation *in vivo*, we developed a conditional knockout and lineage-tracing system for *Caenorhabditis elegans*. Combined lineage-specific gene inactivation and genetic screening revealed extensive redundancies between previously identified cell cycle inhibitors and the SWI/SNF chromatin-remodeling complex. Loss of either SWI/SNF or G1/S-inhibitor function in muscle precursor cells caused limited defects, while simultaneous inactivation of these regulators resulted in massive over-proliferation and a unique *C. elegans* tumor phenotype. Further genetic analyses support that SWI/SNF acts in concert with *hlh-1* MyoD, antagonizes Polycomb-mediated transcriptional repression, and suppresses *cye-1* Cyclin E transcription to arrest cell division of muscle precursors. Thus, SWI/SNF and G1/S inhibitors provide alternative mechanisms to arrest cell cycle progression during terminal differentiation. This is particularly important considering the frequent mutation of SWI/SNF genes in human cancers.

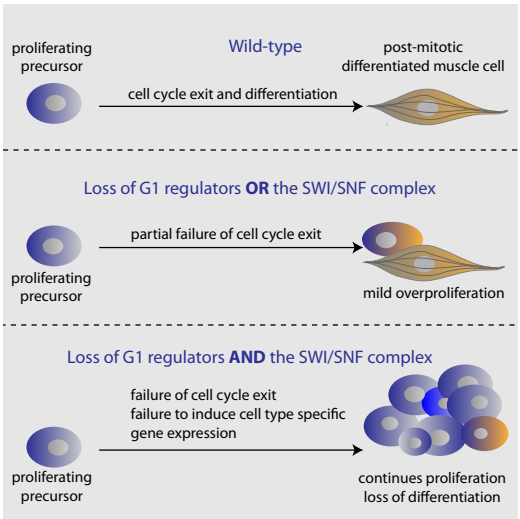

Introduction

The development and maintenance of tissues and organisms depend on close coordination between cell proliferation and differentiation. Early embryos contain rapidly proliferating totipotent cells, whereas adult tissues predominantly consist of non-dividing cells with specialized morphologies and functions (Buttitta and Edgar, 2007). In general, cell specialization involves a gradual process of lineage restriction, followed by permanent exit from the division cycle and terminal differentiation. The mechanisms that arrest cell proliferation during differentiation are crucial for tumor suppression but limit tissue regeneration. Despite this importance, it remains poorly understood how cell proliferation and differentiation are inversely regulated during development, and how temporary quiescence differs from permanent cell cycle arrest.

The primary mechanism to arrest cell division is inhibition of Cyclin Dependent Kinases (CDKs), the key positive regulators of the cell division cycle. CDK4/6-cyclin D and CDK2-cyclin E kinases promote cell cycle entry during the G1-phase of the cell cycle (van den Heuvel and Dyson, 2008). Various levels of regulation counteract CDK-cyclin activation to prevent unscheduled progression from G1 into S-phase. G1/S inhibitors include members of the retinoblastoma tumor suppressor (Rb) protein family, which act as transcriptional repressors together with E2F transcription factors. Phosphorylation of pRb by active CDKs triggers its release from E2F and allows activating E2Fs to induce transcription of cyclin E and other cell cycle genes. In addition, CDK inhibitory proteins (CKIs) oppose G1/S progression. CKIs of the INK4 protein family, such as $p16^{INK4A}$, associate with CDK4/6 kinases and prevent their interaction with D-type cyclins. In contrast, CKIs of the CIP/KIP family associate with CDK-cyclin complexes, and are particularly important for inhibiting CDK2-cyclin E. Ubiquitin-dependent protein degradation provides yet another level of G1/S inhibition. This involves the Anaphase Promoting Complex/Cyclosome (APC/C) in association with the FZR1/Cdh1 coactivator, as well as Skp1, Cullin, F-box factor (SCF) complexes. APC/C and SCF are both E3 ubiquitin ligases that target cell cycle regulatory proteins for degradation.

Cell differentiation is ultimately determined at the level of gene expression. As a well-studied example, muscle differentiation involves a regulatory network of MyoD and other myogenic transcription factors, together with general transcription factors and histone modification/chromatin remodeling complexes (Puri and Mercola, 2012). Other transcription factors mediate differentiation into, for instance, specific blood cell types or neurons. Mutations associated with human cancer frequently affect cell cycle regulators, but also transcription factors and chromatin regulators with critical functions in differentiation (Kandoth *et al.*, 2013). In particular, transcriptional repressors and activators of the polycomb group (PcG) and Trithorax group (TrxG), respectively, are strongly associated with cell fate and tumor formation. In fact, mutations in a subclass of TrxG genes, which encode subunits of Switch/Sucrose nonfermentable (SWI/SNF) chromatin remodeling complexes, were recently found among the most common mutations in human cancer (Kadoch *et al.*, 2013; Kandoth *et al.*, 2013; Wang *et al.*, 2014). These findings highlight the importance of

understanding how the combinatorial activity of cell cycle regulators, transcription factors and chromatin remodelers coordinate cell cycle arrest and differentiation.

The nematode *Caenorhabditis elegans* provides an attractive animal system in which to study the control of cell cycle exit during development. *C. elegans* develops through a highly reproducible pattern of cell proliferation and differentiation (Sulston and Horvitz, 1977; Sulston and Schierenberg, 1983). The animal's transparency and well-described lineage allow characterization of mutants with single cell resolution. Extra cell division (hyperplasia) of somatic cells was first observed in the lineage-abnormal mutants *lin-23* β-TrCP and *cul-1* (*lin-19*), which lack the function of an SCF-like E3 ubiquitin ligase (Kipreos *et al*., 1996, 2000). Loss of *cki-1* Kip1 also results in extra cell division (Hong *et al*., 1998; Boxem and van den Heuvel, 2001; Fukuyama *et al*., 2003). In contrast, mutation of the single *C. elegans* Rb-related gene, *lin-35*, or the APC/C coactivator *fzr-1* FZR1/Cdh1 leads to substantial hyperplasia only when combined with loss of other negative cell cycle regulators (Boxem and van den Heuvel, 2001; Fay *et al*., 2002). Notably, such double mutants still form apparently normal differentiated post-mitotic cells, and uncontrolled over-proliferation of somatic cells has thus far not been described for *C. elegans*.

To study cell cycle arrest during the process of differentiation, we created a system for tissue specific gene inactivation and lineage tracing. This allowed inactivation of multiple genes in a single precursor cell, while fluorescently marking all daughter cells. Combining this system with RNAi of candidate genes revealed multiple levels of control that together provide robust arrest of cell division during terminal differentiation. We observed a surprising degree of redundancy between well-known negative regulators of the cell cycle and the SWI/SNF chromatin-remodeling complex. Only combined inactivation of the SWI/SNF complex and G1/S-inhibitors resulted in tumorous over-proliferation of muscle precursor cells. Our results support that SWI/SNF-dependent chromatin remodeling provides global transcriptional control not only of cell-type specific genes but also of positive and negative cell cycle regulators. This provides an alternative mechanism for control of cell cycle exit during terminal differentiation and likely is relevant for the tumor suppressor function of SWI/SNF genes.

Results

A CRE-lox-based recombination and lineage tracing system for *C. elegans*

We assumed that cell cycle withdrawal during differentiation depends on multiple regulators and is essential for viability. Hence, to genetically dissect developmental control of cell cycle exit, we aimed to induce multiple gene alterations in a lineage-specific manner. Hereto, we developed a CRE-lox-based recombination and lineage tracing system for *C. elegans* (Figure 1A). This system combines a recombination vector that includes a gene of

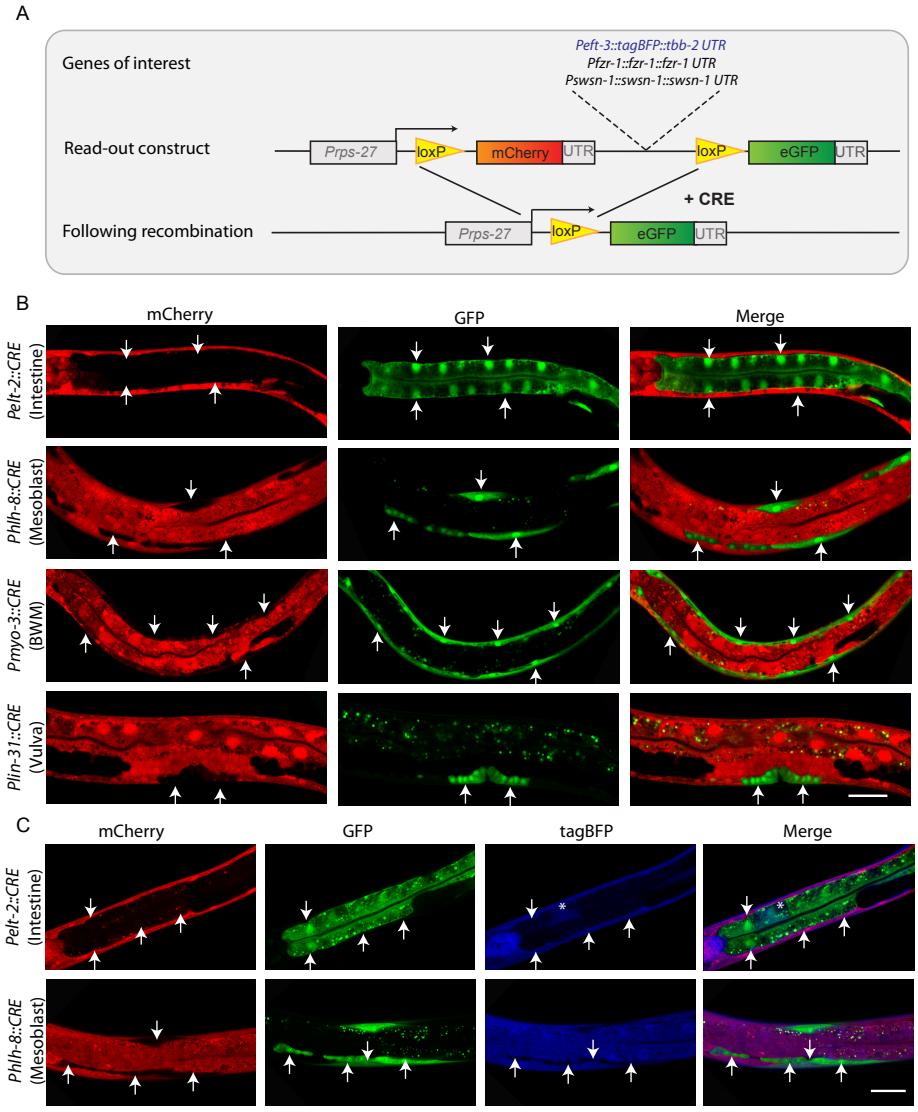

Figure 1. Lineage tracing and tissue-specific knockout in *C. elegans*. (A) Overview of the CRE-lox-based recombination system, which combines tissue specific gene inactivation with switching mCherry to eGFP expression to allow lineage tracing. The single copy integrated plasmid without gene of interest is used as a recombination reporter (read-outlox). *Peft-3::tagBFP, swsn-1* and *fzr-1* were studied as genes of interest. (B) Examples of lineage specific recombination and lineage tracing following tissue-specific CRE expression from the indicated promoters. Arrows indicate cells that switched mCherry to eGFP expression (C) CRE-lox-based recombination causes loss of expression of a tagBFP reporter gene of interest (A), single copy integrated into the genome. CRE expressed from the indicated promoters resulted in loss of mCherry and tagBFP expression, while eGFP was induced (indicated by arrows). Asterisk (*) indicates mCherry-negative intestinal cell with residual tagBFP fluorescence. Scale bar 20 µm. See also Figures S1 and S2, Table S1 and Table S2.

interest, a homozygous genomic mutation of the gene and tissue-specific expression of the CRE recombinase. This allows tissue-specific gene loss and simultaneous visualization of knockout cells by altered expression of fluorescent proteins.

We started with a recombination-reporter construct (*read-out^{lox}*) that expresses the mCherry fluorescent protein from the universally active ribosomal subunit *rps-27* promoter (Figure 1A). *LoxP* recombination sites were placed upstream of the mCherry coding sequences and downstream of a polyadenylation/transcriptional stop signal (*let-858* 3'UTR). This is followed by eGFP coding sequences without promoter, causing CRE-induced recombination to induce a switch from mCherry to eGFP expression (Figure 1A, bottom). Following extensive optimization of the CRE-expressing vectors (Material and Methods), recombination was highly efficient and observed in nearly all animals with a *read-out^{lox}* construct (Table S1).

To examine conditional recombination, we expressed CRE under the control of a heat shock-inducible promoter (*Phsp-16.2*) and a variety of promoters with lineage-specific activity. Recombination was readily detected by expression of eGFP, coincident with mCherry loss, and occurred in the expected lineages in nearly all animals (Figure 1B, data not shown). Dependent on the promoter used, additional cell types sometimes showed eGFP expression (Table S1). For instance, early embryonic expression of CRE from the *elt-2* GATA4-6 and *hlh-8* TWIST promoters induced recombination as expected in the intestine and mesoblast (M) lineage, respectively. However, both promoters showed some additional activity in the somatic gonad, and *Phlh-8::CRE* also induced recombination in embryonic bodywall muscles (BWM), mostly in the head region of the animal. In practice, this level of transcriptional noise did not pose a problem as it usually caused recombination of only one allele (as concluded from coincident mCherry and eGFP expression) in a few specific cells.

Several adjustments expanded the versatility of the system. We introduced alternative lox sites (*loxP, loxN* and *lox2272)* for reliable recombination of multiple genes in the same cell (Fig. S1, Table S2). Moreover, we created read-out constructs that switch from mCherry to tagBFP expression, to allow lineage tracing in combination with use of GFP-reporter transgenes (Fig. S1). Finally, we tested whether CRE-induced recombination is likely to cause loss of function of the gene of interest.

DNA injected into the *C. elegans* gonad regularly forms multi-copy arrays that remain present extra-chromosomally (Mello *et al.*, 1991). To exclude that CRE-lox excised DNA fragments are retained through a similar mechanism, we placed tagBFP coding sequences flanked by a general promoter (*Peft-3*) and 3'UTR (*tbb-2 3'*UTR) between the *loxP* sites in the recombination vector (Figure 1A). Genomic integration of this vector resulted in animals with mCherry and tagBFP expression in all somatic cells. Lineage specific CRE expression resulted in loss of mCherry and tagBFP expression (Figure 1C), although tagBFP fluorescence lasted somewhat longer than mCherry fluorescence. Recombination could be induced even in post-mitotic cells, based on eGFP expression and mCherry loss in bodywall muscle, but tagBFP expression perdured in these cells (Figure 1B, S2). Thus, cell division likely helps creating a loss of gene function with this approach. In the intestine and mesoblast lineages, tagBFP was completely absent in all later stage larvae examined.

In summary, CRE-lox recombination allows efficient lineage-specific loss of function in *C. elegans*, and knockout cells can be readily visualized based on fluorescent protein expression.

General inhibitors of G1/S progression show lineage-dependent contributions

We focused our analysis of cell cycle exit on the intestine and post-embryonic mesoderm lineage of the mesoblast. Nuclear divisions in the intestine are sensitive to cell cycle deregulation (Boxem and van den Heuvel, 2001, 2002; Saito *et al.*, 2004; Korzelius *et al.*, 2011), while the M-lineage is particularly attractive for proliferation-differentiation studies. The mesoblast (M) is formed at approximately 4 hours of embryonic development and remains quiescent until halfway the first larval stage (L1) (Sulston and Schierenberg, 1983) (Figure 2A). Cell divisions in L1 generate 16 M daughter cells that undergo terminal differentiation, and two ventral precursor cells known as sex myoblasts (SMs). The SMs migrate anteriorly to align with the gonad during L2 development (Figures 2A, B) (Sulston and Horvitz, 1977). Starting in the late L3 stage, each SM goes through three rounds of division to form a total of 16 vulval and uterine muscles that are used for egg laying, and are known as sex muscles. Thus, the M-lineage includes multiple periods of proliferation, temporal arrest and terminal differentiation over a substantial part of the animal's development.

We first examined whether the *lin-35* Rb and *fzr-1* FZR1/Cdh1 inhibitors of G1/S progression contribute to cell cycle arrest in the intestine and M-lineage. Inactivation of *lin-35* by RNAi or putative null mutation (*n745*) combined with *fzr-1* loss of function results in a larval lethal and sterile phenotype, with extra cell divisions in multiple lineages (Fay *et al.*, 2002). For lineage specific loss of function, we placed a *fzr-1* genomic fragment in the reporter plasmid (Figure 1A). Mos1-mediated single copy insertion (MosSCI) of this plasmid rescued the *fzr-1(ku298)* strong loss-of-function mutation, as it restored viability, fertility and cell cycle exit in *lin-35(RNAi* or *n745);fzr-1(ku298)* double mutant larvae (Figure 2C, 3A). For simplicity, we use *fzr-1^{lox}* to indicate the combination of *fzr-1^{lox}* transgene and *fzr-1(ku298)* allele (Table S7 lists complete genotypes of all strains). Intestine-specific CRE expression (*Pelt-2::CRE*) in *lin-35(RNAi);fzr-1^{lox}* animals caused extra division of intestinal nuclei, similar to the extra intestinal divisions in *lin-35(RNAi);fzr-1(ku298)* larvae (Figure 2C; Table S3). In contrast to the latter, however, *lin-35(RNAi)* animals with CRE-induced *fzr-1* loss were fully fertile and viable. Thus, validating our system, *Pelt-2::CRE* expression induced intestine specific *fzr-1* inactivation while leaving other tissues unaffected.

Remarkably, examination of the M-lineage revealed that *lin*-35 Rb and *fzr-1* are not critical for cell division control in this lineage. Use of the *read-out^{lox}* reporter helped determine that *lin-35(RNAi* or *n745);fzr-1(ku298)* double mutants undergo normal temporal arrest of SM cell division and cell cycle exit during terminal differentiation (Figure 2D, Table S4). Not surprisingly, lineage-specific loss of *fzr-1^{lox}* combined with *lin-35* inactivation also did not alter the cell division and differentiation pattern in the postembryonic mesoderm lineage (Figure 2D, Table S4). Thus, *lin-35* Rb and *fzr-1* show lineage-dependent requirements,

and other cell cycle regulators are sufficient for temporal and permanent cell cycle arrest in the M-lineage.

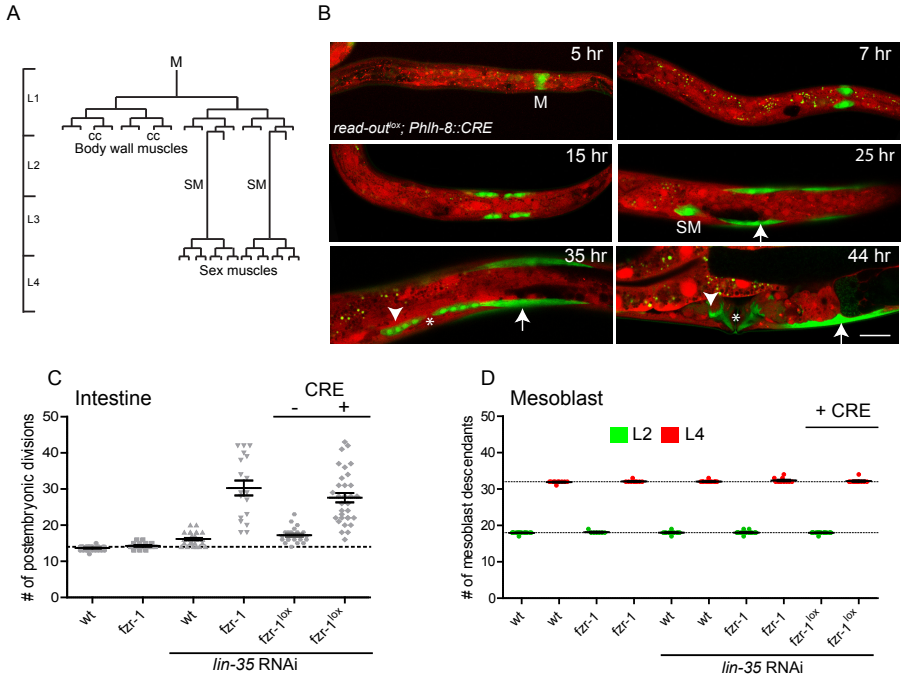

Figure 2. Lineage-specific requirement for *lin-35* Rb and *fzr-1* FZR1/Cdh1 in cell cycle arrest. (A) Mesoblast (M) lineage and division pattern in the hermaphrodite. Cell divisions generate 18 M daughter cells in the L1 stage. 16 of these cells differentiate into bodywall muscle cells and coelomocytes (CC). Two sex myoblasts (SM) migrate anteriorly and divide again in the third larval stage to form muscles required for egg laying. (B) Fluorescence microscopy images of mesoblast descendants (eGFP positive, green), visualized by CRE-loxP-based recombination of the read-outlox reporter (Figure 1) following *Phlh-8::CRE* expression. Arrows: differentiated bodywall muscle. Arrowheads: daughter cells from the SM, * indicates the position of the vulva. Scale bar: 20 µm. (C and D) Comparison between a homozygous *fzr-1(ku298)* strong loss-of-function mutant and lineage-specific *fzr-1*^{lox} knockout. (C) Number of postembryonic nuclear divisions in the intestine upon inactivation of *fzr-1* alone or *fzr-1* and *lin-35*. (D) Number of mesoblast descendants upon inactivation of *fzr-1*, or *fzr-1* and *lin-35*, in L2 and L4. Graphs show mean ± s.e.m; each dot represents a single animal, the dotted line indicates the average number in WT. See also Table S3 and Table S4.

Reliable cell cycle arrest through multiple levels of control

To identify regulators that control temporal cell cycle exit in muscle precursor cells, we performed a candidate-based RNAi screen. This included all genes with a reported cell cycle inhibitory function in *C. elegans* as well as transcription factors and chromatin modifiers with a potential contribution in cell cycle arrest (Table S5). Gene knockdown by feeding

RNAi was tested in parallel in the M-lineage reporter strain (*read-out*^{lox};*Phlh-8::CRE*) and in M-lineage double mutant animals *lin-35(n745);fzr-1*^{lox}*;Phlh-8::CRE* (Table S4). We identified six genes that when singly inactivated by RNAi interfered with M-lineage cell cycle exit in the read-out control strain. These genes encode the well-known *C. elegans* CDK inhibitor CKI-1 Kip1, and two SCF-like E3 ubiquitin ligase subunits, CUL-1 and LIN-23 β-TrCP (Figure 3A; Figure S3, Table S4; quantified for sex muscles). In addition, inhibition of three subunits of the SWI/SNF chromatin-remodeling complex allowed extra divisions in the M-lineage (Figures 3A and S3; Table S4). Thus, the function of each of these genes is critical for correct cell cycle exit in the mesoblast lineage. At the same time, differentiated muscle cells were still formed following knockdown of these genes, and the number of sex muscles at most doubled (Figure 3A).

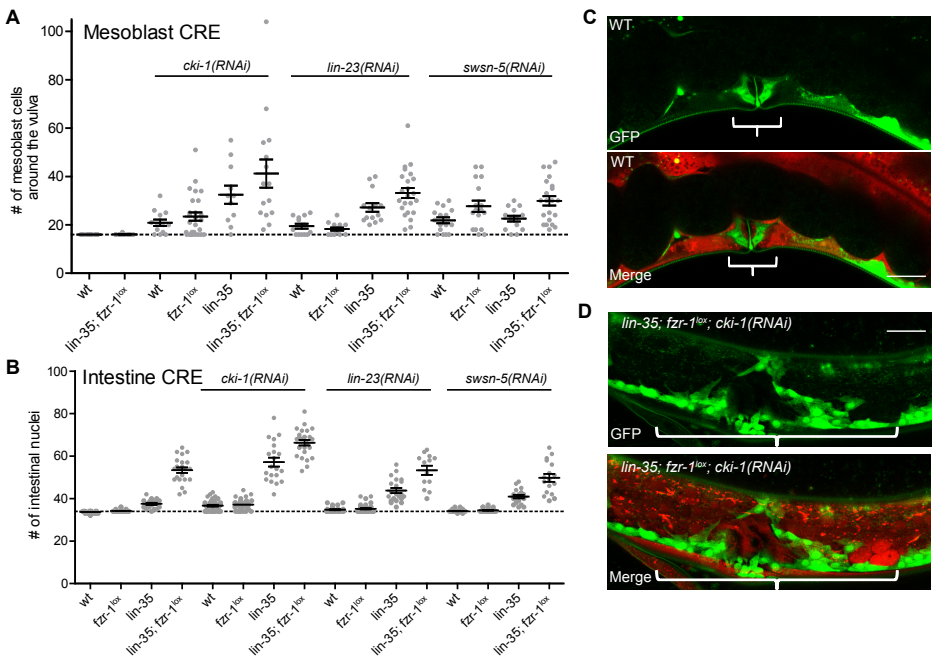

Figure 3. Cooperative control of cell cycle exit by G1/S inhibitors and SWI/SNF subunits. (A-D) RNAi of the indicated genes combined with *lin-35* null mutation and lineage-specific *fzr-1* knockout. (A) Quantification of the number of mesoblast descendants localized around the vulva for the indicated genotypes. (B) Quantification of the number of intestinal nuclei for the indicated genotypes. Graphs show mean ± s.e.m. Each dot represents a single animal, the dotted line indicates the average numbers in WT. (C and D) Fluorescence microscopy images of mesoblast descendants (eGFP positive). Bracket indicates vulva region. (C) *read-out*^{lox}*:Phlh-8::CRE* control animal with 16 sex muscles. (D) illustration of animal with a substantial over-proliferation phenotype, following RNAi of *cki-1* in *lin-35(n745);fzr-1*^{lox}*;Phlh-8::CRE* larvae. Scale bars represent 20 µm. See also Figure S3, Table S3, Table S4, Table S5 and Table S6.

When tested in combination, the different levels of control were found to act partly redundantly in promoting cell cycle exit. Even though the parental strain *lin-35(n745); fzr-1^{lox};Phlh-8::CRE* showed a normal M-lineage division pattern, the presence of *lin-35* and *fzr-1* single or double mutations substantially increased the numbers of M-descendants when combined with RNAi of either *cki-1* Kip1, *lin-23* β-TrCP, *cul-1* Cullin1, or the SWI/SNF genes *swsn-1* BAF155/170, *swsn-5* (*snfc-5*) SNF5/INI1, and *swsn-2.1* BAF60 (Figures 3A, S2, Table S4). Specifically, when combined with *cki-1(RNAi)*, the *lin-35(n745)* and *fzr-1(ku298)* single mutations significantly enhanced the number of M-descendants around the vulva, and the triple gene inactivation resulted in further increased numbers of cell division (Figures 3A,C,D, S3, Table S4). Similarly, the *lin-23* RNAi phenotype was significantly stronger in *lin-35* single mutants, while the strongest effects were observed in *lin-35;fzr-1^{lox};hlh-8::CRE* mutants. Hyperplasia of vulval muscles induced by RNAi of SWI/SNF genes was enhanced by *fzr-1* mutation in the mesoblast lineage (Figures 3A, S3, Table S4). While the effect of *lin-35* mutation could possibly arise from enhanced RNAi (Wang *et al.*, 2005), this is not the case for *fzr-1* loss.

Comparing the results in the M-lineage to the intestine, lineage-dependent differences were observed again. Only *cki-1* RNAi further increased the number of nuclear divisions in the intestine of *lin-35(n745);fzr-1^{lox};Pelt-2::CRE* double mutants (Figures 3B; S3, Table S3). RNAi of *lin-23* and *cul-1* increased the number of divisions of intestinal nuclei in *lin-35(n745)* single mutant larvae. By contrast, inactivation of SWI/SNF subunits did not affect the number of divisions in the intestine (Figures 3B, S3; see discussion). While the relative contribution of each regulator varies between cell lineages, these results show that multiple levels of control act in cooperation to arrest the cell cycle both in the intestine and mesoblast lineage.

G1/S inhibitors act largely redundantly with the SWI/SNF complex in cell cycle exit

To better define SWI/SNF contribution in cell cycle control, we examined additional mutant combinations. SWI/SNF components form highly conserved chromatin remodeling complexes that use ATPase activity to remodel nucleosome positions, thereby increasing or reducing access to transcriptional regulators (reviewed in: (Wilson and Roberts, 2011). The complexes contain several core subunits, including an ATPase subunit known as Brahma (BRM) in *Drosophila,* human BRM (hBRM) and BRM-Related Gene 1 (BRG1), and SWSN-4 in *C. elegans*. BRM/BRG1 associated factors (BAFs) include other core subunits (*swsn-1* BAF155/170 and *swsn-5* BAF47/SNF5/INI1 in *C. elegans*), as well as additional accessory and signature subunits (Table S6) (Sawa *et al.*, 2000; Shibata *et al.*, 2012; Riedel *et al.*, 2013). Based on signature subunit composition, two different complexes, BAF and PBAF, have been distinguished. While *swsn-4* was not present in our RNAi libraries, the other SWI/SNF core subunits *swsn-1* and *swsn-5*, as well as the accessory subunit *swsn-2.1* (BAF60/SMARCD3), were found to induce extra M-lineage divisions in our screen (Figure S3, Table S5). RNAi for three different PBAF-specific components (*pbrm-1* BAF180/Polybromo),

swsn-7 BAF200/ARID2, *swsn-9* BRD7) did not result in a cell division phenotype (Table S5). Thus, SWI/SNF activity, and possibly specifically a *C. elegans* BAF-related complex, appears to contribute to cell cycle arrest.

As loss of SWI/SNF-complex function is incompatible with viability, we created lineage specific knockout strains for further analysis. For technical reasons, we focused on the *swsn-1(os22)* temperature-sensitive allele, which causes strong loss of function at the non-permissive temperature of 25 °C, while being viable at 15 °C (Material and Methods). Similar to the effect of *swsn-5* RNAi, shift of *swsn-1^{lox};Phlh-8::CRE* embryos from 15 to 25 °C increased the number of M descendants (Figure 4A, Figure S3; note that *swsn-1^{lox}* refers to the combined *swsn-1(os22)* mutation and *swsn-1^{lox}* single copy rescuing transgene). Combining *swsn-1* inactivation with single *lin-35*, *cki-1*, or *fzr-1* mutation or RNAi further increased the number of M descendants (Figure 4A). Remarkably, lineage-specific inactivation of *swsn-1* combined with RNAi of either *cul-1* or *lin-23* resulted in a massive increase in M-lineage descendants, which was further enhanced by *fzr-1* inactivation (Figures 4B,C, S4, Table S4). Similarly, *swsn-1^{lox};Phlh-8::CRE* combined with *lin-35(n745)* and *cki-1(RNAi)* resulted in a dramatic over-proliferation phenotype, which was even stronger when combined with *fzr-1^{lox}* (Figures 4B,D, S4; Table S4). While the use of non-null alleles may contribute to this enhanced effect, the limited over-proliferation observed after severe knockdown of individual SWI/SNF genes or G1/S inhibitors stood in stark contrast with the phenotype of combined mutants (Figures 2-4). Even double or triple loss of function of the canonical G1/S inhibitors caused limited defects, which were greatly enhanced by simultaneous *swsn-1* inhibition. These results demonstrate that the SWI/SNF complex and G1/S inhibitors provide substantially overlapping contributions in promoting cell cycle exit.

Tumorous over-proliferation of somatic cells in *C. elegans*

Several additional observations confirm that the combined inactivation of *swsn-1* and previously characterized G1 regulators causes uncontrolled cell proliferation and a tumorous phenotype. First, to examine whether individual cells or large multinucleated cells are formed, we dissected *lin-23(RNAi);swsn-1^{lox};Phlh-8::CRE* animals in iso-osmotic medium. Upon cutting the cuticle, cells streamed from the carcass, including many individual green fluorescent cells (Figure 4E). Addition of DAPI did not result in DNA staining of these eGFP-positive cells in iso-osmotic medium, while DAPI staining of fixed animals indicates a normal DNA content of the eGFP positive cells (Figure 4G, data not shown). This indicates that the M-lineage descendants contain an intact plasma membrane. Thus, the combined loss of *swsn-1* and G1/S inhibitors leads to the formation of many extra individual cells.

To further characterize the phenotype, we performed live observations of single animals by combined immunofluorescence and Differential Interference Contrast (DIC) microscopy. We observed increased numbers of M descendant cells in the early L2 stage, but not before completion of the L1 division pattern (Figure 4F). We followed M-lineage divisions in four individual *fzr-1^{lox};swsn-1^{lox};lin-23(RNAi);Phlh-8::CRE* animals from the mo-

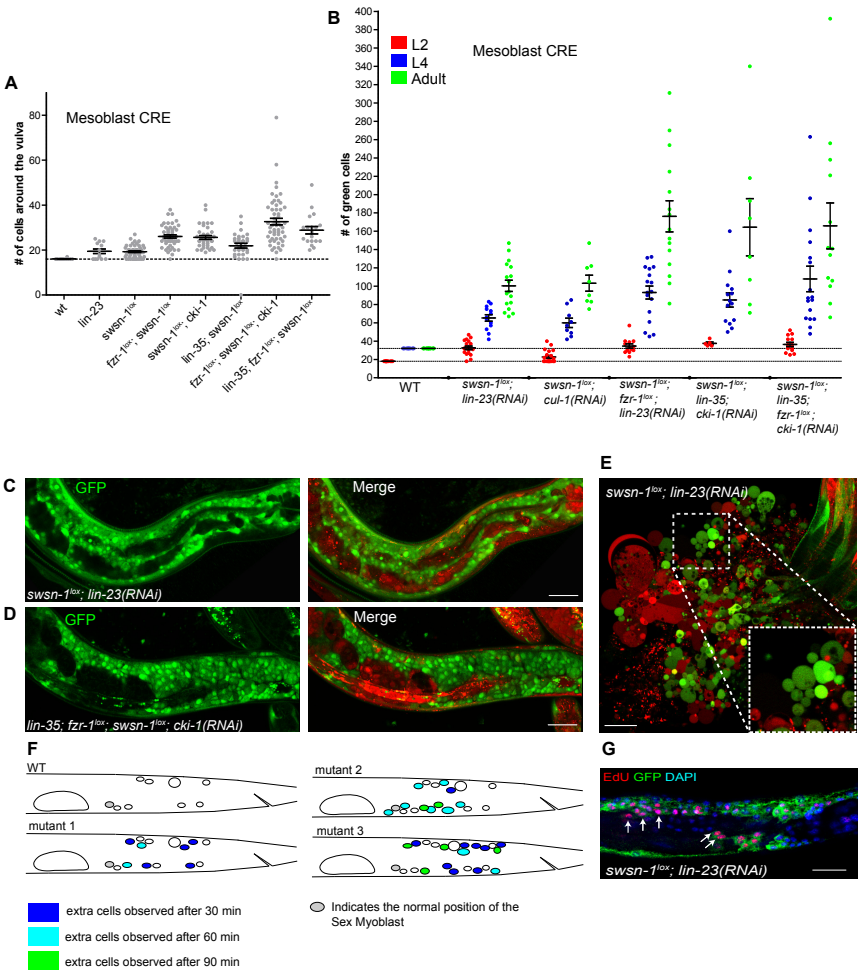

Figure 4. Combined inactivation of *swsn-1* with G1/S inhibitors leads to dramatically increased proliferation in the mesoblast lineage. (A and B) RNAi of the indicated genes combined with l*in-35(n745)* null mutation and lineage specific inactivation of *swsn-1* and *fzr-1*. (A) Quantification of the number of mesoblast descendants localized around the vulva. (B) Quantification of the total number of mesoblast descendants of the indicated genotypes in L2 (red), L4 (blue) and adult (green). Graphs show mean ± s.e.m.; each dot represents a single animal, dotted lines in the graphs indicate average WT number.(C and D) Representative fluorescent images of mesoblast over-proliferation (green, eGFP positive) in animals of indicated mutant genotypes. (E) Fluorescence microscopy image of cells following dissection of animals as in panel (D) in iso-osmotic medium. (F) Graphical illustrations of lineage analysis of proliferation patterns in young *fzr-1lox; swsn-1lox; lin-23(RNAi)* animals, based on combined immunofluoresence and DIC microscopy. Animals containing 18 posterior myoblast daughter cells (as in WT) were imaged every 30 minutes to follow the initial steps of the overproliferation phenotype. Only the left half of the animals, with 9 M-daughter cells, is shown in the cartoons. Dark blue, light blue and green circles: cells formed during the first 30 min of imaging, between 30 and 60 min, or between 60 and 90 min after the start of the experiment, respectively. Grey cell indicates the initial SM. (G) Incorporation of EdU (red) in mutant M descendants (green) during L2-L4 development. Nuclei are marked with DAPI (blue). Scale bars represent 20 µm. See also Figure S4, Table S3 and Table S4.

ment that 8 daughter cells are formed. In all four animals, apparently normal cell divisions continued in the M-lineage, which resulted in the generation of 18 daughter cells at normal positions (Compare to: Figures 2A, B). Mutant animals synchronized by developmental staging all showed 8 to 18 M-derived cells at 12 hours of larval development. In the large majority (22 of 24) of these larvae the pattern of M descendants was normal, while 2 showed abnormal positioning of M daughters, but no extra cells. Following the 18 cell-stage, divisions in the M-lineage continued in 4 out of 5 mutants, while the corresponding cells in wild-type animals undergo prolonged cell cycle arrest (Figure 4F). Extra divisions were observed in every quadrant, with continued proliferation of daughter cells that normally become post-mitotic and initiate terminal differentiation at this stage.

We examined incorporation of the thymidine analog EdU to visualize DNA synthesis. Combined detection of EdU and immunohistochemical staining of eGFP demonstrated continued DNA synthesis in M daughters of lineage-specific *swsn-1* knockdown, *lin-23(RNAi)* larvae (Figure 4G). Quantification of cell numbers by counting the eGFP-positive cells indicated that the number of M descendants increased substantially during the L2 stage, and also during the L3 and L4 stages (Figure 4B). These numbers approximately doubled again during a 24-hour timespan of development from L4 into the adult stage, at which time no somatic cell division takes place in the wild type (Figure 4B). Reduced viability and cell disintegration prevented counting at later time points. Amazingly, some young adults contained well over 300 M-lineage cells, formed from a single precursor in three days time and corresponding to approximately a third of the somatic cells in a normal adult animal. Together, these data show that combined loss of *swsn-1* and G1/S inhibitors results in tumorous over-proliferation in the *C. elegans* soma.

The SWI/SNF complex cooperates with *hlh-1* MyoD in cell cycle exit

In contrast to the G1/S inhibitors, a function of the SWI/SNF complex in cell cycle exit is poorly defined. Previous chromatin immunoprecipitation (ChIP) experiments identified several thousand *C. elegans* genes associated with SWI/SNF subunits (Riedel *et al.*, 2013). Examining the available chromatin immunoprecipitation (ChIP) data of SWSN-1::GFP and SWSN-4::GFP (Riedel *et al.*, 2013), we observed SWI/SNF promoter occupancy at 8 out of 9 negative regulators of cell cycle progression, and 3 out of 8 positive regulators (Figure S5). SWI/SNF-dependent chromatin remodeling is particularly important for the coordinated switching of gene expression programs during lineage commitment (Wilson and Roberts, 2011; Eroglu *et al.*, 2014). As human MyoD acts in concert with SWI/SNF components (de la Serna *et al.*, 2001; Puri and Mercola, 2012), the *C. elegans* SWI/SNF complex may act together with the myogenic transcription factors of the M-lineage, in particular HLH-1 MyoD. Chromatin association of HLH-1 MyoD has been extensively characterized in previous experiments (Lei *et al.*, 2010; Boyle *et al.*, 2014). Visual inspection of promoter regions showed strong overlap between SWI/SNF and HLH-1 occupancy, not only at muscle-specific genes (e.g. *myo-3* myosin), but also at several positive (*cdk-4, cye-1)* and nega-

tive *(cki-1, cki-2, cdc-14)* G1 regulatory genes (Figure S6). Using a temperature sensitive *hlh-1* MyoD allele, we observed that partial *hlh-1* loss of function at 25 °C resulted in increased numbers of M descendants around the vulva, to a similar extent as *hlh-1, swsn-1* double mutants (Figure 5A, Table S4). While this supports a concerted function, the *hlh-1(cc561*ts*)* phenotype resulted largely from SM duplication, whereas extra M-lineage divisions following *swsn-1* loss appeared more random (Figure 4F). When combined with *lin-23* RNAi*,* the *hlh-1* mutation caused severe over-proliferation to a similar degree as mesoblast specific *swsn-1* inactivation (Figure 5B, Table S4). Combining *hlh-1(cc561*ts*)* and *swsn-1* knockout with *lin-23(RNAi)* further increased M-lineage proliferation, which may reflect incomplete loss of function or point to partially non-overlapping contributions of *hlh-1* and *swsn-1*. Nevertheless, the substantial overlap in over-proliferation phenotypes indicates that SWI/SNF and HLH-1 MyoD act together to induce cell cycle arrest in the transition of proliferating precursor cells to differentiated post-mitotic muscle cells.

SWI/SNF antagonizes PcG gene function and controls positive and negative cell cycle regulators

SWI/SNF chromatin remodeling has been proposed to antagonize transcriptional repression by Polycomb group (PcG) proteins. *C. elegans* uses a protein complex of MES-2, MES-3 and MES-6 with similarity to the Polycomb Repressive Complex 2 (PRC2) (Gaydos *et al.*, 2012). We observed that RNAi of the PcG-related genes *mes-2* EZH2 and *mes-3* significantly suppressed over-proliferation induced by *swsn-1* mutation or *fzr-1, swsn-1* double mutation (Figure 5C, Table S4). Thus, the over-proliferation phenotype may result from PcG-mediated repression of genes that normally are SWI/SNF-dependently induced during muscle differentiation.

When combined with M-lineage specific *fzr-1* and *swsn-1* inactivation, strong RNAi of *mes-2* EZH2 or *mes-3* reduced the extra divisions only in part (Figure 5C). As loss of *fzr-1* alone does not alter the M-lineage, these observations appear to indicate that SWI/SNF also has functions unrelated to antagonizing PcG. *C. elegans* SWI/SNF proteins occupy promoters of positive as well as negative regulators of cell division (Figure S5; Riedel *et al.*, 2013). Hence, the SWI/SNF complex could stimulate cell cycle exit through transcriptional activation of G1/S inhibitors, and in addition through transcriptional silencing of cell cycle entry promoting genes such as *cye-1* Cyclin E. To examine this possibility, we created a *cye-1* transcriptional reporter. This *Pcye-1::tagBFP* reporter was expressed in post-mitotic M-derived muscle cells of lineage-specific *swsn-1* mutants, in contrast to the corresponding cells in wild-type control animals (Figure 5D, E). These data support SWI/SNF-mediated transcriptional repression of *cye-1* cyclin E during cell cycle withdrawal.

To extend these observations, we performed single molecule FISH (smFISH) experiments for positive (*cye-1, cdk-4*) and negative (*cki-1, cdc-14*) cell cycle regulators identified as potentially SWI/SNF and HLH-1-regulated genes (Figure S6). We also included *myo-3* myosin, as an example of a probable SWI/SNF and HLH-1 MyoD-regulated muscle-specific gene (Figure S6). *cyd-1* Cyclin D was not identified as a SWI/SNF target in previous ChIP

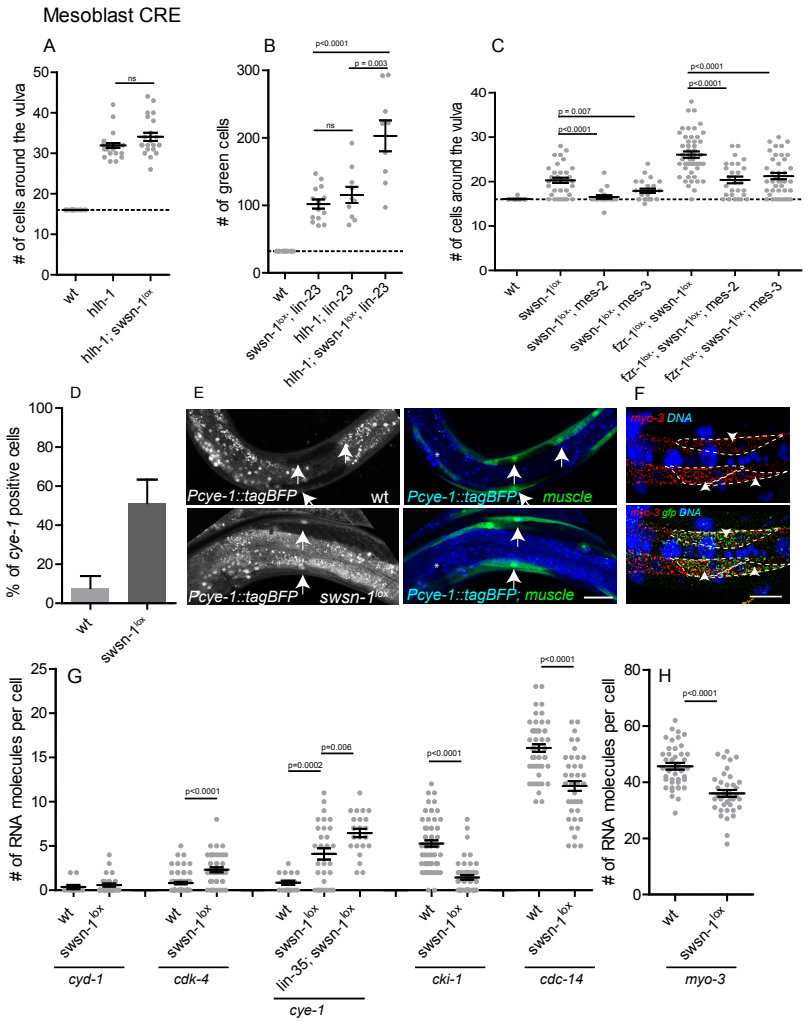

Figure 5. Control of cell cycle arrest and differentiation by SWI/SNF chromatin remodeling. (A-B) Quantification of the number of mesoblast descendants in wild-type and *hlh-1(cc561ts)* animals at the non-permissive temperature, combined with lineage specific inactivation of *swsn-1* (A) and/or *lin-23* RNAi (B). (C) Quantification of mesoblast descendants around the vulva in *swsn-1* or *fzr-1;swsn-1* mutants in combination with *mes-2* EZH2 or *mes-3* RNAi. (D) Quantification of the percentage post-mitotic muscle cells expressing *Pcye-1::tagBFP* in WT and mutants with M-lineage specific *swsn-1* inactivation. (E) Representative fluorescence microscopy images of animals quantified in (D). (F) smFISH staining using Cy5 labeled probes for *myo-3* and TMR labeled probes for GFP. (G-H) Detection of cell cycle and muscle-specific gene transcripts using smFISH, showing the number of fluorescent spots corresponding to the indicated mRNAs in post-mitotic muscle cells of the indicated genotypes. Arrows indicate differentiated M lineage muscles (green). Graphs show mean ± s.e.m.; each dot represents a single animal (A-C) or single cell (D, G). Dotted lines (A-C) indicate average WT numbers. Scale bar: 20 µm in (E), 5 µm in (F). See also Figures S5 and S6, and Table S3 and S4.

experiments and served as a control (Figure S5; (Riedel *et al*., 2013). Simultaneous smFISH labeling with anti-eGFP probes helped visualize the M-derived muscle cells in *read-out*^{lox}; *hlh-8::CRE* control animals and *swsn-1*^{lox} mutants (Figure 5F).

We detected *cye-1* and *cdk-4* mRNA expression in post-mitotic muscle cells of M-lineage-specific *swsn-1* mutants (Figure 5G). The corresponding muscle cells in control animals basically did not express *cye-1* mRNA, and showed significantly fewer *cdk-4* mRNA molecules. Conversely, the numbers of *cki-1, cdc-14,* and *myo-3* mRNA molecules in M-lineage muscle cell were substantially reduced in *swsn-1* mutants, compared to wild-type controls (Figure 5G, 5H). Neither the control nor *swsn-1* mutants expressed *cyd-1* mRNA in arrested M-lineage muscle cells (Figure 5G). Thus, only the G1/S regulator genes with a SWI/SNF-occupied promoter showed significantly induced (*cye-1* and *cdk-4*) or reduced (*cki-1* and *cdc-14*) expression following *swsn-1* inactivation. Importantly, the *cye-1* transcript numbers further increased when the *swsn-1* mutation was combined with a *lin-35(n745)* mutation (Figure 5G). This observation lends support for independent yet cooperative functions of SWI/SNF and *lin-35* Rb complexes in *cye-1* cyclin E repression. Together, these results support that the SWI/SNF complex contributes to both positive and negative regulation of cell cycle gene expression during muscle differentiation.

Combined G1/S inhibitor and SWI/SNF loss leads to continued proliferation of muscle precursors

The over-proliferating cells could remain present as undifferentiated precursor cells, become highly undifferentiated or obtain an in-between or random fate. To distinguish between these possibilities, we examined several markers for M-lineage descendants. The HLH-8 Twist transcription factor is expressed in undifferentiated precursor cells of the M-lineage, but not in the differentiated muscle cells and coelomocytes (Corsi *et al*., 2000). We examined expression of a *Phlh-8::tagBFP* transcriptional reporter in the *read-out*^{lox} strain and two M-lineage mutant strains (Figures 6A-C). Expression of tagBFP was apparent in all precursor cells of the M-lineage, including the migrating sex myoblasts (SM). However, at the time of muscle differentiation, tagBFP expression disappeared (Figure 6A). In *swsn-1* M-lineage knockout mutants treated with *lin*-23 RNAi, approximately half of the daughter cells maintained *Phlh-8::tagBFP* expression, even at late larval stages. This number increased considerably when *swsn-1 lin*-23 double inactivation was combined with *fzr-1* loss (49.8% versus 81.7% tagBFP-positive M descendants in the double versus triple mutant, respectively; Figures 6B, 6C, S7). Thus, increased proliferation in the M-lineage correlated with a higher percentage of M descendants maintaining expression of the *hlh-8* Twist precursor cell reporter. We also examined actin and UNC-15 paramyosin expression and organization, as markers for muscle differentiation. As visualized by immunohistochemical analysis, the eGFP-positive M-lineage derived bodywall muscle cells intercalated with the embryonic body muscles and formed well-organized myofilaments (Figure 6D, 6F, top). The eGFP positive M-descendants in *lin-23(RNAi) fzr-1*^{lox}*;swsn-1*^{lox}*;Phlh-8::CRE* mutants rarely showed organized myofilaments, and the majority did not show detectable actin or UNC-

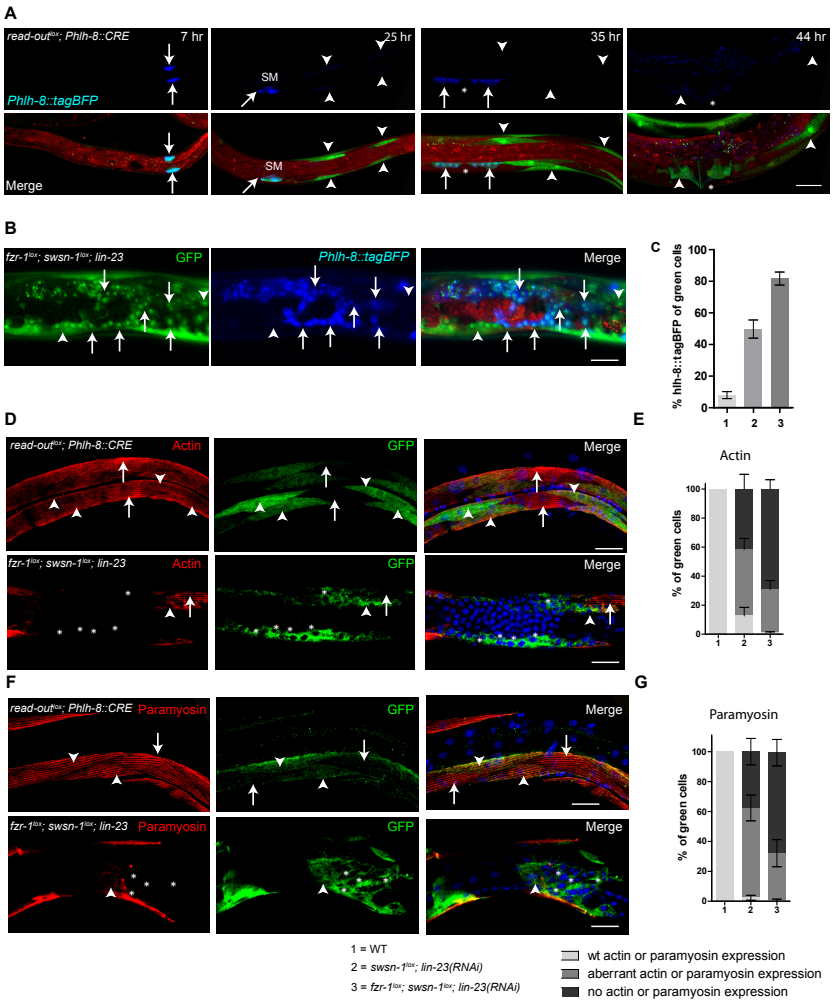

Figure 6. Limited differentiation of over-proliferating mesoblast descendants. (A-B) Fluorescence microscopy images showing *hlh-8* Twist promoter activity (tagBFP, Blue) in M-daughter cells (eGFP-positive, green). (A) Wild-type control, tagBFP is visible in precursor cells (arrows), but not in differentiated muscle cells (arrowheads). Asterisks (*) indicate the position of the vulva. (B) *fzr-1^{lox}; swsn-1^{lox}; lin-23(RNAi)* mesoblast mutant. M-derived cells with *Phlh-8::tagBFP* expression are indicated by arrows, without *Phlh-8::tagBFP* expression with a arrowhead. (C) Percentage of green cells positive for *Phlh-8::tagBFP* in animals of the indicated genotypes (bottom). (D and F) Staining of muscle differentiation markers, actin (red, D) and paramyosin (red, F) in L4 wild-type and mutant larvae. GFP: mesoblast descendants are visualized by anti-GFP antibody staining (green), nuclei by DNA staining (DAPI, blue). Arrows indicate non-mesoblast derived differentiated muscle cells (GFP absent), arrowheads indicate mesoblast descendants (green) expressing actin (red) or paramyosin (red), * indicates mesoblast descendants (green), without expression of actin (red) or paramyosin (red). (E and G) Percentage of cells with well-organized myofilaments (light grey), aberrant morphology of myofilaments (middle grey) or absence of myofilaments (dark grey) based on actin (E) or paramyosin (G) staining in animals of the indicated genotypes (bottom). Graphs show mean ± s.e.m. Scale bars: 20 µm. See also Figure S7.

15 paramyosin expression (Figures 6D-G, S7). However, muscle markers were expressed in some cells, and the percentage of actin or paramyosin expressing cells was substantially higher in *lin-23(RNAi);swsn-1*^{lox}*;Phlh-8::CRE* mutants with wild-type *fzr-1*, compared to mutants that also lacked *fzr-1* function. This is consistent with the proliferating M-lineage cells either maintaining progenitor status or initiating incomplete muscle differentiation. These observations highlight the inverse regulation of cell proliferation and differentiation.

Discussion

Our experiments based on CRE-lox-mediated recombination and lineage tracing uncovered tissue-type specific regulatory mechanisms for cell division arrest that cause tumorous over-proliferation of somatic cells when deregulated in *C. elegans*. We found five distinct levels of control to contribute to cell cycle exit: CDK inhibitory protein expression, LIN-35 Rb-mediated transcriptional repression, APC/C^{FZR1} and SCF^{LIN-23} catalyzed protein degradation, and SWI/SNF-mediated chromatin remodeling. These controls appear largely redundant and partly additive, together creating a highly robust decision to exit the cell division cycle. The contribution of SWI/SNF-mediated chromatin remodeling is critical, as excessive over-proliferation occurred only when inactivation of G1/S inhibitors was combined with SWI/SNF gene loss. Our data together with the described molecular functions support a model in which the different G1/S inhibitors and SWI/SNF complex provide alternative mechanisms to block the cell cycle machinery, converging at the CDK-4/Cyclin D and CDK-2/Cyclin E kinases and initiation of DNA synthesis (Figure 7).

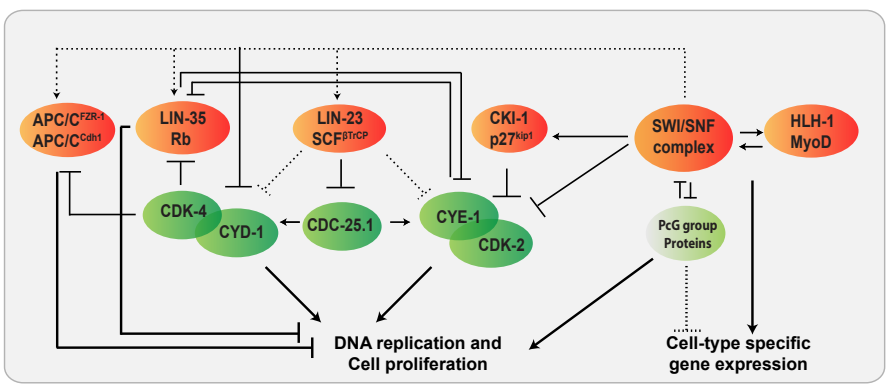

Figure 7. Model for developmental arrest of cell division. Ub-dependent protein degradation, Rb-mediated transcriptional repression, and association of CDK-inhibitory proteins with CDK/cyclin complexes, promote cell cycle arrest. During terminal differentiation, SWI/SNF complexes in cooperation with lineage-specific transcription factors provide an additional level of control. The different G1/S inhibitors and SWI/SNF complex cooperate by providing alternative levels of control over the basic cell cycle regulators, with each level antagonizing CDK-4/CYD-1 cyclin D and/or CDK-2/CYE-1 cyclin E kinase activity. Together, these regulators provide a highly robust control network for cell cycle exit. See also Figures S5 and S6.

The cell cycle arrest network is complex, because the regulators involved act redundantly, have multiple substrates, and provide feedback control. The Rb/E2F and SWI/SNF complexes affect the transcription of many genes, and the APC/C^{FZR-1} and SCF^{LIN-23} E3 ligases target multiple proteins for degradation. Nevertheless, a limited number of regulatory steps may be crucial for cell cycle exit. We found LIN-35 Rb and SWI/SNF to converge on *cye-1* Cyclin E transcriptional repression, while CKI-1 likely blocks CDK-2/CYE-1 Cyclin E kinase activity. Moreover, CUL-1 and LIN-23 β-TrCP have been implicated in G1 cyclin protein degradation (Kipreos *et al.*, 1996, 2000), while experimental evidence points to SCF^{LIN-23} catalyzed degradation of the CDK-cyclin activating phosphatase CDC-25.1 (Hebeisen and Roy, 2008). Targets of the APC/C^{FZR-1} are currently not known in *C. elegans*. Our recent results indicate that FZR-1 and LIN-35 RB are the most critical substrates of CDK-4/cyclin D kinases (The *et al.*, 2015). As such, combined loss of *lin-35* Rb and *fzr-1* alleviates cell cycle arrest by bypassing the requirement for CDK-4/cyclin D kinase activity. That mesoblast descendants do not continue proliferation in *lin-35* Rb, *fzr-1* double mutants likely reflects requirement for CDK-2/Cyclin E activation for S-phase initiation. In the double mutants, CDK-2/Cyclin E activity is still inhibited through CKI-1 Kip1 association, SCF^{LIN-23}-induced degradation of CDC-25.1, and SWI/SNF-dependent cyclin E transcriptional repression. Such alternative and partly non-overlapping levels of G1 CDK-cyclin inhibition can explain the observed genetic interactions between the different regulators (Figure 7).

SWI/SNF chromatin remodeling complexes act as global regulators of transcription. *Drosophila* SWI/SNF genes were identified as TrxG members with a positive role in Homeotic (HOX) gene expression or antagonism of PcG-mediated silencing (Schuettengruber *et al.*, 2011). Suppression of the *swsn-1* over-proliferation phenotype by PcG-related gene knockdown indicates that the antagonism between SWI/SNF and PcG gene function is conserved in *C. elegans*. Re-introduction of human SNF5 (BAF47/INI1) in SNF5-mutant rhabdoid tumor cells was found to induce PcG complex removal, transcription of the p16^{INK4A} and p21^{CIP1} genes, and cell proliferation arrest (Chai *et al.*, 2005; Kia *et al.*, 2008; Kuwahara *et al.*, 2013). Similarly, our results could be explained by PcG-mediated silencing of G1/S inhibitor genes that are normally activated by the SWI/SNF complex. However, this cannot explain the enhanced expression of positive cell cycle regulators in the *swsn-1* mutant. Transcriptional suppression by SWI/SNF-mediated chromatin remodeling could indirectly result from an induced factor, as has recently been described in *Drosophila* neural stem cells (Eroglu *et al.*, 2014). In contrast, our data, based on SWI/SNF promoter occupancy combined with reporter expression and smFISH experiments, support a direct contribution of SWI/SNF-mediated chromatin remodeling in transcriptional repression of *cye-1* and *cdk-4*. Together, these data are consistent with the model that SWI/SNF-mediated chromatin remodeling antagonizes PcG and promotes transcription of negative cell cycle regulators during differentiation, while simultaneously acting in cooperation with pRb to repress the transcription of positive regulators.

We found SWI/SNF gene function to be crucial for cell cycle arrest in the mesoblast lineage, but not in the intestine. Notably, differentiated embryonic intestinal cells do not

exit the cell cycle as they continue nuclear divisions and rounds of DNA synthesis during larval development (Hedgecock and White, 1985). In contrast, cells in the M-lineage transition from proliferating precursors to terminally differentiated post-mitotic cells (Sulston and Horvitz, 1977). This transition combines cell cycle withdrawal with activation of a muscle-specific gene expression program. Previous studies of differentiating myoblasts implicated SWI/SNF-mediated chromatin remodeling in muscle-specific gene expression (de la Serna *et al.*, 2001; Puri and Mercola, 2012). This activation of cell-type specific gene expression likely coincides with SWI/SNF-mediated chromatin remodeling at cell cycle gene promoters (see above, Figure 7). Transcriptional activation and inactivation of cell cycle genes by the SWI/SNF complex provides a mechanism for cell cycle exit that may be employed specifically during terminal differentiation, and which still can be effective when multiple G1/S inhibitors are lost. This could be the main difference between permanent cell cycle arrest and temporary quiescence.

Recent cancer genome sequencing studies and identification of additional SWI/SNF accessory and signature factors have revealed that inactivation of SWI/SNF components occurs in a broad spectrum of human cancers, at an astonishing average frequency of nearly 20% (Kadoch *et al.*, 2013; Kandoth *et al.*, 2013; Wang *et al.*, 2014). The mutation frequencies vary greatly among SWI/SNF subunits and cancer types, emphasizing the importance of cellular context and SWI/SNF complex composition. Selective pressure in cancer can be expected to particularly benefit mutations that prevent early lineage transitions and maintain an immortal stem or progenitor state. At the same time, mutations that sustain cell proliferation are near universally present in human cancer (Hanahan and Weinberg, 2011). Further studies will be needed to understand the cell-type specific and combinatorial activities of SWI/SNF components and transcription factors in proliferation versus differentiation decisions, and their interplay with cell cycle control genes in human cancer.

Materials and Methods

Strains, Culture and CRE expression

The genotypes of strains used in this study are listed in Table S7. *C. elegans* was cultured on NGM plates seeded with OP50 bacteria and generally maintained at 20 °C. Strains containing the *swsn-1(os22*ts*)* or *hlh-1(cc561*ts*)* mutation were maintained at 15 °C and shifted to 25 °C for mutant phenotype analysis. The use of the temperature sensitive *swsn-1(os22*ts*)* mutation was chosen because the floxed *swsn-1* transgene did not rescue embryonic development of *swsn-1(tm4567)* deletion mutant animals. Larval development was restored by the transgene, indicating that the failure to complement was likely caused by germline silencing of the *swsn-1* transgene. The *swsn-5(ok622)* (*snfc-5*) deletion strain was also not suitable for our studies, as we found this strain to contain residual *swsn-5* function, as published by (Large and Mathies, 2014).

The CRE recombinase was first used in *C. elegans* by the Hajnal lab (Hoier *et al.*, 2000) and, independently of this study, further explored by the Mitani lab (Kage-Nakadai *et al.*, 2014). In initial experiments, coinjection of a vector for general CRE recombinase expression (*Psur-5::CRE*) and the recombination reporter (*read-out*^{lox}) resulted in transgenic animals with a low number of eGFP positive cells in multiple lineages. We optimized the efficiency of CRE-recombination through multiple adjustments. Motivated by CRE results in mammalian cells (Lin *et al.*, 2004), we added an N-terminal FLAG-tag and EGL-13 nuclear localization signal to the CRE coding sequence. Moreover, we introduced introns and optimized the codon usage for *C. elegans* (Redemann *et al.*, 2011). Finally, the CRE expression vectors were inserted in the genome as single copy-transgenes (Frøkjær-Jensen *et al.*, 2012). These adjustments resulted in efficient recombination.

RNA-mediated interference

Bacterial cultures of *E. coli* HT115 containing L4440 empty vector or vector with genomic or ORF gene inserts were grown o/n, three times concentrated and seeded onto NGM plates containing 12,5 µg/ml Tetracycline, 100 µg/ml Ampicillin and 2mM IPTG. In the initial screen, L4 animals of the indicated strains were placed on RNAi plates and the number of green cells (Intestine or Mesoblast) in the progeny was analyzed in L3 animals (Intestine) or late L4/young adults (Mesoblast). If this resulted in close to 100% sterility or embryonic lethality (*swsn-5* and *swsn-1*), we started feeding RNAi in the L1 stage and analyzed the number of mesoblast descendents in L4 animals of the same generation. A different RNAi approach was used in order to analyze the role of either *lin-23*, *cul-1* or *cki-1* in *swsn-1(os22ts)*; *swsn-1*^{lox} mutants. Since the *swsn-1* rescue construct could not rescue germ line development at the restrictive temperature, L4 animals were grown for two days on plates containing either *lin-23, cul-1* or *cki-1* RNAi at 15 °C, followed by a hypochlorite treatment to isolate the embryos. Embryos were placed in M9 at 25 °C, in order to inactivate *swsn-1*, and hatched over night. Hatched animals were placed on RNAi plates at 25 °C and the number of green cells was analyzed 34 hours later (late L4/young adult stage). Note: *lin-23* RNAi results in high percentage of embryonic lethality, by starting with many L4 animals we were able to obtain enough animals for analysis. For *mes-2* and *mes-3,* exposure to feeding RNAi was needed for two generations in order to obtain a highly penetrant sterile phenotype. To obtain strong RNAi phenotypes for *mes-2* and *mes-3,* we started RNAi treatment as L4 animals (P0). The next generation (F1) was bleached, and eggs (F2) were hatched at 25 °C to inactivate *swsn-1(os22*ts*)* (see above). The number of mesoblast descendents was quantified in L4/young adult animals in the F2 generation.

Quantification of the number of mesoblast descendents

Expression of *hlh-8::CRE* in combination with the recombination reporter (*read-out*^{lox}) allowed us to specifically visualize the mesoblast lineage (GFP positive). Extra division events were quantified by counting the number of GFP-positive cells. In our analysis, we

either focused on the total number of green cells or only on the mesoblast descendents in the region around the vulva. Images of the over-proliferation phenotypes were obtained using a Zeiss LSM700 Confocal microscope.

In approximately 90% of the animals expressing *hlh-8::CRE*, recombination and GFP expression was detected in some non-mesoblast derived head muscle cells as well (Table S2). Usually these a-specific recombination events did not pose a problem as it resulted in recombination of only one allele (as concluded from coincident mCherry and eGFP expression). In addition, the head region could easily be excluded from our analysis. In approximately 10% of the animals we also observed recombination in the somatic gonad. Since these cells are located in the same region as the mesoblast cells surrounding the vulva careful analysis is required to exclude these cells from our quantifications. The cells of the somatic gonad can be excluded based on several criteria. Similar to the head muscle cells, usually cells of the somatic gonad also appeared to recombine only one of the alleles, resulting in coincident mCherry and eGFP expression. In addition, the cells of the somatic gonad are located in a different plane compared to the sex muscle cells from the mesoblast lineage. Moreover, cells in the somatic gonad have a different size and morphology in comparison to the mesoblast-derived cells. Finally, in case of severe overproliferation, the overproliferation usually started in the posterior part of the animal and migration of the SMs towards the vulva region failed.

Molecular Cloning

For the generation of the MosSCI *loxP* constructs, a general cassette of *Prps-27::loxP::SV40nls::mCherry::let-858UTR::loxP::SV40nls::GFP::let-858UTR* was created in pCFJ35. Codon-optimized mCherry was amplified from *pMa-mCherry* (a kind gift from Tony Hyman) and cloned into pPD158.85 with *Bam*HI and *Eco*RI creating a *mCherry::let-858::UTR* construct. An 841 bp promoter fragment of *rps-27* was amplified by PCR from genomic N2 DNA, using a reverse primer containing the *loxP* site (ATAACTTCGTATA **GCATACAT** TATACGAAGTTAT)(Livet *et al.*, 2007). This fragment was cloned into an *mCherry::let858* construct using *Pst*1 and *Xba*I sites. Codon-optimized eGFP was amplified from *pMa-meGFP* (a kind gift from Tony Hyman) and used to replace mCherry in the above described construct, creating *loxP::SV40nls::eGFP::let-858UTR*. This fragment was PCR amplified and cloned into the *Prps-27::loxP::nls::mCherry::let858UTR* vector, giving rise to the read-out reporter plasmid: *Prps-27::loxP::SV40nls::mCherry::let-858UTR::loxP::SV40nls::GFP::let-858UTR*. Finally, this construct was cloned into the pCFJ356 Mos ChrIV vector. The final construct contains a unique *Not*1 site, directly upstream of the second *loxP* site, which has been used in subsequent cloning steps to create the combined read-out and rescue constructs for the genes of interest.

To generate the *fzr-1* read-out and rescue construct, a region containing 2.2 kb of *fzr-1* promoter sequence, previously shown to be sufficient for *fzr-1(ku298)* rescue by D. Fay (Fay *et al.*, 2002), the *fzr-1* gene, and 1kb 3'UTR was amplified from Fosmid WRM-0635dH03, using primers containing a *Not*1 site. This fragment was cloned into the

Prps-27::loxP::SV40nls::mCherry::let-858UTR::loxP::SV40nls::GFP::let-858UTR read-out construct, using *Not*1 to create *Prps-27::loxP::SV40nls::mCherry::let-858UTR::Pfzr-1::fzr-1::fzr-1UTR::loxP::SV40nls::GFP::let-858UTR*.

To generate the *swsn-1* read-out and rescue construct, we amplified the *swsn-1* rescue construct from pPS1.7 (a kind gift from H. Sawa; (Sawa *et al*., 2000)) containing 2.0 kb of the *swsn-1* promoter region, the *swsn-1* gene including intron 1 and 2, followed by the *unc-54 3'UTR*. In order to prevent cross-reactivity between the *lox*-sites on different chromosomes we used site directed mutagenesis to change the *loxP* site into a *loxN* site (ATAACTTCGTATA **GTATACCT** TATACGAAGTTAT)(Livet *et al*., 2007) in the general read-out construct. The *swsn-1* rescuing PCR fragment was subsequently cloned into the *loxN*-containing read-out construct *Prps-27::loxN::SV40nls::mCherry::let-858UTR::loxN::SV40nls::GFP::let-858UTR*, using the unique *Not*1 site, thereby creating the final construct *Prps-27::loxN::SV40nls::mCherry::let-858UTR::Pswsn-1::swsn-1::unc-54UTR::loxN::SV40nls::GFP::let-858UTR*. This construct was cloned into the PCFJ350 vector and single copy integrated on Chr V by MosSCI (Frøkjær-Jensen *et al*., 2012).

To generate the *hlh-8::CRE* construct, a 518 bp promoter fragment directly upstream of the *hlh-8* ATG was amplified from genomic N2 DNA with a forward primer containing *Xba*I and reverse primer containing a *Pac*I site. A 330 bp *tbb-2 3'UTR* was amplified from genomic N2 DNA with a forward primer containing *Pac*I and a reverse primer with a *Spe*I site. The two resulting PCR products were ligated into *Xba*I and *Spe*I digested PCFJ355, to generate the *hlh-8::tbb-2 3'UTR* construct. In the final step we digested the *egl-13NLS::codoptCRE* from the pUC57 vector with *Pac*I and *Not*1 and ligated the CRE constructs in between the *Phlh-8* and *tbb-2 3'UTR* to generate the *Phlh-8::egl-13nls::CRE::tbb-2 3'UTR* construct. To generate the *Pelt-2::egl-13nls::CRE::tbb-2 3'UTR* construct, the *hlh-8* promoter was replaced by a 3.6 kb promoter region of *elt-2* using *Xba*I and *Xma*I restriction sites.

In order to generate the *Pcye-1::tagBFP::unc-54* read-out construct, GFP was replaced by tagBFP in the PKM1110 vector (Brodigan *et al*., 2003). PKM1110 contains a 3.1 kb promoter of *cye-1* as well as the first two exons and first intron of *cye-1,* and was previously shown to drive GFP expression consistent with S-phase (Brodigan *et al*., 2003).

Immunohistochemical analysis

For immuno-staining with antibodies, animals were fixed using the Bouin's fixative protocol (Van den Heuvel and Kipreos, 2012). In short: animals were fixed for 30 min. at RT in 400 µl Bouin's fix + 400 µl methanol and 10 µl β-mercaptoethanol, three times freeze-thawed and again tumbled for 30 min in fixative at RT. For permeabilization, the fixative was removed and exchanged for borate-Triton-β-mercaptoethanol (BTB: 1xBorate Buffer, 0.5% Triton and 2% β-mercaptoethanol) solution. Animals were tumbled 3 times for 1 hour in BTB solution at RT. After the final step, animals were washed with PBS-0.05% Tween and incubated in block-solution (10% BSA and 10% goat serum). Staining with primary antibodies was performed overnight at 4 °C, incubation with secondary antibodies

for 2 hours at RT. Primary antibodies used in this study are: rabbit anti-GFP (Life Technologies A6455, 1:100), mouse anti-GFP (Roche, 1:100), mouse anti UNC-15 paramyosin (Developmental Studies Hybridoma Bank, 1:3), rabbit anti-actin (Cytoskeleton, AAN01 1:100). Secondary antibodies used in this study: Goat anti-rabbit Alexa Fluor 488, goat anti-rabbit Alexa Fluor 568, goat anti-mouse Alexa Fluor 488, goat anti-mouse Alexa Fluor 568 (Invitrogen). Animals were mounted in Prolong Anti-Fade Gold with DAPI (Molecular Probes) and analyzed using a Zeiss LSM700 Confocal microscope.

EdU incorporation was used to visualize DNA replication during later stages of development (Van den Heuvel and Kipreos, 2012). *swsn-1(os22);swsn-1*^{lox} L4 animals were placed on *lin-23* RNAi plates at 15 °C. Every few hours the parents were removed from the plates and embryos were shifted to 25 °C. Once these semi-synchronized batches of animals had reached the L2 stage, animals were collected and placed on NGM plates seeded with EdU-containing MG1693 (thy$^-$) *E. coli* bacteria. Animals were grown at 25°C until L4 and fixed following the Bouin's-fixative protocol. Permeabilization was followed by a Click-IT reaction, using the Click-IT EdU Alexa Fluor 594 kit (Invitrogen) as described previously and according to the manufacturer's instructions (Invitrogen) (Van den Heuvel and Kipreos, 2012). Subsequently, immunohistochemical staining was used to detect GFP-positive cells, as described above.

Single molecule Fluorescence in Situ Hybridization

Single molecule Fluorescence In Situ Hybridization (smFISH) was performed as described previously (Raj *et al.*, 2010) and www.singlemoleculefish.com, with some adaptations to the general protocol. In brief, 48 (*cye-1*), 46 (*cyd-1*), 35 (*cdk-4*), 24 (*GFP*), 48 (*myo-3*), 23 (*cki-1*) or 48 (*cdc-14*) oligonucleotide probes directed against the coding sequence of the indicated genes were designed, making use of the website www.singlemoleculefish.com, and obtained labeled with Cy5 except for except for the probes against GFP which were labeled with TAMRA (GFP).

Synchronized (starved) L1 animals were fed for 26 hours on OP50 at 25 °C, followed by fixation with Bouin's fixative. After permeabilization in borate-Triton-β-mercaptoethanol solution, hybridization was performed as described previously (Raj *et al.*, 2010). Animals were tumbled overnight at 32 °C in 100 µl hybridization solution (20% formamide) to which 0.2 µl of 25 µM stock (*cyd-1, cdk-2*, GFP and *myo-3*) or 0,5 µl of 25 µM stock (*cki-1*, *cdc-14* and *cdk-4*) was added, resulting in a final probe concentration of 50 or 125 nM. Following overnight incubation at 32 °C, samples were washed 4x for 1 hour in wash buffer (20% formamide) at 32 °C. DAPI was added to the final wash step in order to visualize the nuclei. Shortly before imaging, samples were mounted in anti-bleach GLOX buffer.

smFISH data were imaged using a Leica MM-AF Microscope with filter settings for DAPI, TMR and Cy5. Quantification of the number of mRNA molecules was performed by drawing a region around the cell of interest, marked by the presence of TMR spots. In this region, the number of Cy5 spots was quantified. For each condition, at least 8 animals, and multiple cells per animal, were used for quantifications.

Microscopy and quantification of cell numbers

Cell division events were quantified by counting the number of GFP-positive cells in the intestine or mesoblast lineage. For relatively weak phenotypes, mesoblast descendants were counted in the region around the vulva. For stronger phenotypes, we counted the total number of eGFP cells, as indicated in the text and figures. Images acquisition and quantifications of mesoblast descendants expressing the *Pcye-1::tagBFP* or *Phlh-8::tagBFP* transcriptional reporters, UNC-15 paramyosin or actin are described in the extended experimental procedures.

Statistical analysis

Sample sizes were not pre-determined, instead all available animals of the right stage and genotype were counted. smFISH data are included from at least 8 independent animals, reporter expression and cell numbers from at least 10 independent animals. Graphs and data analysis were produced using GraphPad Prism 5. Plots indicate all data points, as well as the mean (average) ± s.e.m. As the data essentially fit normal distributions, unpaired two-tailed Student's t tests were used to examine statistical significance of the difference between means.

Acknowledgement

We thank A. Akhmanova, H. Sawa, S. Mitani, A. Hyman, A. Pozniakovsky, G. Wachsman and B. Scheres for reagents and strains. T. Middelkoop, M. Bienko, A. van Oudenaarden and the Hubrecht Imaging Center for assistance with smFISH experiments, C. Riedel for access to SWI/SNF ChIP data, M. Boxem for help with data analysis, F. Holstege, M. Boxem, I. The, and A. Thomas for critically reading the manuscript, and members of the van den Heuvel and Boxem groups for help and discussion. Several strains were provided by the CGC, which is funded by the NIH Office of Research Infrastructure Programs (P40 OD010440). This work is part of research program 819.02.016, financed by the Netherlands Organization for Scientific Research (NWO).

Author contributions

S.R. performed all experiments. S.v.d.H. and S.R. designed the experiments, analyzed the data, and wrote the manuscript.

Supporting Information

A

Lox variant	Sequence
LoxP	ATAACTTCGTATA **GCATACAT** TATACGAAGTTAT
Lox2272	ATAACTTCGTATA **GGATACTT** TATACGAAGTTAT
LoxN	ATAACTTCGTATA **GTATACCT** TATACGAAGTTAT

B

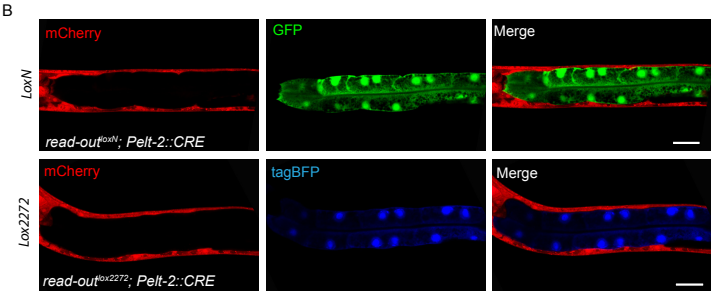

Supplementary Figure 1. Cell type specific recombination and lineage tracing using *loxN* and *lox2272*. (A). Overview of the tested and used lox-site variants in this study. (B) Fluorescent microscopy images of CRE-lox-based recombination in the intestine using *loxN* and *lox2272* sites in the read-out reporter construct. The recombination reporter containing the *loxN* (*read-out*^{loxN}) sites switches from mCherry to eGFP, whereas the *lox2272*-containing recombination reporter (*read-out*^{lox2272}) switches from mCherry to tagBFP expression upon CRE-induced recombination. Scale bar represents 20 µm.

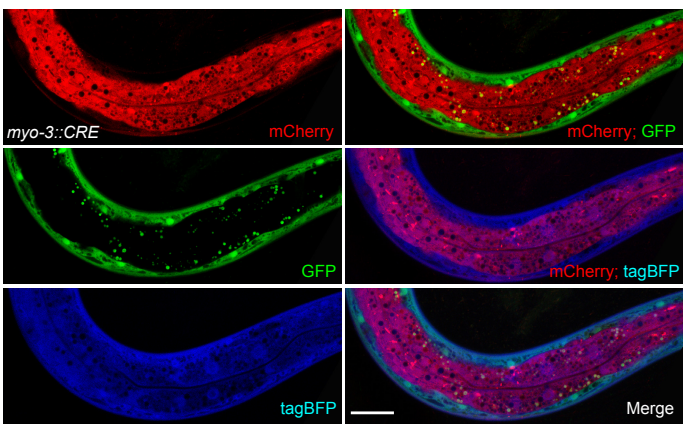

Supplementary Figure 2. CRE expression in post-mitotic muscle cells induces recombination but not loss of tagBFP gene of interest expression. The tagBFP coding sequence, flanked by a general promoter (*Peft-3*) and 3' UTR (*tbb-2 3' UTR*) was placed in the read-outlox recombination construct and single copy integrated into the genome. Lineage specific CRE expression in post-mitotic muscle cells driven by *Pmyo-3* resulted in loss of mCherry and induction of eGFP expression. However, in contrast to results in proliferating cells, loss of expression of the tagBFP gene of interest was not observed. Scale bar indicates 20 µm. See also Figure 1, Figure S1, Table S1 and Table S2.

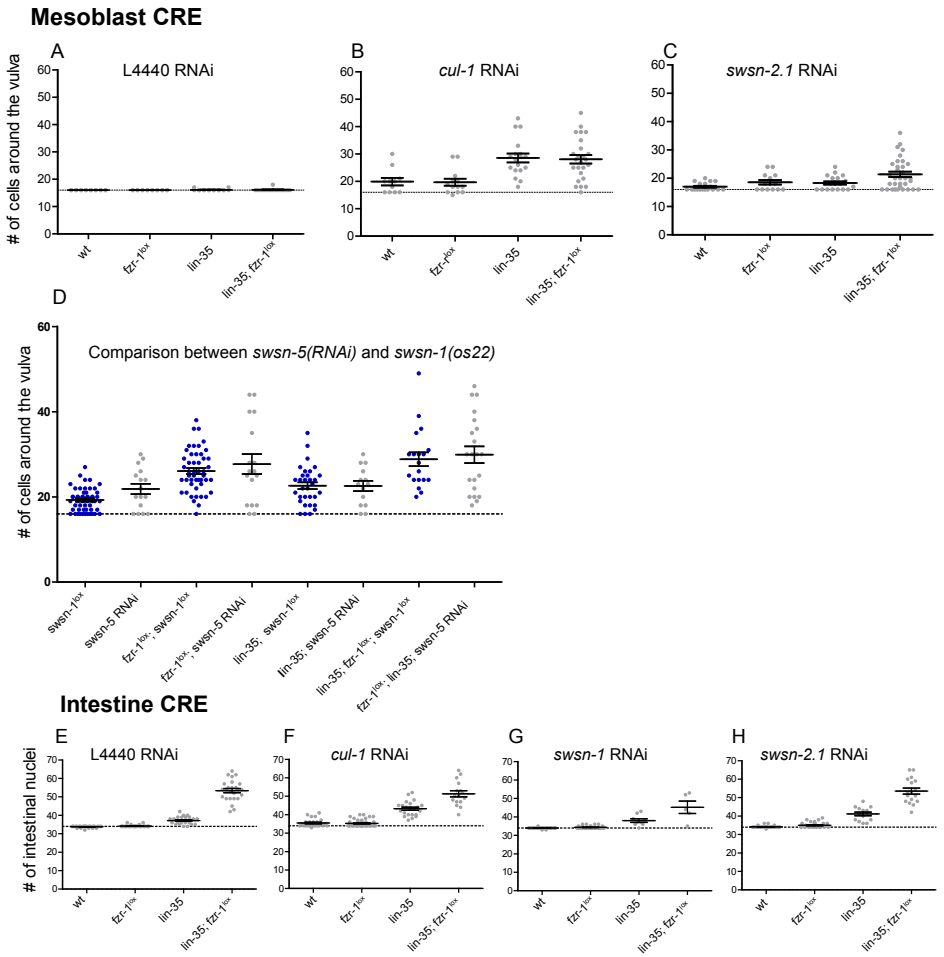

Supplementary Figure 3. Cooperative control of cell cycle exit by G1/S inhibitors and SWI/SNF subunits. (A-C) Quantification of the number of mesoblast descendants around the vulva upon RNAi of the indicated genes combined with *lin-35* null mutation and lineage specific *fzr-1* knockout, or empty vector (L4440) control RNAi. (D) Comparison between the number of mesoblast descendants localized around the vulva upon lineage-specific inactivation of *swsn-1* and RNAi of *swsn-5*. (E-H) Quantification of the number of intestinal nuclei upon RNAi of the indicated genes combined with *lin-35* null mutation and lineage-specific *fzr-1* knockout. Graphs show mean ± s.e.m., each dot represents the number of cells in a single animal. Dotted line in the graph represents average number in the WT.

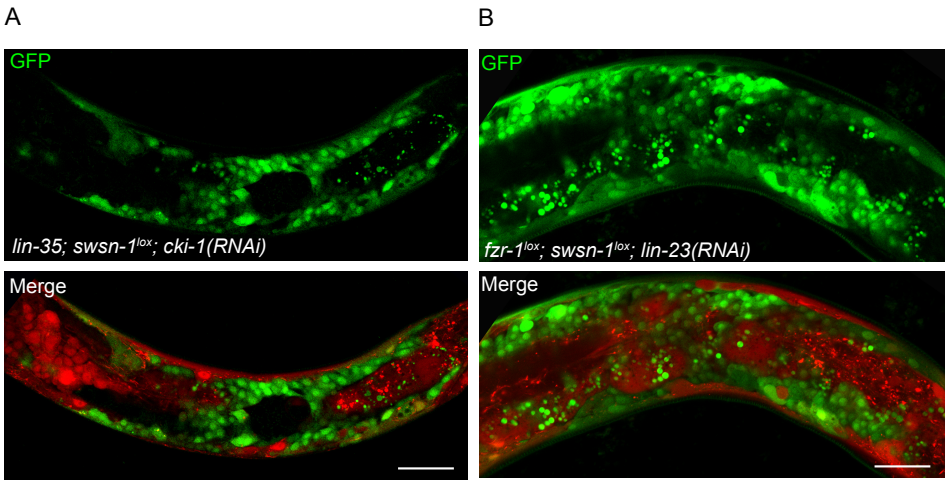

Supplementary Figure 4. Combined inactivation of swsn-1 with G1/S inhibitors leads to dramatically increased proliferation in the mesoblast lineage. (A and B) Representative fluorescence microscopy images of mesoblast overproliferation (green cells) in mutant animals of the indicated genotype. Scale bars represent 20 μm.

Supplementary Figure 5. SWSN-1 and SWSN-4 binding near positive and negative cell cycle regulatory genes. Data from Chromatin immunoprecipitation-sequencing (ChIP-seq) experiments by Riedel *et al.,* (2013) reveal SWSN-1::GFP (top) and SWSN-4::GFP (bottom) association with genomic DNA near negative (left) and positive (right) cell cycle regulators. Binding site traces of SWI/SNF subunits are detected near promoter regions of all examined negative cell cycle regulators, except for *wee-1.1.* In addition, at least 2 of 8 positive cell cycle regulators, *cye-1* and *cdk-4*, show SWI/SNF binding near their regulatory regions. The data from Riedel *et al.*, were loaded into the USCS genome browser to reveal binding site traces. Al profiles shown have the same scale as the *fzr-1* profile, with exception of *lin-35*, *cdk-2* and *cdc-25.2*, for which a larger region is shown, with the same scale bar as shown for *lin-35.*

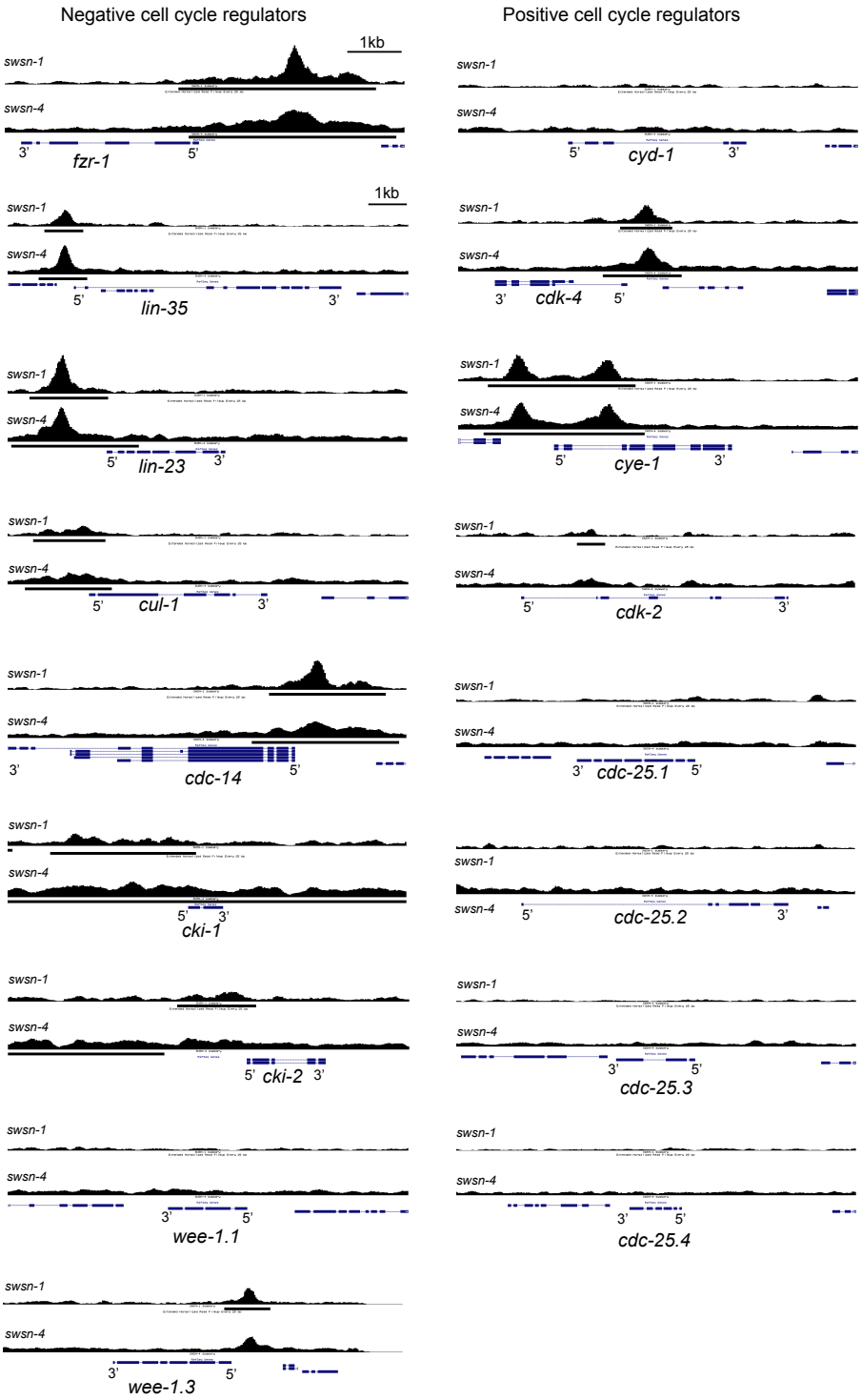
Negative cell cycle regulators
Positive cell cycle regulators
1kb
swsn-1
swsn-4
3'
fzr-1
5'
cyd-1
lin-35
cdk-4
lin-23
cye-1
cul-1
cdk-2
cdc-14
cdc-25.1
cki-1
cdc-25.2
cki-2
cdc-25.3
wee-1.1
cdc-25.4
wee-1.3

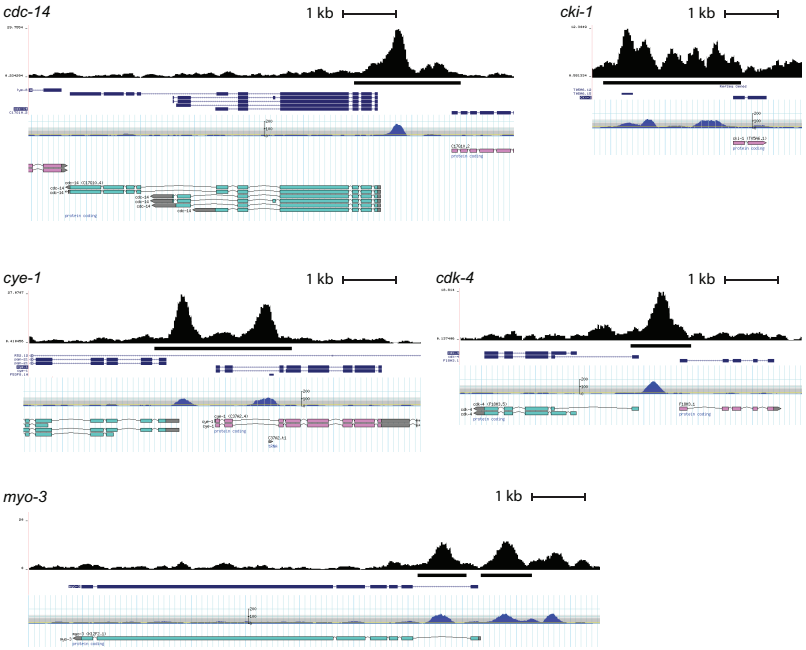

Supplementary Figure 6. Overlap between SWSN-1 and HLH-1 binding sites at promoter regions of *cdc-14*, *cki-1*, *cye-1* and *cdk-4*. Comparing data from ChIP-seq experiments by (Riedel *et al*., 2013) and (Boyle *et al*., 2014) reveals overlapping putative SWSN-1 and HLH-1 binding sites. Top of each panel shows binding site tracks for SWSN-1, based on data from Riedel *et al*., loaded into the USCS genome browser. Bottom part of each panel illustrates binding sites for HLH-1, as identified by the Snyder group, in the Wormbase GBrowse display. In all four cell cycle regulators (including two positive and two negative cell cycle regulators) overlap between HLH-1 and SWI/SNF promoter binding can be observed.

Supplementary Figure 7. Loss of cell cycle arrest coincides with failure of differentiation in over-proliferating mesoblast descendants. Expression of *Phlh-8::tagBFP*, a marker of mesoblast precursor cells in *swsn-1$^{lox;}$ lin-23(RNAi)* animals (A) and *fzr-1$^{lox;}$swsn-1$^{lox;}$ lin-23(RNAi)* animals (B). Arrowheads indicate mesoblast descendants without hlh-8::tagBFP expression, arrows indicate mesoblast descendants with *Phlh-8::tagBFP* expression. (C and D) Staining of the muscle differentiation marker actin (red) in *swsn-1^{lox};lin-23(RNAi)* animals (C) and *fzr-1^{lox};swsn-1^{lox};lin-23(RNAi)* animals (D) Mesoblast descendants show anti-GFP staining (green), nuclei are stained with DAPI (blue). In *swsn-1^{lox};lin-23(RNAi)* animals most mesoblast descendants still express actin, but fail to form organized myofilaments (C). In *fzr-1^{lox};swsn-1^{lox};lin-23(RNAi)* animals most mesoblast descendants fail to express actin, and fail to form organized myofilaments. (E and F) Staining of the muscle differentiation marker paramyosin (red) in *swsn-1^{lox};lin-23(RNAi)* animals (E) and *fzr-1^{lox};swsn-1^{lox};lin-23(RNAi)* animals (F) Mesoblast descendants show anti-GFP staining (green), nuclei are stained with DAPI (blue). In *swsn-1^{lox};lin-23(RNAi)* animals most mesoblast descendants still express paramyosin, but fail to form organized myofilaments (E). In *fzr-1^{lox};swsn-1^{lox};lin-23(RNAi)* animals most mesoblast descendants fail to express paramyosin and fail to form organized myofilaments (F). Arrows indicate non-mesoblast derived differentiated muscle cells (GFP absent), arrowheads indicate mesoblast descendants (green) with expression of actin (red) or paramyosin (red), * indicates mesoblast descendants (green), without expression of actin (red) or paramyosin (red). Scale bars represent 20 µm.

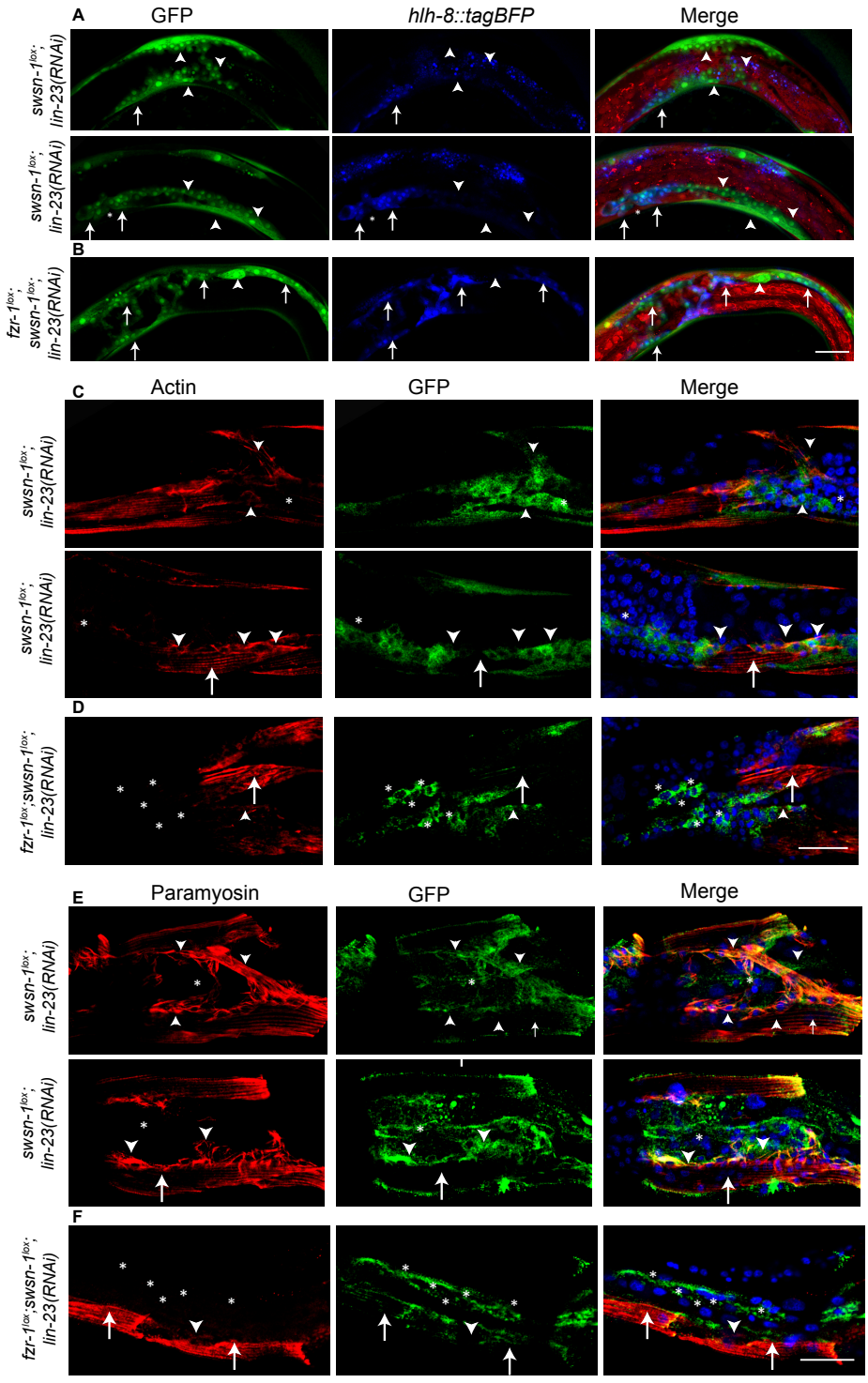
A
GFP
hlh-8::tagBFP
Merge
swsn-1lox; lin-23(RNAi)
swsn-1lox; lin-23(RNAi)
B
fzr-1lox; swsn-1lox; lin-23(RNAi)
C
Actin
GFP
Merge
swsn-1lox; lin-23(RNAi)
swsn-1lox; lin-23(RNAi)
D
fzr-1lox;swsn-1lox; lin-23(RNAi)
E
Paramyosin
GFP
Merge
swsn-1lox; lin-23(RNAi)
swsn-1lox; lin-23(RNAi)
F
fzr-1lox;swsn-1lox; lin-23(RNAi)

Supplementary Table 1. Efficiency and specificity of CRE-loxP-based recombination in *C. elegans*

Promoter used for CRE expression	Temp (°C)	Mesoblast	Intestine	Body wall muscle	Somatic gonad	Seam cells
Phlh-8 (mesoblast)	15	97	0	81*	4	0
	20	100	0	91*	9	0
	25	99	0	92*	20	1
Pelt-2 (intestine)	15	0	100	0	94	0
	20	0	100	0	93	0
	25	0	100	4	97	0
Pmyo-3 (bwm)	15	0	0	100	0	0
	20	0	0	100	0	0
	25	0	0	100	0	1

Efficiency and specificity of CRE-loxP-based recombination in *C. elegans* at 15, 20 and 25 °C. Numbers represent % of animals showing recombination, mean of three independent experiments. In each experiment 100 animals were counted. *Note that most of the body wall muscle cells in which recombination was detected were located in the head region

Supplementary Table 2. Efficiency of recombination using *lox2272* and *loxN* sites

Promoter used for CRE expression	Temp (°C)	lox2272	loxN
Phlh-8 (mesoblast)	20	98 (97-100)	96 (91-99)
Pelt-2 (intestine)	20	100 (100-100)	100 (99-100)

Efficiency of CRE-lox-based recombination in *C. elegans* at 20 °C. Numbers represent % of animals showing recombination, mean of three independent experiments. Minimum and maximum values are shown in between brackets. In each experiment 100 animals were counted.

Supplementary Table 3. Quantification of the number of intestinal nuclei for all genotypes used in this study

Genotype	Quantification Intestine (mean ± s.e.m)	
	number of nuclei	post-embryonic divisions
WT	33.7 ± 0.1 (N= 25)	13.7 ± 0.1 (N= 31)
fzr-1(ku298); fzr-1^{lox}; Pelt-2::CRE	34.2 ± 0.1 (N= 28)	14.3 ± 0.2 (N= 18)
lin-35(n745); read-out^{lox}; Pelt-2::CRE	37.5 ± 0.5 (N= 19)	16.2 ± 0.3 (N= 29)
lin-35(n745); fzr-1(ku298)		30.3 ± 2.1 (N= 18)
lin-35(n745); fzr-1(ku298); fzr-1^{lox}		17.2 ± 0.4 (N= 32)
lin-35(n745); fzr-1(ku298); fzr-1^{lox}; Pelt-2::CRE	53.4 ± 1.3 (N= 22)	27.6 ± 1.3 (N= 24)
cki-1(RNAi)	36.7 ± 0.4 (N= 37)	
fzr-1(ku298); fzr-1^{lox}; Pelt-2::CRE; cki-1(RNAi)	37.1 ± 0.4 (N= 38)	
lin-35(n745); read-out^{lox}; Pelt-2::CRE; cki-1(RNAi)	57.1 ± 2.1 (N= 20)	
lin-35(n745); fzr-1(ku298); fzr-1^{lox};Pelt-2::CRE; cki-1(RNAi)	66.3 ± 1.3 (N= 26)	
lin-23 (RNAi)	34.8 ± 0.2 (N= 30)	
fzr-1(ku298); fzr-1^{lox}; Pelt-2::CRE; lin-23(RNAi)	35.2 ± 0.3 (N= 38)	
lin-35(n745); read-out^{lox}; Pelt-2::CRE; lin-23(RNAi)	43.8 ± 1.2 (N= 21)	
lin-35(n745); fzr-1(ku298); fzr-1^{lox}; Pelt-2::CRE; lin-23(RNAi)	53.3 ± 2.2 (N= 13)	
cul-1(RNAi)	35.5 ± 0.4 (N= 25)	
fzr-1(ku298); fzr-1^{lox}; Pelt-2::CRE; cul-1(RNAi)	35.3 ± 0.3 (N= 44)	
lin-35(n745); read-out^{lox}; Pelt-2::CRE; cul-1(RNAi)	43.2 ± 0.9 (N= 22)	
lin-35(n745); fzr-1(ku298); fzr-1^{lox}; Pelt-2::CRE; cul-1(RNAi)	51.3 ± 1.7 (N= 16)	
swsn-5(RNAi)	34.1 ± 0.1 (N= 33)	
fzr-1(ku298); fzr-1^{lox}; Pelt-2::CRE; swsn-5(RNAi)	34.5 ± 0.2 (N= 32)	
lin-35(n745); read-out^{lox}; Pelt-2::CRE; swsn-5(RNAi)	40.9 ± 0.8 (N= 18)	
lin-35(n745); fzr-1(ku298); fzr-1^{lox}; Pelt-2::CRE; swsn-5(RNAi)	49.8 ± 1.9 (N= 17)	
swsn-2.1(RNAi)	34.2 ± 0.1 (N= 31)	
fzr-1(ku298); fzr-1^{lox}; Pelt-2::CRE; swsn-2.1 (RNAi)	35.0 ± 0.3 (N= 31)	
lin-35 (n745); read-out^{lox}; Pelt-2::CRE; swsn-2.1 (RNAi)	41.1 ± 1.0 (N= 14)	
lin-35 (n745); fzr-1(ku298);fzr-1^{lox}; Pelt-2::CRE; swsn-2.1 (RNAi)	53.5 ± 1.6 (N= 17)	
swsn-1(RNAi)	33.9 ± 0.0 (N= 35)	
fzr-1(ku298); fzr-1^{lox}; Pelt-2::CRE; swsn-1(RNAi)	34.3 ± 0.1 (N= 37)	
lin-35(n745); read-out^{lox}; Pelt-2::CRE; swsn-1(RNAi)	38.0 ± 1.0 (N= 9)	
lin-35(n745); fzr-1(ku298); fzr-1^{lox}; Pelt-2::CRE; swsn-1(RNAi)	45.2 ± 3.4 (N= 5)	

Supplementary Table 4. Quantification of the number of mesoblast descendants for all genotypes used in this study

Genotype	Mesoblast descendants (eGFP (+), mean ± s.e.m.)	
	Total number of nuclei	Cells around the vulva
WT	31.9 ± 0.1 (N= 20)	16.0 ± 0.0 (N= 25)
fzr-1(ku298); fzr-1^{lox}; Phlh-8::CRE	32.4 ± 0.2 (N= 18)	16.1 ± 0.1 (N= 15)
lin-35(n745); read-out^{lox}; Phlh-8::CRE	32.6 ± 0.1 (N= 34)	16.1 ± 0.1 (N= 19)
lin-35(n745); fzr-1(ku298); fzr-1^{lox}; Phlh-8::CRE	32.2 ± 0.2 (N= 22)	16.1 ± 0.1 (N= 14)
cki-1(RNAi)		20.8 ± 1.3 (N= 13)
fzr-1(ku298); fzr-1^{lox}; Phlh-8::CRE; cki-1(RNAi)		23.4 ± 1.7 (N= 27)
lin-35(n745); read-out^{lox}; Phlh-8::CRE; cki-1(RNAi)		32.4 ± 3.8 (N= 11)
lin-35(n745); fzr-1(ku298); fzr-1^{lox}; Phlh-8::CRE; cki-1(RNAi)		41.2 ± 5.9 (N= 15)
lin-23(RNAi)		19.5 ± 1.0 (N= 13)
fzr-1(ku298); fzr-1^{lox}; Phlh-8::CRE; lin-23(RNAi)		18.3 ± 0.6 (N= 15)
lin-35(n745); read-out^{lox}; Phlh-8::CRE; lin-23(RNAi)		27.2 ± 1.8 (N= 14)
lin-35(n745); fzr-1(ku298); fzr-1^{lox}; Phlh-8::CRE; lin-23(RNAi)		33.2 ± 2.1 (N=23)
cul-1(RNAi)		19.9 ± 1.4 (N= 11)
fzr-1(ku298); fzr-1^{lox}; Phlh-8::CRE; cul-1(RNAi)		19.7 ± 1.3 (N= 13)
lin-35(n745); read-out^{lox}; Phlh-8::CRE; cul-1(RNAi)		28.6 ± 1.6 (N= 18)
lin-35(n745); fzr-1(ku298); fzr-1^{lox}; Phlh-8::CRE; cul-1(RNAi)		28.1 ± 1.5 (N= 25)
swsn-5(RNAi)		21.9 ± 1.2 (N= 16)
fzr-1(ku298); fzr-1^{lox};Phlh-8::CRE; swsn-5(RNAi)		27.7 ± 2.3 (N= 17)
lin-35(n745); read-out^{lox}; Phlh-8::CRE; swsn-5(RNAi)		22.6 ± 1.2 (N= 14)
lin-35(n745); fzr-1(ku298); fzr-1^{lox}; Phlh-8::CRE; swsn-5(RNAi)		30.0 ± 2.0 (N= 21)
swsn-2.1(RNAi)		17.0 ± 0.3 (N= 18)
fzr-1(ku298); fzr-1^{lox}; Phlh-8::CRE; swsn-2.1(RNAi)		18.6 ± 0.6 (N= 14)
lin-35(n745); read-out^{lox}; Phlh-8::CRE; swsn-2.1(RNAi)		18.3 ± 0.6 (N= 29)
lin-35(n745); fzr-1(ku298); fzr-1^{lox}; Phlh-8::CRE; swsn-2.1(RNAi)		21.4 ± 1.0 (N= 33)
swsn-1(os22); swsn-1^{lox}; Phlh-8::CRE		19.3 ± 0.4 (N= 53)
fzr-1(ku298); fzr-1^{lox}; swsn-1(os22); swsn-1^{lox}; Phlh-8::CRE		26.1 ± 0.7 (N= 48)
lin-35(n745); swsn-1(os22); swsn-1^{lox}; Phlh-8::CRE		21.9 ± 1.0 (N= 32)
lin-35(n745); fzr-1(ku298); fzr-1^{lox}; swsn-1(os22); swsn-1^{lox}; Phlh-8::CRE		28.8 ± 1.6 (N= 19)
swsn-1(os22); swsn-1^{lox}; Phlh-8::CRE; cki-1(RNAi)		25.6 ± 0.8 (N= 36)

Supplementary Table 4 continued		
Genotype	**Mesoblast descendents (eGFP (+) mean ± s.e.m**	
	Total number of nuclei	Cells around de vulva
fzr-1(ku298); fzr-1^{lox}; swsn-1(os22); swsn-1^{lox}; Phlh-8::CRE; cki-1(RNAi)		32.0 ± 1.5 (N= 55)
lin-35(n745); swsn-1(os22); swsn-1^{lox}; Phlh-8::CRE; cki-1(RNAi)	153.2 ± 25.9 (N= 10)	
lin-35(n745); fzr-1(ku298); fzr-1^{lox};swsn-1(os22); swsn-1^{lox}; Phlh-8::CRE; cki-1(RNAi)	154.0 ± 26.1 (N= 14)	
swsn-1(os22); swsn-1^{lox}; Phlh-8::CRE; lin-23(RNAi)	100.4 ± 6.1 (N= 17)	
fzr-1(ku298); fzr-1^{lox}; swsn-1(os22); swsn-1^{lox}; Phlh-8::CRE; lin-23(RNAi)	176.3 ± 17.0 (N= 15)	
hlh-1(cc561): Phlh-8::CRE		31.9 ± 0.6 (N= 26)
hlh-1(cc561): swsn-1(os22); swsn-1^{lox}; Phlh-8::CRE		34.1 ± 1.0 (N= 20)
hlh-1(cc561): Phlh-8::CRE; lin-23 (RNAi)	115.4 ± 12.0 (N= 10)	
hlh-1(cc561): swsn-1(os22); swsn-1^{lox}; Phlh-8::CRE; lin-23(RNAi)	202.8 ± 22.8 (N= 9)	
swsn-1(os22); swsn-1^{lox}; Phlh-8::CRE; mes-2(RNAi)		16.5 ± 0.4 (N= 20)
swsn-1(os22); swsn-1^{lox}; Phlh-8::CRE; mes-3(RNAi)		17.9 ± 0.5 (N= 22)
fzr-1(ku298); fzr-1^{lox}; swsn-1(os22); swsn-1^{lox}; Phlh-8::CRE; mes-2(RNAi)		20.4 ± 0.8 (N= 27)
fzr-1(ku298); fzr-1^{lox}; swsn-1(os22); swsn-1^{lox}; Phlh-8::CRE; mes-3(RNAi)		21.2 ± 0.7 (N= 40)

Supplementary Table 5. List of genes tested in the RNAi screen to identify regulators of cell cycle exit in the mesoblast lineage

			extra cells	
Genes tested	**Gene**	**Human homolog**	**wt**	***lin-35; fzr-1***
Proliferation Inhibitors				
lin-23	K10B2.1	β-TrCP	+	+
cul-1	D2045.6	Cullin 1	+	+
cul-4	F45E12.3	Cullin 4	-	-
gmn-1	Y75B8a.17	Geminin	-	+
cdc-14	C17G10.4	Cdc14	-	-
cki-1	T05A6.1	Cip/Kip p27Kip1	+	+
daf-18	T07A9.6	PTEN	-	-
daf-16	RI3H8.1	FOXO	-	-
dcr-1	K12H4.8	Dicer	-	-
alg-1	F48F7.1	Argonaute orthologue	-	-

Supplementary Table 5. Continued

			extra cells	
Genes tested	**Gene**	**Human homolog**	**wt**	***lin-35; fzr-1***
Differentiation factors				
hlh-8	C02B8.4	TWIST	-	-
hlh-1	B0304.1	MyoD	-	+
TGF-β signaling				
lon-3	Zk836.1	Collagen	-	-
lon-1	F48E8.1	member of CRISP family	-	-
Chromatin silencing				
sop-2	C50E10.4	related to PcG proteins	-	-
set-1	T26A5.7	histone lysine N methyl transferase	-	-
hda-1	C53A5.3	histone deacetylase	-	-
met-2	R05D3.11	SETDB1	-	-
set-25	Y43F4B.3	H3 lysine-9 methyl transferase	-	-
hpl-1	K08h2.6	heterochromatin protein 1	-	-
hpl-2	K01G5.2	heterochromatin protein 2	-	-
rbr-2	ZK593.4	JARID1A	-	-
lin-53	K07A1.12	RbAp48	-	-
Polycomb				
mes-2	R06A4.7	Enhancer of Zeste	-	-
mes-3	F54C1.3	Part of Polycomb complex	-	-
mes-6	C09G4.5	Extra sex comb	-	-
SWI/SNF				
swsn-1	Y113G7b.23	BAF155, BAF170	+	+
swsn-5	R07E5.3	hSNF5/INI1	+	+
swsn-2.1	Zk1128.5	BAF60	+	+
swsn-2.2	C18E3.2	BAF60	-	-
pbrm-1	C26C6.1	BAF180	-	-
swsn-7	C08B11.3	BAF200	-	-
swsn-9	C01H6.7	BRD7	-	-

Supplementary Table 6. List of predicted *C. elegans* SWI/SNF subunits with their function and human homologues

C. elegans gene	Alternative name	Sequence name	Human homologue	Function
swsn-4	*psa-4*	F01G4.1	BRG/BRM	ATPase core subunit
swsn-1	*psa-1*	Y113G7b.23	BAF155/SMARCC1 BAF170/SMARCC2	core subunit
swsn-5	*snfc-5*	R07E5.3	hSNF5/INI1/SMRACB1	core subunit
swsn-2.1	*ham-3; tag-246*	ZK1128.5	BAF60/SMARCD3	accessory subunit
swsn-2.2		C18E3.2	BAF60/SMARCD3	accessory subunit
swsn-3		Y71H2AM.17	BAF57/SMARCE1	accessory subunit
swsn-6	*psa-13*	ZK616.4	BAF53	accessory subunit
swsn-8	*psa-10, Iss-4, let-526*	C01G8.9	hOSA/BAF250/ARID1A	signature subunit
pbrm-1	*tag-185*	C26C6.1	BAF180/PBRM	signature subunit
swsn-7		C08B11.3	BAF200/ARID2	signature subunit
swsn-9	*tag-298*	C01H6.7	BRD7	signature subunit

Supplementary Table 7. Overview of Strains Used in this Study, Related to Experimental Procedures

Strain number	Genotype
SV1361	*unc-119(ed3) III; heIs105 [rps-27::loxP::nls::mCherry::let-858UTR::lox::nls::gfp::let-858UTR] IV*
SV1438	*heSi141 [shorthlh-8::flag::CRE::tbb-2] X*
SV1439	*heSi142 [elt-2::flag::CRE::tbb-2] X*
SV1440	*unc-119(ed3) III;heIs105 [rps-27::loxP::nls::mCherry::let-858UTR::loxP::nls::gfp::let-858UTR] IV; heSi141 [shorthlh-8::flag::CRE::tbb-2] X*
SV1441	*lin-35(n745) I; fzr-1(ku298)II; unc-119(ed3) III; heSi143 [rps-27::loxP::mCherry::let-858::pfzr-1::fzr-1::fzr-1UTR::loxP::GFP::let-858UTR] IV; heSi141 [shorthlh-8::flag::CRE::tbb-2] X*
SV1445	*lin-35(n745); unc-119(ed3) III; heIs105 [rps-27::loxP::nls::mCherry::let-858UTR::loxP::nls::gfp::let-858UTR] IV; heSi141 [shorthlh-8::CRE] X*
SV1446	*unc-119(ed3) III;heIs105 [rps-27::loxP::nls::mCherry::let-858::UTR::loxP::nls::gfp::let-858UTR] IV; heSi142 [elt-2::CRE]X*
SV1447	*fzr-1(ku298)II; unc-119(ed3) III; heSi143 [rps-27::loxP::mCherry::let-858::pfzr-1::fzr-1::utrfzr-1 loxP::GFP::let-858UTR] IV; heSi142 [elt-2::CRE]X*
SV1448	*fzr-1(ku298)II; unc-119(ed3) III; heSi143 [rps-27::loxP::mCherry::let-858::pfzr-1::fzr-1::fzr-1UTR::loxP::GFP::let-858UTR] IV; heSi141 [hlh-8::CRE]X*
SV1570	*lin-35(n745); unc-119(ed3) III; heIs105 [rps-27::loxP::nls::mCherry::let-858UTR::loxP::nls::gfp::let-858UTR] IV; heSi142 [elt-2::CRE]x*
SV1571	*lin-35(n745) I; fzr-1(ku298)II; unc-119(ed3) III; heSi143 [rps-27::loxP::mCherry::let-858::pfzr-1::fzr-1::fzr-1UTR::loxP::GFP::let-858UTR] IV; heSi142 [elt-2::CRE] X*

Supplementary Table 7. Continued	
Strain number	**Genotype**
SV1572	*fzr-1(ku298)II; unc-119(ed3) III; heIs105 [rps-27::loxP::nls::mCherry::let-858UTR::loxP::nls::gfp::let-858UTR] IV; heSi141 [hlh8::CRE]X*
SV1573	*fzr-1(ku298)II; unc-119(ed3) III; heIs105 [rps-27::loxP::nls::mCherry::let-858UTR::loxP::nls::gfp::let-858UTR] IV; heSi142 [elt-2::CRE]X*
SV1578	*unc-119(ed3) III; heIs105 [rps-27::loxP::nls::mCherry::let-858UTR::loxP::nls::gfp::let-858UTR] IV; swsn-1(os22); heSi164 [rps-27::loxN::nls::mCherry::let-858UTR::Pswsn-1::swsn-1::unc-54UTR::loxN::nls::gfp::let-858UTR] V*
SV1579	*fzr-1(ku298);unc-119(ed3) III ; heSi143 [rps-27::loxP::mCherry::let-858::pfzr-1::fzr-1::fzr-1UTR::loxP::GFP::let-858UTR] IV; swsn-1(os22); heSi164 [rps-27::loxN::nls::mCherry::let-858UTR::Pswsn-1::swsn-1::unc-54UTR::loxN::nls::gfp::let-858UTR] V*
SV1580	*lin-35(n745); unc-119(ed3) III; heIs105 [rps-27::loxP::nls::mCherry::let-858UTR::loxP::nls::gfp::let-858UTR] IV; swsn-1(os22); heSi164 [rps-27::loxN::nls::mCherry::let-858UTR::Pswsn-1::swsn-1::unc-54UTR::loxN::nls::gfp::let-858UTR] V*
SV1581	*lin-35(n745); fzr-1(ku298);unc-119(ed3) III ; heSi143 [rps-27::loxP::mCherry::let-858::pfzr-1::fzr-1::fzr-1UTR::loxP::GFP::let-858UTR] IV; swsn-1(os22); heSi164 [rps-27::loxN::nls::mCherry::let-858UTR::Pswsn-1::swsn-1::unc-54UTR::loxN::nls::gfp::let-858UTR] V*
SV1595	*unc-119 (edIII); heIs105 [rps-27::loxP::nls::mCherry::let-858UTR::loxP::nls::gfp::let-858UTR] IV; swsn-1 (os22); heSi164 [rps-27::loxN::nls::mCherry::let-858UTR::Pswsn-1::swsn-1::unc-54UTR::loxN::nls::gfp::let-858UTR] V; heEx508 [Pcye-1::tagBFP]*
SV1601	*hlh-1(cc561); unc-119 (ed3) III; heIs105 [rps-27::loxP::nls::mCherry::let-858UTR::loxP::nls::gfp::let-858UTR] IV; heSi141 [shorthlh-8::flag::CRE::tbb-2] X*
SV1602	*hlh-1(cc561); unc-119(ed3) III; heIs105 [rps-27::loxP::nls::mCherry::let-858UTR::loxP::nls::gfp::let-858UTR] IV; swsn-1(os22); heSi164 [rps-27::loxN::nls::mCherry::let-858UTR::Pswsn-1::swsn-1::unc-54UTR::loxN::nls::gfp::let-858UTR] V; heSi141 [shorthlh-8::flag::CRE::tbb-2] X*
SV1603	*unc-119 (ed3) III;heIs105 [rps-27::loxP::nls::mCherry::let-858UTR::loxP::nls::gfp::let-858UTR] IV; heSi141 [shorthlh-8::flag::CRE::tbb-2] X; heEx509 [Phlh-8::tagBFP]*
SV1604	*unc-119(ed3) III; heIs105 [rps-27::loxP::nls::mCherry::let-858UTR::loxP::nls::gfp::let-858UTR] IV; swsn-1(os22); heSi164 [rps-27::loxN::nls::mCherry::let-858UTR::Pswsn-1::swsn-1::unc-54UTR::loxN::nls::gfp::let-858UTR]; heSi141 [shorthlh-8::flag::CRE::tbb-2] X; heEx509 [Phlh-8::tagBFP]*
SV1631	*heEx513 [rps-27::loxN::nls::mCherry::let-858UTR::loxN::nls::gfp::let-858UTR; elt-2::CRE; lin-48::tdTomato]*
SV1633	*heEx515 [rps-27::lox2272::nls::mCherry::let-858UTR::lox2272::nls::tagBFP::let-858UTR; elt-2::CRE; lin-48::tdTomato]*

Chapter 7

CRE-lox-mediated inducible expression and a split-CRE system in *C. elegans*

Suzan Ruijtenberg, Lotte van Rijnberk*, Sanne Boersma* & Sander van den Heuvel

* these authors contributed equally to the work

Manuscript in preparation for publication

Developmental Biology, Faculty of Sciences, Department of Biology, Utrecht University, Padualaan 8, 3584 CH Utrecht, The Netherlands.

Abstract

Temporal and tissue-specific control of gene expression provide powerful strategies to study gene function in multi-cellular organisms. CRE-lox-mediated DNA recombination has been widely used to induce or inactivate gene expression in a specific subset of cells. Here we describe the development and characterization of a CRE-lox mediated cell-type specific gene expression system for *C. elegans* and demonstrate permanent induction of gene expression in a tissue specific manner. In order to further increase the cell-type specificity of the system and to combine spatial resolution with temporal control we created a *C. elegans* version of the split-CRE system. In the split-CRE system, the CRE recombinase is divided into two inactive protein fragments that can each be expressed under the control of a tissue- or temporal specific promoter. Only in those cells where expression patterns of the two promoters overlap, CRE activity will be reconstituted and recombination induced. Using this system we were able to catalyze DNA recombination in specific cells at a defined moment during development, thereby introducing a second dimension to the cell-type specific control of gene expression.

Introduction

Conditional knockouts and inducible expression of genes of interest provide powerful approaches to study cell-type specific gene function in multi-cellular organisms. One of the methods to control gene expression in a spatio-temporal manner makes use of site-specific CRE-lox-mediated recombination. CRE-lox-mediated recombination depends on the binding of the CRE protein to two 34 bp lox sites flanking the target DNA. Depending on the orientation of the lox sites, binding of CRE results in either excision or inversion of the DNA between the lox sites. Excision occurs when both lox sites are positioned in the same orientation, and leaves a single lox site behind.

Since the description of the CRE-lox system in eukaryotic cells in 1987, it has been adapted and used in a wide variety of organisms ranging from plants to mice (Sauer, 1987; Sauer and Henderson, 1988). The first description of CRE-lox-mediated recombination in *C. elegans* stems from 2000 (Hoier *et al.*, 2000). However, the number of studies that have since reported use of the CRE-lox system has remained limited in *C. elegans*. Efficient recombination and gene excision requires use of single copy transgenes, which remained challenging for many years. With the development of methods that allow single copy insertion into the genome, including MosSCI, TALENs and CRISPR/Cas9-based approaches, conditional gene manipulation by CRE-lox-mediated recombination has become more feasible (Frøkjaer-Jensen *et al.*, 2008; Wood *et al.*, 2011; Friedland *et al.*, 2013; Waaijers *et al.*, 2013). Indeed, we and others have recently described the development and systemic use of CRE-lox-mediated recombination to generate conditional knockouts in *C. elegans* (Chapter 6 in this thesis and Hubbard, 2014; Kage-Nakadai *et al.,* 2014).

Here we further expand the possibilities and opportunities of CRE-lox-mediated recombination in *C. elegans*. We adapted our knockout system to create a cell-type specific inducible expression system, as well as a so called split-CRE system (Jullien *et al.*, 2003; Hirrlinger *et al.*, 2009; Rodrigues *et al.*, 2012). The split-CRE system is based on the separation of the CRE recombinase in an N-terminal and C-terminal fragment, both expressed under their own regulatory sequences. CRE activity will be reconstituted and recombination induced only at the intersection of the expression patterns of both fragments. Since CRE expression becomes dependent on simultaneous activity of two promoters, higher cell-type specificity can be achieved and spatial and temporal specificity can be combined.

Results and discussion

Construct design for cell-type specific inducible gene expression

To induce cell-type specific gene expression, we adapted our earlier described CRE-lox-based recombination and lineage tracing system (Figure 1A) (Chapter 6, this thesis). We designed a general recombination cassette that contains the ubiquitously active *eft-3* promoter to drive the expression of mCherry (Figure 1B). mCherry is followed by the *let-858*

3'UTR, previously described to function as a transcriptional terminator preventing the expression of downstream sequences (Davis *et al.*, 2008). mCherry and the *let-858* 3'UTR are flanked by loxP sites and followed by the coding sequence of a gene of interest (e.g. *let-60,* as described below; Figure 1B). Tissue-specific expression of CRE triggers the removal of mCherry and the *let-858* 3'UTR and places the *eft-3* promoter adjacent to the coding sequence of the gene of interest. This results in transgene expression in tissues of interest and can be visualized by the loss of mCherry. One of the main advantages of this CRE-lox-mediated induction of gene expression is the permanent and stable induction of transgenes, in contrast to promoter driven transgenes which may only be transiently expressed.

Vulva specific overexpression of Ras *let-60(gf)*

As a proof of principle, we aimed to specifically induce a gain-of-function mutation of *let-60* Ras in the vulval lineage. Normal induction of vulva formation depends on activation of the Ras pathway, and gain-of-function (gf) mutant alleles of *let-60* Ras induce the formation of multiple vulva (Muv phenotype) (Beitel *et al.*, 1990; Han and Sternberg, 1990). We reasoned that vulva specific and permanent induction of *let-60(gf)* expression would likewise result in a Muv phenotype.

To allow inducible expression, we placed the *let-60(gf)* sequence downstream of mCherry and *let-858* 3'UTR to generate *Peft-3::mCherry::let-858-3'UTR^{lox}::let-60(gf)* (referred to as the *let-60(gf)^{lox}* construct). CRE expression from the *lin-31* FOXB2 promoter was used to induce vulva specific recombination. As a control, we combined *Plin-31::CRE* expression with our previously described recombination reporter (*read-out^{lox}*) (Figure 1A) (Chapter 6, this thesis). In short, this read-out construct contains a ubiquitously active *rps-27* promoter, which drives the expression of mCherry. mCherry is flanked by two loxP sites and followed by GFP. Upon recombination, mCherry will be excised and GFP will be expressed in all subsequent cells of the lineage. Indeed, *Plin-31::CRE* catalyzes recombination in vulval precursor cells as visualized by the formation of a GFP positive vulva (Figure 1C). As a second control, we injected the inducible *let-60(gf)* construct into the *read-out^{lox}* containing line in the absence of *Plin-31::CRE*. As expected, no recombination or Muv phenotype was observed (Table 1). In contrast, induction of *let-60(gf)* in the *read-out^{lox}; Plin-31::CRE* line resulted in a Muv phenotype in 28% of the transgenic progeny and 65 % of the viable, transgenic progeny (Figure 1D, F, Table 1). These results indicate that CRE-lox mediated recombination can be used to permanently induce the expression of a gene of interest in a cell-type specific manner in *C. elegans*.

Together with the induction of a Muv phenotype, an unexpected lethal blister phenotype and larval lethality were observed (Table 1). Analysis of GFP expression showed that expression of *Plin-31::CRE* not only induced recombination in the vulval precursor cells, but also in one or more seam cells in almost half of the animals (20/42). Since this most likely causes *let-60(gf)* expression in these seam cells, this may be the explanation for the observed blister phenotype and lethality. Indeed, when we injected the *let-60(gf)^{lox}* construct into a line in which CRE is expressed under the control of a seam cell specific promoter,

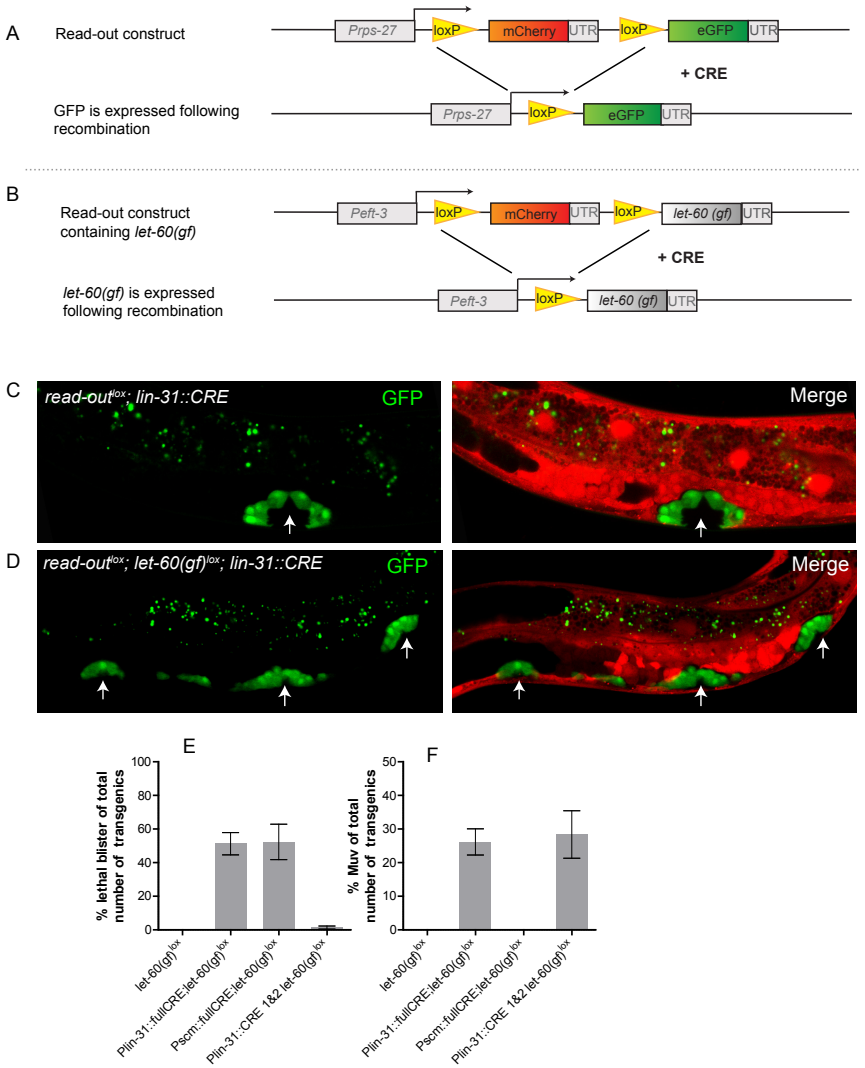

Figure 1. Cell-type specific inducible expression of *let-60(gf)* Ras. (A) Schematic overview of the recombination reporter (*read-out*^{lox}), which allows the visualization of CRE-mediated recombination. (B) Schematic overview of the CRE-lox-mediated induction of *let-60(gf)*. (C) Representative fluorescence microscopy images of *Plin-31::CRE*-mediated recombination in vulval cells, as visualized by a switch from mCherry to GFP expression. (D) Fluorescence microscopy images of *Plin-31::CRE*-mediated recombination in the presence of the *let-60(gf)*^{lox} construct, resulting in the formation of multiple GFP positive vulva. Arrows indicate examples of cells in which recombination has occurred. Scale bar indicates 20 μm. (E, F) Percentage lethal blister (E) and Multivulva (F) of total transgenic animals observed in the indicated genotypes. Error bars indicate s.e.m. See Table 1.

Pscm::CRE, we observed a lethal blister phenotype in more than 50% of the F1 animals (Table 1, Figure 1E). These observations highlight the need for methods that allow more spatially restricted and temporally controlled CRE expression. One such method is the split-CRE method, in which the CRE recombinase is reconstituted from two partial polypeptides (Jullien *et al.*, 2003; Hirrlinger *et al.*, 2009; Rodrigues *et al.*, 2012). By expressing these polypeptides from different promoters, CRE function can be restricted to a specific cell type and/or developmental time.

Table 1. Overview of the observed phenotypes upon induced expression of *let-60(gf)^{lox}*.

	Total number F1			% of transgenic animals			
	# of P0	Mean # of F1	Embryonic lethal	Larval lethal	Blister lethal	Multi vulva	Wild type
N2	11	224,7	0,7%	-	-	-	-
read-out^{lox}; Plin-31::CRE	5	200,8	0,7%	-	-	-	-
read-out^{lox}; let-60(gf)^{lox}(ex)	11	191,5	2,1%	0,1%	0%	0%	99,9%
read-out^{lox}; Plin-31::CRE; let-60(gf)^{lox}(ex)	10	139,4	5,0%	10,3%	47,1%	27,9% (65,5%)	14,7% (34,5%)
Pscm::CRE ; let-60(gf) ^{lox} (ex)	8	180,2	3,82%	2,8%	52,4%	0 (0%)	44,9% (100%)
Plin-31::CRE part 1 & 2 let-60(gf) ^{lox}(ex)	9	171,1	2,53%	0,7%	1,4%	28,4% (33,3%)	69,5% (66,7%)

The percentage embryonic lethality is defined as the number of dead embryos, divided by the total number of progeny of the injected P0. The percentage of Muv, larval lethal, lethal blister and wild-type is determined as the number of F1 animals with the indicated phenotype divided by the total number of transgenic F1 and is therefore not displayed for the non-injected animals. The numbers in brackets indicate the percentage of animals with the indicated phenotype divided by the number of viable F1 progeny. Injected constructs are indicated in blue.

Creation of *C. elegans* split-CRE constructs.

As shown above, CRE-mediated recombination can be used in *C. elegans* to inactivate or activate genes of interest in a specific cell type. The spatial specificity of recombination depended in these experiments on the promoters available to drive CRE expression. While for some tissues highly specific promoters are available, in many other cases the expression pattern of a single promoter is insufficient to define a distinct cell type. Moreover, with the previously described system it is impossible to independently control spatial and temporal specificity, since CRE expression is determined either by a cell type- or temporal (heat shock)-specific promoter. To increase the specificity of the CRE-lox recombination system in *C. elegans,* we developed a CRE-based complementation, or split-CRE system as previously reported for mice and zebrafish (Hirrlinger *et al.*, 2009; Rodrigues *et al.*, 2012). In the split-CRE system, the CRE recombinase is expressed as two separate protein fragments which can functionally complement each other. Only at the intersection of the expression patterns of both fragments, CRE activity will be reconstituted and recombination induced. Based on previous work, the CRE coding region was divided in two parts. The N-terminal

(part 1) contained amino acids 19-59, and the C-terminal (part 2) contained amino acids 60-343. To promote association of the two CRE parts *in vivo*, a coiled coil GCN4 dimerization domain was fused to the N-terminus of both Part 1 and Part 2 via a flexible linker (Figure 2A) (Jullien *et al.*, 2003; Hirrlinger *et al.*, 2009). The first 18 amino acids of CRE can be missed and were excluded from part 1 to facilitate interaction between the dimerization domains (Jullien *et al.*, 2003). As for the full length CRE described above, the DNA sequences for each part were codon optimized for use in *C. elegans* and also encode a flag-tag and a *C. elegans* specific *egl-13* nuclear localization signal (NLS) (Figure 2A). The two constructed split-CRE protein fragments were expressed under the control of a variety of promoters, including an inducible heat-shock promoter and several promoters with lineage specific activity (For an overview of all split-CRE constructs: Table 2).

Table 2. Overview of split-CRE constructs.

Promoter	Expression	Full lenght CRE	CRE part 1	CRE part 2
Phlh-8	mesoblast	yes	yes	yes
Pscm	seam cells	yes	yes	yes
Pmyo-3	body wall muscle cells	yes	yes	yes
Plin-31	vulva precursor cells	yes	yes	yes
Phsp-16.48	heat shock, multiple tissues	no	yes	yes
Phsp-16.41	heat shock, multiple tissues	yes	yes	yes
Pegl-17	multiple cell types	yes	yes	yes
Punc-86	neurons	yes	yes	yes

Split-CRE induced recombination in *C. elegans*: efficient recombination and higher levels of specificity

To examine the recombination activity of the split-CRE proteins, we analyzed their ability to induce an integrated *read-out*^{lox} reporter to switch mCherry expression to eGFP expression (Figure 1A) (see above; Chapter 6). Without CRE expression, or when only one of the split-CRE parts was expressed, recombination-induced switching of the *read-out*^{lox} vector was not observed (Table 3). In contrast, simultaneous expression of both split-CRE parts from the same promoter induced recombination in general in more than 70% of the transgenic animals (Figure 2C, Table 3). Tissue specificity was largely as expected for the promoters used: *Pscm* (seam cells) (Figure 2B), *Plin-31* (Hypodermal Pn.p ventral cord precursor cells), *Phlh-8* (mesoblast lineage) or *Phsp-16.48* (heat shock, variety of tissues). Nearly all cells of the lineage switched from red to green in animals, where recombination was observed. For instance, approximately 90% of the seam cell became GFP positive in animals with *Pscm* controlled part 1 and part 2 CRE expression (Figure 2C, Table 3). These data demonstrate that a split-CRE-based approach can be used in *C. elegans* to efficiently induce CRE-lox-mediated recombination.

Table 3. Overview of the recombination efficiency upon expression of split-CRE Part 1 and 2.

		Split CRE part 2				
		Pscm	*Plin-31*	*Phlh-8*	*Phsp-16.48*	*No Part 2*
Split CRE part 1	*Pscm*	**94.2%** (90-100%)	na	na	**45,0%** (30-60%)	0,0%
	Plin-31	na	**75,3%** (66-80%)	na	**49,5** (20-88%)	0,0%
	Phlh-8	na	na	88.7% (71-100%)	68,1% (47-91%)	0,0%
	Phsp-16.48	**77.8%** (51-100%)	**52,6%** (42-61%)	**38,0%** (8-79%)	**100%** (100-100%)	0,0%
	No Part 1	0.0%	0.0%	0.0%	0.0%	0.0%

Efficiency is defined as the percentage of animals in which a CRE-mediated switch from mCherry to GFP is observed in the tissue of interest. For each combination, at least three lines and at least 10 animals per line were analyzed. The efficiency of the individual parts was quantified in 2 different lines, at least 15 animals per line were quantified. Mean efficiency is shown in bold, range is shown between brackets. na = Not applicable, since promoter combinations with known non-overlapping expression patterns were not tested.

Tissue specific expression of full length CRE (for clarity, indicated below as fullCRE) induced recombination in the expected cell type in nearly all animals. However, dependent on the promoter used, some additional cell types showed GFP expression as well. Remarkably, in the split-CRE-based approach, these unexpected recombination events occurred less frequently. For example, aspecific recombination in a few non-mesoblast derived body wall muscle cells was observed in 90 % of the *Phlh-8::fullCRE* expressing animals, this percentage dropped to 31 % for animals simultaneously expressing *Phlh-8:: CRE Part 1* and *Phlh-8::CRE Part 2*. Similarly, while 48 % of the *Plin-31::fullCRE* expressing animals showed recombination in seam cells, no GFP positive seam cells were observed in animals expressing *Plin-31::CRE Part 1* and *Plin-31::CRE Part* 2.

To further explore and take advantage of the increased recombination specificity, we expressed *let-60(gf)*^{lox} with *Plin-31::CRE Part 1* and *Plin-31::CRE Part* 2. The characterizations described above indicated a lethal blister phenotype associated with *let-60(gf)* expression resulting from noisy *Plin-31::CRE* activity in the seam cells or hypodermis. We reasoned that the increased recombination specificity of the *Plin-31* split-CRE combination might result in a Muv phenotype without the associated blister lethal phenotype. Indeed, the percentage of blistered lethal F1 animals dropped from 47% to 1% when *let-60(gf)*^{lox} and *Plin-31* split-CRE constructs were coinjected, compared to the combination with *Plin-31::fullCRE* (Table 1, Figure 1E, F). By contrast, the two CRE combinations resulted in a similar percentage of F1 Muv animals. We were never able to obtain stable transgenic lines from *Plin-31::fullCRE*; *let-60(gf)*^{lox} F1 animals. However, more than half of the singled *Plin-31::CRE Part1 Plin-31::CRE Part2; let-60(gf)*^{lox} animals gave rise to stable transgenic lines. In these lines, on average approximately 65% of the F2 animals was Muv, which closely resembles the percentage of recombination efficiency of *Plin-31::CRE Part1 Plin-31::CRE*

Part2 animals. Also animals that were non-Muv in the first generation gave rise to F2 animals with a Muv phenotype indicating that the phenotype is partially penetrant. These data demonstrate that, by expressing the CRE recombinase as two independent fragments, higher levels of specificity are obtained compared to the use of full CRE constructs. The explanation for this reduced background may be the compound probability of noisy transcription from two independent promoters.

Spatio-temporal control of CRE-lox-mediated recombination

In order to manipulate gene expression in a specific cell type and at a defined moment during development, we aimed to expresse one part of the CRE recombinase under the control of a cell-type specific promoter and the other part under the control of the heat-shock-dependent *hsp-16.48* promoter. We first tested heat-shock-dependent recombination in animals expressing *Phsp-16.48::CRE Part 1* together with *Phsp-16.48::CRE Part 2* in the presence of the *read-out*^{lox} recombination reporter. Heat-shock treatment for one hour at 34 °C resulted in recombination in 100% of the animals, with GFP positive cells in a wide variety of tissues, including the intestine, muscles, seam cells, the vulva, hypodermis and neurons. In contrast, in control animals not exposed to heat-shock, 3 out of 53 animals showed GFP expression in only a single cell. Thus, *Phsp-16.48::CRE Part 1-Phsp-16.48::CRE Part 2* transgenic animals show efficient heat-shock dependent recombination (Table 3).

Next, we tested the effect of combined expression of cell-type specific (*Pscm*, *Phlh-8* or *Plin-31*) driven CRE expression of CRE Part 1 with heat-shock driven expression of CRE Part 2 and *vice versa*. Animals were again heat-shocked for one hour at 34 °C and dependent on the specific combination, recombination efficiency was analyzed eight to ten hours after heat-shock. Indeed, all tested combinations showed recombination in the expected tissues at defined moments during development with an efficiency ranging from 38% (mesoblast) to 78% (seam cells) (Figure 2D; Table 3). We conclude that combining split-CRE expression from a cell-type specific promoter with expression from a heat-shock promoter allows temporal and tissue-specific control of recombination. Moreover, these experiments indicate that functional CRE activity can be achieved upon expression of *CRE Part 1-CRE Part 2*, even when co-expression of both parts coincides only transiently, as is most likely the case for all heat-shock combinations.

Using the combination of *Phsp-16.48::CRE Part 1* and *Pscm::CRE Part 2* we further characterized the efficiency and dynamics of spatio-temporal dependent induction of recombination. To determine the percentage of seam cells in which recombination occurred, animals were heat-shocked at 12 hours of development and GFP expression in seam cells was analyzed 12 hours later. In animals expressing *Pscm::CRE Part 1-Pscm::CRE Part 2*, approximately 90% of the seam cells were positive for GFP. Animals expressing *Phsp-16.48::CRE Part 1* and *Pscm::CRE Part 2* showed a lower percentage, with approximately 50-60% GFP-positive seam cells. The lower recombination efficiency in the latter combination may be explained by not completely overlapping expression from the *hsp-16.48* and *scm* promoters and is in agreement with our observation that heat-shock induced recombination only oc-

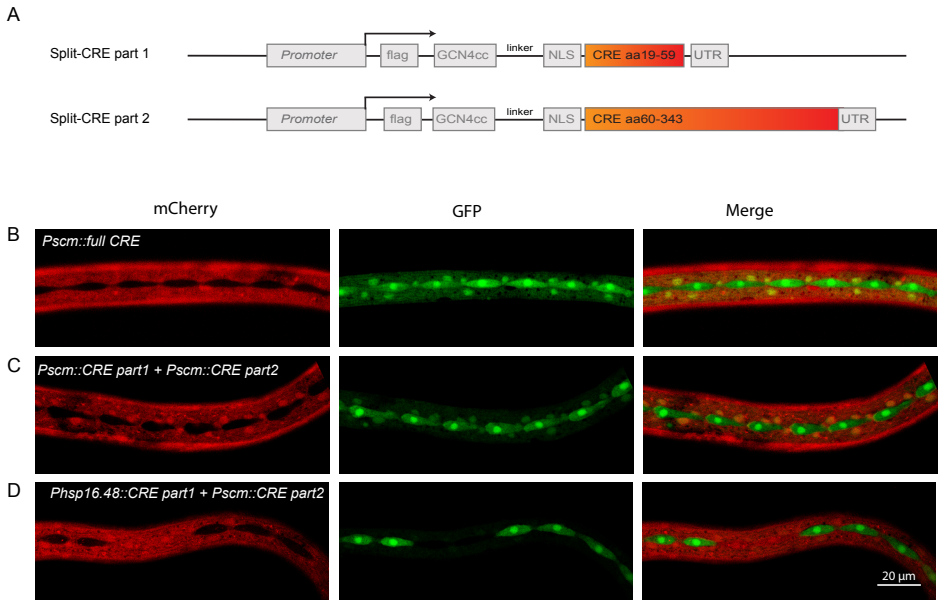

Figure 2. Description and characterization of the split-CRE system in *C. elegans*. (A) Overview of split-CRE fragments. CRE Part 1 (top) consists of amino acid 19-59, CRE Part 2 (bottom) consists of amino acid 60-343. Both parts are fused to a constitutively active coiled-coil interaction domain from yeast GCN4 (GCN4cc). Both parts are codon optimized for the use in *C. elegans*, and fused to a flag tag and *egl-13* NLS. (B-D) Representative fluorescence microscopy images illustrating *Pscm::fullCRE* (B), *Pscm::CRE Part 1* and *Pscm::CRE Part 2* (C) or heat-shocked *Phsp-16.48::CRE Part 1*- and *Pscm::CRE Part 2*- mediated (D) recombination of the read-out reporter. Scale bar indicates 20 µm.

curred in a subset of seam cells. GFP positive seam cells were mostly observed as pairs, indicating that the recombination occurred early after heat-shock.

In summary, CRE-lox-mediated recombination provides a powerful strategy to manipulate gene expression in a tissue- and temporal specific manner in *C. elegans*. In order to increase spatial specificity and to combine spatial and temporal control, we developed a split-CRE system. We divided the CRE recombinase into two fragments and expressed these fragments under the control of cell-type specific or heat-shock dependent promoters. Only in those cells that express both promoters at the same moment during development, functional CRE activity was reconstituted, resulting in CRE-mediated recombination. This split-CRE approach enables the labeling and manipulation of a distinct cell type, for which the expression pattern of a single promoter is insufficient. In addition, combining heat-shock driven and germline specific split CRE constructs may offer the possibility to generate germline clones in *C. elegans*. Finally, the split-CRE system substantially increases the recombination specificity, and in addition allows simultaneous temporal and spatial control of gene expression.

Materials and Methods

C. elegans culturing and transgenesis

C. elegans strains were cultured on NGM plates seeded with *E. coli* OP50 according to standard protocols. Strains were maintained at 20 °C, except for those strains that contained heat-shock promoter driven CRE constructs, which were maintained at 15 °C to prevent leakage from the heat-shock promoter. In order to quantify recombination efficiency at specific developmental time points, animals were synchronized by hypochlorite treatment, followed by hatching in M9 buffer. Animals were then allowed to develop for the appropriate amount of time. In order to induce expression from the *hsp-16.48* promoter, animals were heat-shocked for 1 hour at 34 °C, recovered for 30 min. at 15 °C, grown at 20 °C or 25 °C and analyzed 8 to 10 hours after heat-shock treatment (as indicated in the text). Transgenic lines were created as described previously (Mello *et al.*, 1991). To examine recombination activity of the split-CRE proteins both parts were injected at 20 ng/µl into the *read-out*^{lox} strain (SV1361) (Chapter 6). For each combination multiple transgenic lines were obtained and recombination efficiency was analyzed in at least three independent lines.

Phenotypic analysis upon induction of *let-60(gf)*^{lox}

To determine the phenotypes associated with the CRE-dependent induction of *let-60(gf)*^{lox}, L4 animals of the indicated genotypes (first column Table 1, black) were selected on day one and injected with the indicated constructs (first column Table 1, blue) and singled on day two. These P0 animals were transferred to new plates every 24 hours and the number of larvae and unhatched (dead) embryos was quantified 24 hours after removal of the parent. During the following four days the total number of transgenic animals as well as the number of larval lethal, blister lethal and multi-vulva animals was scored. Only P0 animals which gave rise to transgenic F1 animals were used for further analysis.

Molecular Cloning

To create the split CRE constructs, we replaced the CRE coding region in the previously described fullCRE constructs (Chapter 6) by either the N-terminal part (Part 1, a.a. 19-59) or the C-terminal part (Part 2, a.a. 60-343). The final constructs contained the *hlh-8* promoter, a GCN4 dimerization domain (AAGCAACTCGAGGATAAGGTCGAGGAGCTTCTCTCTAAGAACTACCACCTTGAGAACGAGGTCGCTCGTCTTAAGAAGCTTGTCGGAGAGCGT) a flexible linker (ATGTCCCGTCGTCGTAAGGCCAACCCAACCAAGCTCTCCGAGAACGCCAAGAAGCTCGCCAAGGAGG), a *C. elegans* specific *egl-13* NLS followed by the split CRE coding sequences codon optimized for the use in *C. elegans* (Hirrlinger *et al.*, 2009). The promoter was flanked by an N terminal AvrII site and a C-terminal PacI site which were used to replace the *hlh-8* promoter with other tissue- and temporal-specific promoters used in this study (Table S1).

To create the *Peft-3::loxP::mCherry::let-858-3'UTR::loxP::let-60(gf)::unc-54-3'UTR* construct we used GA cloning to replace the *rps-27* promoter with the *eft-3* promoter in the *read-out*^{lox} construct *(Prps-27::loxP::SV40nls::mCherry::let-858UTR::loxP::SV40nls::GFP::let-858UTR)* (Chapter 6). This *eft-3* promoter is flanked by an upstream BssHII and downstream AscI cloning site and followed by a *loxP* site. The GFP and the second *let-858 3'UTR* sequences in the read-out construct were replaced by the *let-60(gf)* and *unc-54 3'UTR* sequence using the unique Not1 site upstream of GFP and the AflII site downstream of the second *let-858 3'UTR* The *let-60(gf)* sequence was amplified from mutants containing the n1046 allele, in which bp 38 is changed from a G to A, resulting in a G to E change at amino acid 13 of *let-60*.

Chapter 8

Summary and Discussion

Suzan Ruijtenberg & Sander van den Heuvel

Developmental Biology, Faculty of Sciences, Department of Biology, Utrecht University,
Padualaan 8, 3584 CH Utrecht, The Netherlands.

Summary

During development, cells face the important decision whether to continue to proliferate, or to exit the cell division cycle and differentiate. Improved insight into the molecular mechanisms that arrest the cell cycle during terminal differentiation is important for our understanding of normal development, as well as for cancer research and regenerative medicine. The work described in this thesis aims to contribute to our understanding of cell cycle exit, the mechanisms that coordinate cell cycle arrest with differentiation, and the maintenance of a nonproliferative state in terminally differentiated cells (Figure 1).

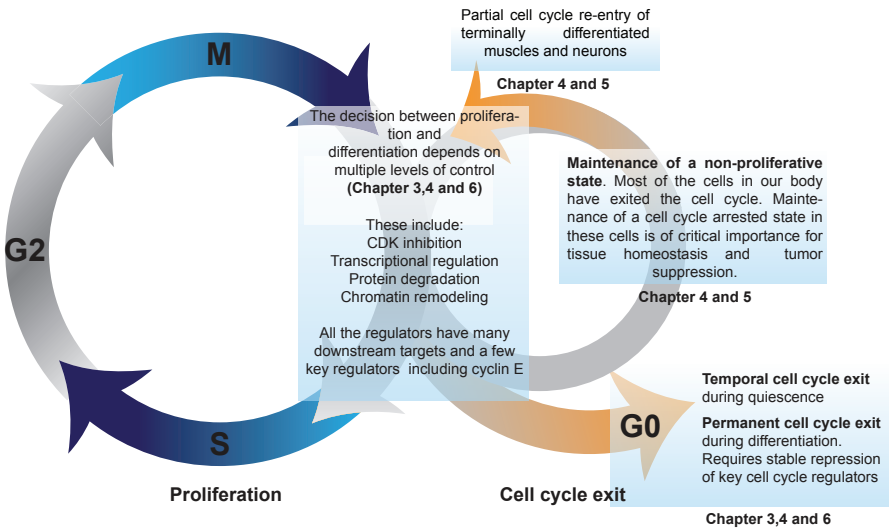

Figure 1. Overview of the different topics addressed in this thesis with regard to the different phases of the cell cycle.

The decision to arrest cell division and withdraw from the cell division cycle is made during the G1 phase of the cell cycle. Progression through G1 and the transition from G1 into S-phase is controlled by the combined activity of positive and negative regulators. Positive regulators include the G1 CDK-cyclin complexes CDK4/6-cyclin D and CDK2-cyclin E. **Chapter 3** describes the identification of the critical downstream targets of CDK4/6-cyclin D in *C. elegans*: LIN-35 Rb and FZR-1. We found that Rb-mediated transcriptional repression and APC/C^{FZR1}-mediated protein degradation act in parallel to inhibit G1/S progression, and that their phosphorylation by CDK4/6-cyclin D counteracts these inhibitory functions. Importantly, our data indicate that these mechanisms are conserved, as we also observed synergy between Rb and FZR-1 knockdown in bypassing the cell division arrest induced by the CDK4/6-specific inhibitor PD-0332991 in human breast cancer cells.

During development most cells eventually exit the cell cycle permanently to enter a

terminally differentiated and post-mitotic state. In **Chapter 4 and 5** we investigated the arrested state of muscle cells and neurons, and examined to what extent these terminally differentiated cells responded to cell cycle inducing signals. We found that overexpression of the G1 CDK-cyclins in *C. elegans* muscle cells triggered the expression of many cell division genes without interfering with the differentiation status **(Chapter 4)**. Tissue-specific transcriptional profiling and single molecule FISH experiments revealed that CDK-4/CYD-1 and CDK-2/CYE-1 induced a substantial and overlapping cell cycle-related set of genes, and in addition that CYD-1/CDK-4 influenced gene expression of large numbers of metabolism-related genes. In spite of this, CDK-cyclin expression did not induce complete muscle cell division and failed to induce some key cell cycle regulators, such as *cye-1*, *cdc-25.1*, and *cdk-2*. This indicates that in general cell cycle gene expression remains remarkably flexible in differentiated muscle cells, and that tight control of a few regulatory genes maintains a stable post-mitotic state.

In **Chapter 5**, we investigated whether G1 CDK-cyclin complexes execute similar effects in terminally differentiated *C. elegans* and rat-hippocampal neurons. Forced expression of CDK-4/CYD-1 and loss of the negative cell cycle regulator *fzr-1* in *C. elegans* neurons induced partial cell cycle re-entry. Importantly, we obtained similar results in rat-hippocampal neurons, indicating that mechanisms that maintain cell cycle arrest of terminally differentiated neurons may be conserved between *C. elegans* and mammals.

The transition from proliferating precursors to post-mitotic differentiated cells requires tight coordination between cell cycle exit and cellular differentiation. To study the mechanisms that coordinate cell cycle arrest with differentiation, we created a CRE-lox based recombination system for tissue-specific gene inactivation and lineage tracing in *C. elegans* **(Chapter 6)**. Combining cell-type specific knock-outs with RNAi of candidate genes revealed that exit from the cell division cycle is regulated by multiple, redundantly acting levels of control. While loss of either the SWI/SNF complex or G1/S regulators induced only limited defects, combined inactivation resulted in tumorous over-proliferation of muscle precursor cells. Further genetic analysis and single molecule FISH experiments indicated that the SWI/SNF complex acts together with the muscle specific transcription factor MyoD and regulates both the expression of genes involved in cell cycle control and cell differentiation. Understanding the role of the SWI/SNF complex in cell cycle exit during differentiation is of particular importance considering the frequent mutation of genes encoding SWI/SNF genes subunits in human cancer.

In **Chapter 7,** we describe additional and novel applications of the CRE-lox based recombination system as introduced in Chapter 6. This includes the generation of a cell-type specific inducible gene expression system and the development and characterization of a split-CRE system. In this system, the CRE recombinase is reconstituted from independently expressed N- and C-terminal protein fragments. By using the split-CRE system, increased specificity of recombination can be achieved and spatial and temporal control of gene expression can be obtained.

The final chapter **(Chapter 8)** discusses the results described in this thesis in relation to recent literature data.

Discussion

Proper development requires tight control of cell proliferation and differentiation. On the one hand, cells need to be formed in the right numbers, while on the other hand, cell division needs to stop at the correct moment during development. Exit from the cell division cycle can be either temporal and reversible, or permanent as cells become terminally differentiated. Below we will discuss our findings regarding the regulators involved in cell cycle exit, the mechanisms controlling temporal versus permanent withdrawal from the cell division cycle, and the coordination of permanent cell cycle exit with differentiation. In the last part we will discuss the use of *C. elegans* as a model system for cell cycle studies.

Cell cycle exit: multiple levels of control and a few key regulators

Progression through the cell cycle depends on the activation of CDK-cyclin complexes. As cells exit the cell cycle and stop proliferation, multiple levels of control counteract CDK-cyclin activity. This includes Rb-mediated transcriptional repression, activation of CDK inhibitors, and ubiquitin mediated protein degradation by the Anaphase Promoting Complex/Cyclosome (APC/C) and Skp1, Cullin, F-box factor (SCF) protein complexes. In addition, histone modification and chromatin remodeling complexes can inhibit CDK and cyclin expression by remodeling and modifying the epigenetic landscape at the promoters of these genes. As cells exit the cell cycle permanently, become post-mitotic and initiate differentiation, transcription factors (TF) likely act together with these chromatin remodeling complexes as well as G1 regulators to inhibit CDK activity and induce expression of cell-type specific genes. Taken together, exit from the cell division cycle is controlled at multiple levels and involves many regulators, with a critical role for SWI/SNF-dependent chromatin remodeling (Chapter 6).

Adding complexity, most of these regulators have many downstream targets. Rb binding to E2F for example prevents the expression of a substantial number of S-phase genes. Likewise, the APC/C and the SCF complex target multiple proteins for degradation. The SWI/SNF complex has even been found associated with thousands of genes, and is involved in gene expression control of many genes (Wilson and Roberts, 2011; Riedel *et al.*, 2013). Moreover, extensive redundancies and several positive and negative feedback mechanisms exist between these regulators, creating a highly complex network, to ensure that cells exit the cell cycle at the right time during development.

Most likely, not all regulators and downstream targets are equally important and perhaps only a few may critically determine whether cells withdraw from the cell cycle or continue to divide. Our data indicate that cyclin E might act as such a critical and tightly controlled key regulator in this network. Multi-level control over cyclin E expression was observed in single molecule mRNA detection experiments, where we found cyclin E mRNA levels to depend on at least two different mechanisms: Rb mediated transcriptional regulation and SWI/SNF dependent chromatin remodeling (Chapter 6). Cyclin E activity is also controlled by CDK inhibitors and by SCF-mediated protein degradation (Reed,

2003), indicating at least four regulatory mechanisms controlling cyclin E expression and activity.

Interestingly, overexpression of CDK-4/CYD-1 in terminally differentiated muscle cells resulted in the expression of hundreds of cell cycle genes, but failed to induce cyclin E. This finding indicates that additional safeguards control and inhibit cyclin E expression in these cells (Chapter 3). As cyclin E was shown to be repressed by the SWI/SNF complex in muscle precursor cells of the mesoblast lineage (Chapter 6), SWI/SNF may also act as a repressor of Cyclin E transcription in terminally differentiated muscle cells, despite the activation of CDK-4/CYD-1. The SWI/SNF complex however predominantly acts as a positive regulator of gene expression and counteracts PcG-mediated transcriptional repression. As such, PcG function could also be responsible for the silencing of cyclin E expression in differentiated muscle cells, and SWI/SNF activity may be required to induce cyclin E transcription in these cells. With the tools and insights obtained in our studies, we could now test these hypotheses by combining SWI/SNF or PcG disruption with CDK-4/CYD-1 expression in terminally differentiated muscle cells.

The combined activity of many different cell cycle regulators creates a highly robust network controlling cell cycle entry and exit. The need for such a complex network and the importance of all individual components has been questioned, since loss of some key components only has mild effects on cell cycle progression. In addition, much more simplified networks have been shown to be able to control cell division. Mice mutant for all D-type cyclins or CDK4 and CDK6 for example develop until late embryogenesis (Kozar *et al.*, 2004; Malumbres *et al.*, 2004). In yeast, expression of only a single CDK can be sufficient for ordered progression through the cell cycle (Coudreuse and Nurse, 2010). Likewise, we found in *C. elegans* that upon inhibition of three key regulators of G1 progression, Cyclin D, Rb, and FZR1, cell cycle entry and exit remained relatively normal (Chapter 3). In these triple mutant animals other cell cycle regulators must be capable of controlling ordered progression through and timely exit from the cell cycle. These controls are likely to converge on the regulation of CDK2-cyclin E kinase activity. However, multiple redundantly acting mechanisms probably act together during development in order to integrate external and internal signals under a wide variety of conditions, to accurately control the timing of cell cycle entry and exit, and to prevent uncontrolled and tumorous overproliferation. An interesting computational modeling study recently described the coordination between proliferation and differentiation during *C. elegans* vulva development (Weinstein *et al.*, 2015). This study predicted the formation of a highly connective network formed by cell cycle and differentiation regulators, which is in agreement with our experimental observations (Weinstein *et al.*, 2015). Similar to our findings in muscles, some general cell cycle regulators seem to be more important within the network for correct development than others (Weinstein *et al.*, 2015). Future experiments and computational modeling will be required to further unravel the interaction between the currently known players and to identify the critical nodes within these regulatory networks.

Temporal versus permanent cell cycle exit

During development, cells can either temporarily stop proliferation and enter a state called quiescence, or permanently exit the cell cycle during terminal differentiation. Quiescence has been mostly studied in cell culture and refers to a reversible state, which allows cell cycle re-entry in the presence of the correct proliferative signals. In contrast, post-mitotic terminally differentiated cells that have permanently exited the cell cycle are insensitive to these proliferative signals, even to those that promoted proliferation prior to differentiation (Buttitta and Edgar, 2007). While we did not address the upstream signals, our work reveals some of the differences between the mechanisms involved in temporal versus permanent withdrawal from the cell cycle. Both forms of arrest are characterized by the presence of hypophosphorylated pRb and high levels of CDK inhibitors (Buttitta and Edgar, 2007). Our studies in *C. elegans* emphasize the tissue-specific contribution of these G1 inhibitors and the involvement of additional levels of control (Chapter 3, 5, and 6).

In temporarily arrested quiescent cells, G1 inhibitors repress CDK-cyclin activity while maintaining the possibility of de-repression upon cell cycle re-entry. Permanent cell cycle exit in contrast, needs to coincide with a stable and permanent inhibition of CDK-cyclin activity, which requires substantially different mechanisms and regulators. To investigate the mechanisms underlying cell cycle exit during terminal differentiation, we studied the transition from proliferating precursors to terminally differentiated muscle cells in the mesoblast lineage. We found that, in contrast to temporal cell cycle exit, permanent cell cycle exit during muscle differentiation is dependent on the combined activity of the canonical G1 regulators, SWI/SNF remodeling complexes, and the transcription factor MyoD (Chapter 6). Also in other systems, SWI/SNF function has been associated with the transition from proliferating precursors to terminally differentiated cells. Exchange of SWI/SNF subunits may also trigger transitions; for instance, incorporation of the BAF60c subunit into the SWI/SNF complex at the expense of BAF60a/BAF60b is essential during MyoD- dependent muscle development (Simone *et al.*, 2004; Puri and Mercola, 2012). Similarly, in proliferating neuronal precursors, the SWI/SNF complex contains the BAF45a and BAF53a subunits, while BAF45b and c and BAF53b are incorporated as these precursors exit the cell cycle and become terminally differentiated neurons. Modulating the specific subunit composition effects both cell cycle exit and expression of neuron specific genes, highlighting the importance of SWI/SNF subunit composition during cell cycle exit and differentiation (Lessard *et al.*, 2007). Changing the chromatin structure might be particularly important during terminal differentiation as it enables permanent and stable repression of CDK-cyclin activity, thereby ensuring cell cycle arrest and maintenance of the nonproliferative state of differentiated cells.

While cell cycle withdrawal during terminal differentiation is in principle non-reversible, it appears to be more reversible in some cell-types than in others (Buttitta and Edgar, 2007). One of the examples often used to illustrate the possibility of cell cycle re-entry of terminally differentiated cells is the proliferation of horizontal interneurons in the retina upon inactivation of members of the Rb family (Ajioka *et al.*, 2007). However, other neuronal cell types do not re-enter the cell cycle under the same conditions. Analysis of the

chromatin structure revealed that horizontal interneurons have a more open chromatin structure compared to rods or Müller cells for example, which may explain why horizontal interneurons are more susceptible to activation of the cell cycle machinery (Davis and Dyer, 2010). So far, we can only speculate about why these cells have a more open chromatin structure and how this specific histone code is achieved. Interestingly, however, BAF53a, a subunit of the SWI/SNF complex mostly associated with proliferating precursors is also expressed in some of the differentiated retinal neurons. Similarly, the SWI/SNF ATPase subunit BRG1 is expressed in both proliferating precursors and in differentiated neurons of the retina (Davis and Dyer, 2010). These observations indicate that cell-type specific changes in the SWI/SNF subunit composition may contribute to cell-type specific changes in chromatin structure, resulting in differential probability to re-enter the cell cycle. Understanding why reversibility of cell cycle varies between different cell-types will contribute to our understanding of the mechanisms involved in this process and how quiescence differs from permanent cell cycle exit.

Coordinating cell cycle exit with differentiation

During the past decades many regulators required for cell division have been identified and investigated. Simultaneously, our knowledge of the molecules and mechanisms involved in fate determination and differentiation has significantly increased. Still, at the interface of these two fundamental processes our understanding is lacking. In particular, substantial progress can be made in understanding the inverse relationship between proliferation and differentiation. The temporal coupling between cell cycle exit and differentiation could in theory be explained by the activation of independent regulators that through positive and negative feedback mechanisms jointly regulate cell cycle exit and differentiation. Alternatively, a single regulator, able to directly control both cell cycle exit and differentiation, may be responsible for the tight coordination between the two processes. During development most likely a combination of these mechanisms is involved. The results described in Chapter 6 indeed provide evidence for tight coordination between the two processes, which is achieved by cell cycle regulators that affect differentiation, transcription factors that influence proliferation, and chromatin remodeling complexes that regulate both general cell cycle and cell-type specific genes.

Combined inactivation of the SCF subunit *lin-23* β-TrcP and the SWI/SNF chromatin remodeling complex resulted in substantial overproliferation in the mesoblast lineage in *C. elegans* (Chapter 6). The number of cells even further increased when this was combined with the inactivation of *fzr-1* FZR1. Along with the increase in proliferation capacity, loss of expression of differentiation markers, such as paramyosin and actin, was observed. Comparing the triple mutant (*fzr-1^{lox}; swsn-1^{lox}; lin-23(RNAi)*) to the double mutant (*swsn-1^{lox}; lin-23(RNAi)*), an increase in proliferation and concomitant loss of differentiation marker expression was observed, emphasizing the strict inverse relationship between proliferation and differentiation. Interestingly, the difference between the two conditions is the absence of the cell cycle inhibitor *fzr-1* FZR1, providing an example of how manipulation of the cell

cycle machinery influences differentiation. In the same study, we showed that loss of one of the key transcription factors involved in muscle differentiation, *hlh-1* MyoD, resulted in a defect in cell cycle exit and increased number of cells in the mesoblast lineage. This is in agreement with studies in other organisms and tissue culture systems where transcription factors, including MyoD, were shown to be involved in cell cycle control (Introduction in this thesis; Myster and Duronio, 2000). In addition, the detection of mRNA expression by smFISH showed that the SWI/SNF chromatin remodeling complex acts as a dual function regulator, simultaneously controlling genes associated with differentiation, for example the muscle specific gene *myo-3*, and cell cycle regulators including *cye-1*, *cdk-4*, *cki-1,* and *cdc-14* (Chapter 6). These results support that the coupling of cell cycle exit and differentiation involves the combined activity of cell cycle regulators, transcription factors and chromatin remodeling complexes. It is not unlikely that future work will identify even additional levels of regulation such as translational control (Kronja and Orr-Weaver, 2011), and microRNA regulation of mRNA degradation and accessibility (Bueno and Malumbres, 2011). All these mechanisms are likely to form part of the regulatory network responsible for the inverse regulation of proliferation and differentiation.

Paradoxically, work described in Chapters 4 and 5 indicates that cell cycle arrest and differentiation do not necessary need to coincide. At least a partial cell cycle program can be induced in differentiated muscle cells and neurons, without noticeably interfering with the differentiation state of these cells. However, so far we have not been able to induce mitosis and continued proliferation in terminally differentiated cells. While this might be the consequence of our approach which includes the continued expression of the induced G1 CDK-cyclins, the differentiated state of the cells may still prevent cell division. Similar experiments in which positive cell cycle regulators were overexpressed and negative regulators inhibited in terminally differentiated cells, have also been performed in other organisms and other cell-types (Chen and Segil, 1999; Roy *et al*., 2002; Wirth *et al*., 2004; Sage *et al*., 2005; Ajioka *et al*., 2007; Buttitta *et al*., 2007, 2010; Remus *et al*., 2009; Pajcini *et al*., 2010; Tian *et al*., 2015). In some cases this resulted in partial cell cycle re-entry, in other cases in full proliferation in combination with loss of differentiation. Only in a few cases proliferation of fully differentiated cells was observed (Sage *et al*., 2005; Ajioka *et al*., 2007; Pajcini *et al*., 2010). Understanding the differences between the cells in which mitosis can be induced and those that are insensitive to cell cycle promoting signals could further reveal the mechanisms that obstruct proliferation in differentiated cells.

One of the reasons to aim for proliferation of differentiated cells is to investigate whether this could be a valid approach for future regenerative therapies. During the past decades, substantial progress in the field of regenerative medicine has been made by creating new and functional tissues *in vitro,* starting from tissue specific stem cells or from induced pluripotent stem cells (Bellin *et al*., 2012; Mummery *et al*., 2012; Yui *et al*., 2012). However, tissue specific stem cells are not available for every tissue, and it remains challenging to generate differentiated cells from iPS cells in numbers sufficient for therapeutic applications. With our work, we aim to contribute to and explore the potential for regenerative therapies that start from terminally differentiated cells, as these cells will be available

in every tissue. While obviously of importance, re-activation of the cell cycle will involve activation of proto-oncogenes and the inhibition of tumor suppressors, with risks of uncontrolled and tumorous proliferation of these cells. Therefore, a subsequent challenge will be to temporarily induce proliferation, for example to create and expand a committed progenitor population, and to induce proliferation only until sufficient cell numbers are formed.

C. elegans as a model system for cell cycle studies: conserved mechanisms and clinical relevance

Most of the work described in this thesis has been performed by making use of the small nematode *C. elegans*. This final part of the discussion will restate our reasons for studying the mechanisms underlying cell cycle exit in *C. elegans*, and describe how data obtained in *C. elegans* can be translated to mammalian systems. *C. elegans* was introduced as a model system in the 1960s by Sydney Brenner and has since been an important model system for studies of a wide variety of biological processes including cell cycle progression. One of the most powerful features of *C. elegans* is its invariant cell lineage, which means that somatic cells enter and exit the cell cycle at fixed moments within the developmental program. This, together with the animal's transparency, efficient genetics, and the available cell cycle and tissue specific markers, allowed us to follow and investigate cell cycle progression with single cell resolution in a multicellular organism.

While these properties make *C. elegans* suitable for cell cycle studies, there are additional reasons for our choice to use *C. elegans* as a model system in our studies. Most of the cell cycle regulators that exist in gene families in higher eukaryotes are represented by single genes in *C. elegans*. As a consequence, regulatory networks are simpler, helping identification of gene functions and regulatory pathways. More importantly, by studying cell division in a developing animal, we may identify levels of regulation that are not important for single cell eukaryotes or cells in tissue culture. Indeed, we encountered several examples of tissue-specific requirements during cell cycle exit. For example, proper cell cycle exit in the intestine depends critically on the activity of LIN-35 Rb and FZR-1, while their function is not essential for cell cycle exit in the mesoblast lineage. *Vice versa*, SWI/SNF function is critical for cell cycle exit of mesoblast daughters, but not for intestinal cells (Chapter 6). Finally, while loss of FZR-1 was sufficient to induce S-phase marker expression in neurons, expression of this marker in muscle cells required simultaneous inhibition of FZR-1 and Rb (Chapter 3). These cell-type specific differences may be explained by variations in the cell cycle, the outcome of cell cycle exit (quiescence versus terminal differentiation), or cell-type specific differences in the interplay between cell cycle regulators and transcriptional regulators in a given cell-type. Understanding how these cell-type specific differences are achieved and how variations in regulatory networks control cell cycle in one versus the other tissue will expand our knowledge of regulatory pathways and routes for the correct timing of cell cycle progression.

The findings obtained in model organisms ultimately serve to both increase our

fundamental understanding of important biological processes such as development, and to better understand human disease. Therefore, it is necessary to critically evaluate and functionally validate findings acquired in *C. elegans* in a mammalian system. In this thesis two examples are described where we indeed validated the *C. elegans* results in a mammalian system. As a first example, we found functional conservation of the regulators involved in the maintenance of a post-mitotic state in neurons of *C. elegans* and the rat hippocampus (Chapter 5). In both type of neurons, overexpression of CDK4/6-cyclin D or loss of FZR1 resulted in partial cell cycle re-entry, making it likely that additional findings obtained in *C. elegans* can also be translated to a mammalian system.

Secondly, our finding regarding the role of Rb and FZR in G1 control appears to be relevant for our understanding of cell cycle regulation in human breast cancer cells. We found in *C. elegans* that loss of Rb and FZR could bypass the requirement for Cyclin D (Chapter 3). Human breast cancer cells, grown in the presence of the CDK4/6 inhibitor PD-033299 inhibitor stop proliferation (similar to CDK-4 inactivation in *C. elegans*). Simultaneous inhibition of Rb and FZR1 in these PD-0332991 treated cells bypassed the induced inhibition of proliferation and resulted in substantial proliferation. Importantly, we observed synergy between Rb and FZR1 knockdown in bypassing PD-0332991 arrest, which demonstrates how *C. elegans* can contribute to insights relevant for human disease. These findings predict that cancer cells with mutant Rb or a compromised FZR1 pathway may show reduced sensitivity to CDK4/6 inhibitor treatment, which could be of substantial clinical importance.

The frequent mutation of genes encoding SWI/SNF subunits in human cancer validates the relevance of our findings that SWI/SNF contributes critically to cell cycle exit in *C. elegans*. So far, we have not tested the role of the SWI/SNF complex in proliferation control in mammalian cell differentiation models, or addressed the consequences of SWI/SNF loss in human cancer cells. However, experiments in mice and human cell lines performed by others are in agreement with our results as they report an important role for the SWI/SNF complex in lineage commitment and muscle development (Puri and Mercola, 2012).

Taken together, the development of an organism with all the specific cell-types, tissues and, organs, requires tight control over both proliferation and cell specification. In contrast, continued proliferation as observed in cancer cells may arise from loss of proliferation control or from a failure to differentiate. Here we have focused on the mechanisms that regulate the progression from G1 into S-phase, temporal versus permanent cell cycle exit, the maintenance of a differentiated post-mitotic state and the coordination between cell cycle exit and differentiation. Redundantly acting regulators and the involvement of many different control mechanisms including transcription repression, protein degradation, CDK inhibition, and chromatin remodeling together ensure proper development and the correct temporal coupling between cell cycle exit and differentiation. Improvements in our understanding of these mechanisms will be of great fundamental and clinical importance, both in terms of cancer biology and regenerative therapies.

Addendum

References

Adachi, M., Roussel, M.F., Havenith, K., and Sherr, C.J. (1997). Features of macrophage differentiation induced by p19INK4d, a specific inhibitor of cyclin D-dependent kinases. Blood *90*, 126–137.

Ajioka, I., Martins, R. A. P., Bayazitov, I.T., Donovan, S., Johnson, D. A., Frase, S., Cicero, S. A., Boyd, K., Zakharenko, S.S., and Dyer, M. A. (2007). Differentiated horizontal interneurons clonally expand to form metastatic retinoblastoma in mice. Cell *131*, 378–390.

Alarcon-Vargas, D., Zhang, Z., Agarwal, B., Challagulla, K., Mani, S., and Kalpana, G. V (2006). Targeting cyclin D1, a downstream effector of INI1/hSNF5, in rhabdoid tumors. Oncogene *25*, 722–734.

Ali, F., Hindley, C., McDowell, G., Deibler, R., Jones, A., Kirschner, M., Guillemot, F., and Philpott, A. (2011). Cell cycle-regulated multi-site phosphorylation of Neurogenin 2 coordinates cell cycling with differentiation during neurogenesis. Development *138*, 4267–4277.

Amon, A., Irniger, S., and Nasmyth, K. (1994). Closing the cell cycle circle in yeast: G2 cyclin proteolysis initiated at mitosis persists until the activation of G1 cyclins in the next cycle. Cell *77*, 1037–1050.

Anders, L., Ke, N., Hydbring, P., Choi, Y.J., Widlund, H.R., Chick, J.M., Zhai, H., Vidal, M., Gygi, S.P., Braun, P., *et al.* (2011). A systematic screen for CDK4/6 substrates links FOXM1 phosphorylation to senescence suppression in cancer cells. Cancer Cell *20*, 620–634.

Ankeny, R.A. (2001). The natural history of *Caenorhabditis elegans* research. Nat. Rev. Genet. *2*, 474–479.

Arias, E.E., and Walter, J.C. (2007). Strength in numbers: preventing rereplication via multiple mechanisms in eukaryotic cells. Genes Dev. *21*, 497–518.

Armstrong, J.A., Bieker, J.J., and Emerson, B.M. (1998). A SWI/SNF–related chromatin remodeling complex, E-RC1, Is required for tissue-specific transcriptional regulation by EKLF *In vitro*. Cell *95*, 93–104.

Asp, P., Blum, R., Vethantham, V., Parisi, F., Micsinai, M., Cheng, J., Bowman, C., Kluger, Y., and Dynlacht, B.D. (2011). Genome-wide remodeling of the epigenetic landscape during myogenic differentiation. Proc. Natl. Acad. Sci. U. S. A. *108*, E149–E158.

Mac Auley, A., Werb, Z., and Mirkes, P.E. (1993). Characterization of the unusually rapid cell cycles during rat gastrulation. Development *117*, 873–883.

Baig, J., Chanut, F., Kornberg, T.B., and Klebes, A. (2010). The chromatin-remodeling protein Osa interacts with CyclinE in *Drosophila* eye imaginal discs. Genetics *184*, 731–744.

Bandara, L.R., and La Thangue, N.B. (1991). Adenovirus E1a prevents the retinoblastoma gene product from complexing with a cellular transcription factor. Nature *351*, 494–497.

Barnes, A.P., and Polleux, F. (2009). Establishment of axon-dendrite polarity in developing neurons. Annu. Rev. Neurosci. *32*, 347–381.

Barta, T., Dolezalova, D., Holubcova, Z., and Hampl, A. (2013). Cell cycle regulation in human embryonic stem cells: links to adaptation to cell culture. Exp. Biol. Med. *238*, 271–275.

Bashir, T., Dorrello, N.V., Amador, V., Guardavaccaro, D., and Pagano, M. (2004). Control of the SCF(Skp2-Cks1) ubiquitin ligase by the APC/C(Cdh1) ubiquitin ligase. Nature *428*, 190–193.

Bassermann, F., Eichner, R., and Pagano, M. (2014). The ubiquitin proteasome system - implications for cell cycle control and the targeted treatment of cancer. Biochim. Biophys. Acta *1843*, 150–162.

Beitel, G.J., Clark, S.G., and Horvitz, H.R. (1990). *Caenorhabditis elegans* ras gene let-60 acts as a switch in the pathway of vulval induction. Nature *348*, 503–509.

Bell, S.P., and Dutta, A. (2002). DNA replication in eukaryotic cells. Annu. Rev. Biochem. *71*, 333–374.

Bellin, M., Marchetto, M.C., Gage, F.H., and Mummery, C.L. (2012). Induced pluripotent stem cells: the new patient? Nat. Rev. Mol. Cell Biol. *13*, 713–726.

Bennett, M.D., Leitch, I.J., Price, H.J., and Johnston, J.S. (2003). Comparisons with Caenorhabditis (approximately 100 Mb) and *Drosophila* (approximately 175 Mb) using flow cytometry show genome size in *Arabidopsis* to be approximately 157 Mb and thus approximately 25% larger than the Arabidopsis genome initiative estimate . Ann. Bot. *91*, 547–557.

Berger, C., Kannan, R., Myneni, S., Renner, S., Shashidhara, L.S., and Technau, G.M. (2010). Cell cycle independent role of Cyclin E during neural cell fate specification in *Drosophila* is mediated by its regulation of Prospero function. Dev. Biol. *337*, 415–424.

Berger, C., Pallavi, S.K., Prasad, M., Shashidhara, L.S., and Technau, G.M. (2005). A critical role for cyclin E in cell fate determination in the central nervous system of *Drosophila* melanogaster. Nat. Cell Biol. *7*, 56–62.

Bernstein, B.E., Mikkelsen, T.S., Xie, X., Kamal, M., Huebert, D.J., Cuff, J., Fry, B., Meissner, A., Wernig, M., Plath, K., *et al.* (2006). A bivalent chromatin structure marks key developmental genes in embryonic stem cells. Cell *125*, 315–326.

Berriz, G.F., King, O.D., Bryant, B., Sander, C., and Roth, F.P. (2003). Characterizing gene sets with FuncAssociate. Bioinformatics *19*, 2502–2504.

Bettinger, J.C., Lee, K., and Rougvie, A.E. (1996). Stage-specific accumulation of the terminal differentiation factor LIN-29 during *Caenorhabditis elegans* development. Development *122*, 2517–2527.

Biedermann, B., Wright, J., Senften, M., Kalchhauser, I., Sarathy, G., Lee, M.-H., and Ciosk, R. (2009). Translational repression of cyclin E prevents precocious mitosis and embryonic gene activation during *C. elegans* meiosis. Dev. Cell *17*, 355–364.

Bienvenu, F., Jirawatnotai, S., Elias, J.E., Meyer, C.A., Mizeracka, K., Marson, A., Frampton, G.M., Cole, M.F., Odom, D.T., Odajima, J., *et al.* (2010). Transcriptional role of cyclin D1 in development revealed by a genetic-proteomic screen. Nature *463*, 374–378.

Blais, A., and Dynlacht, B.D. (2007). E2F-associated chromatin modifiers and cell cycle control. Curr. Opin. Cell Biol. *19*, 658–662.

Blais, A., van Oevelen, C.J.C., Margueron, R., Acosta-Alvear, D., and Dynlacht, B.D. (2007). Retinoblastoma tumor suppressor protein-dependent methylation of histone H3 lysine 27 is associated with irreversible cell cycle exit. J. Cell Biol. *179*, 1399–1412.

Blanchard, D.P., Georlette, D., Antoszewski, L., and Botchan, M.R. (2014). Chromatin reader L(3)mbt requires the Myb-MuvB/DREAM transcriptional regulatory complex for chromosomal recruitment. Proc. Natl. Acad. Sci. U. S. A. *111*, E4234–E4243.

Blomen, V.A., and Boonstra, J. (2007). Cell fate determination during G1 phase progression. Cell. Mol. Life Sci. *64*, 3084–3104.

Blow, J.J., and Dutta, A. (2005). Preventing re-replication of chromosomal DNA. Nat. Rev. Mol. Cell Biol. *6*, 476–486.

Bondar, T., Kalinina, A., Khair, L., Kopanja, D., Nag, A., Bagchi, S., and Raychaudhuri, P. (2006). Cul4A and DDB1 associate with Skp2 to target p27Kip1 for proteolysis involving the COP9 signalosome. Mol. Cell. Biol. *26*, 2531–2539.

Bousset, K., and Diffley, J.F. (1998). The Cdc7 protein kinase is required for origin firing during S phase. Genes Dev. *12*, 480–490.

Boxem, M., and van den Heuvel, S. (2001). *lin-35* Rb and *cki-1* Cip/Kip cooperate in developmental regulation of G1 progression in *C. elegans*. Development *128*, 4349–4359.

Boxem, M., and van den Heuvel, S. (2002). *C. elegans* class B synthetic multivulva genes act in G(1) regulation. Curr. Biol. *12*, 906–911.

Boxem, M., Srinivasan, D.G., and van den Heuvel, S. (1999). The *Caenorhabditis elegans* gene *ncc-1* encodes a cdc2-related kinase required for M phase in meiotic and mitotic cell divisions, but not for S phase. Development *126*, 2227–2239.

Boyle, A.P., Araya, C.L., Brdlik, C., Cayting, P., Cheng, C., Cheng, Y., Gardner, K., Hillier, L.W., Janette, J., Jiang, L., *et al.* (2014). Comparative analysis of regulatory information and circuits across distant species. Nature *512*, 453–456.

Bracken, A.P., Dietrich, N., Pasini, D., Hansen, K.H., and Helin, K. (2006). Genome-wide mapping of Polycomb target genes unravels their roles in cell fate transitions. Genes Dev. *20*, 1123–1136.

Branzei, D., and Foiani, M. (2010). Maintaining genome stability at the replication fork. Nat. Rev. Mol. Cell Biol. *11*, 208–219.

Brauchle, M., Baumer, K., and Gonczy, P. (2003). Differential activation of the DNA replication checkpoint contributes to asynchrony of cell division in *C. elegans* embryos. Curr. Biol. *13*, 819–827.

Braun, T., and Gautel, M. (2011). Transcriptional mechanisms regulating skeletal muscle differentiation, growth and homeostasis. Nat. Rev. Mol. Cell Biol. *12*, 349–361.

Brenner, S. (1974). The genetics of *Caenorhabditis elegans*. Genetics *77*, 71–94.

Brodigan, T.M., Liu, J. i, Park, M., Kipreos, E.T., and Krause, M. (2003). Cyclin E expression during development in *Caenorhabditis elegans*. Dev. Biol. *254*, 102–115.

Brower, V. (2014). Cell cycle inhibitors make progress. J. Natl. Cancer Inst. *106*.

Brumby, A.M., Zraly, C.B., Horsfield, J.A., Secombe, J., Saint, R., Dingwall, A.K., and Richardson, H. (2002). *Drosophila* cyclin E interacts with components of the Brahma complex. EMBO J. *21*, 3377–3389.

Buck, S.H., Chiu, D., and Saito, R.M. (2009). The cyclin-dependent kinase inhibitors, *cki-1* and *cki-2*, act in overlapping but distinct pathways to control cell cycle quiescence during *C. elegans* development. Cell Cycle *8*, 2613–2620.

Buckingham, M., and Rigby, P.W.J. (2014). Gene regulatory networks and transcriptional mechanisms that control myogenesis. Dev. Cell *28*, 225–238.

Bueno, M.J., and Malumbres, M. (2011). MicroRNAs and the cell cycle. Biochim. Biophys. Acta *1812*, 592–601.

Busanello, A., Battistelli, C., Carbone, M., Mostocotto, C., and Maione, R. (2012). MyoD regulates p57kip2 expression by interacting with a distant cis-element and modifying a higher order chromatin structure. Nucleic Acids Res. *40*, 8266–8275.

Buttitta, L.A., and Edgar, B.A. (2007). Mechanisms controlling cell cycle exit upon terminal differentiation. Curr. Opin. Cell Biol. *19*, 697–704.

Buttitta, L. A., Katzaroff, A.J., and Edgar, B. a (2010). A robust cell cycle control mechanism limits E2F-induced proliferation of terminally differentiated cells *in vivo*. J. Cell Biol. *189*, 981–996.

Buttitta, L.A., Katzaroff, A.J., Perez, C.L., de la Cruz, A., and Edgar, B.A. (2007). A double-assurance mechanism controls cell cycle exit upon terminal differentiation in *Drosophila*. Dev. Cell *12*, 631–643.

Byun, T.S., Pacek, M., Yee, M., Walter, J.C., and Cimprich, K.A. (2005). Functional uncoupling of MCM helicase and DNA polymerase activities activates the ATR-dependent checkpoint. Genes Dev. *19*, 1040–1052.

Calder, A., Roth-Albin, I., Bhatia, S., Pilquil, C., Lee, J.H., Bhatia, M., Levadoux-Martin, M., McNicol, J., Russell, J., Collins, T., *et al.* (2013). Lengthened G1 phase indicates differentiation status in human embryonic stem cells. Stem Cells Dev. *22*, 279–295.

Calegari, F., and Huttner, W.B. (2003). An inhibition of cyclin-dependent kinases that lengthens, but does not arrest, neuroepithelial cell cycle induces premature neurogenesis. J. Cell Sci. *116*, 4947–4955.

Calegari, F., Haubensak, W., Haffner, C., and Huttner, W.B. (2005). Selective lengthening of the cell cycle in the neurogenic subpopulation of neural progenitor cells during mouse brain development. J. Neurosci. *25*, 6533–6538.

Cao, Y., Yao, Z., Sarkar, D., Lawrence, M., Sanchez, G.J., Parker, M.H., MacQuarrie, K.L., Davison, J., Morgan, M.T., Ruzzo, W.L., *et al.* (2010). Genome-wide MyoD binding in skeletal muscle cells: a potential for broad cellular reprogramming. Dev. Cell *18*, 662–674.

Cardozo, T., and Pagano, M. (2004). The SCF ubiquitin ligase: insights into a molecular machine. Nat. Rev. Mol. Cell Biol. *5*, 739–751.

Caretti, G., Di Padova, M., Micales, B., Lyons, G.E., and Sartorelli, V. (2004). The Polycomb Ezh2 methyltransferase regulates muscle gene expression and skeletal muscle differentiation. Genes Dev. *18*, 2627–2638.

Ceol, C.J., and Horvitz, H.R. (2001). *dpl-1* DP and *efl-1* E2F Act with *lin-35* Rb to antagonize ras signaling in *C. elegans* vulval vevelopment. Mol. Cell *7*, 461–473.

Chai, J., Charboneau, A.L., Betz, B.L., and Weissman, B.E. (2005). Loss of the hSNF5 gene concomitantly inactivates p21CIP/WAF1 and p16INK4a activity associated with replicative senescence in A204 rhabdoid tumor cells. Cancer Res. *65*, 10192–10198.

Chellappan, S.P., Hiebert, S., Mudryj, M., Horowitz, J.M., and Nevins, J.R. (1991). The E2F transcription factor is a cellular target for the RB protein. Cell *65*, 1053–1061.

Chen, P., and Segil, N. (1999). p27(Kip1) links cell proliferation to morphogenesis in the developing organ of Corti. Development *126*, 1581–1590.

Chen, T., and Dent, S.Y.R. (2014). Chromatin modifiers and remodellers: regulators of cellular differentiation. Nat. Rev. Genet. *15*, 93–106.

Cheng, T., Rodrigues, N., Shen, H., Yang, Y., Dombkowski, D., Sykes, M., and Scadden, D.T. (2000). Hematopoietic stem cell quiescence maintained by p21cip1/waf1. Science *287*, 1804–1808.

Chi, W., and Reinke, V. (2006). Promotion of oogenesis and embryogenesis in the *C. elegans* gonad by EFL-1/DPL-1 (E2F) does not require LIN-35 (pRB). Development *133*, 3147–3157.

Choe, K.S., Ujhelly, O., Wontakal, S.N., and Skoultchi, A.I. (2010). PU.1 directly regulates cdk6 gene expression, linking the cell proliferation and differentiation programs in erythroid cells. J. Biol. Chem. *285*, 3044–3052.

Choi, Y.J., and Anders, L. (2014). Signaling through cyclin D-dependent kinases. Oncogene *33*, 1890–1903.

Choi, Y.J., Li, X., Hydbring, P., Sanda, T., Stefano, J., Christie, A.L., Signoretti, S., Look, A.T., Kung, A.L., von Boehmer, H., *et al.* (2012). The requirement for cyclin D function in tumor maintenance. Cancer Cell *22*, 438–451.

Ciemerych, M.A., and Sicinski, P. (2005). Cell cycle in mouse development. Oncogene *24*, 2877–2898.

Cinquin, O., Crittenden, S.L., Morgan, D.E., and Kimble, J. (2010). Progression from a stem cell-like state to early differentiation in the *C. elegans* germ line. Proc. Natl. Acad. Sci. U. S. A. *107*, 2048–2053.

Claycomb, J.M., and Orr-Weaver, T.L. (2005). Developmental gene amplification: insights into DNA replication and gene expression. Trends Genet. *21*, 149–162.

Clayton, J.E., van den Heuvel, S.J.L., and Saito, R.M. (2008). Transcriptional control of cell-cycle quiescence during *C. elegans* development. Dev. Biol. *313*, 603–613.

Clijsters, L., Ogink, J., and Wolthuis, R. (2013). The spindle checkpoint, APC/C(Cdc20), and APC/C(Cdh1) play distinct roles in connecting mitosis to S phase. J. Cell Biol. *201*, 1013–1026.

Clucas, C., Cabello, J., Büssing, I., Schnabel, R., and Johnstone, I.L. (2002). Oncogenic potential of a C.elegans cdc25 gene is demonstrated by a gain-of-function allele. EMBO J. *21*, 665–674.

Cobrinik, D. (2005). Pocket proteins and cell cycle control. Oncogene *24*, 2796–2809.

Coller, H.A., Sang, L., and Roberts, J.M. (2006). A new description of cellular quiescence. PLoS Biol. *4*, e83.

Coronado, D., Godet, M., Bourillot, P.-Y., Tapponnier, Y., Bernat, A., Petit, M., Afanassieff, M., Markossian, S., Malashicheva, A., Iacone, R., *et al.* (2013). A short G1 phase is an intrinsic determinant of naïve embryonic stem cell pluripotency. Stem Cell Res. *10*, 118–131.

Corsi, A.K., Kostas, S.A., Fire, A., and Krause, M. (2000). *Caenorhabditis elegans* twist plays an essential role in non-striated muscle development. Development *127*, 2041–2051.

Coudreuse, D., and Nurse, P. (2010). Driving the cell cycle with a minimal CDK control network. Nature *468*, 1074–1079.

Crooks, G.E., Hon, G., Chandonia, J.-M., and Brenner, S.E. (2004). WebLogo: a sequence logo generator. Genome Res. *14*, 1188–1190.

Cui, M., Fay, D.S., and Han, M. (2004). *lin-35*/Rb cooperates with the SWI/SNF complex to control *Caenorhabditis elegans* larval development. Genetics *167*, 1177–1185.

Dalton, S. (2013). G1 compartmentalization and cell fate coordination. Cell *155*, 13–14.

Dambournet, D., Machicoane, M., Chesneau, L., Sachse, M., Rocancourt, M., El Marjou, A., Formstecher, E., Salomon, R., Goud, B., and Echard, A. (2011). Rab35 GTPase and OCRL phosphatase remodel lipids and F-actin for successful cytokinesis. Nat. Cell Biol. *13*, 981–988.

Datar, S.A., Jacobs, H.W., de la Cruz, A.F., Lehner, C.F., and Edgar, B.A. (2000). The *Drosophila* cyclin D-Cdk4 complex promotes cellular growth. EMBO J. *19*, 4543–4554.

Davis, D.M., and Dyer, M.A. (2010). Retinal progenitor cells, differentiation, and barriers to cell cycle reentry. Curr. Top. Dev. Biol. *93*, 175–188.

Davis, M.W., Morton, J.J., Carroll, D., and Jorgensen, E.M. (2008). Gene activation using FLP recombinase in *C. elegans*. PLoS Genet. *4*, e1000028.

Dehay, C., and Kennedy, H. (2007). Cell-cycle control and cortical development. Nat. Rev. Neurosci. *8*, 438–450.

Dephoure, N., Zhou, C., Villén, J., Beausoleil, S.A., Bakalarski, C.E., Elledge, S.J., and Gygi, S.P. (2008). A quantitative atlas of mitotic phosphorylation. Proc. Natl. Acad. Sci. U. S. A. *105*, 10762–10767.

Dick, F.A., and Rubin, S.M. (2013). Molecular mechanisms underlying RB protein function. Nat. Rev. Mol. Cell Biol. *14*, 297–306.

Dietrich, N., Bracken, A.P., Trinh, E., Schjerling, C.K., Koseki, H., Rappsilber, J., Helin, K., and Hansen, K.H. (2007). Bypass of senescence by the polycomb group protein CBX8 through direct binding to the INK4A-ARF locus. EMBO J. *26*, 1637–1648.

Dimova, D.K., and Dyson, N.J. (2005). The E2F transcriptional network: old acquaintances with new faces. Oncogene *24*, 2810–2826.

Dimova, D.K., Stevaux, O., Frolov, M. V, and Dyson, N.J. (2003). Cell cycle-dependent and cell cycle-independent control of transcription by the *Drosophila* E2F/RB pathway. Genes Dev. *17*, 2308–2320.

Doitsidou, M., Flames, N., Lee, A.C., Boyanov, A., and Hobert, O. (2008). Automated screening for mutants affecting dopaminergic-neuron specification in *C. elegans*. Nat. Methods *5*, 869–872.

Dotti, C.G., Sullivan, C.A., and Banker, G.A. (1988). The establishment of polarity by hippocampal neurons in culture. J. Neurosci. *8*, 1454–1468.

Dozier, C., Kagoshima, H., Niklaus, G., Cassata, G., and Bürglin, T.R. (2001). The *Caenorhabditis elegans* Six/sine oculis class homeobox gene ceh-32 is required for head morphogenesis. Dev. Biol. *236*, 289–303.

Duronio, R.J., and O'Farrell, P.H. (1995). Developmental control of the G1 to S transition in *Drosophila*: cyclin E is a limiting downstream target of E2F. Genes Dev. *9*, 1456–1468.

Dyson, N., Howley, P.M., Münger, K., and Harlow, E. (1989). The human papilloma virus-16 E7 oncoprotein is able to bind to the retinoblastoma gene product. Science *243*, 934–937.

Efroni, S., Duttagupta, R., Cheng, J., Dehghani, H., Hoeppner, D.J., Dash, C., Bazett-Jones, D.P., Le Grice, S., McKay, R.D.G., Buetow, K.H., *et al.* (2008). Global transcription in pluripotent embryonic stem cells. Cell Stem Cell *2*, 437–447.

Eguren, M., Manchado, E., and Malumbres, M. (2011). Non-mitotic functions of the Anaphase-Promoting Complex. Semin. Cell Dev. Biol. *22*, 572–578.

Emmerich, J., Meyer, C.A., de la Cruz, A.F.A., Edgar, B.A., and Lehner, C.F. (2004). Cyclin D does not provide essential Cdk4-independent functions in *Drosophila*. Genetics *168*, 867–875.

Encalada, S.E., Martin, P.R., Phillips, J.B., Lyczak, R., Hamill, D.R., Swan, K.A., and Bowerman, B. (2000). DNA replication defects delay cell division and disrupt cell polarity in early *Caenorhabditis elegans* embryos. Dev. Biol. *228*, 225–238.

Encalada, S.E., Willis, J., Lyczak, R., and Bowerman, B. (2005). A spindle checkpoint functions during mitosis in the early *Caenorhabditis elegans* embryo. Mol. Biol. Cell *16*, 1056–1070.

Eroglu, E., Burkard, T.R., Jiang, Y., Saini, N., Homem, C.C.F., Reichert, H., and Knoblich, J.A. (2014). SWI/SNF complex prevents lineage reversion and induces temporal patterning in neural stem cells. Cell *156*, 1259–1273.

Faber, P.W., Alter, J.R., MacDonald, M.E., and Hart, A.C. (1999). Polyglutamine-mediated dysfunction and apoptotic death of a *Caenorhabditis elegans* sensory neuron. Proc. Natl. Acad. Sci. U. S. A. *96*, 179–184.

Fay, D.S., and Han, M. (2000). Mutations in cye-1, a *Caenorhabditis elegans* cyclin E homolog, reveal coordination between cell-cycle control and vulval development. Development *127*, 4049–4060.

Fay, D.S., Keenan, S., and Han, M. (2002). *fzr-1* and *lin-35*/Rb function redundantly to control cell proliferation in *C. elegans* as revealed by a nonbiased synthetic screen. Genes Dev. *16*, 503–517.

Feng, H., Zhong, W., Punkosdy, G., Gu, S., Zhou, L., Seabolt, E.K., and Kipreos, E.T. (1999). CUL-2 is required for the G1-to-S-phase transition and mitotic chromosome condensation in *Caenorhabditis elegans*. Nat. Cell Biol. *1*, 486–492.

Figliola, R., and Maione, R. (2004). MyoD induces the expression of p57Kip2 in cells lacking p21Cip1/Waf1: overlapping and distinct functions of the two cdk inhibitors. J. Cell. Physiol. *200*, 468–475.

Filipczyk, A.A., Laslett, A.L., Mummery, C., and Pera, M.F. (2007). Differentiation is coupled to changes in the cell cycle regulatory apparatus of human embryonic stem cells. Stem Cell Res. *1*, 45–60.

Finn, R.S., Dering, J., Conklin, D., Kalous, O., Cohen, D.J., Desai, A.J., Ginther, C., Atefi, M., Chen, I., Fowst, C., *et al.* (2009). PD 0332991, a selective cyclin D kinase 4/6 inhibitor, preferentially inhibits proliferation of luminal estrogen receptor-positive human breast cancer cell lines *in vitro*. Breast Cancer Res. *11*, R77.

Fire, A., and Waterston, R.H. (1989). Proper expression of myosin genes in transgenic nematodes. EMBO J. *8*, 3419–3428.

Flames, N., and Hobert, O. (2009). Gene regulatory logic of dopamine neuron differentiation. Nature *458*, 885–889.

Flemming, A.J., Shen, Z.Z., Cunha, A., Emmons, S.W., and Leroi, A.M. (2000). Somatic polyploidization and cellular proliferation drive body size evolution in nematodes. Proc. Natl. Acad. Sci. U. S. A. *97*, 5285–5290.

Flowers, S., Nagl, N.G., Beck, G.R., and Moran, E. (2009). Antagonistic roles for BRM and BRG1 SWI/SNF complexes in differentiation. J. Biol. Chem. *284*, 10067–10075.

Forcales, S. V, Albini, S., Giordani, L., Malecova, B., Cignolo, L., Chernov, A., Coutinho, P., Saccone, V., Consalvi, S., Williams, R., *et al.* (2012). Signal-dependent incorporation of MyoD-BAF60c into Brg1-based SWI/SNF chromatin-remodelling complex. EMBO J. *31*, 301–316.

Fox, P.M., Vought, V.E., Hanazawa, M., Lee, M.-H., Maine, E.M., and Schedl, T. (2011). Cyclin E and CDK-2 regulate proliferative cell fate and cell cycle progression in the *C. elegans* germline. Development *138*, 2223–2234.

Fox, R.M., Watson, J.D., Von Stetina, S.E., McDermott, J., Brodigan, T.M., Fukushige, T., Krause, M., and Miller, D.M. (2007). The embryonic muscle transcriptome of *Caenorhabditis elegans*. Genome Biol. *8*, R188.

Frescas, D., and Pagano, M. (2008). Deregulated proteolysis by the F-box proteins SKP2 and beta-TrCP: tipping the scales of cancer. Nat. Rev. Cancer *8*, 438–449.

Friedland, A.E., Tzur, Y.B., Esvelt, K.M., Colaiácovo, M.P., Church, G.M., and Calarco, J.A. (2013). Heritable genome editing in *C. elegans* via a CRISPR-Cas9 system. Nat. Methods *10*, 741–743.

Frith, M.C., Fu, Y., Yu, L., Chen, J.-F., Hansen, U., and Weng, Z. (2004). Detection of functional DNA motifs via statistical over-representation. Nucleic Acids Res. *32*, 1372–1381.

Frøkjaer-Jensen, C., Davis, M.W., Hopkins, C.E., Newman, B.J., Thummel, J.M., Olesen, S.-P., Grunnet, M., and Jorgensen, E.M. (2008). Single-copy insertion of transgenes in *Caenorhabditis elegans*. Nat. Genet. *40*, 1375–1383.

Frøkjær-Jensen, C., Davis, M.W., Ailion, M., and Jorgensen, E.M. (2012). Improved Mos1-mediated transgenesis in *C. elegans*. Nat. Methods *9*, 117–118.

Fry, D.W., Harvey, P.J., Keller, P.R., Elliott, W.L., Meade, M., Trachet, E., Albassam, M., Zheng, X., Leopold, W.R., Pryer, N.K., *et al.* (2004). Specific inhibition of cyclin-dependent kinase 4/6 by PD 0332991 and associated antitumor activity in human tumor xenografts. Mol. Cancer Ther. *3*, 1427–1438.

Fujita, M., Takeshita, H., and Sawa, H. (2007). Cyclin E and CDK2 repress the terminal differentiation of quiescent cells after asymmetric division in *C. elegans*. PLoS One *2*, e407.

Fukushige, T., Hawkins, M.G., and McGhee, J.D. (1998). The GATA-factor *elt-2* is essential for formation of the *Caenorhabditis elegans* intestine. Dev. Biol. *198*, 286–302.

Fukuyama, M., Gendreau, S.B., Derry, W.B., and Rothman, J.H. (2003). Essential embryonic roles of the CKI-1 cyclin-dependent kinase inhibitor in cell-cycle exit and morphogenesis in *C. elegans*. Dev. Biol. *260*, 273–286.

Galli, M., Muñoz, J., Portegijs, V., Boxem, M., and Heck, A.J.R., and Van den Heuvel S.J.L. (2011) aPKC phosphorylates LIN-5 / NuMA to position the mitotic spindle during asymmetric division. Nat. Cell Biol. *13*, 1132-1138

Gaydos, L.J., Rechtsteiner, A., Egelhofer, T.A., Carroll, C.R., and Strome, S. (2012). Antagonism between MES-4 and Polycomb repressive complex 2 promotes appropriate gene expression in *C. elegans* germ cells. Cell Rep. *2*, 1169–1177.

Gérard, C., Gonze, D., and Goldbeter, A. (2012). Effect of positive feedback loops on the robustness of oscillations in the network of cyclin-dependent kinases driving the mammalian cell cycle. FEBS J. *279*, 3411–3431.

Van Gilst, M.R., Hadjivassiliou, H., Jolly, A., and Yamamoto, K.R. (2005). Nuclear hormone receptor NHR-49 controls fat consumption and fatty acid composition in *C. elegans*. PLoS Biol. *3*, e53.

Gordon, G.M., and Du, W. (2011). Conserved RB functions in development and tumor suppression. Protein Cell *2*, 864–878.

Guha, M. (2012). Cyclin-dependent kinase inhibitors move into Phase III. Nat. Rev. Drug Discov. *11*, 892–894.

Guha, M. (2013). Blockbuster dreams for Pfizer's CDK inhibitor. Nat. Biotechnol. *31*, 187.

Gunawardena, R.W., Fox, S.R., Siddiqui, H., and Knudsen, E.S. (2007). SWI/SNF activity is required for the repression of deoxyribonucleotide triphosphate metabolic enzymes via the recruitment of mSin3B. J. Biol. Chem. *282*, 20116–20123.

Guo, K., and Walsh, K. (1997). Inhibition of myogenesis by multiple cyclin-Cdk complexes. Coordinate regulation of myogenesis and cell cycle activity at the level of E2F. J. Biol. Chem. *272*, 791–797.

Guo, K., Wang, J., Andrés, V., Smith, R.C., and Walsh, K. (1995). MyoD-induced expression of p21 inhibits cyclin-dependent kinase activity upon myocyte terminal differentiation. Mol. Cell. Biol. *15*, 3823–3829.

Halevy, O., Novitch, B.G., Spicer, D.B., Skapek, S.X., Rhee, J., Hannon, G.J., Beach, D., and Lassar, A.B. (1995). Correlation of terminal cell cycle arrest of skeletal muscle with induction of p21 by MyoD. Science *267*, 1018–1021.

Han, M., and Sternberg, P.W. (1990). let-60, a gene that specifies cell fates during *C. elegans* vulval induction, encodes a ras protein. Cell *63*, 921–931.

Hanahan, D., and Weinberg, R.A. (2011). Hallmarks of cancer: The next generation. Cell *144*, 646–674.

Hardwick, L.J.A., and Philpott, A. (2014). Nervous decision-making: to divide or differentiate. Trends Genet. *30*, 254–261.

Harrison, M.M., Ceol, C.J., Lu, X., and Horvitz, H.R. (2006). Some *C. elegans* class B synthetic multivulva proteins encode a conserved LIN-35 Rb-containing complex distinct from a NuRD-like complex. Proc. Natl. Acad. Sci. U. S. A. *103*, 16782–16787.

Harrison, M.M., Lu, X., and Horvitz, H.R. (2007). LIN-61, one of two *Caenorhabditis elegans* malignant-brain-tumor-repeat-containing proteins, acts with the DRM and NuRD-like protein complexes in vulval development but not in certain other biological processes. Genetics *176*, 255–271.

Hart, A.C., Kass, J., Shapiro, J.E., and Kaplan, J.M. (1999). Distinct signaling pathways mediate touch and osmosensory responses in a polymodal sensory neuron. J. Neurosci. *19*, 1952–1958.

Hartwell, L.H., and Weinert, T.A. (1989). Checkpoints: controls that ensure the order of cell cycle events. Science *246*, 629–634.

Havens, C.G., and Walter, J.C. (2009). Docking of a specialized PIP Box onto chromatin-bound PCNA creates a degron for the ubiquitin ligase CRL4Cdt2. Mol. Cell *35*, 93–104.

Hebeisen, M., and Roy, R. (2008). CDC-25.1 stability is regulated by distinct domains to restrict cell division during embryogenesis in *C. elegans*. Development *135*, 1259–1269.

Hedgecock, E.M., and White, J.G. (1985). Polyploid tissues in the nematode *Caenorhabditis elegans*. Dev. Biol. *107*, 128–133.

Hendricks, K.B., Shanahan, F., and Lees, E. (2004). Role for BRG1 in cell cycle control and tumor suppression. Mol. Cell. Biol. *24*, 362–376.

Herrup, K., and Yang, Y. (2007). Cell cycle regulation in the postmitotic neuron: oxymoron or new biology? Nat. Rev. Neurosci. *8*, 368–378.

Van den Heuvel, S., and Dyson, N.J. (2008). Conserved functions of the pRB and E2F families. Nat. Rev. Mol. Cell Biol. *9*, 713–724.

Heuvel, S.J.L., van der, and Harlow, E. (1993). Distinct roles for cyclin-dependent kinases in cell cycle control. Science *262*, 2050–2054.

Heuvel, S.J.L., van der and Kipreos, E.T. (2012). *C. elegans* Cell Cycle Analysis. Methods Cell Biol. *107*, 265–294.

Heuvel, S.J.L., van der, van Laar, T., The, I., and van der Eb, A.J. (1993). Large E1B proteins of adenovirus types 5 and 12 have different effects on p53 and distinct roles in cell transformation. J. Virol. *67*, 5226–5234.

Higa, L.A., Yang, X., Zheng, J., Banks, D., Wu, M., Ghosh, P., Sun, H., and Zhang, H. (2006). Involvement of CUL4 ubiquitin E3 ligases in regulating CDK inhibitors Dacapo/p27Kip1 and cyclin E degradation. Cell Cycle *5*, 71–77.

Hindley, C., Ali, F., McDowell, G., Cheng, K., Jones, A., Guillemot, F., and Philpott, A. (2012). Post-translational modification of Ngn2 differentially affects transcription of distinct targets to regulate the balance between progenitor maintenance and differentiation. Development *139*, 1718–1723.

Hirabayashi, Y., Suzki, N., Tsuboi, M., Endo, T.A., Toyoda, T., Shinga, J., Koseki, H., Vidal, M., and Gotoh, Y. (2009). Polycomb limits the neurogenic competence of neural precursor cells to promote astrogenic fate transition. Neuron *63*, 600–613.

Hirrlinger, J., Scheller, A., Hirrlinger, P.G., Kellert, B., Tang, W., Wehr, M.C., Goebbels, S., Reichenbach, A., Sprengel, R., Rossner, M.J., *et al.* (2009). Split-cre complementation indicates coincident activity of different genes *in vivo*. PLoS One *4*, e4286.

Hoier, E.F., Mohler, W.A., Kim, S.K., and Hajnal, A. (2000). The *Caenorhabditis elegans* APC-related gene *apr-1* is required for epithelial cell migration and Hox gene expression. Genes Dev. *14*, 874–886.

Holland, E.C. (2001). Gliomagenesis: genetic alterations and mouse models. Nat. Rev. Genet. *2*, 120–129.

Holstege, F.C., Jennings, E.G., Wyrick, J.J., Lee, T.I., Hengartner, C.J., Green, M.R., Golub, T.R., Lander, E.S., and Young, R.A. (1998). Dissecting the regulatory circuitry of a eukaryotic genome. Cell *95*, 717–728.

Holway, A.H., Kim, S.-H., La Volpe, A., and Michael, W.M. (2006). Checkpoint silencing during the DNA damage response in *Caenorhabditis elegans* embryos. J. Cell Biol. *172*, 999–1008.

Hong, Y., Roy, R., and Ambros, V. (1998). Developmental regulation of a cyclin-dependent kinase inhibitor controls postembryonic cell cycle progression in *Caenorhabditis elegans*. *3597*, 3585–3597.

Horvitz, H.R., and Sulston, J.E. (1980). Isolation and genetic characterization of cell-lineage mutants of the nematode *Caenorhabditis elegans*. Genetics *96*, 435–454.

Huang, J.N., Park, I., Ellingson, E., Littlepage, L.E., and Pellman, D. (2001). Activity of the APC(Cdh1) form of the anaphase-promoting complex persists until S phase and prevents the premature expression of Cdc20p. J. Cell Biol. *154*, 85–94.

Hubbard, E.J.A. (2014). FLP/FRT and Cre/lox recombination technology in *C. elegans*. Methods *68*, 417–424.

Iavarone, A., King, E.R., Dai, X.-M., Leone, G., Stanley, E.R., and Lasorella, A. (2004). Retinoblastoma promotes definitive erythropoiesis by repressing Id2 in fetal liver macrophages. Nature *432*, 1040–1045.

Inoue, H., Giannakopoulos, S., Parkhurst, C.N., Matsumura, T., Kono, E.A., Furukawa, T., and Tanese, N. (2011). Target genes of the largest human SWI/SNF complex subunit control cell growth. Biochem. J. *434*, 83–92.

Irniger, S., and Nasmyth, K. (1997). The anaphase-promoting complex is required in G1 arrested yeast cells to inhibit B-type cyclin accumulation and to prevent uncontrolled entry into S-phase. J. Cell Sci. *110*, 1523–1531.

Jacobs, J.J., Kieboom, K., Marino, S., DePinho, R.A., and van Lohuizen, M. (1999). The oncogene and Polycomb-group gene *bmi-1* regulates cell proliferation and senescence through the ink4a locus. Nature *397*, 164–168.

Jaspersen, S.L., Charles, J.F., and Morgan, D.O. (1999). Inhibitory phosphorylation of the APC regulator Hct1 is controlled by the kinase Cdc28 and the phosphatase Cdc14. Curr. Biol. *9*, 227–236.

Jaworski, J., Kapitein, L.C., Gouveia, S.M., Dortland, B.R., Wulf, P.S., Grigoriev, I., Camera, P., Spangler, S.A., Di Stefano, P., Demmers, J., *et al.* (2009). Dynamic microtubules regulate dendritic spine morphology and synaptic plasticity. Neuron *61*, 85–100.

Jeong, J., Verheyden, J.M., and Kimble, J. (2011). Cyclin E and Cdk2 control GLD-1, the mitosis/meiosis decision, and germline stem cells in *Caenorhabditis elegans*. PLoS Genet. *7*, e1001348.

Jorgensen, E.M., and Mango, S.E. (2002). The art and design of genetic screens: *Caenorhabditis elegans*. Nat. Rev. Genet. *3*, 356–369.

Juliandi, B., Abematsu, M., and Nakashima, K. (2010). Chromatin remodeling in neural stem cell differentiation. Curr. Opin. Neurobiol. *20*, 408–415.

Jullien, N., Sampieri, F., Enjalbert, A., and Herman, J.-P. (2003). Regulation of Cre recombinase by ligand-induced complementation of inactive fragments. Nucleic Acids Res. *31*, e131.

Kadoch, C., Hargreaves, D.C., Hodges, C., Elias, L., Ho, L., Ranish, J., and Crabtree, G.R. (2013). Proteomic and bioinformatic analysis of mammalian SWI/SNF complexes identifies extensive roles in human malignancy. Nat. Genet. *45*, 592–601.

Kaech, S., and Banker, G. (2006). Culturing hippocampal neurons. Nat. Protoc. *1*, 2406–2415.

Kage-Nakadai, E., Imae, R., Suehiro, Y., Yoshina, S., Hori, S., and Mitani, S. (2014). A conditional knockout toolkit for *Caenorhabditis elegans* based on the Cre/loxP recombination. PLoS One *9*, e114680.

Kamath, R.S., Fraser, A.G., Dong, Y., Poulin, G., Durbin, R., Gotta, M., Kanapin, A., Le Bot, N., Moreno, S., Sohrmann, M., *et al.* (2003). Systematic functional analysis of the *Caenorhabditis elegans* genome using RNAi. Nature *421*, 231–237.

Kandoth, C., McLellan, M.D., Vandin, F., Ye, K., Niu, B., Lu, C., Xie, M., Zhang, Q., McMichael, J.F., Wyczalkowski, M.A., *et al.* (2013). Mutational landscape and significance across 12 major cancer types. Nature *502*, 333–339.

Kang, H., Cui, K., and Zhao, K. (2004). BRG1 controls the activity of the retinoblastoma protein via regulation of p21CIP1/WAF1/SDI. Mol. Cell. Biol. *24*, 1188–1199.

Kapitein, L.C., Yau, K.W., and Hoogenraad, C.C. (2010). Microtubule dynamics in dendritic spines. Methods Cell Biol. *97*, 111–132.

Kia, S.K., Gorski, M.M., Giannakopoulos, S., and Verrijzer, C.P. (2008). SWI/SNF mediates polycomb eviction and epigenetic reprogramming of the INK4b-ARF-INK4a locus. Mol. Cell. Biol. *28*, 3457–3464.

Kim, J., and Kipreos, E.T. (2008). Control of the Cdc6 replication licensing factor in metazoa: the role of nuclear export and the CUL4 ubiquitin ligase. Cell Cycle *7*, 146–150.

Kim, J., Feng, H., and Kipreos, E.T. (2007). *C. elegans* CUL-4 prevents rereplication by promoting the nuclear export of CDC-6 via a CKI-1-dependent pathway. Curr. Biol. *17*, 966–972.

Kim, K.H., and Roberts, C.W.M. (2014). Mechanisms by which SMARCB1 loss drives rhabdoid tumor growth. Cancer Genet. *207*, 365–372.

Kim, Y., and Kipreos, E.T. (2007a). The *Caenorhabditis elegans* replication licensing factor CDT-1 is targeted for degradation by the CUL-4/DDB-1 complex. Mol. Cell. Biol. *27*, 1394–1406.

Kim, Y., and Kipreos, E.T. (2007b). Cdt1 degradation to prevent DNA re-replication: conserved and non-conserved pathways. Cell Div. *2*, 18.

Kim, Y., Starostina, N.G., and Kipreos, E.T. (2008). The CRL4Cdt2 ubiquitin ligase targets the degradation of p21Cip1 to control replication licensing. Genes Dev. *22*, 2507–2519.

Kim, Y., Deshpande, A., Dai, Y., Kim, J.J., Lindgren, A., Conway, A., Clark, A.T., and Wong, D.T. (2009). Cyclin-dependent kinase 2-associating protein 1 commits murine embryonic stem cell differentiation through retinoblastoma protein regulation. J. Biol. Chem. *284*, 23405–23414.

Kipreos, E.T. (2005a). *C. elegans* cell cycles: invariance and stem cell divisions. Nat. Rev. Mol. Cell Biol. *6*, 766–776.

Kipreos, E.T. (2005b). Ubiquitin-mediated pathways in *C. elegans*. WormBook 1–24.

Kipreos, E.T., Lander, L.E., Wing, J.P., He, W.W., and Hedgecock, E.M. (1996). *cul-1* is required for cell cycle exit in *C. elegans* and identifies a novel gene family. Cell *85*, 829–839.

Kipreos, E.T., Gohel, S.P., and Hedgecock, E.M. (2000). The *C. elegans* F-box/WD-repeat protein LIN-23 functions to limit cell division during development. Development *127*, 5071–5082.

Kirienko, N. V, and Fay, D.S. (2007). Transcriptome profiling of the *C. elegans* Rb ortholog reveals diverse developmental roles. Dev. Biol. *305*, 674–684.

Kitzmann, M., and Fernandez, A. (2001). Crosstalk between cell cycle regulators and the myogenic factor MyoD in skeletal myoblasts. Cell. Mol. Life Sci. *58*, 571–579.

Kitzmann, M., Vandromme, M., Schaeffer, V., Carnac, G., Labbé, J.C., Lamb, N., and Fernandez, A. (1999). cdk1- and cdk2-mediated phosphorylation of MyoD Ser200 in growing C2 myoblasts: role in modulating MyoD half-life and myogenic activity. Mol. Cell. Biol. *19*, 3167–3176.

Korenjak, M., and Brehm, A. (2005). E2F-Rb complexes regulating transcription of genes important for differentiation and development. Curr. Opin. Genet. Dev. *15*, 520–527.

Korenjak, M., Taylor-Harding, B., Binné, U.K., Satterlee, J.S., Stevaux, O., Aasland, R., White-Cooper, H., Dyson, N., and Brehm, A. (2004). Native E2F/RBF complexes contain Myb-interacting proteins and repress transcription of developmentally controlled E2F target genes. Cell *119*, 181–193.

Korzelius, J., and van den Heuvel, S. (2007). Replication licensing: oops! ... I did it again. Curr. Biol. *17*, R630–R632.

Korzelius, J., The, I., Ruijtenberg, S., Prinsen, M.B.W., Portegijs, V., Middelkoop, T.C., Koerkamp, M.J.G., Holstege, F.C.P., Boxem, M., and van den Heuvel, S. (2011a). *Caenorhabditis elegans* cyclin D/CDK4 and cyclin E/CDK2 induce distinct cell cycle re-entry programs in differentiated muscle cells. PLoS Genet. *7*.

Korzelius, J., The, I., Ruijtenberg, S., Portegijs, V., Xu, H., Horvitz, H.R., and Van den Heuvel, S. (2011b). *C. elegans* MCM-4 is a general DNA replication and checkpoint component with an epidermis-specific requirement for growth and viability. Dev. Biol. *350*, 358–369.

Kostić, I., and Roy, R. (2002). Organ-specific cell division abnormalities caused by mutation in a general cell cycle regulator in *C. elegans*. Development *129*, 2155–2165.

Kowenz-Leutz, E., and Leutz, A. (1999). A C/EBPβ Isoform Recruits the SWI/SNF complex to activate myeloid Genes. Mol. Cell *4*, 735–743.

Kozar, K., Ciemerych, M.A., Rebel, V.I., Shigematsu, H., Zagozdzon, A., Sicinska, E., Geng, Y., Yu, Q., Bhattacharya, S., Bronson, R.T., *et al.* (2004). Mouse development and cell proliferation in the absence of D-cyclins. Cell *118*, 477–491.

Kranenburg, O., Scharnhorst, V., Van der Eb, A.J., and Zantema, A. (1995). Inhibition of cyclin-dependent kinase activity triggers neuronal differentiation of mouse neuroblastoma cells. J. Cell Biol. *131*, 227–234.

Krause, M., and Liu, J. Somatic muscle specification during embryonic and post-embryonic development in the nematode *C. elegans*. Wiley Interdiscip. Rev. Dev. Biol. *1*, 203–214.

Kronja, I., and Orr-Weaver, T.L. (2011). Translational regulation of the cell cycle: when, where, how and why? Philos. Trans. R. Soc. Lond. B. Biol. Sci. *366*, 3638–3652.

Kuwahara, Y., Charboneau, A., Knudsen, E.S., and Weissman, B.E. (2010). Reexpression of hSNF5 in malignant rhabdoid tumor cell lines causes cell cycle arrest through a p21(CIP1/WAF1)-dependent mechanism. Cancer Res. *70*, 1854–1865.

Kuwahara, Y., Wei, D., Durand, J., and Weissman, B.E. (2013). SNF5 reexpression in malignant rhabdoid tumors regulates transcription of target genes by recruitment of SWI/SNF complexes and RNAPII to the transcription start site of their promoters. Mol. Cancer Res. *11*, 251–260.

De la Serna, I.L., Carlson, K.A., and Imbalzano, A.N. (2001). Mammalian SWI/SNF complexes promote MyoD-mediated muscle differentiation. Nat. Genet. *27*, 187–190.

De la Serna, I.L., Ohkawa, Y., Berkes, C.A., Bergstrom, D.A., Dacwag, C.S., Tapscott, S.J., and Imbalzano, A.N. (2005). MyoD targets chromatin remodeling complexes to the myogenin locus prior to forming a stable DNA-bound complex. Mol. Cell. Biol. *25*, 3997–4009.

De la Serna, I.L., Ohkawa, Y., and Imbalzano, A.N. (2006). Chromatin remodelling in mammalian differentiation: lessons from ATP-dependent remodellers. Nat. Rev. Genet. *7*, 461–473.

Labib, K., and Diffley, J.F. (2001). Is the MCM2-7 complex the eukaryotic DNA replication fork helicase? Curr. Opin. Genet. Dev. *11*, 64–70.

Labib, K., Kearsey, S.E., and Diffley, J.F. (2001). MCM2-7 proteins are essential components of prereplicative complexes that accumulate cooperatively in the nucleus during G1-phase and are required to establish, but not maintain, the S-phase checkpoint. Mol. Biol. Cell *12*, 3658–3667.

Lacomme, M., Liaubet, L., Pituello, F., and Bel-Vialar, S. (2012). NEUROG2 drives cell cycle exit of neuronal precursors by specifically repressing a subset of cyclins acting at the G1 and S phases of the cell cycle. Mol. Cell. Biol. *32*, 2596–2607.

Lancaster, M.A., and Knoblich, J.A. (2014). Generation of cerebral organoids from human pluripotent stem cells. Nat. Protoc. *9*, 2329–2340.

Lange, C., and Calegari, F. (2010). Cdks and cyclins link G1 length and differentiation of embryonic, neural and hematopoietic stem cells. Cell Cycle *9*, 1893–1900.

Lange, C., Huttner, W.B., and Calegari, F. (2009). Cdk4/cyclinD1 overexpression in neural stem cells shortens G1, delays neurogenesis, and promotes the generation and expansion of basal progenitors. Cell Stem Cell *5*, 320–331.

Large, E.E., and Mathies, L.D. (2014). *Caenorhabditis elegans* SWI/SNF Subunits Control Sequential Developmental Stages in the Somatic Gonad. G3 Genes|Genomes|Genetics *4*, 471–483.

Laugesen, A., and Helin, K. (2014). Chromatin Repressive Complexes in Stem Cells, Development, and Cancer. Cell Stem Cell *14*, 735–751.

Lazaro, J.-B., Bailey, P.J., and Lassar, A.B. (2002). Cyclin D-cdk4 activity modulates the subnuclear localization and interaction of MEF2 with SRC-family coactivators during skeletal muscle differentiation. Genes Dev. *16*, 1792–1805.

Lee, Y., Dominy, J.E., Choi, Y.J., Jurczak, M., Tolliday, N., Camporez, J.P., Chim, H., Lim, J.-H., Ruan, H.-B., Yang, X., *et al.* (2014). Cyclin D1-Cdk4 controls glucose metabolism independently of cell cycle progression. Nature *510*, 547–551.

Lei, H., Fukushige, T., Niu, W., Sarov, M., Reinke, V., and Krause, M. (2010). A widespread distribution of genomic CeMyoD binding sites revealed and cross validated by ChIP-Chip and ChIP-Seq techniques. PLoS One *5*, e15898.

Lenhard, B., and Wasserman, W.W. (2002). TFBS: Computational framework for transcription factor binding site analysis. Bioinformatics *18*, 1135–1136.

Lessard, J., Wu, J.I., Ranish, J.A., Wan, M., Winslow, M.M., Staahl, B.T., Wu, H., Aebersold, R., Graef, I.A., and Crabtree, G.R. (2007). An essential switch in subunit composition of a chromatin remodeling complex during neural development. Neuron *55*, 201–215.

Van Leuken, R., Clijsters, L., and Wolthuis, R. (2008). To cell cycle, swing the APC/C. Biochim. Biophys. Acta *1786*, 49–59.

Lewis, P.W., Beall, E.L., Fleischer, T.C., Georlette, D., Link, A.J., and Botchan, M.R. (2004). Identification of a *Drosophila* Myb-E2F2/RBF transcriptional repressor complex. Genes Dev. *18*, 2929–2940.

Li, L., and Vaessin, H. (2000). Pan-neural Prospero terminates cell proliferation during *Drosophila* neurogenesis. Genes Dev. *14*, 147–151.

Li, V.C., Ballabeni, A., and Kirschner, M.W. (2012). Gap 1 phase length and mouse embryonic stem cell self-renewal. Proc. Natl. Acad. Sci. U. S. A. *109*, 12550–12555.

Li, W., Wu, G., and Wan, Y. (2007). The dual effects of Cdh1/APC in myogenesis. FASEB J. *21*, 3606–3617.

Lilly, M.A., and Duronio, R.J. (2005). New insights into cell cycle control from the *Drosophila* endocycle. Oncogene *24*, 2765–2775.

Lim, D.A., Huang, Y.-C., Swigut, T., Mirick, A.L., Garcia-Verdugo, J.M., Wysocka, J., Ernst, P., and Alvarez-Buylla, A. (2009). Chromatin remodelling factor Mll1 is essential for neurogenesis from postnatal neural stem cells. Nature *458*, 529–533.

Lin, Q., Jo, D., Gebre-Amlak, K.D., and Ruley, H.E. (2004). Enhanced cell-permeant Cre protein for site-specific recombination in cultured cells. BMC Biotechnol. *4*, 25.

Lipinski, M.M., and Jacks, T. (1999). The retinoblastoma gene family in differentiation and development. Oncogene *18*, 7873–7882.

Litovchick, L., Sadasivam, S., Florens, L., Zhu, X., Swanson, S.K., Velmurugan, S., Chen, R., Washburn, M.P., Liu, X.S., and DeCaprio, J.A. (2007). Evolutionarily conserved multisubunit RBL2/p130 and E2F4 protein complex represses human cell cycle-dependent genes in quiescence. Mol. Cell *26*, 539–551.

Liu, M., Iavarone, A., and Freedman, L.P. (1996). Transcriptional activation of the human p21(WAF1/CIP1) gene by retinoic acid receptor. Correlation with retinoid induction of U937 cell differentiation. J. Biol. Chem. *271*, 31723–31728.

Livet, J., Weissman, T.A., Kang, H., Draft, R.W., Lu, J., Bennis, R.A., Sanes, J.R., and Lichtman, J.W. (2007). Transgenic strategies for combinatorial expression of fluorescent proteins in the nervous system. Nature *450*, 56–62.

Lozano, E., Saez, A.G., Flemming, A.J., Cunha, A., and Leroi, A.M. (2006). Regulation of growth by ploidy in *Caenorhabditis elegans*. Curr. Biol. *16*, 493–498.

Lu, X., and Horvitz, H.R. (1998). *lin-35* and lin-53, two genes that antagonize a *C. elegans* ras Pathway, encode proteins similar to Rb and its binding protein RbAp48. Cell *95*, 981–991.

Lukas, C., Sørensen, C.S., Kramer, E., Santoni-Rugiu, E., Lindeneg, C., Peters, J.M., Bartek, J., and Lukas, J. (1999). Accumulation of cyclin B1 requires E2F and cyclin-A-dependent rearrangement of the anaphase-promoting complex. Nature *401*, 815–818.

Lünenbürger, H., Lanvers-Kaminsky, C., Lechtape, B., and Frühwald, M.C. (2010). Systematic analysis of the antiproliferative effects of novel and standard anticancer agents in rhabdoid tumor cell lines. Anticancer. Drugs *21*, 514–522.

Machida, Y.J., Hamlin, J.L., and Dutta, A. (2005). Right place, right time, and only once: replication initiation in metazoans. Cell *123*, 13–24.

Maduro, M., and Pilgrim, D. (1995). Identification and cloning of unc-119, a gene expressed in the *Caenorhabditis elegans* nervous system. Genetics *141*, 977–988.

Maduzia, L.L., Gumienny, T.L., Zimmerman, C.M., Wang, H., Shetgiri, P., Krishna, S., Roberts, A.F., and Padgett, R.W. (2002). *lon-1* regulates *Caenorhabditis elegans* body size downstream of the dbl-1 TGF beta signaling pathway. Dev. Biol. *246*, 418–428.

Mahmoud, A.I., Kocabas, F., Muralidhar, S.A., Kimura, W., Koura, A.S., Thet, S., Porrello, E.R., and Sadek, H.A. (2013). Meis1 regulates postnatal cardiomyocyte cell cycle arrest. Nature *497*, 249–253.

Mailand, N., and Diffley, J.F.X. (2005). CDKs promote DNA replication origin licensing in human cells by protecting Cdc6 from APC/C-dependent proteolysis. Cell *122*, 915–926.

Malumbres, M., and Barbacid, M. (2009). Cell cycle, CDKs and cancer: a changing paradigm. Nat. Rev. Cancer *9*, 153–166.

Malumbres, M., Sotillo, R., Santamaría, D., Galán, J., Cerezo, A., Ortega, S., Dubus, P., and Barbacid, M. (2004). Mammalian cells cycle without the D-type cyclin-dependent kinases Cdk4 and Cdk6. Cell *118*, 493–504.

Margaritis, T., Lijnzaad, P., van Leenen, D., Bouwmeester, D., Kemmeren, P., van Hooff, S.R., and Holstege, F.C.P. (2009). Adaptable gene-specific dye bias correction for two-channel DNA microarrays. Mol. Syst. Biol. *5*, 266.

Martinez, A.-M., and Cavalli, G. (2014). The role of Polycomb Group Proteins in Cell Cycle Regulation During Development. Cell Cycle *5*, 1189–1197.

Matsumoto, A., Takeishi, S., Kanie, T., Susaki, E., Onoyama, I., Tateishi, Y., Nakayama, K., and Nakayama, K.I. (2011). p57 is required for quiescence and maintenance of adult hematopoietic stem cells. Cell Stem Cell *9*, 262–271.

Matsushime, H., Quelle, D.E., Shurtleff, S.A., Shibuya, M., Sherr, C.J., and Kato, J.Y. (1994). D-type cyclin-dependent kinase activity in mammalian cells. Mol. Cell. Biol. *14*, 2066–2076.

Matsuura, I., Denissova, N.G., Wang, G., He, D., Long, J., and Liu, F. (2004). Cyclin-dependent kinases regulate the antiproliferative function of Smads. Nature *430*, 226–231.

Matushansky, I., Radparvar, F., and Skoultchi, A.I. (2000). Reprogramming leukemic cells to terminal differentiation by inhibiting specific cyclin-dependent kinases in G1. Proc. Natl. Acad. Sci. U. S. A. *97*, 14317–14322.

McGarry, T.J., and Kirschner, M.W. (1998). Geminin, an inhibitor of DNA replication, is degraded during mitosis. Cell *93*, 1043–1053.

Méchali, M. (2010). Eukaryotic DNA replication origins: many choices for appropriate answers. Nat. Rev. Mol. Cell Biol. *11*, 728–738.

Mello, C., and Fire, A. (1995). DNA transformation. Methods Cell Biol. *48*, 451–482.

Mello, C.C., Kramer, J.M., Stinchcomb, D., and Ambros, V. (1991). Efficient gene transfer in *C.elegans*: extrachromosomal maintenance and integration of transforming sequences. EMBO J. *10*, 3959–3970.

Meyer, C.A., Jacobs, H.W., Datar, S.A., Du, W., Edgar, B.A., and Lehner, C.F. (2000). *Drosophila* Cdk4 is required for normal growth and is dispensable for cell cycle progression. EMBO J. *19*, 4533–4542.

Meyer, C.A., Jacobs, H.W., and Lehner, C.F. (2002). Cyclin D-cdk4 is not a master regulator of cell multiplication in *Drosophila* embryos. Curr. Biol. *12*, 661–666.

Mikkelsen, T.S., Ku, M., Jaffe, D.B., Issac, B., Lieberman, E., Giannoukos, G., Alvarez, P., Brockman, W., Kim, T.-K., Koche, R.P., *et al.* (2007). Genome-wide maps of chromatin state in pluripotent and lineage-committed cells. Nature *448*, 553–560.

Moerman, D.G., and Williams, B.D. (2006). Sarcomere assembly in *C. elegans* muscle. WormBook 1–16.

Morita, K., Flemming, A.J., Sugihara, Y., Mochii, M., Suzuki, Y., Yoshida, S., Wood, W.B., Kohara, Y., Leroi, A.M., and Ueno, N. (2002). A *Caenorhabditis elegans* TGF-beta, DBL-1, controls the expression of LON-1, a PR-related protein, that regulates polyploidization and body length. EMBO J. *21*, 1063–1073.

Morris, E.J., and Dyson, N.J. (2001). Retinoblastoma protein partners. Adv. Cancer Res. *82*, 1–54.

Müller, H., and Helin, K. (2000). The E2F transcription factors: key regulators of cell proliferation. Biochim. Biophys. Acta - Rev. Cancer *1470*, M1–M12.

Müller, J., Hart, C.M., Francis, N.J., Vargas, M.L., Sengupta, A., Wild, B., Miller, E.L., O'Connor, M.B., Kingston, R.E., and Simon, J.A. (2002). Histone methyltransferase activity of a *Drosophila* Polycomb group repressor complex. Cell *111*, 197–208.

Mummery, C.L., van den Brink, C.E., and de Laat, S.W. (1987). Commitment to differentiation induced by retinoic acid in P19 embryonal carcinoma cells is cell cycle dependent. Dev. Biol. *121*, 10–19.

Mummery, C.L., Zhang, J., Ng, E.S., Elliott, D.A., Elefanty, A.G., and Kamp, T.J. (2012). Differentiation of human embryonic stem cells and induced pluripotent stem cells to cardiomyocytes: a methods overview. Circ. Res. *111*, 344–358.

Münger, K., Werness, B.A., Dyson, N., Phelps, W.C., Harlow, E., and Howley, P.M. (1989). Complex formation of human papillomavirus E7 proteins with the retinoblastoma tumor suppressor gene product. EMBO J. *8*, 4099–4105.

Muñoz, J., Stange, D.E., Schepers, A.G., van de Wetering, M., Koo, B.-K., Itzkovitz, S., Volckmann, R., Kung, K.S., Koster, J., Radulescu, S., *et al.* (2012). The Lgr5 intestinal stem cell signature: robust expression of proposed quiescent "+4" cell markers. EMBO J. *31*, 3079–3091.

Myster, D.L., and Duronio, R.J. (2000). To differentiate or not to differentiate? Curr. Biol. *10*, R302–R304.

Nagl, N.G., Wang, X., Patsialou, A., Van Scoy, M., and Moran, E. (2007). Distinct mammalian SWI/SNF chromatin remodeling complexes with opposing roles in cell-cycle control. EMBO J. *26*, 752–763.

Narasimha, A.M., Kaulich, M., Shapiro, G.S., Choi, Y.J., Sicinski, P., and Dowdy, S.F. (2014). Cyclin D activates the Rb tumor suppressor by mono-phosphorylation. Elife *3*, e02872.

Nass, R., Hall, D.H., Miller, D.M., and Blakely, R.D. (2002). Neurotoxin-induced degeneration of dopamine neurons in *Caenorhabditis elegans*. Proc. Natl. Acad. Sci. U. S. A. *99*, 3264–3269.

Nguyen, V.Q., Co, C., and Li, J.J. (2001). Cyclin-dependent kinases prevent DNA re-replication through multiple mechanisms. Nature *411*, 1068–1073.

Nystrom, J., Shen, Z.-Z., Aili, M., Flemming, A.J., Leroi, A., and Tuck, S. (2002). Increased or decreased levels of *Caenorhabditis elegans lon-3,* a gene encoding a collagen, cause reciprocal changes in body length. Genetics *161*, 83–97.

O'Farrell, P.H. (2011). Quiescence: early evolutionary origins and universality do not imply uniformity. Philos. Trans. R. Soc. Lond. B. Biol. Sci. *366*, 3498–3507.

O'Farrell, P.H., Stumpff, J., and Su, T.T. (2004). Embryonic cleavage cycles: how is a mouse like a fly? Curr. Biol. *14*, R35–R45.

Pajcini, K. V., Corbel, S.Y., Sage, J., Pomerantz, J.H., and Blau, H.M. (2010). Transient inactivation of Rb and ARF yields regenerative cells from postmitotic mammalian muscle. Cell Stem Cell *7*, 198–213.

Papetti, M., and Skoultchi, A.I. (2007). Reprogramming leukemia cells to terminal differentiation and growth arrest by RNA interference of PU.1. Mol. Cancer Res. *5*, 1053–1062.

Papetti, M., Wontakal, S.N., Stopka, T., and Skoultchi, A.I. (2010). GATA-1 directly regulates p21 gene expression during erythroid differentiation. Cell Cycle *9*, 1972–1980.

Paridaen, J.T.M.L., and Huttner, W.B. (2014). Neurogenesis during development of the vertebrate central nervous system. EMBO Rep. *15*, 351–364.

Parisi, T., Beck, A.R., Rougier, N., McNeil, T., Lucian, L., Werb, Z., and Amati, B. (2003). Cyclins E1 and E2 are required for endoreplication in placental trophoblast giant cells. EMBO J. *22*, 4794–4803.

Park, M., and Krause, M.W. (1999). Regulation of postembryonic G(1) cell cycle progression in *Caenorhabditis elegans* by a cyclin D/CDK-like complex. Development *126*, 4849–4860.

Parker, S.B., Eichele, G., Zhang, P., Rawls, A., Sands, A.T., Bradley, A., Olson, E.N., Harper, J.W., and Elledge, S.J. (1995). p53-independent expression of p21Cip1 in muscle and other terminally differentiating cells. Science *267*, 1024–1027.

Patel, T., Tursun, B., Rahe, D.P., and Hobert, O. (2012). Removal of Polycomb repressive complex 2 makes *C. elegans* germ cells susceptible to direct conversion into specific somatic cell types. Cell Rep. *2*, 1178–1186.

Pauklin, S., and Vallier, L. (2013). The cell-cycle state of stem cells determines cell fate propensity. Cell *155*, 135–147.

Van de Peppel, J., Kemmeren, P., van Bakel, H., Radonjic, M., van Leenen, D., and Holstege, F.C.P. (2003). Monitoring global messenger RNA changes in externally controlled microarray experiments. EMBO Rep. *4*, 387–393.

Pesin, J.A., and Orr-Weaver, T.L. (2008). Regulation of APC/C activators in mitosis and meiosis. Annu. Rev. Cell Dev. Biol. *24*, 475–499.

Petrella, L.N., Wang, W., Spike, C. a, Rechtsteiner, A., Reinke, V., and Strome, S. (2011). synMuv B proteins antagonize germline fate in the intestine and ensure *C. elegans* survival. Development *138*, 1069–1079.

Phelan, M.L., Sif, S., Narlikar, G.J., and Kingston, R.E. (1999). Reconstitution of a core chromatin remodeling complex from SWI/SNF subunits. Mol. Cell *3*, 247–253.

Pick, J.E., Wang, L., Mayfield, J.E., and Klann, E. (2013). Neuronal expression of the ubiquitin E3 ligase APC/C-Cdh1 during development is required for long-term potentiation, behavioral flexibility, and extinction. Neurobiol. Learn. Mem. *100*, 25–31.

Polager, S., and Ginsberg, D. (2009). p53 and E2f: partners in life and death. Nat. Rev. Cancer *9*, 738–748.

Polley, S.R.G., Kuzmanov, A., Kuang, J., Karpel, J., Lažetić, V., Karina, E.I., Veo, B.L., and Fay, D.S. (2014). Implicating SCF complexes in organogenesis in *Caenorhabditis elegans*. Genetics *196*, 211–223.

Popov, N., and Gil, J. (2010) Epigenetic regulation of the INK4b-ARF-INK4a locus: in sickness and in health. Epigenetics *5*, 685–690.

Porrello, E.R., Mahmoud, A.I., Simpson, E., Hill, J.A., Richardson, J.A., Olson, E.N., and Sadek, H.A. (2011). Transient regenerative potential of the neonatal mouse heart. Science. *331*, 1078–1080.

Portales-Casamar, E., Thongjuea, S., Kwon, A.T., Arenillas, D., Zhao, X., Valen, E., Yusuf, D., Lenhard, B., Wasserman, W.W., and Sandelin, A. (2010). JASPAR 2010: the greatly expanded open-access database of transcription factor binding profiles. Nucleic Acids Res. *38*, D105–D110.

Praitis, V., Casey, E., Collar, D., and Austin, J. (2001). Creation of low-copy integrated transgenic lines in *Caenorhabditis elegans*. Genetics *157*, 1217–1226.

Puri, P.L., and Mercola, M. (2012). BAF60 A, B, and Cs of muscle determination and renewal. Genes Dev. *26*, 2673–2683.

Puyol, M., Martín, A., Dubus, P., Mulero, F., Pizcueta, P., Khan, G., Guerra, C., Santamaría, D., and Barbacid, M. (2010). A synthetic lethal interaction between K-Ras oncogenes and Cdk4 unveils a therapeutic strategy for non-small cell lung carcinoma. Cancer Cell *18*, 63–73.

Raj, A., van den Bogaard, P., Rifkin, S.A., van Oudenaarden, A., and Tyagi, S. (2008). Imaging individual mRNA molecules using multiple singly labeled probes. Nat. Methods *5*, 877–879.

Raj, A., Rifkin, S.A., Andersen, E., and van Oudenaarden, A. (2010). Variability in gene expression underlies incomplete penetrance. Nature *463*, 913–918.

Rampalli, S., Li, L., Mak, E., Ge, K., Brand, M., Tapscott, S.J., and Dilworth, F.J. (2007). p38 MAPK signaling regulates recruitment of Ash2L-containing methyltransferase complexes to specific genes during differentiation. Nat. Struct. Mol. Biol. *14*, 1150–1156.

Rao, S.S., Chu, C., and Kohtz, D.S. (1994). Ectopic expression of cyclin D1 prevents activation of gene transcription by myogenic basic helix-loop-helix regulators. Mol. Cell. Biol. *14*, 5259–5267.

Redemann, S., Schloissnig, S., Ernst, S., Pozniakowsky, A., Ayloo, S., Hyman, A. a, and Bringmann, H. (2011). Codon adaptation-based control of protein expression in *C. elegans*. Nat. Methods *8*, 250–252.

Reed, S.I. (2003). Ratchets and clocks: the cell cycle, ubiquitylation and protein turnover. Nat. Rev. Mol. Cell Biol. *4*, 855–864.

Reimann, J.D., Freed, E., Hsu, J.Y., Kramer, E.R., Peters, J.M., and Jackson, P.K. (2001). Emi1 is a mitotic regulator that interacts with Cdc20 and inhibits the anaphase promoting complex. Cell *105*, 645–655.

Remus, D., Blanchette, M., Rio, D.C., and Botchan, M.R. (2005). CDK phosphorylation inhibits the DNA-binding and ATP-hydrolysis activities of the *Drosophila* origin recognition complex. J. Biol. Chem. *280*, 39740–39751.

Remus, D., Beuron, F., Tolun, G., Griffith, J.D., Morris, E.P., and Diffley, J.F.X. (2009). Concerted loading of Mcm2-7 double hexamers around DNA during DNA replication origin licensing. Cell *139*, 719–730.

Reynaud, E.G., Pelpel, K., Guillier, M., Leibovitch, M.P., and Leibovitch, S.A. (1999). p57(Kip2) stabilizes the MyoD protein by inhibiting cyclin E-Cdk2 kinase activity in growing myoblasts. Mol. Cell. Biol. *19*, 7621–7629.

Reynaud, E.G., Leibovitch, M.P., Tintignac, L.A., Pelpel, K., Guillier, M., and Leibovitch, S.A. (2000). Stabilization of MyoD by direct binding to p57(Kip2). J. Biol. Chem. *275*, 18767–18776.

Richard-Parpaillon, L., Cosgrove, R.A., Devine, C., Vernon, A.E., and Philpott, A. (2004). G1/S phase cyclin-dependent kinase overexpression perturbs early development and delays tissue-specific differentiation in *Xenopus*. Development *131*, 2577–2586.

Riedel, C.G., Dowen, R.H., Lourenco, G.F., Kirienko, N. V, Heimbucher, T., West, J.A., Bowman, S.K., Kingston, R.E., Dillin, A., Asara, J.M., *et al.* (2013). DAF-16 employs the chromatin remodeller SWI/SNF to promote stress resistance and longevity. Nat. Cell Biol. *15*, 491–501.

Robatzek, M., and Thomas, J.H. (2000). Calcium/calmodulin-dependent protein kinase II regulates *Caenorhabditis elegans* locomotion in concert with a G(o)/G(q) signaling network. Genetics *156*, 1069–1082.

Rodrigues, A., Christen, B., Martí, M., and Izpisúa Belmonte, J.C. (2012). Skeletal muscle regeneration in *Xenopus* tadpoles and zebrafish larvae. BMC Dev. Biol. *12*, 9.

Roepman, P., Wessels, L.F.A., Kettelarij, N., Kemmeren, P., Miles, A.J., Lijnzaad, P., Tilanus, M.G.J., Koole, R., Hordijk, G.-J., van der Vliet, P.C., *et al.* (2005). An expression profile for diagnosis of lymph node metastases from primary head and neck squamous cell carcinomas. Nat. Genet. *37*, 182–186.

Rosenbauer, F., and Tenen, D.G. (2007). Transcription factors in myeloid development: balancing differentiation with transformation. Nat. Rev. Immunol. *7*, 105–117.

Roy, K., de la Serna, I.L., and Imbalzano, A.N. (2002a). The myogenic basic helix-loop-helix family of transcription factors shows similar requirements for SWI/SNF chromatin remodeling enzymes during muscle differentiation in culture. J. Biol. Chem. *277*, 33818–33824.

Roy, P.J., Stuart, J.M., Lund, J., and Kim, S.K. (2002b). Chromosomal clustering of muscle-expressed genes in *Caenorhabditis elegans*. Nature *418*, 975–979.

Rual, J.-F., Ceron, J., Koreth, J., Hao, T., Nicot, A.-S., Hirozane-Kishikawa, T., Vandenhaute, J., Orkin, S.H., Hill, D.E., van den Heuvel, S., *et al.* (2004). Toward improving *Caenorhabditis elegans* phenome mapping with an ORFeome-based RNAi library. Genome Res. *14*, 2162–2168.

Sadasivam, S., and DeCaprio, J.A. (2013). The DREAM complex: master coordinator of cell cycle-dependent gene expression. Nat. Rev. Cancer *13*, 585–595.

Sage, C., Huang, M., Karimi, K., Gutierrez, G., Vollrath, M.A., Zhang, D.-S., García-Añoveros, J., Hinds, P.W., Corwin, J.T., Corey, D.P., *et al.* (2005). Proliferation of functional hair cells *in vivo* in the absence of the retinoblastoma protein. Science *307*, 1114–1118.

Saito, R.M., Perreault, A., Peach, B., Satterlee, J.S., and van den Heuvel, S. (2004). The CDC-14 phosphatase controls developmental cell-cycle arrest in *C. elegans*. Nat. Cell Biol. *6*, 777–783.

Salic, A., and Mitchison, T.J. (2008). A chemical method for fast and sensitive detection of DNA synthesis *in vivo*. Proc. Natl. Acad. Sci. U. S. A. *105*, 2415–2420.

Salomoni, P., and Calegari, F. (2010). Cell cycle control of mammalian neural stem cells: putting a speed limit on G1. Trends Cell Biol. *20*, 233–243.

Sang, L., Coller, H.A., and Roberts, J.M. (2008). Control of the reversibility of cellular quiescence by the transcriptional repressor HES1. Science *321*, 1095–1100.

Sarnow, P., Ho, Y.S., Williams, J., and Levine, A.J. (1982). Adenovirus E1b-58kd tumor antigen and SV40 large tumor antigen are physically associated with the same 54 kd cellular protein in transformed cells. Cell *28*, 387–394.

Sauer, B. (1987). Functional expression of the cre-lox site-specific recombination system in the yeast Saccharomyces cerevisiae. Mol. Cell. Biol. *7*, 2087–2096.

Sauer, B., and Henderson, N. (1988). Site-specific DNA recombination in mammalian cells by the Cre recombinase of bacteriophage P1. Proc. Natl. Acad. Sci. U. S. A. *85*, 5166–5170.

Savage-Dunn, C. (2005). TGF-beta signaling. WormBook 1–12.

Sawa, H., Kouike, H., and Okano, H. (2000). Components of the SWI/SNF complex are required for asymmetric cell division in *C. elegans*. Mol. Cell *6*, 617–624.

Sawai, C.M., Freund, J., Oh, P., Ndiaye-Lobry, D., Bretz, J.C., Strikoudis, A., Genesca, L., Trimarchi, T., Kelliher, M.A., Clark, M., *et al.* (2012). Therapeutic targeting of the cyclin D3:CDK4/6 complex in T cell leukemia. Cancer Cell *22*, 452–465.

Scheffner, M., Werness, B.A., Huibregtse, J.M., Levine, A.J., and Howley, P.M. (1990). The E6 oncoprotein encoded by human papillomavirus types 16 and 18 promotes the degradation of p53. Cell *63*, 1129–1136.

Schmitz, C., Kinge, P., and Hutter, H. (2007). Axon guidance genes identified in a large-scale RNAi screen using the RNAi-hypersensitive *Caenorhabditis elegans* strain nre-1(hd20) lin-15b(hd126). Proc. Natl. Acad. Sci. U. S. A. *104*, 834–839.

Schuettengruber, B., Chourrout, D., Vervoort, M., Leblanc, B., and Cavalli, G. (2007). Genome regulation by polycomb and trithorax proteins. Cell *128*, 735–745.

Schuettengruber, B., Martinez, A.-M., Iovino, N., and Cavalli, G. (2011). Trithorax group proteins: switching genes on and keeping them active. Nat. Rev. Mol. Cell Biol. *12*, 799–814.

Schwab, M., Lutum, A.S., and Seufert, W. (1997). Yeast Hct1 is a regulator of Clb2 cyclin proteolysis. Cell *90*, 683–693.

Sela, Y., Molotski, N., Golan, S., Itskovitz-Eldor, J., and Soen, Y. (2012). Human embryonic stem cells exhibit increased propensity to differentiate during the G1 phase prior to phosphorylation of retinoblastoma protein. Stem Cells *30*, 1097–1108.

Sherr, C.J. (2004). Principles of tumor suppression. Cell *116*, 235–246.

Sherr, C.J., and Roberts, J.M. (1999). CDK inhibitors: positive and negative regulators of G1-phase progression. Genes Dev. *13*, 1501–1512.

Shibata, Y., Uchida, M., Takeshita, H., Nishiwaki, K., and Sawa, H. (2012). Multiple functions of PBRM-1/Polybromo- and LET-526/Osa-containing chromatin remodeling complexes in *C. elegans* development. Dev. Biol. *361*, 349–357.

Siatecka, M., Lohmann, F., Bao, S., and Bieker, J.J. (2010). EKLF directly activates the p21WAF1/CIP1 gene by proximal promoter and novel intronic regulatory regions during erythroid differentiation. Mol. Cell. Biol. *30*, 2811–2822.

Signoretti, S., Di Marcotullio, L., Richardson, A., Ramaswamy, S., Isaac, B., Rue, M., Monti, F., Loda, M., and Pagano, M. (2002). Oncogenic role of the ubiquitin ligase subunit Skp2 in human breast cancer. J. Clin. Invest. *110*, 633–641.

Sigrist, S.J., and Lehner, C.F. (1997). *Drosophila* fizzy-related down-regulates mitotic cyclins and is required for cell proliferation arrest and entry into endocycles. Cell *90*, 671–681.

Simone, C., Forcales, S.V., Hill, D.A., Imbalzano, A.N., Latella, L., and Puri, P.L. (2004). p38 pathway targets SWI-SNF chromatin-remodeling complex to muscle-specific loci. Nat. Genet. *36*, 738–743.

Singh, A.M., and Dalton, S. (2009). The cell cycle and Myc intersect with mechanisms that regulate pluripotency and reprogramming. Cell Stem Cell *5*, 141–149.

Singh, A.M., Chappell, J., Trost, R., Lin, L., Wang, T., Tang, J., Matlock, B.K., Weller, K.P., Wu, H., Zhao, S., *et al.* (2013). Cell-cycle control of developmentally regulated transcription factors accounts for heterogeneity in human pluripotent cells. Stem Cell Reports *1*, 532–544.

Singh, K., Cassano, M., Planet, E., Sebastian, S., Jang, S.M., Sohi, G., Faralli, H., Choi, J., Youn, H.-D., Dilworth, F.J., *et al.* (2015). A KAP1 phosphorylation switch controls MyoD function during skeletal muscle differentiation. Genes Dev. *29*, 513–525.

Skaar, J.R., and Pagano, M. (2008). Cdh1: a master G0/G1 regulator. Nat. Cell Biol. *10*, 755–757.

Skaar, J.R., and Pagano, M. (2009). Control of cell growth by the SCF and APC/C ubiquitin ligases. Curr. Opin. Cell Biol. *21*, 816–824.

Skapek, S.X., Rhee, J., Spicer, D.B., and Lassar, A.B. (1995). Inhibition of myogenic differentiation in proliferating myoblasts by cyclin D1-dependent kinase. Science *267*, 1022–1024.

Skapek, S.X., Rhee, J., Kim, P.S., Novitch, B.G., and Lassar, A.B. (1996). Cyclin-mediated inhibition of muscle gene expression via a mechanism that is independent of pRB hyperphosphorylation. Mol. Cell. Biol. *16*, 7043–7053.

Smith, M.E., Cimica, V., Chinni, S., Jana, S., Koba, W., Yang, Z., Fine, E., Zagzag, D., Montagna, C., and Kalpana, G. V (2011). Therapeutically targeting cyclin D1 in primary tumors arising from loss of Ini1. Proc. Natl. Acad. Sci. U. S. A. *108*, 319–324.

Song, A., Wang, Q., Goebl, M.G., and Harrington, M.A. (1998). Phosphorylation of nuclear MyoD is required for its rapid degradation. Mol. Cell. Biol. *18*, 4994–4999.

Sonnichsen, B., Koski, L.B., Walsh, A., Marschall, P., Neumann, B., Brehm, M., Alleaume, A.-M., Artelt, J., Bettencourt, P., Cassin, E., *et al.* (2005). Full-genome RNAi profiling of early embryogenesis in *Caenorhabditis elegans*. Nature *434*, 462–469.

Sparmann, A., and van Lohuizen, M. (2006). Polycomb silencers control cell fate, development and cancer. Nat. Rev. Cancer *6*, 846–856.

Spencer, S.L., Cappell, S.D., Tsai, F.-C., Overton, K.W., Wang, C.L., and Meyer, T. (2013). The proliferation-quiescence decision is controlled by a bifurcation in CDK2 activity at mitotic exit. Cell *155*, 369–383.

Staehling-Hampton, K., Ciampa, P.J., Brook, A., and Dyson, N. (1999). A genetic screen for modifiers of E2F in *Drosophila* melanogaster. Genetics *153*, 275–287.

Stead, E., White, J., Faast, R., Conn, S., Goldstone, S., Rathjen, J., Dhingra, U., Rathjen, P., Walker, D., and Dalton, S. (2002). Pluripotent cell division cycles are driven by ectopic Cdk2, cyclin A/E and E2F activities. Oncogene *21*, 8320–8333.

Stiernagle, T. (2006). Maintenance of *C. elegans*. WormBook 1–11.

Stiewe, T. (2007). The p53 family in differentiation and tumorigenesis. Nat. Rev. Cancer *7*, 165–168.

Sulston, J.E., and Brenner, S. (1974). The DNA of *Caenorhabditis elegans*. Genetics *77*, 95–104.

Sulston, J.E., and Horvitz, H.R. (1977). Post-embryonic cell lineages of the nematode, *Caenorhabditis elegans*. Dev. Biol. *56*, 110–156.

Sulston, J.E., and Horvitz, H.R. (1981). Abnormal cell lineages in mutants of the nematode *Caenorhabditis elegans*. Dev. Biol. *82*, 41–55.

Sulston, J.E., and Schierenberg, E. (1983). The embryonic cell lineage of the nematode *Caenorhabditis elegans*. *119*, 64–119.

Sumrejkanchanakij, P., Tamamori-Adachi, M., Matsunaga, Y., Eto, K., and Ikeda, M.-A. (2003). Role of cyclin D1 cytoplasmic sequestration in the survival of postmitotic neurons. Oncogene *22*, 8723–8730.

Suzuki, Y., Yandell, M.D., Roy, P.J., Krishna, S., Savage-Dunn, C., Ross, R.M., Padgett, R.W., and Wood, W.B. (1999). A BMP homolog acts as a dose-dependent regulator of body size and male tail patterning in *Caenorhabditis elegans*. Development *126*, 241–250.

Talluri, S., and Dick, F.A. (2012). Regulation of transcription and chromatin structure by pRB: here, there and everywhere. Cell Cycle *11*, 3189–3198.

Tapscott, S.J., Davis, R.L., Thayer, M.J., Cheng, P.F., Weintraub, H., and Lassar, A.B. (1988). MyoD1: a nuclear phosphoprotein requiring a Myc homology region to convert fibroblasts to myoblasts. Science *242*, 405–411.

Tateishi, Y., Matsumoto, A., Kanie, T., Hara, E., Nakayama, K., and Nakayama, K.I. (2012). Development of mice without Cip/Kip CDK inhibitors. Biochem. Biophys. Res. Commun. *427*, 285–292.

Tenen, D.G. (2003). Disruption of differentiation in human cancer: AML shows the way. Nat. Rev. Cancer *3*, 89–101.

Teng, F.Y.H., and Tang, B.L. (2005). APC/C regulation of axonal growth and synaptic functions in postmitotic neurons: the Liprin-alpha connection. Cell. Mol. Life Sci. *62*, 1571–1578.

The, I., Ruijtenberg, S., Bouchet, B.P., Cristobal, A., Prinsen, M.B.W., van Mourik, T., Koreth, J., Xu, H., Heck, A.J.R., Akhmanova, A., *et al.* (2015). Rb and FZR1/Cdh1 determine CDK4/6-cyclin D requirement in *C. elegans* and human cancer cells. Nat. Commun. *6*, 5906.

Tian, Y., Liu, Y., Wang, T., Zhou, N., Kong, J., Chen, L., Snitow, M., Morley, M., Li, D., Petrenko, N., *et al.* (2015). A microRNA-Hippo pathway that promotes cardiomyocyte proliferation and cardiac regeneration in mice. Sci. Transl. Med. *7*, 279ra38–ra279ra38.

Tintignac, L.A., Leibovitch, M.P., Kitzmann, M., Fernandez, A., Ducommun, B., Meijer, L., and Leibovitch, S.A. (2000). Cyclin E-cdk2 phosphorylation promotes late G1-phase degradation of MyoD in muscle cells. Exp. Cell Res. *259*, 300–307.

Toogood, P.L., Harvey, P.J., Repine, J.T., Sheehan, D.J., VanderWel, S.N., Zhou, H., Keller, P.R., McNamara, D.J., Sherry, D., Zhu, T., *et al.* (2005). Discovery of a potent and selective inhibitor of cyclin-dependent kinase 4/6. J. Med. Chem. *48*, 2388–2406.

Trojer, P., Li, G., Sims, R.J., Vaquero, A., Kalakonda, N., Boccuni, P., Lee, D., Erdjument-Bromage, H., Tempst, P., Nimer, S.D., *et al.* (2007). L3MBTL1, a histone-methylation-dependent chromatin lock. Cell *129*, 915–928.

Tsikitis, M., Zhang, Z., Edelman, W., Zagzag, D., and Kalpana, G. V (2005). Genetic ablation of Cyclin D1 abrogates genesis of rhabdoid tumors resulting from Ini1 loss. Proc. Natl. Acad. Sci. U. S. A. *102*, 12129–12134.

Tursun, B., Cochella, L., Carrera, I., and Hobert, O. (2009). A toolkit and robust pipeline for the generation of fosmid-based reporter genes in *C. elegans*. PLoS One *4*, e4625.

Vaart, B., van der, van Riel, W.E., Doodhi, H., Kevenaar, J.T., Katrukha, E.A., Gumy, L., Bouchet, B.P., Grigoriev, I., Spangler, S.A., Yu, K. Lou, *et al.* (2013). CFEOM1-associated kinesin KIF21A is a cortical microtubule growth inhibitor. Dev. Cell *27*, 145–160.

Vaccarello, G., Figliola, R., Cramerotti, S., Novelli, F., and Maione, R. (2006). p57Kip2 is induced by MyoD through a p73-dependent pathway. J. Mol. Biol. *356*, 578–588.

Versteege, I., Sévenet, N., Lange, J., Rousseau-Merck, M.F., Ambros, P., Handgretinger, R., Aurias, A., and Delattre, O. (1998). Truncating mutations of hSNF5/INI1 in aggressive paediatric cancer. Nature *394*, 203–206.

Visintin, R., Prinz, S., and Amon, A. (1997). CDC20 and CDH1: a family of substrate-specific activators of APC-dependent proteolysis. Science *278*, 460–463.

Vizcaíno, J.A., Deutsch, E.W., Wang, R., Csordas, A., Reisinger, F., Ríos, D., Dianes, J.A., Sun, Z., Farrah, T., Bandeira, N., *et al.* (2014). ProteomeXchange provides globally coordinated proteomics data submission and dissemination. Nat. Biotechnol. *32*, 223–226.

Voet, M., van der, Lorson, M.A., Srinivasan, D.G., Bennett, K.L., and van den Heuvel, S. (2009). *C. elegans* mitotic cyclins have distinct as well as overlapping functions in chromosome segregation. Cell Cycle *8*, 4091–4102.

Voigt, P., Tee, W.-W., and Reinberg, D. (2013). A double take on bivalent promoters. Genes Dev. *27*, 1318–1338.

Voncken, J.W., Roelen, B.A.J., Roefs, M., de Vries, S., Verhoeven, E., Marino, S., Deschamps, J., and van Lohuizen, M. (2003). Rnf2 (Ring1b) deficiency causes gastrulation arrest and cell cycle inhibition. Proc. Natl. Acad. Sci. U. S. A. *100*, 2468–2473.

Waaijers, S., Portegijs, V., Kerver, J., Lemmens, B.B.L.G., Tijsterman, M., van den Heuvel, S., and Boxem, M. (2013). CRISPR/Cas9-targeted mutagenesis in *Caenorhabditis elegans*. Genetics *195*, 1187–1191.

Wang, D., Kennedy, S., Conte, D., Kim, J.K., Gabel, H.W., Kamath, R.S., Mello, C.C., and Ruvkun, G. (2005). Somatic misexpression of germline P granules and enhanced RNA interference in retinoblastoma pathway mutants. Nature *436*, 593–597.

Wang, X., Haswell, J.R., and Roberts, C.W.M. (2014). Molecular pathways: SWI/SNF (BAF) complexes are frequently mutated in cancer: mechanisms and potential therapeutic insights. Clin. Cancer Res. *20*, 21–27.

Wäsch, R., Robbins, J. a, and Cross, F.R. (2010). The emerging role of APC/CCdh1 in controlling differentiation, genomic stability and tumor suppression. Oncogene *29*, 1–10.

Wei, W., Ayad, N.G., Wan, Y., Zhang, G.-J., Kirschner, M.W., and Kaelin, W.G. (2004). Degradation of the SCF component Skp2 in cell-cycle phase G1 by the anaphase-promoting complex. Nature *428*, 194–198.

Weinstein, N., Ortiz-Gutiérrez, E., Muñoz, S., Rosenblueth, D.A., Álvarez-Buylla, E.R., and Mendoza, L. (2015). A model of the regulatory network involved in the control of the cell cycle and cell differentiation in the *Caenorhabditis elegans* vulva. BMC Bioinformatics *16*, 81.

Werness, B.A., Levine, A.J., and Howley, P.M. (1990). Association of human papillomavirus types 16 and 18 E6 proteins with p53. Science *248*, 76–79.

White, J., and Dalton, S. (2005). Cell cycle control of embryonic stem cells. Stem Cell Rev. *1*, 131–138.

White, J., Stead, E., Faast, R., Conn, S., Cartwright, P., and Dalton, S. (2005). Developmental activation of the Rb-E2F pathway and establishment of cell cycle-regulated cyclin-dependent kinase activity during embryonic stem cell differentiation. Mol. Biol. Cell *16*, 2018–2027.

White, S.M., Constantin, P.E., and Claycomb, W.C. (2004). Cardiac physiology at the cellular level: use of cultured HL-1 cardiomyocytes for studies of cardiac muscle cell structure and function. Am. J. Physiol. Heart Circ. Physiol. *286*, H823–H829.

Whyte, P., Buchkovich, K.J., Horowitz, J.M., Friend, S.H., Raybuck, M., Weinberg, R.A., and Harlow, E. (1988). Association between an oncogene and an anti-oncogene: the adenovirus E1A proteins bind to the retinoblastoma gene product. Nature *334*, 124–129.

Wilkinson, G., Dennis, D., and Schuurmans, C. (2013). Proneural genes in neocortical development. Neuroscience *253*, 256–273.

Wilson, B.G., and Roberts, C.W.M. (2011). SWI/SNF nucleosome remodellers and cancer. Nat. Rev. Cancer *11*, 481–492.

Wilson, B.G., Wang, X., Shen, X., McKenna, E.S., Lemieux, M.E., Cho, Y.-J., Koellhoffer, E.C., Pomeroy, S.L., Orkin, S.H., and Roberts, C.W.M. (2010). Epigenetic antagonism between polycomb and SWI/SNF complexes during oncogenic transformation. Cancer Cell *18*, 316–328.

Winn, J., Carter, M., Avery, L., and Cameron, S. (2011). Hox and a newly identified E2F co-repress cell death in *Caenorhabditis elegans*. Genetics *188*, 897–905.

Wirt, S.E., Adler, A.S., Gebala, V., Weimann, J.M., Schaffer, B.E., Saddic, L. a, Viatour, P., Vogel, H., Chang, H.Y., Meissner, A., *et al.* (2010). G1 arrest and differentiation can occur independently of Rb family function. J. Cell Biol. *191*, 809–825.

Wirth, K.G., Ricci, R., Giménez-Abián, J.F., Taghybeeglu, S., Kudo, N.R., Jochum, W., Vasseur-Cognet, M., and Nasmyth, K. (2004). Loss of the anaphase-promoting complex in quiescent cells causes unscheduled hepatocyte proliferation. Genes Dev. *18*, 88–98.

Wood, A.J., Lo, T.-W., Zeitler, B., Pickle, C.S., Ralston, E.J., Lee, A.H., Amora, R., Miller, J.C., Leung, E., Meng, X., *et al.* (2011). Targeted genome editing across species using ZFNs and TALENs. Science *333*, 307.

Wu H, Kerr MK, Cui X and Churchill GA (2002) MAANOVA: a software package for the analysis of spotted cDNA microarray experiments. The analysis of gene expression data:methods and software*:* 313-341

Xiao, Y., Bedet, C., Robert, V.J.P., Simonet, T., Dunkelbarger, S., Rakotomalala, C., Soete, G., Korswagen, H.C., Strome, S., and Palladino, F. (2011). *Caenorhabditis elegans* chromatin-associated proteins SET-2 and ASH-2 are differentially required for histone H3 Lys 4 methylation in embryos and adult germ cells. Proc. Natl. Acad. Sci. U. S. A. *108*, 8305–8310.

Xu, X.L., Fang, Y., Lee, T.C., Forrest, D., Gregory-Evans, C., Almeida, D., Liu, A., Jhanwar, S.C., Abramson, D.H., and Cobrinik, D. (2009). Retinoblastoma has properties of a cone precursor tumor and depends upon cone-specific MDM2 signaling. Cell *137*, 1018–1031.

Yanagi, K., Mizuno, T., Tsuyama, T., Tada, S., Iida, Y., Sugimoto, A., Eki, T., Enomoto, T., and Hanaoka, F. (2005). *Caenorhabditis elegans* geminin homologue participates in cell cycle regulation and germ line development. J. Biol. Chem. *280*, 19689–19694.

Yang, Y., and Herrup, K. (2007). Cell division in the CNS: protective response or lethal event in post-mitotic neurons? Biochim. Biophys. Acta *1772*, 457–466.

Yang, Y.H., Dudoit, S., Luu, P., Lin, D.M., Peng, V., Ngai, J., and Speed, T.P. (2002). Normalization for cDNA microarray data: a robust composite method addressing single and multiple slide systematic variation. Nucleic Acids Res. *30*, e15.

Yu, Q., Geng, Y., and Sicinski, P. (2001). Specific protection against breast cancers by cyclin D1 ablation. Nature *411*, 1017–1021.

Yui, S., Nakamura, T., Sato, T., Nemoto, Y., Mizutani, T., Zheng, X., Ichinose, S., Nagaishi, T., Okamoto, R., Tsuchiya, K., *et al.* (2012). Functional engraftment of colon epithelium expanded *in vitro* from a single adult $Lgr5^+$ stem cell. Nat. Med. *18*, 618–623.

Zachariae, W., Schwab, M., Nasmyth, K., and Seufert, W. (1998). Control of cyclin ubiquitination by CDK-regulated binding of Hct1 to the anaphase promoting complex. Science *282*, 1721–1724.

Zalc, A., Hayashi, S., Auradé, F., Bröhl, D., Chang, T., Mademtzoglou, D., Mourikis, P., Yao, Z., Cao, Y., Birchmeier, C., *et al.* (2014). Antagonistic regulation of p57kip2 by Hes/Hey downstream of Notch signaling and muscle regulatory factors regulates skeletal muscle growth arrest. Development *141*, 2780–2790.

Zantema, A., Schrier, P.I., Davis-Olivier, A., van Laar, T., Vaessen, R.T., and van der Eb, A.J. (1985). Adenovirus serotype determines association and localization of the large E1B tumor antigen with cellular tumor antigen p53 in transformed cells. Mol. Cell. Biol. *5*, 3084–3091.

Zezula, J., Casaccia-Bonnefil, P., Ezhevsky, S.A., Osterhout, D.J., Levine, J.M., Dowdy, S.F., Chao, M. V, and Koff, A. (2001). p21cip1 is required for the differentiation of oligodendrocytes independently of cell cycle withdrawal. EMBO Rep. *2*, 27–34.

Zhang, H.S., Gavin, M., Dahiya, A., Postigo, A.A., Ma, D., Luo, R.X., Harbour, J.W., and Dean, D.C. (2000). Exit from G1 and S phase of the cell cycle is regulated by repressor complexes containing HDAC-Rb-hSWI/SNF and Rb-hSWI/SNF. Cell *101*, 79–89.

Zhang, J.M., Zhao, X., Wei, Q., and Paterson, B.M. (1999a). Direct inhibition of G(1) cdk kinase activity by MyoD promotes myoblast cell cycle withdrawal and terminal differentiation. EMBO J. *18*, 6983–6993.

Zhang, P., Wong, C., Liu, D., Finegold, M., Harper, J.W., and Elledge, S.J. (1999b). p21(CIP1) and p57(KIP2) control muscle differentiation at the myogenin step. Genes Dev. *13*, 213–224.

Zhang, Z.-K., Davies, K.P., Allen, J., Zhu, L., Pestell, R.G., Zagzag, D., and Kalpana, G. V. (2002). Cell Cycle Arrest and Repression of Cyclin D1 Transcription by INI1/hSNF5. Mol. Cell. Biol. *22*, 5975–5988.

Zhong, W., Feng, H., Santiago, F.E., and Kipreos, E.T. (2003). CUL-4 ubiquitin ligase maintains genome stability by restraining DNA-replication licensing. Nature *423*, 885–889.

Zhu, L., and Skoultchi, A.I. (2001). Coordinating cell proliferation and differentiation. Curr. Opin. Genet. Dev. *11*, 91–97.

Zou, L., and Elledge, S.J. (2003). Sensing DNA damage through ATRIP recognition of RPA-ssDNA complexes. Science *300*, 1542–1548.

Nederlandse Samenvatting

Om vanuit één enkele bevruchte eicel een heel organisme te vormen zijn talloze celdelingen nodig. Deze cellen moeten niet alleen worden gevormd, maar zich ook specialiseren en ontwikkelen tot bijvoorbeeld hartcel, spiercel, bloedcel of bot- en vetweefsel. Tijdens dit specialisatieproces verliezen cellen de capaciteit om te delen. Wanneer ze eenmaal spiercel of hersencel geworden zijn, zullen ze dus niet langer in staat zijn om nieuwe cellen te genereren. In weefsels zoals hart of hersenen waarin er weinig nieuwe cellen gegenereerd kunnen worden om de oude te vervangen leidt beschadiging of verlies van cellen als gevolg van bijvoorbeeld een infarct vaak dus ook tot verlies van functie. In andere gevallen blijven cellen juist delen terwijl ze eigenlijk zouden moeten stoppen. Dit ongeremde delen en daaraan gerelateerde verlies van functie is één van de belangrijkste kenmerken van kanker cellen. Hoewel de juiste balans tussen celdeling en celspecialisatie dus van essentieel belang is voor de ontwikkeling en het functioneren van weefsels en organen, zijn de hiervoor belangrijke mechanismen nog maar ten dele bekend.

Om vanuit een moedercel twee nieuwe dochtercellen te creëren moet een cel door verschillende fasen en processen gaan. Het geheel van deze fasen noemen we de celcyclus. In de S-fase wordt het het erfelijk materiaal, het DNA, verdubbeld. In de M-fase of mitose wordt dit DNA verdeeld over de twee toekomstige dochtercellen en vindt de formatie van de twee nieuwe dochtercellen plaats. De S-fase en M-fase worden gescheiden door zogenaamde Gap-fasen (G1 en G2). De G1-fase volgt na mitose, terwijl de G2-fase zich na de S-fase en vóór de M-fase bevindt. De beslissing om door te gaan met delen of de celcyclus te verlaten en te specialiseren wordt gemaakt in de G1-fase van de celcyclus (Figuur 1).

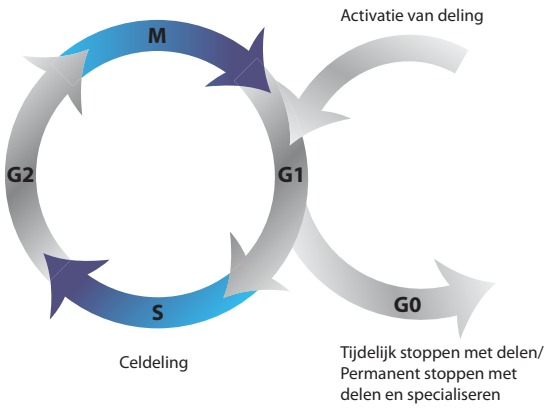

Figuur 1. Overzicht van de celcyclus. Om vanuit één enkele cel twee nieuwe dochtercellen te vormen gaat een cell door verschillende fasen. In de S-fase wordt het DNA, ons erferlijk materiaal, gedupliceerd en tijdens de M-fase wordt dit DNA verdeeld over de twee nieuwe dochtercellen. In de meeste delingen worden de S- en M-fase gescheiden door twee zogenaamde Gap-fasen, de G1 en G2. De beslissing om door te gaan met delen of de celcyclus te verlaten en te stoppen met delen wordt in de G1-fase van de celcyclus gemaakt. Cellen kunnen daarbij zowel tijdelijk als permanent stoppen met delen.

De voortgang door de G1-fase en de transitie van G1 naar S, wordt gereguleerd door een breed scala aan eiwitten die een remmend of stimulerend effect op celdeling kunnen hebben. De belangrijkste en meest bekende groep van positieve celdelingsregulatoren zijn de cyclines en hun partners, de Cycline gereguleerde Kinases (CDKs). Het positive effect van cyclines en CDKs op de voortgang van de celcyclus wordt in balans gehouden door negatieve regulatoren, die de activiteit van cyclines en CDKs remmen. Daarnaast spelen ook specialisatie-inducerende factoren een rol, die de ontwikkeling tot bijvoorbeeld spier of hersencel activeren. Tot slot is ook de organisatie en toegankelijkheid van het DNA, de chromatine structuur, een belangrijke factor bij de beslissing om door te gaan met delen of om te stoppen en te specialiseren.

In dit proefschrift beschrijven wij ons onderzoek naar de mechanismen die ten grondslag liggen aan celdeling en het afstemmen van celdeling met celspecialisatie, alsook de mechanismen die celdeling in gespecialiseerde cellen voorkomen. Hierbij maken we gebruik van de kleine nematode worm *Caenorhabditis elegans* (*C. elegans*). Dit relatief simpele diertje heeft vele voordelen als het gaat om het bestuderen van celdelingsgerelateerde processen. Ten eerste heeft elke worm altijd exact even veel cellen. Het effect van het beinvloeden van biologische processen die celdeling verstoren en bijvoorbeeld tot meer of minder celdeling leiden kan dus heel precies gekwantificeerd worden door het aantal cellen in een weefstel te tellen. Bovendien weten we van elke cel hoeveel uur na de bevruchting deze wordt gevormd, wanneer deze deelt en tot welk celtype deze cel zich zal ontwikkelen. Omdat de worm doorzichtig is kunnen we al deze celdelingen *live* volgen en zichtbaar maken onder de microscoop. Tot slot komen celdelingsmechanismen grotendeels overeen tussen deze worm en meer complexe organismen zoals ook de mens. Ontdekkingen en nieuwe bevindingen opgedaan in de worm zijn dus informatief en van toepassing op de mens en dragen bij aan begrip van humane ziekten.

In het **eerste, inleidende hoofdstuk** bespreken we de verschillende, tot nog toe bekende, factoren en mechanismen die een rol spelen bij het afstemmen van celdeling en celspecialisatie. In het tweede deel van dit hoofdstuk ligt de nadruk vooral op de mechanismen en factoren die celdeling reguleren in *C. elegans*. **Hoofdstuk 2** beschrijft de eiwitten en mechanismen die van belang zijn voor het reguleren van S-fase. We focusen er hierbij vooral op hoe de mechanismen van DNA replicatie verschillen tussen cellen en tussen de verschillende ontwikkelingsstadia van een organisme.

In de **hoofstukken 3 tot en met 7** beschrijven we ons experimentele werk op het gebied van celdeling en celspecialisatie in een zich ontwikkelend organisme. Zoals eerder genoemd wordt de beslissing om wel of niet door te gaan met delen gemaakt in de G1 fase van de celcyclus. Voortgang door de G1-fase wordt gereguleerd door zowel positive als negative regulatoren. De belangrijkste positieve regulatoren voor de G1 fase zijn twee klassen van cycline en CDK complexen: CDK4/6-cycline D en CDK2-cycline E. In **hoofdstuk 3** kijken we naar de functie van het eerste complex, CDK4/6-cycline D, in G1 regulatie. We laten zien dat CDK4/6-cycline D zowel de negatieve cellcyclus regulator pRb als FZR1 kan fosforyleren en remmen en daarmee de progressie van de celcyclus stimuleert. De regulatie

van pRb en FZR is niet alleen van groot belang voor een correcte celdeling in *C. elegans* maar lijkt ook geconserveerd te zijn in humane borstkanker cellen.

In **hoofdstuk 4 en 5** gaan we in op de fundamentele vraag hoe het kan dat gespecialiseerde cellen, zoals spiercellen en hersencellen niet langer in staat zijn om te delen. Daarom onderzoeken we hoe deze cellen reageren op signalen die het delen stimuleren. In hoofdstuk 4 ligt de focus op spiercellen, in hoofdstuk 5 op hersencellen. We beschrijven hoe activatie van de G1 CDKs en cyclines in gespecialiseerde spiercellen leidt tot de activatie van vele celdelingsgerelateerde genen en een gedeeltelijke reactivatie van het celdelingsproces, terwijl spiercel-specifieke genen nauwelijks lijken te veranderen (**hoofstuk 4**). Deze observaties laten zien dat celdeling in ieder geval gedeeltelijk gereactiveerd kan worden in gepecialiseerde spiercellen. Een aantal genen waarvan de expressie essentieel is voor correcte en continue deling konden echter niet geactiveerd worden in deze cellen. Dit suggereert dat er sterke, en voor ons nu nog gedeeltelijk onbekende mechanismen zijn die er voor zorgen dat juist deze essentiële genen worden geïnactiveerd in gespecialiseerde cellen. In **hoofdstuk 5** onderzoeken we vervolgens of de activatie van deze G1 CDKS en cyclines eenzelfde effect heeft in hersencellen. Inderdaad, de overactivatie van deze positieve celcyclus regulatoren of de inactivatie van de negatieve celcyclusregulator FZR1 leidt tot een gedeeltelijke reactivatie van celdeling. Bovendien laten uit rattenhersenen geïsoleerde neuronen vergelijkbare resultaten zien. Deze bevindingen suggereren dat de mechanismen die van belang zijn voor het stoppen met delen en het voorkomen van celdeling in gespecialiseerde hersencellen geconserveerd zijn tussen *C. elegans* en zoogdieren.

Om de mechanismen die celdeling en celspecialisatie op elkaar afstemmen beter te begrijpen ontwikkelden we een methode waarmee genen geïnactiveerd kunnen worden in specifieke cellen in de worm. Deze methode is bovendien zo ontworpen dat de kleur van de cel verandert van rood naar groen wanneer we genen inactiveren. Daardoor zijn we in staat om deze cellen en hun dochters over een langere tijd te volgen. Deze methode is gebaseerd op het zogenaamde CRE-lox recombinatie systeem dat ook in onderzoek met muizen, zebravissen en planten wordt gebruikt. In **hoofdstuk 6** beschrijven we de ontwikkeling en het gebruik van dit systeem en laten we zien dat het stoppen met delen afhankelijk is van vele verschillende factoren. Alleen als we meerdere factoren tegelijkertijd uitschakelen zien we dat voorloperspiercellen niet langer in staat zijn om te stoppen met delen en zich te specialiseren. Er ontstaat dan een tumorachtige ongecontroleerde vermenigvuldiging van cellen waarbij we in sommige gevallen binnen twee dagen een bijna tienvoudige toename zien van het aantal spiercellen. Eén van de belangrijkste regulatoren in dit proces is het SWI/SNF chromatine remodeling complex. Een beter begrip van de rol die dit SWI/SNF complex speelt is van groot belang omdat genen die coderen voor dit complex in veel verschillende humane kankers gemuteerd blijken te zijn.

In **hoofdstuk 7** gaan we verder in op het gebruik en de toepassingen van het op CRE-lox recombinatie systeem zoals beschreven in hoofdstuk 6. Hierin laten we zien dat we met dit systeem niet alleen genen kunnen inactiveren, maar ook activeren. Daarnaast beschrijven we de de ontwikkeling en het gebruik van een zogenaamd split-CRE systeem waarmee

we genexpressie tegelijkertijd in een specifiek celtype en op een specifiek moment tijdens de ontwikkeling kunnen regelen.

Het **laatste hoofdstuk (hoofdstuk 8)** geeft een samenvating van de resultaten beschreven in dit proefschrift. Daarnaast bediscussiëren we deze resultaten in het licht van de recente literatuur met aandacht voor toekomstig onderzoek op het gebied van celdeling en celspecialisatie.

Het werk en de resultaten beschreven in dit proefschrift geven vernieuwde inzichten in verschillende aspecten van celdeling en tonen de complexiteit van de mechanismen die celdeling afstemmen met celspecialisatie. Deze fundamentele kennis kan in de toekomst fungeren als waardevolle basis voor verder klinisch relevant onderzoek op het gebied van kanker en regeneratieve geneeswijzen.

Curriculum Vitae

Suzan Ruijtenberg werd geboren op 19 juli 1985 te Seria, Brunei. Haar lagere schoolperiode bracht ze deels door in Utrecht en deels in Hannover, Duitsland. Na het *cum laude* behalen van haar VWO diploma aan de Stichtse Vrije School in Zeist begon zij in 2004 aan de studie Biomedische Wetenschappen aan de Universiteit Utrecht. In 2007 behaalde ze daar haar Bachelordiploma en in datzelfde jaar begon ze aan de Prestige Master 'Cancer, Genomics, and Developmental Biology'. Haar eerste masterstage van negen maanden verrichtte zij aan de Universiteit Utrecht in het lab van prof. dr. Sander J. L. van den Heuvel onder begeleiding van dr. Inge The en dr. Jerôme Korzelius. Tijdens deze stage richtte zij zich voornamelijk op de vraag wat de essentiële targets zijn van CDK-4/CYD-1 in *C. elegans*. Na deze eerste stage op het gebied van ontwikkelingsbiologie besloot zij zich in haar tweede stage meer te verdiepen in kanker-gerelateerd onderzoek, binnen het lab van dr. Andrea I. McClatchey in het Massachusetts General Hospital, Harvard Medical School in Boston (VS). Hier werkte zij aan de rol van de tumorsuppressor Merlin (NF2) in het ontstaan van borstkanker. Ze deed een laatste stage en schreef haar masterscriptie over de substraatspecificiteit van het Anaphase Promoting Complex/Cyclosome in de groep van prof. dr. Geert J. L. Kops binnen het Universitair Medisch Centrum Utrecht. Na het *cum laude* behalen van haar Masterdiploma in 2009 begon zij in 2010 aan haar promotieonderzoek aan de Universiteit Utrecht in de vakgroep Ontwikkelingsbiologie onder leiding van prof. dr. Sander J.L. van den Heuvel. De resultaten hiervan zijn beschreven in dit proefschrift. Tijdens het promotieonderzoek presenteerde ze haar werk op verscheidene nationale en internationale conferenties waaronder de Cell Cycle Meeting in 2012 en 2014 (Cold Spring Harbour, VS) en de internationale *C. elegans* meeting in 2013 (Los Angeles, VS).

Curriculum Vitae

Suzan Ruijtenberg was born July 19 1985 in Seria, Brunei. She went to primary school both in Utrecht, The Netherlands and in Hannover, Germany. Suzan attended the 'Stichtse Vrije School' in Zeist, where she *cum laude* passed her VWO exam in 2004. In the same year she started her Bachelor studies in Biomedical Sciences at Utrecht University. After three years, she obtained her Bachelor degree and started the biomedical Master "Cancer, Genomics, and Developmental Biology". Her first master rotation project was carried out at the Utrecht University in the Developmental Biology group of prof. dr. Sander J. L. van den Heuvel, under supervision of dr. Inge The and dr. Jerôme Korzelius. During this internship she focused on studying the critical targets of CDK-4/CYD-1 in *C. elegans*. For her second rotation project she moved from developmental biology to the field of cancer biology. In the lab of dr. Andrea I. McClatchey at the Massachusetts General Hospital, Harvard Medical School, Boston USA, she worked on the role of Merlin (NF2) in breast cancer development, using mice and human cell lines as a model system. She performed a final rotation project and wrote her Master thesis on the substrate specificity of the Anaphase Promoting Complex/Cyclosome in the lab of prof. dr. Geert J. L. Kops at the University Medical Center Utrecht, The Netherlands. After obtaining her MSc degree in 2009, *cum laude,* she started her PhD studies in 2010 in the Developmental Biology group of Utrecht University, under supervision of prof. dr. Sander J. L. van den Heuvel. The results of her research are described in this thesis. She presented parts of the work at national and international meetings, among others at the Cell Cycle Meeting in 2012 and 2014 (Cold Spring Harbor, USA) and at the International *C. elegans* meeting in 2013 (Los Angeles, USA).

List of publications

Ruijtenberg, S., van den Heuvel, S. (2015). G1/S inhibitors and the SWI/SNF complex control cell-cycle exit during muscle differentiation. **Cell** *162,* 300-313

The, I.,* **Ruijtenberg, S.**,* Bouchet, B.P., Cristobal, A., Prinsen, M.B.W., van Mourik, T., Koreth, J., Xu, H., Heck, A.J.R., Akhmanova, A., Cuppen, E., Boxem, M., Munoz, J. and van den Heuvel S. (2015). Rb and FZR1/Cdh1 determine CDK4/6-cyclin D requirement in *C. elegans* and human cancer cells. **Nat. Commun.** *6*, 5906.

* These authors contributed equally to the work

Ruijtenberg, S., Van den Heuvel, S., The I. (2011) Book Chapter: DNA Replication and Related Cellular Processes. Edited by dr. Jelena Kusic-Tisma, ISBN: 978-953-307-775-8, InTech

Korzelius, J., The, I., **Ruijtenberg, S.**, Portegijs, V., Xu, H., Horvitz, H.R., and Van den Heuvel, S. (2011). *C. elegans* MCM-4 is a general DNA replication and checkpoint component with an epidermis-specific requirement for growth and viability. **Dev. Biol.** *350*, 358–369.

Korzelius, J., The, I., **Ruijtenberg, S.**, Prinsen, M.B.W., Portegijs, V., Middelkoop, T.C., Koerkamp, M.J.G., Holstege, F.C.P., Boxem, M., and van den Heuvel, S. (2011). *Caenorhabditis elegans* cyclin D/CDK4 and cyclin E/CDK2 induce distinct cell cycle re-entry programs in differentiated muscle cells. **PLoS Genet.** *7(11)*: e1002362

Dankwoord

En dan nu, tot slot de laatste zinnen van dit proefschrift waarin ik graag iedereen die de afgelopen jaren heeft meegewerkt, meegedacht, meegeholpen, luisterde en inspireerde wil bedanken.

Ten eerste mijn promotor Sander van den Heuvel. Sander, de afgelopen jaren heb ik heel veel kansen, mogelijkheden, vrijheid en support gekregen. Ik heb in jouw lab en onder jouw leiding ontzettend veel geleerd en ik kijk met heel veel plezier terug op een intense en mooie AiO periode. Je energie lijkt eindeloos, het glas altijd half vol, de wereld vol mogelijkheden. Zelfs na heel veel jaren wetenschap is de passie voor kennis, weten hoe het zit, een mooi experiment of microscoopplaatje niet verdwenen. En elk experiment leidt ook telkens weer tot een veelheid aan nieuwe plannen en vernieuwde interesses. Af en toe heb ik wel gedacht dat al die mooie plannen misschien alleen haalbaar zijn in een wereld waarin weken en dagen nooit eindigen en er eindeloos veel uren in een dag gaan. Al dan niet haalbaar, waren het die mooie plannen, die mij steeds weer nieuwe perspectieven, richtingen en motivatie brachten en me, zonder twijfel heel veel verder hebben gebracht dan ik ooit had kunnen denken. Bovenal heb ik de afgelopen jaren kunnen werken in een inspirerende omgeving met fijne mensen om me heen die geloofden in mij en in mijn projecten. Sander, heel veel dank!

Inge, ik was trots en blij toen Sander in de zomer van 2007 voorstelde dat jij mijn stage begeleider zou zijn, en wat heb ik veel van je geleerd sindsdien. Vooral ook omdat de rol van begeleider bleef toen ik AiO werd. Nu, bijna acht jaar later is het project van toen afgerond en gepubliceerd. Wat mij betreft is het een voorbeeldproject van een samenwerking waarin we samen zo veel meer konden dan ieder voor zich. Daarmee is het behalve een mooi verhaal, voor mij ook een hele mooie kroon op al onze samenwerkingen, ons samendenken en samenbegeleiden.

Adri, Dank je wel! Ik kan denk ik niet anders zeggen dan dank je wel. Je hebt niet alleen veel betekend in mijn keuze voor de ontwikkelingsbiologie, maar bent ook de afgelopen jaren heel betekenis vol geweest: kritisch, soms wat rechtlijnig, maar bovenal ontzettend betrokken bij mij en bij mijn werk, bij mijn zoektocht naar de juiste projecten, samenwerkingen, mijn plekje in het lab en schrijfstijl. De vele gesprekken en adviezen neem ik mee als hele waardevolle herinneringen. Vincent, al in mijn tweede Bachelor jaar kwam ik bij jou in t "groepje" terecht tijdens de cursus Analysenmethoden. Een beetje intimiderend was je wel: zwarte shirtjes met schreeuwerige teksten, zwarte kisten en lang haar. Maar ook zo ontzettend vriendelijk, behulpzaam en geduldig. De lange haren zijn verdwenen, de zwarte shirtjes verruild voor overhemden, van analist ben je AiO geworden, maar gelukkig zijn de vriendelijkheid, trouw en behulpzaamheid altijd gebleven. Heel veel dank voor alle hulp de afgelopen jaren en ik ben blij dat we zoveel jaren van samenwerken ook gezamenlijk kunnen afsluiten op 16 september als jij als paranimf naast me staat. Mike, uiteindelijk borduurt al mijn werk voort op het jouwe en 'een goed begin is het halve werk' zeggen ze wel eens. Los van het werk aan de celcyclus heb je me de afgelopen jaren veel geholpen en ben je daarin voor mij een hele goede aanvulling op de begeleiding van Sander

geweest. Iemand waarbij ik mijn ideeën kon verifiëren en die altijd klaar stond om te helpen als het ging om computer-gerelateerde zaken die mij soms wat minder liggen. Dank.

I also like to thank all other members of the Developmental Biology group for their help, support, input and inspiring discussions. Thijs, we hebben heel wat jaren samen doorgebracht op de vijfde verdieping van het Kruytgebouw. Ook voor jou zit het promotietraject er nu bijna op en ik wens jou en Lianne ontzettend veel goeds en plezier in het verre Amerika. Suzanne, een heerlijke vrolijke lach, altijd in voor een feestje en een drankje. Ondanks dat je project veel meer vraagt dan de gebruikelijke portie doorzettingsvermogen ben ik er van overtuigd dat het je de komende tijd gaat lukken om het geheel samen te laten komen tot een mooi verhaal en proefschrift. Dank voor al onze gedeelde donderdagmeetings. Lars, maatschappelijk betrokken, wetenschappelijk geïnteresseerd en altijd weet je de juiste vraag te stellen of een prachtig verhaal te vertellen. De afgelopen jaren heb ik steeds je oprechte interesse ervaren, was je nieuwsgierig naar mijn project, blij als het goed ging en was je er ook voor me als het niet mee zat. Dank en succes de komende jaren. Ruben and João, both of you started as master students in the lab and are currently continuing the work as a PhD student. I am sure you both will make something beautiful from your challenging projects. Good luck. Aniek, voor mij was het werk aan het SWI/SNF complex een toevalstreffer, voor jou een bewuste keuze om dit complex verder te bestuderen. Superfijn dat iemand het project doorzet en overneemt en ik wens je heel veel succes. Juliane, you just started in the lab on the already famous project of the wormsorter. I wish you all the best and a wonderful time in Utrecht. Martin en Petra, hoewel jullie focus niet bij de ontwikkelingsbiologie maar op de neurobiologie ligt, heb ik jullie toch ook vaak in de wormenkamer kunnen ontmoeten. Martin, dank voor alle suggesties, input en het mee denken. Petra, heel veel succes bij de allerlaatste stappen van het promotietraject.

Martine, Jana en Herman, zonder goede analist vaart geen enkel lab wel. Martine wat heb ik veel aan je gehad in die beginperiode. Dank voor alle hulp en nog veel meer voor de vriendschap, je heldere kijk, je luisterend oor en gevoel voor humor. Jana en Herman, voor mij waren jullie verhalen en ervaringen van vroeger vaak een heerlijk verfrissend tegengeluid tussen de dagelijkse AiO-sores gesprekken. Herman, dank voor de hulp en de enorme hoeveelheid plaatjes in de laatste anderhalf jaar van mijn AiO periode.

Als beginnende AiO zijn het vooral de ouderejaars AiOs en postdocs waar je tegenop kijkt en van leert. Eén voor één promoveerden jullie en het leek haast onvoorstelbaar dat ik ook ooit zover zou komen, artikelen zou publiceren en zo'n mooi boekje zou schrijven. En nu het bijna zo ver is realiseer ik me meer dan ooit hoe waardevol jullie en jullie gedeelde ervaringen daarin voor mij zijn geweest. Jerôme, Monique, Matilde, Christian, Selma en Marjolein dank jullie wel. Jerôme, voor jou geldt deze dank misschien nog wel het meest, want mijn allereerste ervaringen op het lab waren onder jouw, soms strenge, leiding en het waren absoluut mooie, nuttige en waardevolle ervaringen. Selma, wat hebben we veel jaartjes naast elkaar gestaan en gepipetteerd. Superfijn dat zelfs nu je niet meer in Utrecht werkt je nog zo veel voor dit proefschrift hebt willen doen.

In de afgelopen jaren zijn er ook heel wat studenten geweest die bijgedragen hebben aan de voortgang van het werk en aan mijn eigen ontwikkeling als begeleider. Sander,

mijn eerste scriptie student, David, mijn eerste master student, Henri, Daniel, Stephan, Charlotte, Lotte en Sanne: dank jullie wel. Ik wil hier graag in het bijzonder Stephan, Lotte en Sanne bedanken. Stephan, wat was je zelfstandig en goed op het lab. Zonder al te veel begeleiding lukte het je een heel eigen project op te zetten. Lieve Lotte en Sanne, wat hebben jullie het afgelopen jaar ontzettend hard gewerkt. Wat was het heerlijk om jullie te begeleiden en jullie te zien groeien. Allebei zo verschillend en allebei zo ontzettend goed. Sanne, zelden heb ik iemand ontmoet die zo op haar plek is in de wetenschap. Ongetwijfeld brengt de toekomst nog veel meer mooie labervaringen met zich mee! Lotte, er zijn zoveel verschillende aspecten waar je goed in bent en juist die combinatie maakt je zo bijzonder. Dank voor jullie bijdrage aan mijn AiO-tijd en dit proefschrift.

I also would like to thank Anna, Casper and Paul and all their group members for the nice atmosphere, scientific and non scientific discussions in the hallway of the fifth floor, during meetings or lab outings. Anna, ik heb het laatste jaar meerdere keren aangeklopt voor hulp en advies en ben steeds met nieuwe ideeën, inzichten en heldere adviezen weer je kantoor uit gestapt. Dank je wel. In addition I would like to thank you and Ben for a wonderful collaboration on the role of Rb and FZR in breast cancer cells. Ben, thanks for doing the experiments and for all the advice over the last years. Casper, een gedeelte van het werk beschreven in dit boekje hebben we in jouw lab en met jullie hulp gedaan. Dank. Daarnaast wil ik je bedanken voor de vele korte momenten waarop je me, meestal tussendoor in de gang, in de lift, bij de koffieautomaat van advies hebt voorzien. I would also like to thank all the collaborators who contributed to my work, with a special thanks to Albert Heck, Alba Cristobal, and Javier Muñoz for the mass-spec results, Frank Holstege for the micro-array experiments and Anko de Graaff for giving me the opportunity to use the microscopes in the Hubrecht Institute.

Tot slot wil ik graag de leden van mijn AiO begeleidingscommissie, Geert Kops, Rik Korswagen en Frank Holstege, bedanken. Op het moment zelf is het soms lastig er de vinger op te leggen, maar terugkijkend durf ik wel te zeggen dat sommige van onze gesprekken misschien wel bepalend en op z'n minst sturend zijn geweest voor het verloop van mijn AiO periode.

Naast al deze mensen die de afgelopen jaren hebben bijgedragen aan het wetenschappelijke aspect van mijn bestaan, zijn er nog zovelen die niet direct betrokken zijn bij de inhoud van dit boekje maar die mij wel maken tot wie ik ben en daarmee bijdragen aan mijn kunnen en kennis als wetenschapper. Ten eerste Piet en Alet. Van jongs af aan hebben jullie ons laten zien en ervaren dat de wereld groter is dan Nederland, dat er vele plekke zijn waar je je thuis kan voelen en dat, wanneer je er voor gaat, je er overal iets moois van kan maken. Je moet een beetje geluk hebben als je vanuit de Himmelwiese bij je ouders in de armen stapt en dat geluk, de bijbehorende kansen en mogelijkheden heb ik meer dan gevonden. Bij dat geluk horen ook Jan, Wiebe en Maarten, al lang geen kleine broertjes meer, maar jonge, volwassen mannen, allemaal groter dan ik, die met ambities, overtuigingen, idealen en met een vaak tomeloze energie een wereld vol kansen en mogelijkheden tegemoet treden,

ervoor gaan zonder te zeuren. Het maakt jullie tot prachtmensen waarmee ik graag samen ben.

En als het gaat om 'wie mij maakt tot wie ik ben' denk ik dat vooral diegenen waarmee je vele herinneringen deelt belangrijk zijn. Marjan, Frank, Marijn, Daan en Annelies er zijn veel gezamenlijke herinneringen die ons verbinden, de Johan de Wittstraat als thuis, Kerst, Sinterklaas, bij Oma in de tuin en Friesland. Voor mij zijn het herinneringen aan mooie en belangrijke gebeurtenissen die ongetwijfeld ook in toekomst waardevol blijven voortbestaan.

Met het vinden van mijn lief groeide ook het aantal mensen dat ik familie mag noemen. Hans en Inge, Jan-Wiebe en Lydi, steeds weer weet ik me verzekerd van een warm welkom en interesse.

Naast familie zijn het ook vrienden en de soms jarenlange vriendschappen, gevonden in verschillende fasen in mijn leven, die me dierbaar zijn. Als het gaat om vriendschappen is mijn periode op de Stichtse Vrije School in Zeist heel belangrijk geweest. Zoveel mooie mensen ontmoet, zoveel vriendschappen gevonden in een klas en omgeving waar ik mezelf kon zijn en groeien. Anna en Hanna wat fijn dat we elkaar ook nu nog regelmatig zien. En Anna, wat bijzonder dat mijn lieve 'tweelingzusje' op 16 september weer naast me staat.

Lieve Anne, Sanne, Tessa en Marjan. Wat begon als samen heel hard trainen, samen ploeteren, samen winnen of samen verliezen is inmiddels uitgegroeid tot heel veel meer dan alleen sport. Soms zo verschillend, realiseer ik me heel goed hoe bevoorrecht ik ben, mensen om me heen te hebben waarbij ik verzekerd ben van een luisterend oor, interesse in mijn bestaan en werk, een plek om samen de successen te vieren en gehoord te worden als het tegenzit.

Toen ik op mijn twaalfde lid werd bij de Utrechtse Roeivereniging Viking had ik niet kunnen denken dat 18 jaar later Viking nog steeds zo'n belangrijke rol in mijn leven zou spelen. Viking, een plek waar ik vrienden ontmoette, waar ik kon organiseren en leiding geven, waar ik geleerd heb om te overleggen, samen te werken en te vergaderen, wat het is om te winnen, om door te zetten, maar ook om te verliezen. En waar ik voor het eerst heb ervaren dat dingen soms niet lukken, dat heel graag willen en heel hard trainen geen garantie is voor de overwinning. Iets dat ook zo waar is voor de wetenschap. In al die jaren zijn er in verschillende fasen, verschillende mensen van groot belang geweest. Mederoeiers, coaches, commissie en bestuursleden: allen dank voor een mooie omgeving en samenzijn. Nog bijzonderder misschien, sommigen van jullie zijn ook al die jaren met me mee geroeid en waren belangrijk voor me toen ik op de middelbare school zat, en zijn dat nu nog steeds. Geeske, Edwin, Peter, Hub, Janneke, Simon en Peter en vele anderen dank voor samen zijn, vriendschap en inspiratie. In de afgelopen jaren waarin ik als AiO werkte was juist Viking, de roeiers en hun ouders, vaak de ideale tegenhanger van het meer individualischtische labwerk.

Tot slot, mijn lieve, lieve Super Ties. Wat hebben we het goed samen, geluk dat we elkaar gevonden hebben en aanvullen, en wat ben ik blij met jou. Een eindeloos vertrouwen lijk je in mij te hebben, en steeds blijf je me verzekeren: 'het komt allemaal wel goed'. En mocht het een keer echt te moeilijk voor mij zijn of lijken, ben jij de allereerste die het voor me op zal lossen. Want het zijn juist die dingen die ik moeilijk vind waar jij zo goed in bent. Samen hebben we de afgelopen jaren onze weg gezocht in de wereld van de weteschap, van papers, banen en beurzen, maar ook van student naar grote mensen wereld. Heel, heel graag zoek, en vind ik ook de komende jaren weer samen met jou.

Lieve groet Suzan